Theoretical Models of Dirhodium Catalyzed Reactions and Divergent Heterolytic Fragmentations

By

CROIX JAMES LACONSAY
DISSERTATION

Submitted in partial satisfaction of the requirements for the degree of

DOCTOR OF PHILOSOPHY

in

Chemistry

in the

OFFICE OF GRADUATE STUDIES

of the

UNIVERSITY OF CALIFORNIA

DAVIS

Approved:

Dean J. Tantillo, Chair

Jared T. Shaw

Lee-Ping Wang

Committee in Charge

2022

Dedicated to my mom (Kyle), dad (Michael), and sister (Kaisha)
who prepared me for the road.

All order is doomed, yet the battle is worth while.

- Nathanael West, *Miss Lonelyhearts* (1933)

Reading maketh a full man; conference a ready man; and writing an exact man.

- Sir Francis Bacon

Contents

ABSTRACT OF THE DISSERTATION

Theoretical Models of Dirhodium Catalyzed Reactions and Divergent Heterolytic Fragmentations

The work described in this dissertation builds upon a vast body of work in applied theoretical organic chemistry and spans various sub-disciplines within chemistry. Organic chemistry, organometallic chemistry, and organic chemistry relevant to biological systems—sub-topics of these areas are discussed in this dissertation. A common theme threads through all chapters: computational tools were used to investigate mechanisms of synthetically relevant—and theoretical—reactions to derive general, predictive, and portable models to inform future studies.[*]

Chapter 1 outlines the state of modern, applied theoretical organic chemistry. One role of an applied theoretical organic chemist is to make sense of the complex patterns that emerge out of experimental synthetic organic laboratories. This includes, but is not limited to, deducing mechanistic models that experimentalists can arm themselves with in exploring new reactions. Theoretical chemists use computational methods, in the form of quantum chemistry calculations,

[*] My general research interest and aim is *to solve open questions in organic chemistry using quantum chemistry (computational) tools with an eye towards mechanistic model-generation of fundamental organic reactions*. Through the lens of physical organic chemistry, the "swiss army knife" of organic chemistry, I pursue questions that hold potential to offer valuable insight into reactivity and selectivity of reactions that organic chemists care about, reactions that have broad and direct application in the synthesis of complex organic molecules. Knowledge gained from these mechanistic organic studies help experimental chemists hone their tools (i.e., reactions) to build molecular targets effectively. I aim for my mechanistic models to have broad potential for application in the areas of organic, bio-organic, organometallic, and physical-organic chemistry.

to probe the nuances of organic reaction mechanisms. Chapter 1 discusses these methods along with caveats that inevitably come with limited scientific tools (such as ours).

Part I of this dissertation (which includes Chapters 2-6) homes in on dirhodium(II)-catalyzed reactions and provides examples for which mechanistic details, up until our theoretical investigations, were left in the dark: specifically, mechanistic nuances of ylide-formation/sigmatropic rearrangements (Chapters 2 and 3), donor/donor carbene C-H insertion reactions (Chapters 4 and 5) are described. Specifically for metal-catalyzed ylide-forming reactions, whether dirhodium catalysts are explicitly bound to the ylide intermediate upon subsequent sigmatropic rearrangement (e.g., [1,2]- or [2,3]-shift) remained unknown. A "breadcrumb trail" of evidence in the literature, however, provided ample control experiments for a systematic and comparative theoretical analysis. Reactants, intermediates, and products of synthetically-relevant ylide-formation [1,2]- and [2,3]-rearrangements—and the transition state structures that connect them—were computed with density functional theory. It was found that whether the metal catalyst dissociates before rearrangement *depends on the system*—the most significant factor that directs catalyst dissociation before rearrangement, however, is the steric bulk of the group adjacent to the carbene center. Additionally, computational studies were done in collaboration with the group of Prof. Jared T. Shaw on dirhodium-catalyzed C-H insertion reactions of donor/donor carbenes (Chapter 5). A stepwise mechanism with an S_E2 C-C bond formation was discovered in the C-H insertion reaction. Finally, dirhodium-catalyzed cyclopropanations of cycloheptatriene diazo compounds to semibullvalenes, described in Chapter 6, showcases one example of a theoretical prediction encouraging a synthetic collaboration to test predictions sparked by theory (ongoing).

Part II of this dissertation describes a foray into heterolytic fragmentation reactions. In Chapter 7, computational studies of a designed 1-aza-adamantane model system—by density functional theory, natural bond orbital, *ab initio* molecular dynamics simulations, and external electric field calculations—revealed a divergent fragmentation, one in which a substrate can fragment to two unique products via different mechanistic pathways. Substituents, electrostatic environment, and dynamic effects were found to all influence pathways to competing products.

Chapter 8 provides a portrait of through-bond stereoelectronic effects in products that emerge from a fragmentation reaction, 3-azabicyclo[3.3.1]nonanes. Computational studies of substituent effects, noncovalent interactions, natural bond orbitals, isodesmic reactions, and hydration propensities demonstrated that hyperconjugation/conjugation through-bond effects dominated the different reactivity between two similar compounds—a vinylogous chloride and a vinylogous ester.

Finally, Part III of this dissertation describes an isolated project which benefitted from close collaboration between our group (theory) and the groups of Prof. Reuben Peters (Iowa State University), Prof. Qiang Wang (Sichuan Agricultural University) and Prof. Jeroen Dickschat (University of Bonn), all experimental groups in terpene chemistry. Collaboration between theoretical and experimental groups achieve a depth of mechanistic insight that is potentially missed in the absence of collaboration. This synergy is demonstrated in a collaborative project with all three groups, with whom a plausible mechanism was elucidated for the formation of a natural product, (14*S*)-cleistantha-8,12-diene, from barley diterpene synthase, HvKSL4 (Chapter 9).

PUBLICATIONS

Wang, Q.; Shih, J. -L.; Tsui, K. Y.; **Laconsay, C. J.**; Tantillo, D. J.; May, J. A. "Experimental and Computational Mechanistic Study of Carbonazidate-Initiated Cascade Reactions" *J. Org. Chem.* **2022**, *87*, 8983-9000.

Liang, J.; Merrill, A. T.†; **Laconsay, C. J.**†; Hou, A.; Pu, Q.; Dickschat, J. S.; Tantillo, D. J.; Wang, Q.; Peters, R. J. "Deceptive Complexity in the formation of cleistantha-8,12-diene" *Org. Lett.* **2022**, *24*, 2646-2649.

Laconsay, C. J.†; Rho, T. C.†; Tantillo, D. J. "The Role of Through-Bond Stereoelectronic Effects in the Reactivity of 3-Azabicyclo[3.3.1]nonanes" *J. Org. Chem.* **2022**, *87*, 3378-3388.

Dishman, S.; **Laconsay, C. J.**; Fettinger, J. C.; Tantillo, D. J.; Shaw J. T. "Divergent Stereochemical Outcomes in the Insertion of Donor/Donor Carbenes into the C-H Bonds of Stereogenic Centers" *Chem. Sci.* **2022**, *13*, 1030-1036.

Laconsay, C. J.; Pla-Quintana, A.; Tantillo, D. J. "Effects of Axial Solvent Coordination to Dirhodium Complexes on Reactivity and Selectivity in C-H Insertion Reactions: A Computational Study" *Organometallics* **2021**, *40*, 4120-4132.

Laconsay, C. J.: Tantillo, D. J. "Melding of Experiment and Theory Illuminates Mechanisms of Metal-Catalyzed Rearrangements: Computational Approaches and Caveats" *Synthesis* **2021**, *53*, 3639-3652.

Nair, V. N.; Kojasoy, V.; **Laconsay, C. J.**; Kong, W.; Tantillo, D. J.; Tambar, U. K. "Catalyst Controlled Regiodivergence in Rearrangements of Indole-Based Onium Ylides" *J. Am. Chem. Soc.* **2021**, *143*, 9016-9025.

Laconsay, C.J.; Tantillo, D. J. "Metal-Bound or Free Ylides as Reaction Intermediates in Metal-Catalyzed [2,3]-Sigmatropic Rearrangements? It Depends." *ACS Catalysis* **2021**, *11*, 829-839.

Laconsay, C.J.; Mallick, D.; Shaik, S. "External Electric Fields Interrupt the Concerted Cope Rearrangement of Semibullvalene" *J. Org. Chem.* **2021**, *86, 731-738*

Laconsay, C. J.; Seguin, T. J.; Wheeler, S. E. "Modulating Stereoselectivity through Electrostatic Interactions: SPINOL-Phosphoric Acid Catalyzed Syntheses of 2,3-Dihydroquinazolinones" *ACS Catalysis* **2020**, *10*, 12292-12299.

Laconsay, C. J.; Wedler, H. B.; Tantillo, D. J. "Visualization without Vision – How Blind and Visually Impaired Students and Researchers Engage with Molecular Structures" *Journal of Science Education for Students with Disabilities* **2020**, *23*, 1-21.

Laconsay, C. J.; Tsui, K. Y.; Tantillo, D. J. "Tipping the Balance: Theoretical Interrogation of Divergent Extended Heterolytic Fragmentations" *Chem. Sci.* **2020**, *11*, 2231-2242.

Nickerson, L. A.; Bergstrom, B. D.; Gao, M.; Shiue, Y.; **Laconsay, C. J.**; Culberson, M. R.; Knauss, W. K.; Fettinger, J. C.; Tantillo, D. J.; Shaw, J. T. "Enantioselective Synthesis of Isochromans and Tetrahydroisoquinolines by C-H Insertion of Donor/Donor Carbenes" *Chem. Sci.* **2020**, *11*, 494-498.

Nemes, C. T.; **Laconsay, C. J.**; Galbraith, J. M. "Hydrogen Bonding from a Valence Bond Theory Perspective: The Role of Covalency" *Phys. Chem. Chem. Phys.*, **2018**, *20*, 20963.

James, A. M.; **Laconsay, C. J.**; Galbraith, J. M. "Charge-Shift Corrected Electronegativities and the Effect of Bond Polarity and Substituents on Covalent-Ionic Resonance Energy" *J. Phys. Chem. A* **2017**, *121*, 5190-5195.

Laconsay, C. J.; Galbraith, J. M., "A Valence Bond Theory Treatment of Tetrel-Bonding Interactions" *Computational and Theoretical Chemistry* **2017,** *1116*, 202-206.

Laconsay, C. J.; James, A. M.; Galbraith, J. M. "Effect of Lone Pairs on Molecular Resonance Energy" *J. Phys. Chem. A* **2016**, *120*, 8430-8434.

(† = authors contributed equally.)

ACKNOWLEDGEMENTS

I am indebted to many people who have supported me throughout my life, in and out of graduate school. I dedicate this dissertation to friends and family. Without them, this dissertation would not be possible.

First and foremost, I am grateful to my PhD advisor, Dean Tantillo, for accepting me into his group as a graduate student and for his endless guidance, support, and mentorship. He supported and encouraged me throughout my doctoral studies and led by example. I learned a lot about what it means to be a curious, attentive, and ethical scientist from Dean—for that, I will always be grateful. In the Russian language, the word "scientist" (ученый) literally means "someone who was taught". In this way, I am the scientist I am today because of him.

I am grateful to the mentors on my dissertation committee, who helped me grow as a chemist, and who periodically—when necessary—held my feet to the fire, which further refined my science and ideas. Specifically, I acknowledge Jared Shaw, for his synthetic insight in conversations that stimulated much of the work in this dissertation. I also thank Lee-Ping Wang, who pushed me intellectually in classes and exams, and broadened my knowledge in quantum chemistry, statistical mechanics, and computational methods.

Many experimental and theoretical collaborators helped expand my knowledge about organic chemistry, for which I am deeply grateful. These include Ka Yi Tsui, Sarah Dishman, Volga Kojasoy, Henry (Hoby) Wedler, Amy Merrill, Yusef Ahmed, Wentao Guo, William DeSnoo, Wang Yeuk Kong, Benjamin Bergstrom, Leslie Nickerson, Mingchun Gao, Yuan-Shin Shiue, and Tyler Rho from the Department of Chemistry at UC Davis; Prof. Anna Pla-Quintana from the Institut de Química Computacional i Catàlisi (IQCC) and Departament de Química,

Facultat de Ciències, Universitat de Girona; Vaishnavi Nair and Prof. Uttam Tambar from UT Southwestern Medical Center; Prof. Jeremy May from the University of Houston; Prof. Daniel Romo from Baylor University; Prof. Reuben Peters from Iowa State University; Prof. Benjamin List from Max-Planck-Institut für Kohlenforschung; Prof. Jennifer Hirschi from SUNY Binghamton. I also thank the rest of the Tantillo group for surrounding me with an intellectually stimulating and supportive environment for learning.

I would be remiss if I did not acknowledge my past mentors, who guided me to the intellectual oasis that is theoretical organic chemistry, to whom I will always be grateful: Prof. John Morrison Galbraith and Prof. Jocelyn Nadeau from Marist College; Prof. Steven Wheeler from University of Georgia and my mentor, Dr. Trevor Seguin; Prof. Dibyendu Mallick and Prof. Sason Shaik from The Hebrew University of Jerusalem; and Prof. Roald Hoffmann from Cornell University, who profoundly shaped my ideas (indirectly) through the written word.

Finally, I am deeply grateful for my family—Mom, Dad, Kaisha, and Aaron—and my partner, Jennifer, who all supported me throughout graduate school. Thank you.

Chapter 1

Modern Applied Theoretical Organic Chemistry[†]

There is no nobler aspiration of the human intellect than desire to compass the cause of things.

- T. C. Chamberlin (*The Journal of Geology*, **1897**, *103*, 349-354)

1.1 Introduction

The development and refinement of useful models for organic reactions is the guiding light of applied theoretical organic chemistry. A theoretical organic chemist's *dream* is to have their ideas written down on the glass of a hood and discussed among synthetic chemists, trying to make some sense of their reactions. If our developed models inspire new experiments, increase understanding about the chemical world, and are portable enough to predict new directions (ideally on a napkin), then we have done our job well.

Theoretical organic chemists are motivated by questions such as, 'what is a reaction's mechanism?'; 'what does the stereo-determining transition state structure look like and what is its energy relative to other transition state structures?'; 'why is this product preferred over the other?'; 'what are the physical forces behind this experimental observation?' This field—which inevitably overlaps with parts of computational chemistry—provides answers and opens new questions by

[†] Portions of this chapter are adapted and modified from the following published article: Laconsay, C. J.; Tantillo, D. J. Melding of Experiment and Theory Illuminates Mechanisms of Metal-Catalyzed Rearrangements: Computational Approaches and Caveats, *Synthesis* **2021**, *53*, 3639-3652 with permission from Georg Thieme Verlag KG.

supplying models rooted in quantum mechanics.[1] Theoretical organic chemists wield quantum chemistry calculations as tools in their adventures, be it *ab initio* or density functional theory (DFT) methods (see below). As a result (and in the spirit of Moore's law),[2] advances in computing power have lowered the cost for developing these models: as computing power accelerates so does discovery in theoretical organic chemistry. This has inevitably opened the doors to questions of greater complexity.

The continued advance into unknown chemical space by synthetic groups has increased the demand for satisfactory models for reaction mechanisms (and newfound understanding). Fortunately, faster and more efficient quantum chemical methods (like DFT) have allowed theorists to keep up in some areas. As a result, experimental and theoretical researchers will often venture together—the experimentalist asking 'what', and their theoretically-leaning colleagues asking 'why' (though it is not uncommon for the roles to reverse or for both camps to ask these questions simultaneously). The synergy between these collaborators helps them reach a layer of understanding that is inaccessible to either group if they were to venture new areas alone.

While an experimentalist explores *chemical space*, the possible set of chemical species,[3] a theorist explores the concomitant *potential energy surface* (PES) of one (or more) representative reactions to probe mechanism. Consider a synthetic paper. It will often describe the scope of a reaction (i.e., the chemical space). The breadth of the reaction scope communicates to the reader that their developed method is general, specified under a set of reaction conditions. A theory paper, on the other hand, might describe a one-dimensional "slice" (i.e., the reaction coordinate) of the $3N$-6 potential energy surface (i.e., the PES if it's a non-linear molecule; N being the number of atoms). Whether the described, plausible mechanism is relevant to reactions of similar molecules is much more challenging to show. Nonetheless, despite the different levels of exploration (i.e.,

exploration of chemical space versus energy space), there is much benefit gained by close collaboration between experimental and theory groups—both enhance understanding.

1.2 Mechanistic Models

A reaction mechanism is a *model* that describes how reactants are transformed to products (expressed in an arrow-pushing scheme, a PES picture, a collection of molecular dynamics trajectories, etc.).[4] A *plausible* reaction mechanism is one with which all sets of valid experimental and computational evidence are consistent. Of course, the *validity* of pieces of evidence can be debated. However, if one discounts a piece of evidence in presenting a mechanistic model, the argument for doing so should be clearly stated. In that a mechanism is a model, it *cannot* be proven.[5–8] Rather, the best one can do is sift through the multitude of possible mechanistic models that fit the available data, clearly define criteria for ranking them (or not), and propose future tests (experimental or computational) that can lead to model refinement.[9] After interrogating and refuting hypotheses, one often generates enough confidence in a mechanism to consider it 'valid' or 'accepted,' which it remains until demonstrated otherwise, a notion stemming from, but not exactly aligned with, the ideas described by the philosopher Karl Popper.[10,11] But one must not become too invested in an accepted model, for it could be invalidated by future tests. As Richard Feynman famously stated, "…you must not fool yourself and you are the easiest person to fool."[12] In the words of astronomer John Gribbin, "the best that can be said is that it [the model] has passed all the tests applied so far."[13,14] Of course, a mechanism need not be proven to be useful.[15] Often, a model's utility and virtue lies in its ability to make valuable predictions.[16]

This dissertation focuses on computational studies that provide evidence in support of or against a given reaction mechanism. Modeling mechanisms of complex reactions by quantum chemical calculations is now commonplace;[17–19] however, we are aware of (and agree with) the

notion from philosophers of science that explanations of organic phenomena, as described by organic theory, simply cannot be reducible (in the philosophical sense) to quantum mechanics alone.[20]

The first step of the modeling process in this context generally involves applying computational methods to assess the structural and energetic viability of an arrow-pushing mechanism (hypothesized based on existing experimental evidence) by computing relevant structures (reactants, intermediates, products, and the TSSs connecting them, all of which are called *stationary points*) on a PES (Figure 1.1).

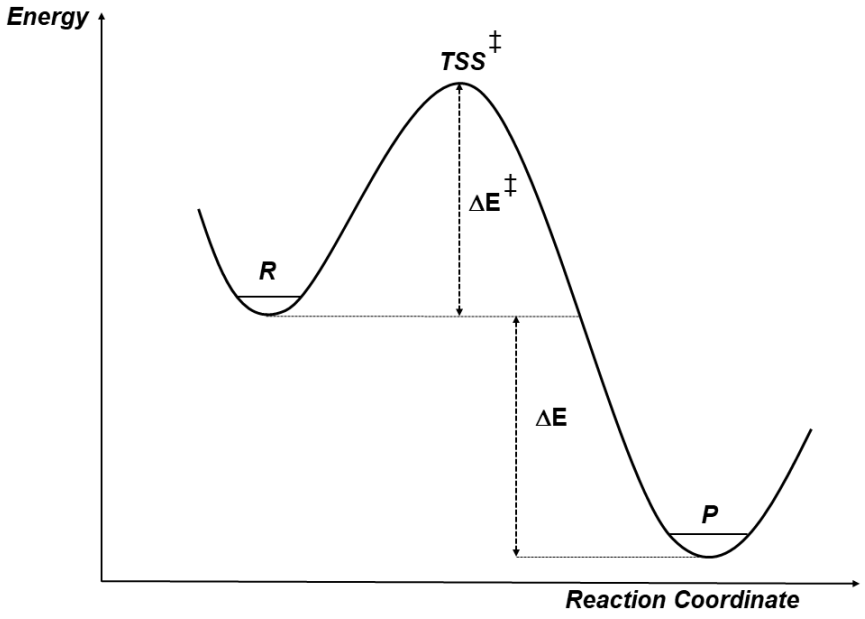

Figure 1.1. Simple potential energy surface, describing the energy change as a reactant (R) transforms to a product (P) through a single transition state structure (TSS) along the reaction coordinate. Horizontal lines in local minima denote zero-point energies for R and P. Activation barrier ($\Delta E^{\ddagger}$) and total energy change (ΔE) are shown.

A PES conveys a molecule's change in energy (E) with respect to changes in structure (tracked by the reaction coordinate). For a molecule with *N* atoms, its internal potential energy will

be represented by a hyperdimensional surface of 3*N*-6 dimensions for non-linear molecules or 3*N*-5 dimensions for linear molecules (for $N \geq 3$). We know these dimensions because each nuclei have three ways of moving (or rotating) in the same direction in three dimensions along (or around) the x, y, and z axes. A PES is often represented with a reduced dimensional reaction coordinate diagram as in Figure 1.1, a one-dimensional "slice" of the hyperdimensional potential energy surface. Note that reduced dimensional PESs chosen based on chemical intuition, of course, have limitations, and tools like *PathReducer*[21] aim to solve these issues by identifying key degrees of freedom that captures the most structural variance in the fewest dimensions. Key to generating PESs (and quantum chemistry, more generally) is the Born-Oppenheimer (BO) approximation, which decouples the movements of nuclei and electrons under the reasonable assumption that nuclei are much heavier than electrons—the view that electrons move in an average field of nuclei and *vice versa*. The BO approximation makes the exploration of a potential energy surface of moving nuclei into solving an electronic Schrödinger equation.

Transition state theory (TST) relates the free energy barrier of a reaction to its rate.[22] A postulated mechanism is consistent with the calculations if computed barriers ($\Delta E^{\ddagger}$, or $\Delta G^{\ddagger}$ when the vertical axis is Gibbs free energy; Figure 1.1) are low enough that the associated rate would be fast enough under the experimental conditions, based on the Eyring equation (uses $\Delta G^{\ddagger}$), in need of revision if computed barriers are much too high, or in need of a deeper dive if computed barriers are borderline, i.e., at the high end or just beyond the range of barriers that are reasonable. This process is iterated until a mechanism is found for which all computed barriers are reasonable and that can account for any side products.[23] A 'good' computed energy profile,[24] therefore, aims to provide a productive and portable model[15] that (i) predicts a reaction mechanism that aligns with laboratory observations, (ii) provides otherwise elusive insight, and (iii) allows new hypotheses to

be generated that can be tested in subsequent experiments.[25] As Plata and Singleton have noted, the "primordial currency of information provided by computational studies consists of the geometries and energies of intermediates and transition states along the mechanism."[26] Thus, rigorously scrutinizing theory's performance against experiment is crucial.[27] For more in-depth discussion of models in chemistry and what makes a good energy profile, we recommend the work of Eisenstein and coworkers.[24]

1.3 Theoretical Approaches and Caveats

1.3.1 Some Quantum Mechanics Basics

All organic chemistry is concerned with nuclei, electrons, and their interactions. Thus, theoretical organic chemists can begin answering mechanistic (and structural) questions in organic chemistry by solving an electronic structure problem, i.e., solving the time-independent Schrödinger equation (eq. 1).

$$\hat{H}|\Psi\rangle = E|\Psi\rangle \tag{1}$$

The Schrödinger equation allows one to associate an energy (E) to a particular set of nuclei oriented in space and its concomitant distribution of electrons, expressed by a wave function (Ψ), and provides a way to obtain a chemical reaction's potential energy surface and other parameters for deriving properties of interest (e.g., activation barriers, energies of reactions, etc.). Solving this equation requires the Hamiltonian operator ($\hat{H}$), which operates on Ψ. $\hat{H}$ is made up of kinetic and potential operators, used to operate on Ψ to obtain Ψ back with an E, an observable—in quantum

mechanics, there is a quantum mechanical operator for every physical observable. We learn much about our molecular world by solving—or, in most cases, *approximating*—the Schrödinger equation. Alas, we can only solve it *exactly* for simple toy models, such as the hydrogen atom and H_2^+ cation. Everything else, that is, everything that concern organic chemists, requires approximations.[28]

Though the history of quantum and computational chemistry begins with *ab initio* methods—wavefunction (Ψ) based electronic structure theories (such as Hartree-Fock theory and post-Hartree-Fock theory)—electron density ($|\Psi|^2$ or ρ) based methods, such as Kohn-Sham density functional theory (DFT), are generally preferred for studying organic systems of the size we are concerned with here because, although the machinery of HF and DFT theories are generally the same, DFT methods are generally cheaper in terms of computational cost. The difference, however, lies in how the energy is calculated: HF theory calculates the energies directly from the orbitals, while DFT calculates the energy from the orbitals and an approximate functional of the electron density.‡

In practice, both methods use a self-consistent field (SCF) approach to approximate solutions to the Schrödinger equation. Within the Hartree-Fock (HF) procedure,[28] for example, an SCF algorithm will begin with a set of nuclear coordinates and an initial guess of the molecular orbitals (one-electron wavefunctions, also called spin orbitals) that describe the positions of the electrons. In HF theory, the *N*-electron system is described by a single Slater determinant—as opposed to methods with multiple determinants, i.e, multiconfigurational methods—where χ_N is the N^{th} molecular (spin) orbital (eq. 1). When expressed as a Slater determinant, the wavefunction satisfies the antisymmetry principle.

‡ For "DFT in a Nutshell", see the following reference by Burke and Wagner: *International Journal of Quantum Chemistry*, **2013**, *113*, 96-101.

$$|\Psi_0\rangle = |\chi_1\chi_2 \cdots \chi_N\rangle \quad (1)$$

According to the variational theorem, the 'best' wavefunction (Ψ_0) is the one with lowest possible energy (E_0) (eq. 2-4). In the equations below, Φ denotes some trial ground state wavefunction, and Ψ_0 denotes the exact ground state wavefunction, and their energies, E_0 and E_Φ, respectively.

$$E_0 \leq \langle\Phi|\hat{H}|\Phi\rangle \quad (2)$$

$$E_0 = \langle\Psi_0|\hat{H}|\Psi_0\rangle \quad (3)$$

$$E_0 \leq E_\Phi \quad (4)$$

The SCF procedure iteratively solves the Schrödinger equation for the set of molecular orbitals that minimizes E. It does this by taking an initial "guess" of molecular orbitals (from a linear combination of atomic orbitals; LCAO), computing the average field 'felt' by each electron, and solving the one-electron Schrödinger equation using Slater determinants to generate a new set of molecular orbitals. The energy is evaluated at each of these steps, and the procedure is repeated iteratively until the average field felt by each electron and orbitals do not change within a set of criteria, in which case the calculation is said to *converge* and reach *self-consistency*, hence *self-consistent field*. Density functional theory SCF calculations proceed in a similar manner except that Fock equations are now Kohn-Sham equations, and the initial guess begins with electron density, not molecular orbitals.[29] The rest of the machinery is effectively the same.

Though *ab initio* methods are useful for reliably obtaining accurate energies[30] relative to DFT methods—and they often are used in subsequent calculations to correct DFT electronic

energies—they often require a prohibitive amount of computer time (*vide infra*). DFT methods, on the other hand, reach similar levels of accuracy at a cheaper computational cost, which greatly motivates their use in geometry optimizations and frequencies analysis, especially when studying organic systems increasingly large numbers of atoms.[17,31–35] Note that reliably obtaining accurate *absolute energies* by DFT is (in most cases) futile: "when DFT results are examined critically, total energies of medium-sized molecules are often in error by one full hartree (627 kcal mol^{-1})".[30] By "accuracy" in mechanistic DFT studies we mean accurate *relative energies*, which rely on cancellation of error. The standard error bars for reaching what is called "chemical accuracy" for relative energetic quantities is within 1 kcal mol^{-1} of experiment or high level computational method.[36] In one sense, computational organic chemistry owes its existence to cancellation of error.

1.3.2 Selecting an Appropriate Theoretical Approach

Since we cannot solve the Schrödinger equation exactly for most systems, choosing an appropriate theoretical approach depends on the system at hand and the type of question being asked. Most of the systems considered in this dissertation are < 300 atoms, and so quantum chemistry methods are most appropriate for typical questions probing mechanism. Below, we home in on metal-catalyzed sigmatropic rearrangements and small organic molecules that undergo heterolytic fragmentations. For most reactions in this realm, DFT is the most suitable theoretical approach. The literature is filled with a continuous stream of updated discussions regarding best practices of DFT on molecular computational chemistry. We recommend a recent article by Grimme for state-of-the-art practices.[37]

As this dissertation focuses prominently on metal-promoted sigmatropic shifts, we discuss in details some general principles for applying computational chemistry to these transformations below, but for thorough tutorials on the nuances involved in modeling organometallic reactions, including nontrivial mistakes, misconceptions, and misinterpretations, we recommend the work of Baik, Peverati, Lan and coworkers.[38–40] Many of the organometallic systems are relatively large, so choosing an appropriate density functional approximation and basis set (i.e., level of theory) is not always trivial.

In addition to organometallic systems, this dissertation discusses small organic systems, such as those involved in heterolytic fragmentations. Heterolytic fragmentation reactions fall within the category of small to medium organic systems, which includes a large swath of compounds. So, finding an appropriate quantum chemistry method (usually DFT) to study fragmentations can be onerous, as it is in any small to medium organic system because there is a 'zoo' of density functional approximations to choose from.[41–44] We, therefore, recommend the general approach: (1) search the literature for computational benchmark studies that establish appropriate computational methods for the system at hand by testing methods against reliable experimental data (e.g., ionization potentials or known, experimentally-derived activation barriers) or high-level of theory reference calculation; (2) if benchmark studies do not exist, then select levels of theory (be it DFT or *ab initio*) appropriate for systems of similar size and conduct a benchmark study against higher-level methods (*vide infra*); (3) test various levels of theory against each other and ask 'do my conclusions depend on the chosen level of theory?'. If the conclusions (qualitative or quantitative) depend on the level of theory, more consideration may be needed.

1.3.3 Recommended Computational Tools (for Relevant Systems)

With the advent of high-performance computing hardware and development of user-friendly quantum chemistry software, the relationship between computation and experiment has strengthened.[45,46] As mentioned above, DFT is currently the standard method of choice for interrogating the mechanisms on which we focus here. Unlike wavefunction theory (WFT) methods, which can be much more computationally demanding, DFT approaches solving electronic structure problems in terms of the electron density rather than the wavefunction (although wavefunction-based algorithms are generally used).[29,47] The choice of DFT methods is generally a practical one; systems of the size (number of electrons) of interest here (i.e., medium to large organic systems) generally cannot be modeled in a justified amount of time with currently-available post-Hartree-Fock WFT methods when DFT methods of similar accuracy can drastically reduce computational cost.[39–45] Much has been written on what recipe of functional and basis set is best to achieve "chemical accuracy" for particular types of organometallic reactions, and we recommend several recent reviews for a more in-depth discussion on this topic.[18,35,39,50] We provide several examples below that highlight the importance of (a) knowing which functionals and basis sets have been validated for particular metals (here, mainly Rh, Cu, and Au) undergoing particular types of reactions (e.g., closed shell versus open shell processes), (b) which functionals and basis sets are affordable but sufficient for addressing conformational complexity and variability of ligand arrangements, and (c) which models of solvation, both implicit and explicit, are appropriate for answering the mechanistic questions at hand.

1.3.4 Choosing a Functional and Basis Set

Choosing a reasonable level of theory for any mechanistic study can be a daunting task.[42,43] Choosing a level of theory then becomes a balancing act between achieving the accuracy required for the particular question at hand and the associated computational cost. One challenge in choosing a level of theory for organometallic reactions is the lack of experimentally-determined rates and concomitant Gibbs free energy barriers, which enable the benchmarking required to accurately deduce an appropriate level of theory.[24]

What combination of functional and basis set do we recommend for metal-promoted sigmatropic shifts? The short, admittedly unsatisfying, answer is *it depends*.[18] The DFT functional determines how the energy is calculated based on the wavefunction and the density. All functionals are approximate and its accuracy depends on the property of interest. The basis set is constructed from linear combinations of a set of basis functions to form the orbitals, and the size of the basis set determines the flexibility of the calculation—the larger the basis set, the more flexible the orbitals. We recommend that new practitioners consult the review by Schoenebeck and coworkers for more in-depth discussion.[18]

We recommend a few starting points for reactions promoted by dirhodium tetracarboxylates, which constitute the bulk of the reactions described here. Some DFT functionals we and others[17,18,24,45] have found useful include ωB97X-D,[51] B3LYP-D3, B3LYP,[52] MN15,[53] PW6B95-D3,[54] and M06.[55] It is now common to use density functionals with a dispersion correction (e.g., DFT-D3 such as B3LYP-D3)[56] to account for medium- and long-range London dispersion (LD) forces—LD is the attractive term in the van der Waals equation and has been shown to be critical in many reactions, but 'unduly underestimated'.[57–59] Indeed, some groups have exploited LD interactions to fine-tune the design of new heterobimetallic paddlewheel complexes,

showcasing the importance of LD as a design element in the development (and computational modeling) of new catalysts.[60,61]

For basis sets to use when optimizing geometries, we have had success using double-ζ basis sets like Ahlrich's def2 basis sets (e.g., def2-SVP[62]) or a double-ζ Pople basis set for non-metals (e.g., 6-31+G(d,p)) plus an effective core potential (ECP) for the transition metals (e.g., SDD[63] or LANL2DZ[64]—we note that LANL2DZ lacks polarization functions but can be added on for certain atoms[65]). Energies can then be reevaluated through single-point calculations with a larger basis set, such as def2-TZVPP or 6-311+G(d,p) (with SDD for the transition metal). Single-point calculations are those in which the nuclear configuration is kept fixed, but the electronic wavefunction is reevaluated to obtain energies. These types of calculations are used to accurately compute the electronic energy of the system with a larger, more flexible basis set. Generally, coupled cluster methods like CCSD(T) are preferable for SP calculations when the system of interest is small enough (e.g., organic molecules), but for the reactions of interest here, such high-level WFT-based methods are not currently feasible. Moreover, some have advised using single-reference post-HF methods with caution when applied to bond breaking and forming transformations involving transition metals.[66] It is worth noting that a much more cost-effective alternative, domain-based local pair natural orbital CCSD(T) (DLPNO-CCSD(T)), has been shown to yield results that have accuracy close to CCSD(T) at a much lower computational cost.[67]

Several caveats are in order regarding basis sets. First, basis set superposition error (BSSE) is attributed to an overestimation of the strengths of intermolecular interactions and thus overestimation of the binding energy between two fragments when small basis sets are used. This can lead, for example, to problems in predicting metal-ligand or metal-substrate binding energies. Second, basis set incompleteness error (BSIE) results from all fragments not having large enough

basis sets composed of appropriate types of basis functions, i.e., not providing results near the complete basis set (CBS) limit.[95] We recommend the tutorial review by Morgante and Peverati, and references therein, for a deeper dive into the sources of these errors and ways to remedy them.[70] In short, however, larger basis sets are usually better, although that is not guaranteed for DFT calculations. It is also generally better to include diffuse basis functions (important for anions and systems with long-range non-covalent interactions) and/or polarization basis functions—which give molecular orbitals the potential for a larger spatial "spread" from the nuclei and increased "flexibility", respectively—when quantitative agreement with experiment is necessary and doing so is cost-effective.[69,70] However, one should be cautious in adding these to smaller basis sets (e.g., double-ζ basis sets).[69] Third, an 'ultrafine' integration grid, (e.g., (99,590) grid at minimum), is recommended, as smaller grids may introduce considerable errors in computed free energies.[71] This grid size is the default grid in commonly used software,[72] but it is prudent to check for one's software of choice. These caveats being mentioned, we would like to re-emphasize that the choice of theoretical method should be rooted in studies (previously reported or carried out during a mechanistic study) in which computational methods are benchmarked against experimental data or, if such data does not exist, against results from higher level theoretical methods.[46] This is true regardless of the type of reaction being studied.

Some metal-carbene reactions may require consideration of electronic states beyond closed shell singlet states—i.e., all electrons paired—in which case, open shell electronic structure calculations become (radically) important.[73,74] DFT methods, however, can still be useful if results are viewed with appropriate caution, e.g., consideration of whether reactivity comes from separate electronic states (DFT is likely okay) or relevant electronic states have multireference character (DFT is not okay).[66,73,75–77] A collaborative experimental and theoretical study of Rh-catalyzed

oxonium ylide formation/[2,3]-rearrangement is a good case in point: Davies and coworkers discovered in their computations that an intermediate directly following the [2,3]-rearrangement transition state revealed other electronic states (closed-, open-shell singlet and triplet states) all within energies close to each other.[78] In other words, it gets electronically complicated after ylide formation and the [2,3]-rearrangement occurs, and as the authors point out, requires multideterminant calculations for a full picture of the energetic landscape. Without employing these methods, however, they came up with a simplified model, which revealed that these states cross near the intermediate region on the PES, which indicates that the [2,3]-rearrangement is more "reactant-like" and spared any radical character. These computational results helped rationalized some of their experimental results.

For the radical-inclined, we recommend the element Fe. Systems involving Fe are infamously challenging to model given the complexity introduced by different spin states. Though this has for many years encouraged theoreticians to avoid Fe, some have admirably taken the plunge.[79,80] Take, for example, the importance of open-shell species in iron-containing systems, which has been crucial in studies of iron porphyrin (heme) carbenes, a source of lively debate. Here, DFT methods are still the method of choice.[81,82] For advice on properly modeling such systems, we direct the reader to recent reviews.[82–84]

1.4 Post-Transition State Bifurcations and Non-Statistical Dynamic Effects

Post-transition state bifurcations (PTSBs) are important phenomena in organic chemistry which, when relevant in a reaction, cannot be adequately captured by classical TST. A PTSB describes a

PES with a fork in the pathway downhill in energy from the transition state along the reaction coordinate to the products (Figure 1.2).

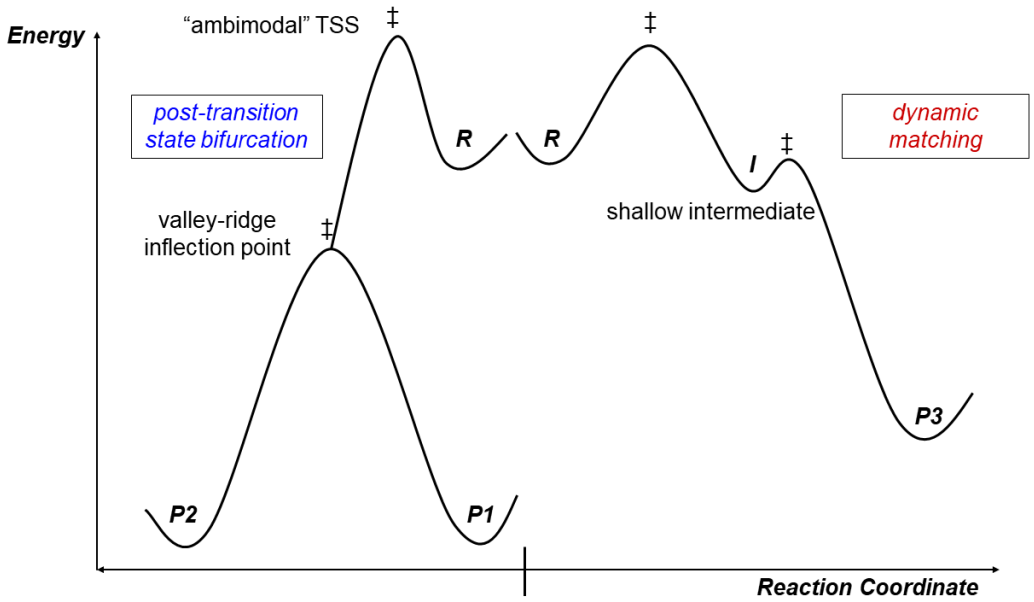

Figure 1.2 Left-hand reaction coordinate (blue): a schematic potential energy surface with a post-transition state bifurcation (PTSB). Right-hand reaction coordinate (red): a schematic potential energy surface ideal for dynamic matching.

Transition state theory and its relatives (e.g., variational TST[85] and Rice-Ramsperger-Kassel-Marcus theory, or RRKM[86]) are all statistical theories. Effects that cannot be explained by these theories, therefore, refer to *non-statistical dynamic effects*. The inherent assumptions of classical TST—that, for example, a single TSS leads to a single product, and that the rate and selectivity of a reaction is independent of the shape of the PES—break down when a PTSB is relevant and non-statistical dynamic effects govern selectivity (*vide infra*).[22,85–89] In these cases, a single TSS can lead to more than one product and the shape of the PES *does* matter for a reaction's selectivity. Much ink has been spilled on this topic since discovery of PTSBs that it would be inappropriate to attempt a thorough review here.[87,90–98] This includes insightful reviews and research articles by past (and current) Tantillo-group members during the years leading up to this dissertation (2017-2022): work from Dr. Stephanie Hare,[21,99–103] Dr. Renan Campos,[104] Dr. Hsiao-

Han Chuang,[105] Dr. Mengna Bai,[106] and (soon to be Dr.) Zhitao Feng.[106,107] However, as Chapter 3 involves a reaction with a PTSB, it *is* appropriate to briefly introduce the topic here. Note: the terms *ambimodal*[108] and *bispericyclic*[90] TSSs fall under the umbrella of reactions with a PTSB. Ambimodal and bispericyclic TSSs simply refer to the TSSs associated with a PTSB. These topics were pioneered by Caramella,[90] and representative papers are cited here.[109–112] Also note that there can be more than one PTSB on a PES! However, they usually follow one another sequentially.[113] Research on PTSBs is ongoing in many groups around the globe, so much so that it is regrettably impossible to mention all of them here.[114–117]

How do we study reactions with a PTSB? We must remember that molecules are not static, despite our valuable depictions[118] of them as static pictures. Roald Hoffmann wrote that "molecules don't sit still".[119] Molecules are dynamic and to model their dynamic behavior we must use molecular dynamics (MD) simulations. In our lab, we use *ab initio* MD (AIMD), sometimes called Born-Oppenheimer MD (BOMD) in trajectory studies to study the dynamic behavior of organic molecules and their effects on reactivity and selectivity. Quantum chemical computations are used to obtain a starting point for the trajectory studies—i.e., a stationary point like a TSS or minimum. With the same level of theory, force constants are computed, and based on reaction temperature, a sample of Boltzmann-weighted energy is randomly distributed in the vibrational modes. These vibrations are used to propagate the trajectories in the forward and backwards direction along the reaction coordinate, with the force constants re-computed at each time step "on the fly" (typically 1 fs time steps; shorter is better, but 1 fs is typically fine given the computational cost of such simulations).[120] Trajectories are run until they reach a new minimum, at which point the trajectories are counted to ascertain information such as the product/reactant selectivity, degree

of recrossing trajectories—trajectories that pass the dividing barrier separating reactant and product more than once—and time required to reach the reactant or product minima.[95]

The governance of nonstatistical dynamic effects in reactions where TST fails is more general than one might think, and even found in textbook reactions.[88,89,121–123] One type of nonstatistical dynamic effect that emerges out of these circumstances—where a shallow intermediate exists downhill in energy from a TSS along a PES, or in cases where the surface around the transition state region if flat—is called *dynamic matching*. When a trajectory approaches a local minimum—say an intermediate along a PES—and holds enough energy and momentum to carry it over the second barrier to the product without rapid redistribution of its internal energy. The trajectory can simply "skip", or spend less time in, the shallow intermediate (Figure 1.2). This phenomenon is what is referred to as *dynamic matching*, as described by Barry Carpenter.[121] Another way this is sometimes stated is that the vibrational modes of the trajectory coming from the first reaction step are such that the so-called *intramolecular (internal) vibrational energy* redistribution (IVR) does not occur rapidly enough to equilibrate in the local minimum (in TST, assumed to be rapid). This will manifest itself in short to long lifetimes of the intermediate structure.[93]

The impact of non-statistical dynamic effects on organic reactions is well-established for small systems in the gas phase or in implicit solvent—little is known in boxes of explicit solvent. In addition, much of our current understanding in this context comes from *potential energy* surfaces (E) of reduced dimensionality and (often) misses crucial information about the *free energy* surface (G). The relevance of non-statistical dynamic effects, therefore, is evidently complicated by solvent effects[103,124] and effects due to entropy.[125,126] This inevitably leaves the door open for

progress in this area. Indeed, much work is *still* needed to fully appreciate entropy and solvent effects on organic reactions.[127,128]

1.5 References

(1) *Applied Theoretical Organic Chemistry*; Tantillo, D. J., Ed.; World Scientific Publishing Europe Ltd.: London, UK, 2018.
(2) Moore, G. M. Cramming More Components onto Integrated Circuits With Unit Cost. *Electronics* **1965**, *38*, 114–117.
(3) Llanos, E. J.; Leal, W.; Luu, D. H.; Jost, J.; Stadler, P. F.; Restrepo, G. Exploration of the Chemical Space and Its Three Historical Regimes. *Proc. Natl. Acad. Sci.* **2019**, *116*, 12660–12665.
(4) Nieves-Quinones, Y.; Singleton, D. A. Dynamics and the Regiochemistry of Nitration of Toluene. *J. Am. Chem. Soc.* **2016**, *138*, 15167–15176.
(5) Buskirk, A.; Baradaran, H. Can Reaction Mechanisms Be Proven? *J. Chem. Educ.* **2009**, *86*, 551.
(6) Lewis, D. E. Response to "Can Reaction Mechanisms Be Proven?" *J. Chem. Educ.* **2009**, *86*, 554.
(7) Brown, T. L. Response to "Can Reaction Mechanisms Be Proven?" *J. Chem. Educ.* **2009**, *86*, 552.
(8) Wade, P. A. Response to "Can Reaction Mechanisms Be Proven?" *J. Chem. Educ.* **2009**, *86*, 558.
(9) Yoon, T. Response to "Can Reaction Mechanisms Be Proven?" *J. Chem. Educ.* **2009**, *86*, 556.
(10) Popper, K. *The Logic of Scientific Discovery*; Routledge: London, 2002.
(11) Popper, K. *Conjectures and Refutations*; Routledge: London, 2014.
(12) Feynman, R. P.; Leighton, R. *Surely You're Joking, Mr. Feynman!*; W. W. Norton Company, 1985.
(13) Gribbin, J. R. *The Fellowship: The Story of a Revolution*; Allen Lane, 2005.
(14) Scott, S. L. The Burden of Disproof. *ACS Catal.* **2019**, *9*, 4706–4708.
(15) Hoffmann, R. Why Buy That Theory? *Am. Sci.* **2003**, *91*.
(16) Dewar, M. J. S. Chemical Implications of .Sigma. Conjugation. *J. Am. Chem. Soc.* **1984**, *106*, 669–682.
(17) Ahn, S.; Hong, M.; Sundararajan, M.; Ess, D. H.; Baik, M.-H. Design and Optimization of Catalysts Based on Mechanistic Insights Derived from Quantum Chemical Reaction Modeling. *Chem. Rev.* **2019**, *119*, 6509–6560.
(18) Sperger, T.; Sanhueza, I. A.; Kalvet, I.; Schoenebeck, F. Computational Studies of Synthetically Relevant Homogeneous Organometallic Catalysis Involving Ni, Pd, Ir, and Rh: An Overview of Commonly Employed DFT Methods and Mechanistic Insights. *Chem. Rev.* **2015**, *115*, 9532–9586.
(19) Meek, S. J.; Pitman, C. L.; Miller, A. J. M. Deducing Reaction Mechanism: A Guide for Students, Researchers, and Instructors. *J. Chem. Educ.* **2016**, *93*, 275–286.
(20) Goodwin, W. Quantum Chemistry and Organic Theory. *Philos. Sci.* **2013**, *80*, 1159–1169.
(21) Hare, S.; Bratholm, L.; Glowacki, D.; Carpenter, B. Low Dimensional Representations

Along Intrinsic Reaction Coordinates and Molecular Dynamics Trajectories Using Interatomic Distance Matrices. *Chem. Sci.* **2019**, *10*, 9954–9968.
(22) Tuñón, I.; Williams, I. H. The Transition State and Cognate Concepts. In *Advances in Physical Organic Chemistry*; Elsevier Ltd., 2019; Vol. 53, pp 29–68.
(23) Watson, W. On Byproducts and Side Products. *Org. Process Res. Dev.* **2012**, *16*, 1877–1877.
(24) Eisenstein, O.; Ujaque, G.; Lledós, A. What Makes a Good (Computed) Energy Profile? In *New Directions in the Modeling of Organometallic Reactions. Topics in Organometallic Chemistry*; Lledós, A., Ujaque, G., Eds.; Springer, 2020; Vol. 67, pp 1–38.
(25) Hare, S. R.; Hudson, B. M.; Tantillo, D. J. Modeling Organic Reactions — General Approaches, Caveats, and Concerns. In *Applied Theoretical Organic Chemistry*; 2018; pp 1–29.
(26) Plata, R. E.; Singleton, D. A. A Case Study of the Mechanism of Alcohol-Mediated Morita Baylis–Hillman Reactions. The Importance of Experimental Observations. *J. Am. Chem. Soc.* **2015**, *137*, 3811–3826.
(27) Pidko, E. A. Toward the Balance between the Reductionist and Systems Approaches in Computational Catalysis: Model versus Method Accuracy for the Description of Catalytic Systems. *ACS Catal.* **2017**, *7*, 4230–4234.
(28) Szabo, A.; Ostlund, N. S. *Modern Quantum Chemistry*; McGraw-Hill, Inc.: New York, 1989.
(29) Burke, K.; Wagner, L. O. DFT in a Nutshell. *Int. J. Quantum Chem.* **2013**, *113*, 96–101.
(30) Hoffmann, R.; Schleyer, P. von R.; Schaefer, H. F. Predicting Molecules-More Realism, Please! *Angew. Chem. Int. Ed.* **2008**, *47*, 7164–7167.
(31) Lam, Y.; Grayson, M. N.; Holland, M. C.; Simon, A.; Houk, K. N. Theory and Modeling of Asymmetric Catalytic Reactions. *Acc. Chem. Res.* **2016**, *49*, 750–762.
(32) Peng, Q.; Duarte, F.; Paton, R. S. Computing Organic Stereoselectivity-from Concepts to Quantitative Calculations and Predictions. *Chem. Soc. Rev.* **2016**, *45*, 6093–6107.
(33) Houk, K. N.; Liu, F. Holy Grails for Computational Organic Chemistry and Biochemistry. *Acc. Chem. Res.* **2017**, *50*, 539–543.
(34) Maji, R.; Mallojjala, S. C.; Wheeler, S. E. Chiral Phosphoric Acid Catalysis: From Numbers to Insights. *Chem. Soc. Rev.* **2018**, *47*, 1142–1158.
(35) Funes-Ardoiz, I.; Schoenebeck, F. Established and Emerging Computational Tools to Study Homogeneous Catalysis—From Quantum Mechanics to Machine Learning. *Chem* **2020**, *6*, 1904–1913.
(36) Perdew, J. P.; Ruzsinszky, A.; Constantin, L. A.; Sun, J.; Csonka, G. I. Some Fundamental Issues in Ground-State Density Functional Theory: A Guide for the Perplexed. *J. Chem. Theory Comput.* **2009**, *5*, 902–908.
(37) Bursch, M.; Mewes, J.; Hansen, A.; Grimme, S. Best Practice DFT Protocols for Basic Molecular Computational Chemistry. *ChemRxiv* **2022**.
(38) Ryu, H.; Park, J.; Kim, H. K.; Park, J. Y.; Kim, S.-T.; Baik, M.-H. Pitfalls in Computational Modeling of Chemical Reactions and How To Avoid Them. *Organometallics* **2018**, *37*, 3228–3239.
(39) Morgante, P.; Peverati, R. The Devil in the Details: A Tutorial Review on Some Undervalued Aspects of Density Functional Theory Calculations. *Int. J. Quantum Chem.* **2020**, *120*, e26332.

(40) Lan, Y. *Computational Methods in Organometallic Catalysis*; Wiley-VCH: Weinheim, Germany, 2021.
(41) Goerigk, L.; Grimme, S. A Thorough Benchmark of Density Functional Methods for General Main Group Thermochemistry, Kinetics, and Noncovalent Interactions. *Phys. Chem. Chem. Phys.* **2011**, *13*, 6670–6688.
(42) Goerigk, L.; Hansen, A.; Bauer, C.; Ehrlich, S.; Najibi, A.; Grimme, S. A Look at the Density Functional Theory Zoo with the Advanced GMTKN55 Database for General Main Group Thermochemistry, Kinetics and Noncovalent Interactions. *Phys. Chem. Chem. Phys.* **2017**, *19*, 32184–32215.
(43) Goerigk, L.; Mehta, N. A Trip to the Density Functional Theory Zoo: Warnings and Recommendations for the User. *Aust. J. Chem.* **2019**, *72*, 563.
(44) Gould, T.; Dale, S. G. Poisoning Density Functional Theory with Benchmark Sets of Difficult Systems. *Phys. Chem. Chem. Phys.* **2022**, *24*, 6398–6403.
(45) Sperger, T.; Sanhueza, I. A.; Schoenebeck, F. Computation and Experiment: A Powerful Combination to Understand and Predict Reactivities. *Acc. Chem. Res.* **2016**, *49*, 1311–1319.
(46) Mata, R. A.; Suhm, M. A. Benchmarking Quantum Chemical Methods: Are We Heading in the Right Direction? *Angew. Chem. Int. Ed.* **2017**, *56*, 11011–11018.
(47) Cohen, A. J.; Mori-Sánchez, P.; Yang, W. Insights into Current Limitations of Density Functional Theory. *Science* **2008**, *321*, 792–794.
(48) Bachrach, S. M. Challenges in Computational Organic Chemistry. *Wiley Interdiscip. Rev. Comput. Mol. Sci.* **2014**, *4*, 482–487.
(49) Tantillo, D. J. Questions in Natural Products Synthesis Research That Can (and Cannot) Be Answered Using Computational Chemistry. *Chem. Soc. Rev.* **2018**, *47*, 7845–7850.
(50) Harvey, J. N.; Himo, F.; Maseras, F.; Perrin, L. Scope and Challenge of Computational Methods for Studying Mechanism and Reactivity in Homogeneous Catalysis. *ACS Catal.* **2019**, *9*, 6803–6813.
(51) Chai, J.-D.; Head-Gordon, M. Long-Range Corrected Hybrid Density Functionals with Damped Atom–Atom Dispersion Corrections. *Phys. Chem. Chem. Phys.* **2008**, *10*, 6615.
(52) Becke, A. D. Density-Functional Thermochemistry. III. The Role of Exact Exchange. *J. Chem. Phys.* **1993**, *98*, 5648–5652.
(53) Yu, H. S.; He, X.; Li, S. L.; Truhlar, D. G. MN15: A Kohn-Sham Global-Hybrid Exchange-Correlation Density Functional with Broad Accuracy for Multi-Reference and Single-Reference Systems and Noncovalent Interactions. *Chem. Sci.* **2016**, *7*, 5032–5051.
(54) Zhao, Y.; Truhlar, D. G. Design of Density Functionals That Are Broadly Accurate for Thermochemistry, Thermochemical Kinetics, and Nonbonded Interactions. *J. Phys. Chem. A* **2005**, *109*, 5656–5667.
(55) Zhao, Y.; Truhlar, D. G. The M06 Suite of Density Functionals for Main Group Thermochemistry, Thermochemical Kinetics, Noncovalent Interactions, Excited States, and Transition Elements: Two New Functionals and Systematic Testing of Four M06-Class Functionals and 12 Other Function. *Theor. Chem. Acc.* **2008**, *120*, 215–241.
(56) Grimme, S.; Antony, J.; Ehrlich, S.; Krieg, H. A Consistent and Accurate Ab Initio Parametrization of Density Functional Dispersion Correction (DFT-D) for the 94 Elements H-Pu. *J. Chem. Phys.* **2010**, *132*, 154104.
(57) Wagner, J. P.; Schreiner, P. R. London Dispersion in Molecular Chemistry - Reconsidering Steric Effects. *Angew. Chem. Int. Ed.* **2015**, *54*, 12274–12296.

(58) Eschmann, C.; Song, L.; Schreiner, P. R. London Dispersion Rather than Steric Hindrance Determines the Enantioselectivity of the Corey-Bakshi-Shibata Reduction. *Angew. Chem. Int. Ed.* **2020**, *60*, 4823–4832.
(59) Solel, E.; Ruth, M.; Schreiner, P. R. London Dispersion Helps Refine Steric A-Values: The Halogens. *J. Org. Chem.* **2021**, *86*, 7701–7713.
(60) Singha, S.; Buchsteiner, M.; Bistoni, G.; Goddard, R.; Furstner, A. A New Ligand Design Based on London Dispersion Empowers Chiral Bismuth − Rhodium Paddlewheel Catalysts. *J. Am. Chem. Soc.* **2021**, *143*, 5666–5673.
(61) Xi, Y.; Su, B.; Qi, X.; Pedram, S.; Liu, P.; Hartwig, J. F. Application of Trimethylgermanyl-Substituted Bisphosphine Ligands with Enhanced Dispersion Interactions to Copper-Catalyzed Hydroboration of Disubstituted Alkenes. *J. Am. Chem. Soc.* **2020**, *142*, 18213–18222.
(62) Weigend, F.; Ahlrichs, R. Balanced Basis Sets of Split Valence, Triple Zeta Valence and Quadruple Zeta Valence Quality for H to Rn: Design and Assessment of Accuracy. *Phys. Chem. Chem. Phys.* **2005**, *7*, 3297.
(63) Fuentealba, P.; Preuss, H.; Stoll, H.; Von Szentpály, L. A Proper Account of Core-Polarization with Pseudopotentials: Single Valence-Electron Alkali Compounds. *Chem. Phys. Lett.* **1982**, *89*, 418–422.
(64) Hay, P. J.; Wadt, W. R. Ab Initio Effective Core Potentials for Molecular Calculations. Potentials for the Transition Metal Atoms Sc to Hg. *J. Chem. Phys.* **1985**, *82*, 270–283.
(65) Check, C. E.; Faust, T. O.; Bailey, J. M.; Wright, B. J.; Gilbert, T. M.; Sunderlin, L. S. Addition of Polarization and Diffuse Functions to the LANL2DZ Basis Set for P-Block Elements. *J. Phys. Chem. A* **2001**, *105*, 8111–8116.
(66) Vogiatzis, K. D.; Polynski, M. V.; Kirkland, J. K.; Townsend, J.; Hashemi, A.; Liu, C.; Pidko, E. A. Computational Approach to Molecular Catalysis by 3d Transition Metals: Challenges and Opportunities. *Chem. Rev.* **2019**, *119*, 2453–2523.
(67) Riplinger, C.; Pinski, P.; Becker, U.; Valeev, E. F.; Neese, F. Sparse Maps—A Systematic Infrastructure for Reduced-Scaling Electronic Structure Methods. II. Linear Scaling Domain Based Pair Natural Orbital Coupled Cluster Theory. *J. Chem. Phys.* **2016**, *144*, 024109.
(68) Boys, S. F.; Bernardi, F. The Calculation of Small Molecular Interactions by the Differences of Separate Total Energies. Some Procedures with Reduced Errors. *Mol. Phys.* **1970**, *19*, 553–566.
(69) Papajak, E.; Zheng, J.; Xu, X.; Leverentz, H. R.; Truhlar, D. G. Perspectives on Basis Sets Beautiful: Seasonal Plantings of Diffuse Basis Functions. *J. Chem. Theory Comput.* **2011**, *7*, 3027–3034.
(70) Papajak, E.; Truhlar, D. G. Efficient Diffuse Basis Sets for Density Functional Theory. *J. Chem. Theory Comput.* **2010**, *6*, 597–601.
(71) Bootsma, A. N.; Wheeler, S. E. Popular Integration Grids Can Result in Large Errors in DFT-Computed Free Energies. *ChemRxiv* **2019**, 1–20.
(72) Frisch, M. J.; Trucks, G. W.; Schlegel, H. B.; Scuseria, G. E.; Robb, M. A.; Cheeseman, J. R.; Scalmani, G.; Barone, V.; Petersson, G. A.; Nakatsuji, H.; et al. Gaussian 16, Revision A.03. Gaussian, Inc.: Willingford, CT 2016.
(73) Bally, T.; Borden, W. T. Calculations on Open-Shell Molecules: A Beginner's Guide. In *Reviews in Computational Chemistry*; 1999; pp 1–97.
(74) Abe, M. Diradicals. *Chemical Reviews*. 2013, pp 7011–7088.

(75) Schreiner, P. R.; Navarro-Vázquez, A.; Prall, M. Computational Studies on the Cyclizations of Enediynes, Enyne-Allenes, and Related Polyunsaturated Systems. *Acc. Chem. Res.* **2005**, *38*, 29–37.
(76) Abe, M.; Ye, J.; Mishima, M. The Chemistry of Localized Singlet 1,3-Diradicals (Biradicals): From Putative Intermediates to Persistent Species and Unusual Molecules with a π-Single Bonded Character. *Chem. Soc. Rev.* **2012**, *41*, 3808.
(77) Stuyver, T.; Chen, B.; Zeng, T.; Geerlings, P.; De Proft, F.; Hoffmann, R. Do Diradicals Behave Like Radicals? *Chem. Rev.* **2019**, *119*, 11291–11351.
(78) Li, Z.; Boyarskikh, V.; Hansen, J. H.; Autschbach, J.; Musaev, D. G.; Davies, H. M. L. Scope and Mechanistic Analysis of the Enantioselective Synthesis of Allenes by Rhodium-Catalyzed Tandem Ylide Formation/[2,3]-Sigmatropic Rearrangement between Donor/Acceptor Carbenoids and Propargylic Alcohols. *J. Am. Chem. Soc.* **2012**, *134*, 15497–15504.
(79) Sun, Y.; Tang, H.; Chen, K.; Hu, L.; Yao, J.; Shaik, S.; Chen, H. Two-State Reactivity in Low-Valent Iron-Mediated C–H Activation and the Implications for Other First-Row Transition Metals. *J. Am. Chem. Soc.* **2016**, *138*, 3715–3730.
(80) Lee, W.; Zhou, J.; Gutierrez, O. Mechanism of Nakamura's Bisphosphine-Iron-Catalyzed Asymmetric $C(sp^2)$–$C(sp^3)$ Cross-Coupling Reaction: The Role of Spin in Controlling Arylation Pathways. *J. Am. Chem. Soc.* **2017**, *139*, 16126–16133.
(81) Khade, R. L.; Zhang, Y. Catalytic and Biocatalytic Iron Porphyrin Carbene Formation: Effects of Binding Mode, Carbene Substituent, Porphyrin Substituent, and Protein Axial Ligand. *J. Am. Chem. Soc.* **2015**, *137*, 7560–7563.
(82) Sharon, D. A.; Mallick, D.; Wang, B.; Shaik, S. Computation Sheds Insight into Iron Porphyrin Carbenes' Electronic Structure, Formation, and N–H Insertion Reactivity. *J. Am. Chem. Soc.* **2016**, *138*, 9597–9610.
(83) Zhang, Y. Computational Investigations of Heme Carbenes and Heme Carbene Transfer Reactions. *Chem. Eur. J.* **2019**, *25*, 13231–13247.
(84) Damiano, C.; Sonzini, P.; Gallo, E. Iron Catalysts with N-Ligands for Carbene Transfer of Diazo Reagents. *Chem. Soc. Rev.* **2020**, *49*, 4867–4905.
(85) Bao, J. L.; Truhlar, D. G. Variational Transition State Theory: Theoretical Framework and Recent Developments. *Chem. Soc. Rev.* **2017**, *46*, 7548–7596.
(86) Jayee, B.; Hase, W. L. Nonstatistical Reaction Dynamics. *Annu. Rev. Phys. Chem.* **2020**, *71*, 289–313.
(87) Rehbein, J.; Carpenter, B. K. Do We Fully Understand What Controls Chemical Selectivity? *Phys. Chem. Chem. Phys.* **2011**, *13*, 20906.
(88) Oyola, Y.; Singleton, D. A. Dynamics and the Failure of Transition State Theory in Alkene Hydroboration. *J. Am. Chem. Soc.* **2009**, *131*, 3130–3131.
(89) Bailey, J. O.; Singleton, D. A. Failure and Redemption of Statistical and Nonstatistical Rate Theories in the Hydroboration of Alkenes. *J. Am. Chem. Soc.* **2017**, *139*, 15710–15723.
(90) Caramella, P.; Quadrelli, P.; Toma, L. An Unexpected Bispericyclic Transition Structure Leading to 4+2 and 2+4 Cycloadducts in the Endo Dimerization of Cyclopentadiene. *J. Am. Chem. Soc.* **2002**, *124*, 1130–1131.
(91) Ess, D. H.; Wheeler, S. E.; Iafe, R. G.; Xu, L.; Çelebi-Ölçüm, N.; Houk, K. N. Bifurcations on Potential Energy Surfaces of Organic Reactions. *Angew. Chem. Int. Ed.* **2008**, *47*, 7592–7601.

(92) Hong, Y. J.; Tantillo, D. J. The Taxadiene-Forming Carbocation Cascade. *J. Am. Chem. Soc.* **2011**, *133*, 18249–18256.
(93) Tantillo, D. J. *Dynamic Effects on Organic Reactions*; Reedijk, J., Ed.; Elsevier Inc.: Waltham, MA, 2018.
(94) Mandal, N.; Datta, A. Dynamical Effects along the Bifurcation Pathway Control Semibullvalene Formation in Deazetization Reactions. *J. Phys. Chem. B* **2018**, *122*, 1239–1244.
(95) Tantillo, D. J. *Beyond Transition State Theory—Non-Statistical Dynamic Effects for Organic Reactions*, 1st ed.; Elsevier Ltd., 2021.
(96) Tantillo, D. J. Dynamic Effects on Organic Reactivity—Pathways to (and from) Discomfort. *J. Phys. Org. Chem.* **2021**, *34*, 1–9.
(97) Kpante, M.; Wolf, L. M. Pathway Bifurcations in the Activation of Allylic Halides by Palladium and Their Influence on the Dynamics of η 1 and η 3 Allyl Intermediates. *J. Org. Chem.* **2021**, *86*, 9637–9650.
(98) Bharadwaz, P.; Maldonado-Domínguez, M.; Srnec, M. Bifurcating Reactions: Distribution of Products from Energy Distribution in a Shared Reactive Mode. *Chem. Sci.* **2021**, *12*, 12682–12694.
(99) Hare, S. R.; Tantillo, D. J. Dynamic Behavior of Rearranging Carbocations - Implications for Terpene Biosynthesis. *Beilstein J. Org. Chem.* **2016**, *12*, 377–390.
(100) Hare, S. R.; Tantillo, D. J. Post-Transition State Bifurcations Gain Momentum-Current State of the Field. *Pure Appl. Chem.* **2017**, *89*, 679–698.
(101) Hare, S. R.; Tantillo, D. J. Cryptic Post-Transition State Bifurcations That Reduce the Efficiency of Lactone-Forming Rh-Carbenoid C-H Insertions. *Chem. Sci.* **2017**, *8*, 1442–1449.
(102) Hare, S. R.; Pemberton, R. P.; Tantillo, D. J. Navigating Past a Fork in the Road: Carbocation−π Interactions Can Manipulate Dynamic Behavior of Reactions Facing Post-Transition-State Bifurcations. *J. Am. Chem. Soc.* **2017**, *139*, 7485–7493.
(103) Hare, S. R.; Li, A.; Tantillo, D. J. Post-Transition State Bifurcations Induce Dynamical Detours in Pummerer-like Reactions. *Chem. Sci.* **2018**, *9*, 8937–8945.
(104) Campos, R. B.; Tantillo, D. J. Designing Reactions with Post-Transition-State Bifurcations: Asynchronous Nitrene Insertions into C–C σ Bonds. *Chem* **2019**, *5*, 227–236.
(105) Chuang, H.-H.; Tantillo, D. J.; Hsu, C.-P. Construction of Two-Dimensional Potential Energy Surfaces of Reactions with Post-Transition-State Bifurcations. *J. Chem. Theory Comput.* **2020**, *16*, 4050–4060.
(106) Bai, M.; Feng, Z.; Li, J.; Tantillo, D. J. Bouncing off Walls – Widths of Exit Channels from Shallow Minima Can Dominate Selectivity Control. *Chem. Sci.* **2020**, *11*, 9937–9944.
(107) Feng, Z.; Tantillo, D. J. Dynamic Effects on Migratory Aptitudes in Carbocation Reactions. *J. Am. Chem. Soc.* **2021**, *143*, 1088–1097.
(108) Pham, H. V.; Houk, K. N. Diels–Alder Reactions of Allene with Benzene and Butadiene: Concerted, Stepwise, and Ambimodal Transition States. *J. Org. Chem.* **2014**, *79* (19), 8968–8976.
(109) Yu, P.; Chen, T. Q.; Yang, Z.; He, C. Q.; Patel, A.; Lam, Y.; Liu, C.; Houk, K. N. Mechanisms and Origins of Periselectivity of the Ambimodal [6 + 4] Cycloadditions of Tropone to Dimethylfulvene. *J. Am. Chem. Soc.* **2017**, *139*, 8251–8258.

(110) Yang, Z.; Dong, X.; Yu, Y.; Yu, P.; Li, Y.; Jamieson, C.; Houk, K. N. Relationships between Product Ratios in Ambimodal Pericyclic Reactions and Bond Lengths in Transition Structures. *J. Am. Chem. Soc.* **2018**, *140*, 3061–3067.
(111) Jamieson, C. S.; Sengupta, A.; Houk, K. N. Cycloadditions of Cyclopentadiene and Cycloheptatriene with Tropones: All Endo -[6+4] Cycloadditions Are Ambimodal. *J. Am. Chem. Soc.* **2021**, *143*, 3918–3926.
(112) Houk, K. N.; Xue, X.; Liu, F.; Chen, Y.; Chen, X.; Jamieson, C. Computations on Pericyclic Reactions Reveal the Richness of Ambimodal Transition States and Pericyclases. *Isr. J. Chem.* **2022**, *62*, 1–18.
(113) Hong, Y. J.; Tantillo, D. J. Biosynthetic Consequences of Multiple Sequential Post-Transition-State Bifurcations. *Nat. Chem.* **2014**, *6*, 104–111.
(114) Lee, S.; Goodman, J. M. Rapid Route-Finding for Bifurcating Organic Reactions. *J. Am. Chem. Soc.* **2020**, *142*, 9210–9219.
(115) Lee, S.; Goodman, J. M. VRAI-Selectivity: Calculation of Selectivity beyond Transition State Theory†. *Org. Biomol. Chem.* **2021**, *19*, 3940–3947.
(116) Wang, X.; Zhang, C.; Jiang, Y.; Wang, W.; Zhou, Y.; Chen, Y.; Zhang, B.; Tan, R. X.; Ge, H. M.; Yang, Z. J.; et al. Influence of Water and Enzyme on the Post-Transition State Bifurcation of NgnD-Catalyzed Ambimodal [6+4]/[4+2] Cycloaddition. *J. Am. Chem. Soc.* **2021**, *143*, 27.
(117) Tremblay, M. T.; Yang, Z. J. The Effect of Zero-point Energy in Simulating Organic Reactions with Post-transition State Bifurcation. *J. Phys. Org. Chem.* **2022**, e4322.
(118) Tantillo, D. J. Drawing Polycyclic Molecules. *ACS Omega* **2021**, *6*, 23008–23014.
(119) Hoffmann, R. Unstable. In *Roald Hoffmann on the Philosophy, Art, and Science of Chemistry*; Oxford University Press, 2012.
(120) Lourderaj, U.; Park, K.; Hase, W. L. Classical Trajectory Simulations of Post-Transition State Dynamics. *Int. Rev. Phys. Chem.* **2008**, *27*, 361–403.
(121) Carpenter, B. K. Dynamic Behavior of Organic Reactive Intermediates. *Angew. Chem. Int. Ed.* **1998**, *37*, 3340–3350.
(122) Wang, Z.; Hirschi, J. S.; Singleton, D. A. Recrossing and Dynamic Matching Effects on Selectivity in a Diels-Alder Reaction. *Angew. Chem. Int. Ed.* **2009**, *48*, 9156–9159.
(123) Carpenter, B. K. Energy Disposition in Reactive Intermediates. *Chem. Rev.* **2013**, *113*, 7265–7286.
(124) Fu, Y.; Bernasconi, L.; Liu, P. Ab Initio Molecular Dynamics Simulations of the S_N1/S_N2 Mechanistic Continuum in Glycosylation Reactions. *J. Am. Chem. Soc.* **2021**, *143*, 1577–1589.
(125) Yang, Z.; Jamieson, C. S.; Xue, X.-S.; Garcia-Borràs, M.; Benton, T.; Dong, X.; Liu, F.; Houk, K. N. Mechanisms and Dynamics of Reactions Involving Entropic Intermediates. *Trends Chem.* **2019**, *1*, 22–34.
(126) Qin, Z.-X.; Tremblay, M.; Hong, X.; Yang, Z. J. Entropic Path Sampling: Computational Protocol to Evaluate Entropic Profile along a Reaction Path. *J. Phys. Chem. Lett.* **2021**, *12*, 10713–10719.
(127) Chin, Y. P.; Krenske, E. H. Nazarov Cyclizations Catalyzed by BINOL Phosphoric Acid Derivatives: Quantum Chemistry Struggles To Predict the Enantioselectivity. *J. Org. Chem.* **2022**, *87*, 1710–1722.
(128) Burrows, C. J.; Harper, J. B.; Sander, W.; Tantillo, D. J. Solvation Effects in Organic Chemistry. *J. Org. Chem.* **2022**, *87*, 1599–1601.

Part I

Theoretical Models of Dirhodium Catalyzed Reactions

Chapter 2

Melding of Experiment and Theory Illuminates Mechanisms of Metal-Catalyzed Rearrangements: Computational Approaches and Caveat[§]

The fertilizer was a blending of interests, where the organic chemist became a theoretician and the theoretician became an organic chemist.

- Jeffrey I. Seeman (*J. Org. Chem.* **2015**, *80*, 11666).

2.1 Introduction

Sigmatropic rearrangements have long been used to facilitate synthetic campaigns toward challenging targets.[1] While, historically, [3,3]-sigmatropic rearrangements have received the most attention, [1,2]- and [2,3]-sigmatropic rearrangements of onium ylides generated via carbene transfer reactions have garnered considerable attention, since they allow for formation of carbon-carbon and/or carbon-heteroatom bonds that can be otherwise difficult to construct. Efforts to achieve these couplings stereoselectively with transition-metal catalysts have enabled reliable and effective methods to introduce new stereogenic centers in complex target molecules.[2,3] The most commonly used transition-metal catalysts for these reactions are rhodium and copper-based

[§] This chapter is an adapted version of the following published article: Laconsay, C. J.; Tantillo, D. J. Melding of Experiment and Theory Illuminates Mechanisms of Metal-Catalyzed Rearrangements: Computational Approaches and Caveats, *Synthesis* **2021**, *53*, 3639-3652 with permission from Georg Thieme Verlag KG.

catalysts,[4,5] but catalysts based on other metals, such as gold,[6,7] ruthenium,[8–11] cobalt,[12,13] palladium,[14–16] silver,[17] nickel,[18] and iron[19–26], have also been developed for these purposes.

In 1981, Doyle and coworkers[27] brought new life to the field of transition-metal catalyzed [2,3]-sigmatropic rearrangements, building on past work by Kirmse and Kapps,[28] by demonstrating utility for organic synthesis (Figure 2.1).[29–36]

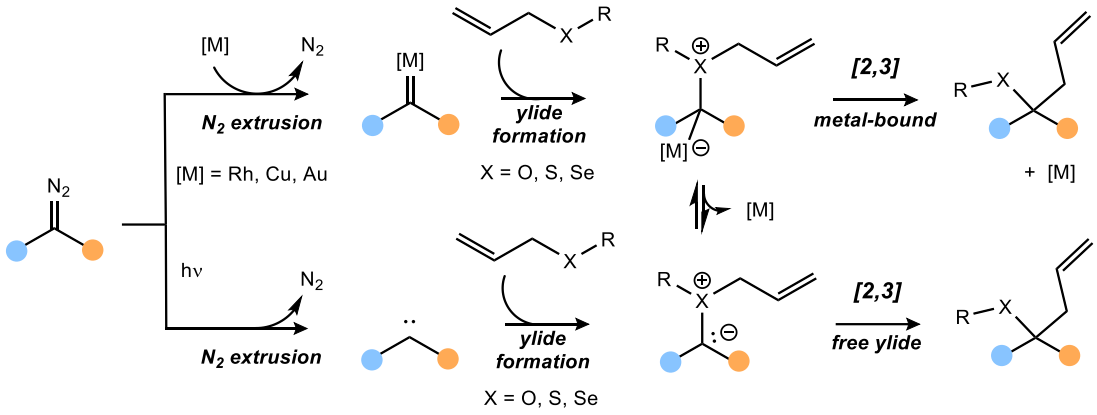

Figure 2.1 Ylide [2,3]-sigmatropic rearrangements via carbene transfer.

Herein, we examine approaches, both theoretical and experimental, for probing the mechanisms of such reactions and feeding the resulting mechanistic knowledge into the reaction design process. Though metal-free carbenes can also form ylides *via* photochemical carbene transfer,[37] this approach has been reviewed elsewhere.[38,39] Recent research on diazo compound activation and carbene transfer by main group elements, such as the use of triarylboranes (e.g., $B(C_6F_5)_3$), has also offered an alternative method to transition-metal catalyzed carbene transfer—this line of research is reviewed elsewhere as well.[40,41]

Many mechanistic aspects of metal-promoted rearrangements are not well-understood. For instance, though these reactions often are employed in a stereoselective manner, the origin of enantioselectivity is not always apparent.[3,42] In addition, it is sometimes unclear which steps in the

path to products actually involve a covalently bound metal.[3,43,44] Freeing such details from the shadows presents an opportunity for discovery.

Experiment and theory provide approaches to studying mechanisms that are often carried out separately or in parallel.[45] However, as we will discuss later, there are benefits from their intertwingling.[46–48] Experimental studies frequently involve control experiments without metals, competition experiments, and kinetic profiling. Computational studies generally involve applying quantum chemical calculations to glean structural and energetic information about relevant reaction intermediates and transition-state structures (TSSs), commonly known as stationary points along a reaction pathway. In some cases, this information is augmented by analyses of noncovalent interactions and dynamic effects.[49–54]

The goal of this chapter is to discuss examples in the literature where experiment and theory both supplied mechanistic details about sigmatropic rearrangements involving metal carbenes, including discussion of computational caveats to consider when studying these transformations, such as the effects of catalyst ligand conformations, solvation and non-statistical dynamic effects. We conclude with an outlook on the current state of the field, asking what questions remain unanswered and how theory and experiment can be merged more seamlessly.

2.2 Conformations and Ligand-Binding Modes

One significant challenge in modeling most reactions is ensuring that the conformational space available on the hyperdimensional potential energy surface ($3N$-6 dimensions for non-linear systems, N = number of atoms) is appropriately sampled. For example, Zimmerman and coworkers investigated the effects of conformational flexibility on reaction rates for reductive elimination of representative nickel bisphosphine catalysts (Figure 2.2).[55] They found that the barriers for

reductive eliminations varied significantly between conformations, providing an important caveat for those working in this field. Low-cost computational methods, such as Grimme's CREST, have proven effective for rapid conformational searching.[56] Even with such tools, capturing the full conformer space—to the extent that one can do so—is still a *significant* challenge, especially when competing non-covalent interactions and increased complexity with more degrees of freedom (e.g., number of alkyl groups) dramatically increase the number of possible conformations.[57]

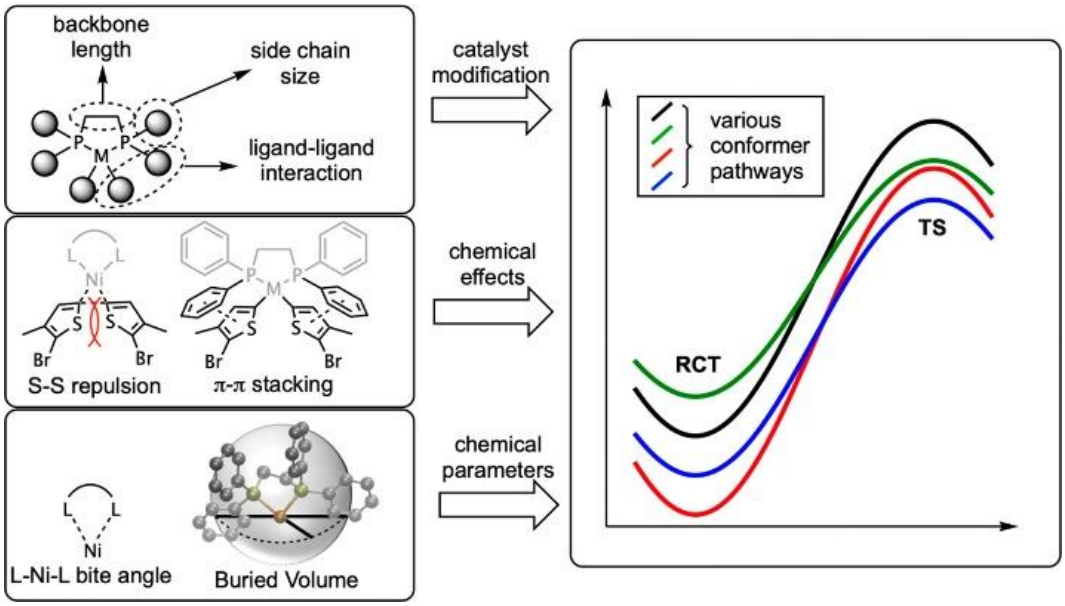

Figure 2.2 Various effects on catalyst ligands that can influence conformer space and the energetically preferred mechanistic pathway. Adapted with permission from Vitek, A. K.; Jugovic, T. M. E.; Zimmerman, P. M. *ACS Catal.* **2020**, *10*, 7136–7145. Copyright 2020 American Chemical Society.

In organometallic chemistry, complexity arises not only from ligands being large and "floppy" but also from ligand-metal binding modes sometimes not being static. In addition, it is important to determine whether multiple conformations of TSSs are close enough in energy to contribute to predicted rates, i.e., TSS conformations within 2-3 kcal/mol of the lowest energy TSS conformation should be accounted for by Boltzmann averaging. For example, in a joint

experimental and theoretical effort, the groups of Takacs (the experimentalist) and Liu (the theorist) demonstrated the critical role of conformationally flexible TADDOL-derived phosphite ligands on reactivity and selectivity in Rh-catalyzed asymmetric hydroboration, highlighting the importance of conformational issues for catalyst/ligand design.[58]

A representative example relevant to metal-promoted [2,3]-sigmatropic shifts involves the use of chiral dirhodium tetracarboxylate paddlewheel (and related) catalysts. In general, chiral ligands in this field are quite large, so ligand conformations can become important.[59–61] For instance, ligand blocking groups around the metal dimer catalyst core can adopt either up (α) or down (β) configurations leading to multiple arrangements (Figure 2.3) that should be considered.[60] And the ligands in each of these arrangements may be able to adopt several different conformations. Similar issues have been described for 4-fold symmetric iron complexes used for CO_2 and O_2 reduction.[62,63]

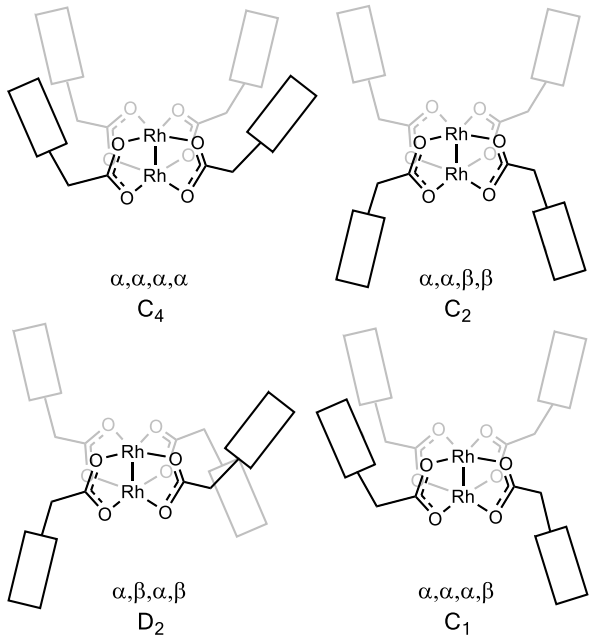

Figure 2.3 Different possible ligand arrangements for chiral dirhodium(II) catalysts and their associated point groups (assuming chiral ligands).

One approach to avoiding the problem of conformational complexity is to carry out calculations using small, inflexible ligands, e.g., formate groups, acetate groups or truncated chiral ligands. While this approach is often reasonable, one must be exceedingly cautious when employing it to assure that important substrate–ligand interactions are not missed. For instance, Hamada and Nemoto found changes in product distributions upon simply changing the ligand type in their dirhodium(II) catalysts from $Rh_2(NHCO^tBu)_4$ to $Rh_2(NHCOMe)_4$ to $Rh_2(OCOMe)_4$ in a Rh-catalyzed carbene insertion into C-N bonds (Figure 2.4).[64]

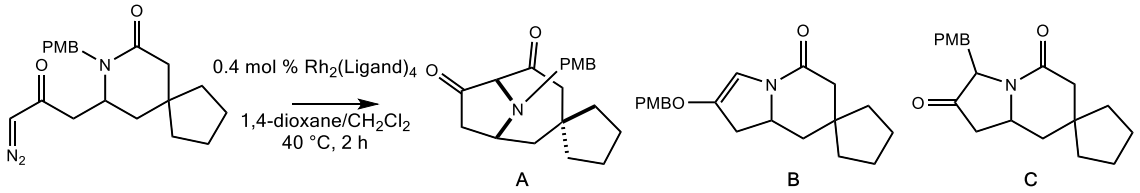

Ligand	Yield of A (%)	Yield of B (%)	Yield of C (%)
NHCO^{t}Bu	82	17	0
NHCOMe	73	17	0
OCOMe	25	16	13

Figure 2.4 Mechanistic experiment on ligand effects in Rh-catalyzed formal insertion into amide C-N bonds. The yield of A, B, and C are dependent on ligand type. Figure adapted from on Hamada and Nemoto.[64]

2.3 Solvation

Accurately modeling the effects of solvent on reactivity has been a longstanding challenge. The more we learn about the ways in which different solvent models can impact computed energies—which inform theoretical predictions/conclusions—the clearer it becomes that treating solvent accurately can make all the difference, especially in cases where the number of components involved is large and/or interactions with solvent molecules are potentially strong.[65,66] As Eisenstein and coworkers described, there are three general approaches to modeling solvent, which

vary in computational cost: (1) implicit (continuum) solvent models, (2) hybrid models of explicit and implicit solvent (sometimes called "hybrid cluster-continuum models" or "microsolvation"), and (3) explicit solvent models.[67] Solvent effects may be drastically important in metal-catalyzed rearrangements. For instance, the Koenigs group discovered a dependence of [1,2]- or [2,3]-sigmatropic rearrangement product yields depending on the solvent in Rh-catalyzed rearrangement reactions.[68] The origin of this solvent-dependence is still unknown.

By far, the least computationally intensive approach, and most widely used today, is the implicit approach. In this crude but useful method to model solvent, the solute is placed within a solvent cavity described by a continuum with a fixed dielectric constant. Practitioners have a choice of implicit solvent models.[69] Frequently used ones include density-based models (SMD)[70] and polarizable continuum models (PCM).[71] As with the choice of level of theory, we caution against haphazardly selecting an implicit solvent model to use. Rather, these solvent models should be applied with the caveat that many were parameterized for particular atomic radii and nonelectrostatic terms. Some solvent models were developed specifically for use with certain functionals and many continuum solvent models are parameterized for reactions occurring at 298 K.[72,73] In general, we recommend comparing computed reaction barriers against experiment (e.g., rates, activation parameters, selectivity) with various models, but it is prudent to make sure that the results are not highly sensitive to the model chosen – that could be a sign of problems with the mechanism, not just the solvation model. If experimental data is lacking for a given reaction, basing the model selection on past benchmarking studies is the next best thing.[74,75]

In some cases, including explicit solvent molecules may be critical to reproduce experimental observations.[76,77] Computing the properties of solutes in a large box of explicit solvent molecules, however, is often not practical (which is the case for many of the reactions

discussed here). In cases where a full statistical treatment of solvent is absolutely necessary, however, such as those in which solvent-solute interactions or solvent reorganization is critical to the mechanism, *ab initio* molecular dynamics (AIMD) methods, in which solvent molecules are treated with quantum chemistry (often semiempirical methods, but ideally with a method as reliable as that used for the solute), can be used.[77–80]

In lieu of modeling a box of explicit solvent, one might be able to model explicit solvent effects with the microsolvation approach. In this approach, only a few explicit solvent molecules around the solute are used within an implicit model for the remainder of the solvent.[66] This approach may be useful in reactions where ionic or zwitterionic species dominate, whose relative energies are not expected to be computed accurately with implicit models.[66] The microsolvation approach is viewed by some (including us) as a last resort effort when the options for accounting for solvent are otherwise exhausted (or computationally intractable), because many systems are adequately modeled in implicit solvent[66] and adequately sampling configurations of explicit solvent molecules is a daunting (and frequently neglected) task.[81,82] A study from our group,[83] for example, indicates that including explicit solvent at the presumably vacant axial position of dirhodium complexes modulates reactivity of dirhodium tetracarboxylates, which aligns with a number of experimental studies that show that axial coordination can influence electronic communication between the two Rh atoms in these complexes.[84–88] In this case, however, the question to be addressed with microsolvation was well-defined. It was specific to a particular position where solvent could bind. Any Lewis base (including reactants) could, in principle, coordinate the vacant, axial coordination site of dirhodium complexes, which may (or may not) have a non-negligible effect on reaction barriers.[89] Considering nuances like these often shed light on particular gray areas of complex mechanisms.

A particularly problematic situation arises when ion pair intermediates occur along a reaction pathway. For instance, in a collaborative experimental and theoretical study with the Tambar group on tandem ylide-formation/rearrangement reactions promoted by Rh and Cu, we proposed a mechanism based on results of DFT calculations (IEFPCM(DCM)-UB3LYP-D3(BJ)/SDD[6-31+G(d,p)]//IEFPCM(DCM)-UB3LYP/LANL2DZ[6-31G(d)]) involving an ion pair intermediate along the pathway to the product (Figure 2.5).[90] It is known that ion pair intermediates (e.g., in carbocation reactions) can be formed and react before surrounding solvent equilibrates, necessitating explicit solvent modeling to account for dynamics.[91] In our case, such modeling was not possible, so we resorted to simply proposing a reactivity model consistent with experiments and shored up by structural comparisons. We hope, however, that explicit solvent modeling of the accuracy we would need will become accessible in the future.

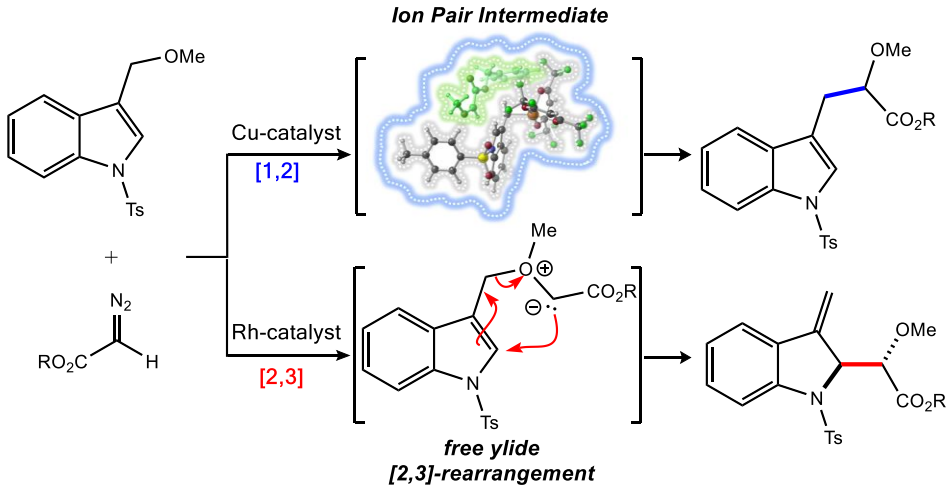

Figure 2.5 Ion pair intermediate is proposed in the Cu-catalyzed pathway to [1,2]-products of indole-based oxonium ylides.

2.4 Synergy of Experiment and Theory—Case Studies

Computational studies on reactions involving transition-metal catalysts have evolved alongside synthetic methodologies, providing useful insight into mechanisms. For instance, a substantial amount of mechanistic insight has been generated by studies involving close collaboration between groups specializing theory and experiment: ranging from C–H[92–95] and Si–H insertion,[96,97] cyclopropanation,[93,98–101] and mapping catalyst space.[102] In this section, we review representative mechanistic studies of metal (mainly Rh and Cu)-catalyzed sigmatropic rearrangement reactions that have benefitted from attention from both experiment and theory camps.

2.4.1 Metal-Bound or Free Ylides?

First, we focus our attention on whether metal catalysts remain bound to substrates for [2,3]-sigmatropic rearrangements catalyzed by Rh(II) and Cu(I) catalysts. Later, we will discuss [1,2]-sigmatropic rearrangements.

Though experimental groups have developed (and are developing) methodology for transition-metal promoted [2,3]-sigmatropic rearrangements—and, in doing so, have carried out control experiments that bear on mechanism—computational work has lagged behind.[38,43,103–105] A key question that emerged from experiment—that is still not definitively clear for many onium ylides formed by Rh(II) and Cu(I) catalysts by carbene transfer—is whether the metal catalyst remains explicitly bound to its substrate during the [2,3]-rearrangement step. The dearth of theoretical insight into this question was brought to our attention *via* recent appeals for theoretical insight in the work of Koenigs and coworkers and through our collaborative work with the Driver, May, Shaw, and Tambar groups.[90,106,107] Hock and Koenigs have stated, “it would still be very

helpful if these experimental findings could be further supported by DFT calculations to improve our understanding of the subtle differences between these rearrangement reactions."[43] We took up this call to action (*vide supra*, Chapter 3).

What experimental evidence was available for us to use in shaping our study? In control experiments where the metal catalyst is varied and all else is kept that same, if stereo-, chemo-, and regioselectivity are unperturbed, then a plausible explanation is that a free ylide is involved. For instance, whereas Clark and Hansen[103] observed a catalyst-dependence on product ratio in their study of metal-catalyzed ylide [2,3]-rearrangements, which led to the conclusion that metal-bound ylides were involved, Wang[104] and Koenigs[108] reported catalyst-*in*dependence on the product ratio for their ylide rearrangement reactions, suggesting the existence of free ylides.

With this precedent, we set out to (1) confirm that our theoretical approaches could provide results consistent with experiments and (2) determine the physical factors that impact whether metal-catalyst remains bound during the rearrangement step, thereby setting the stage for future reaction design.[44] In the four reactions examined, three with Rh and one with Au, we found that our calculations supported the conclusions from control experiments. Here, we utilized the (U)B3LYP/LANL2DZ[6-31G(d)] level of theory to investigate the mechanism (single-point calculations with dispersion correction and with other functionals produced qualitatively similar results). From this study we concluded that the steric bulk adjacent to the carbene center played the most significant role in determining whether a metal catalyst dissociated or remained bound to the ylide intermediate.

Almost simultaneously, Dang and coworkers published a related computational study (SMD(DCM)-M06-L/SDD[6-311++G(d,p)]//M06-L/SDD[6-31G(d)]). They found that allylic iodides and sulfides can form ylides in the presence of Cu(I)-bisoxazoline catalysts that can either

undergo a metal-bound or free ylide rearrangement (Figure 2.6).[109] In particular, iodonium ylides[110] were shown to have Cu bound during the [2,3]-rearrangement while sulfonium ylides rearranged free of Cu catalyst. By computing systems with different substrates, ligands, and solvents, they ascribed this difference to the (thermodynamic) stability of metal-bound and free ylides, which, they suggest, is mainly controlled by the heteroatoms (I or S).[109].

In discussing the nature of the oxonium, sulfonium, and selenonium ylides in our study—wherein we found metal-bound oxonium ylides and free sulfonium and selenonium ylides—we made the point that our conclusions "should not be generalized to all similar ylides undergoing [2,3]-rearrangements."[44] The work by Dang's group bolsters our observation that the nature of the ylide is system-dependent. Enabled by the work done by experimental (and other computational) groups, we seem to have converged on two key factors that determine whether an ylide intermediate is free or metal-bound: (1) steric bulk directly attached to the carbene carbon[44] and, (2) the electronic nature of the heteroatom directly bound to the carbene carbon.[109]

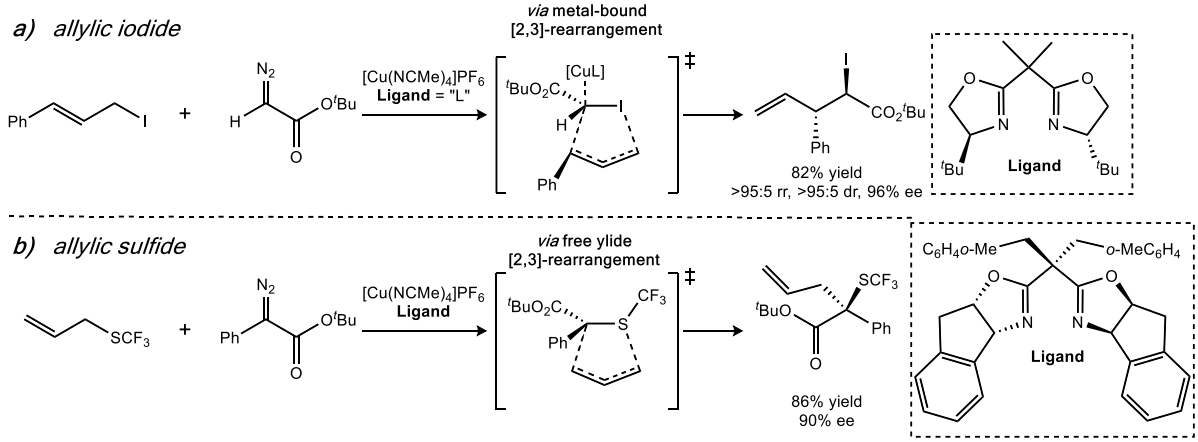

Figure 2.6 Metal-bound and free ylide [2,3]-sigmatropic rearrangements of iodonium and sulfonium ylides supported by DFT calculations. Existence of a free sulfonium ylide and metal-bound iodonium ylide undergoing the [2,3]-sigmatropic rearrangement has implications for experiment. See Liu, Z.; Jin, X.; Dang, Y. *ACS Catal*. **2021**, *11*, 691–702.

Metal dissociation before the end of a catalytic cycle may be more general. For example, Schomaker, Fernández and coworkers reported an aziridinium ylide-formation/[2,3]-rearrangement reaction to form azetidines that appears to involve a free ylide intermediate.[111,112] The authors combined experimental and computational expertise (SMD(DCM)-B3LYP-D3/def2-SVP) to reveal that not only is a free ylide energetically favorable over a Rh-bound ylide, but also that the stereospecificity (enantioretention and high diastereoselectivity) of this reaction can be attributed to a concerted [2,3]-sigmatropic rearrangement (Figure 2.7).[112]

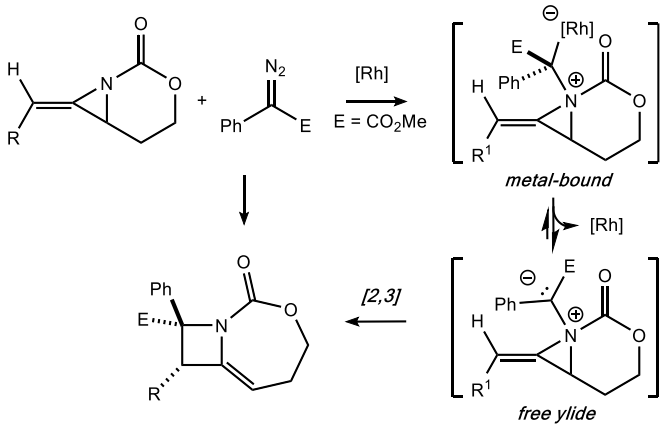

Figure 2.7 A free aziridinium ylide intermediate is predicted to be operative in a concerted [2,3]-rearrangement to azetidines.

Another joint experimental-theoretical study by Koenigs and coworkers led to the conclusion that free ylides are operative in [2,3]-sigmatropic rearrangements of organoselenium compounds with triazoles in the presence of dirhodium catalysts.[89]

Premature catalyst dissociation might afflict ylides undergoing [1,2]-rearrangements (or Stevens rearrangements for ammonium ylides) as well.[32,113–116] For instance, in stereoselective C–H insertions with Rh_2(*R*-PTAD)$_4$ catalysts, forming six-membered ring tetrahydroisoquinolines with high diastereo- and enantioselectivity, Shaw and coworkers observed no [1,2]-rearrangement

side products.[107] In one case, however, they observed a rearrangement product and initiated a collaboration with our group to confirm that this was indeed the case (Figure 2.8). Our calculations ((U)B3LYP/LANL2DZ[6-31G(d)]) revealed that the Rh-catalyst (modeled as $Rh_2(OAc)_4$) dissociated before the [1,2]-rearrangement step. Synergy between theory and experiment, again, illuminated mechanistic detail that might not have been revealed otherwise. These results echo past computational studies by our group, in collaboration with Driver and coworkers, on Rh-promoted indole formation from vinyl/azidoarenes that involved competing [1,5]-shifts.[106] For that reaction, our DFT calculations ((U)M06/SDD[6-31+G(d,p)]) led us to conclude that the Rh catalyst was not necessarily involved in the rearrangement step, since computations without Rh bound corresponded to the experimentally observed selectivity while those with Rh bound did not.

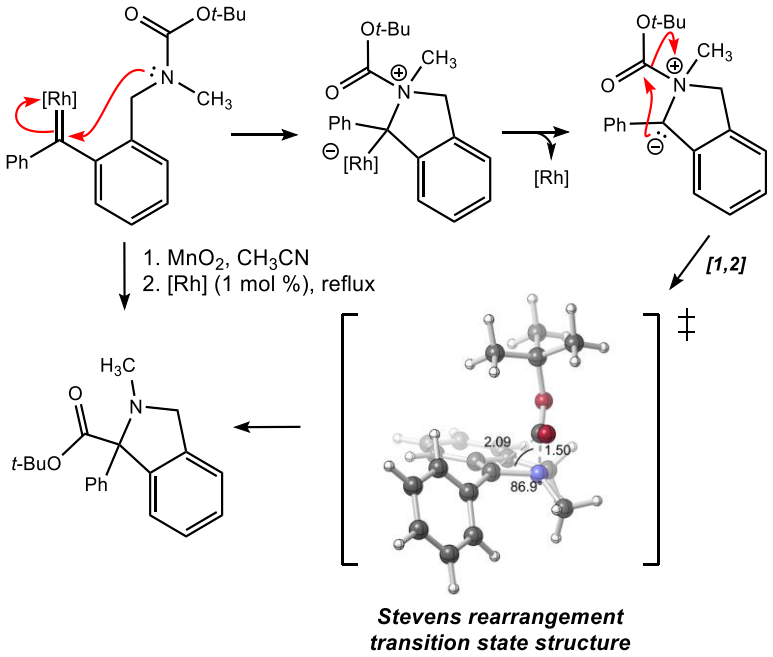

Figure 2.8 Isoindoline product is formed by ylide-formation/Stevens [1,2]-rearrangement in the presence of Rh catalyst. DFT calculations support a free ylide Stevens [1,2]-rearrangement.

While these computational studies do not cover all types of metal-catalyzed sigmatropic rearrangements, they do point to potentially general principles. And while they vary in the degree

of integration between the computational and experimental teams, they show that combining results from both sides can shine light on mechanistic nuances.

2.4.2 Conformations and Ligand-Binding Modes of Paddlewheel Complexes

As mentioned above, ligand binding modes and conformations in chiral dirhodium tetracarboxylate complexes can have important effects on reactivity and selectivity.[117] In a study that reported the crystal structure and computed structure of one such paddlewheel complex, Rh_2(*S*-PTTL)$_4$, Fox and co-workers described the so-called "chiral crown" conformation ($\alpha,\alpha,\alpha,\alpha$) (Figure 2.9). They found that Rh_2(*S*-PTTL)$_4$ crystallized in this arrangement, consistent with the computed lowest-energy form found by DFT calculations (OLYP/TZP).[118] By elucidating the preferred structure of this complex, they were able to pin specific structural features to chemo-, enantio-, and diastereoselectivity of intermolecular cyclopropanation reactions involving Rh_2(*S*-PTTL)$_4$. A similar chiral crown conformation was discovered for Rh_2(*S*-NTTL)$_4$.[119] Subsequent X-ray crystallography and computational studies demonstrated that these chiral crown forms are more general for *tert*-leucine-derived dirhodium paddlewheel complexes,[120] results with implications for the use of these (and potentially other related catalysts) in other reactions, such as [2,3]-sigmatropic shifts.

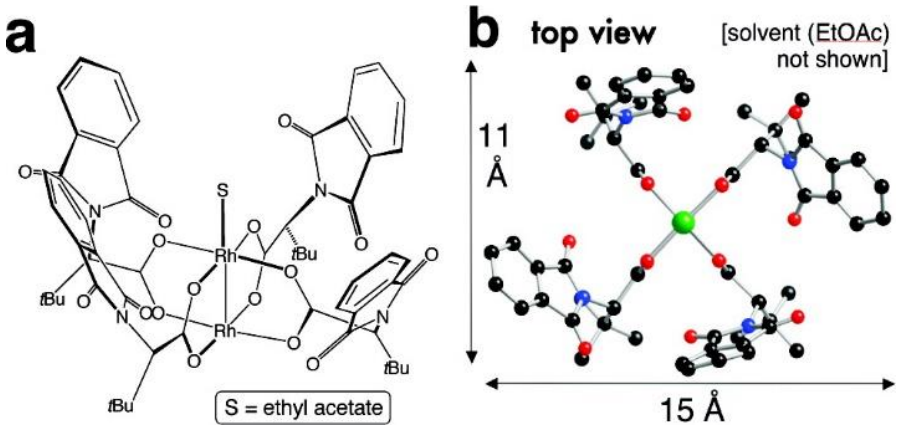

Figure 2.9 Chiral crown conformation of Rh_2(*S*-PTTL)$_4$. Adapted with permission from DeAngelis, A.; Dmitrenko, O.; Yap, G. P. A.; Fox, J. M. *J. Am. Chem. Soc*. **2009**, *131*, 7230–7231. Copyright 2009 American Chemical Society.

2.4.3 No Metal, Just Light

One study by the groups of Koenigs and Xu further highlights the synergy between theory and experiment. Their study revealed interesting diastereoselectivity differences between oxetane and thietane starting materials (Figure 2.10).[121]

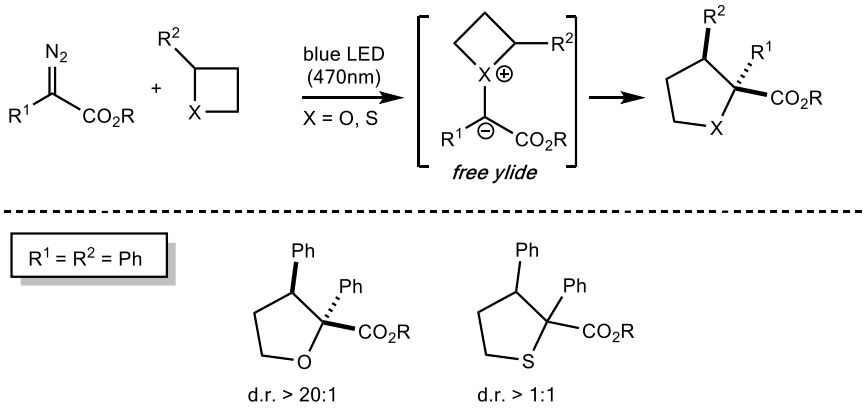

Figure 2.10 Erosion of diastereoselectivity in sulfonium ylides compared to oxonium ylide.

Presumably, after extrusion of nitrogen and carbene formation, a free ylide is generated, which undergoes [1,2]-rearrangement. The origin of observed differences in diastereoselectivity was investigated by DFT calculations (SMD($CHCl_3$)-(U)B3LYP/6-311+G(d,p)//SMD($CHCl_3$)-(U)B3LYP/6-31G(d)), which revealed a diradical pathway for both oxetane and thietane derived ylides. The differences in diastereoselectivity were not attributed to divergent reaction mechanisms, but differences in critical C-O and C-S bond lengths in TSSs (Figure 2.11). One wonders, in the thietane ylides, if this type of reactivity could be controlled by chiral metal catalysts and enable asymmetric reactions using them.

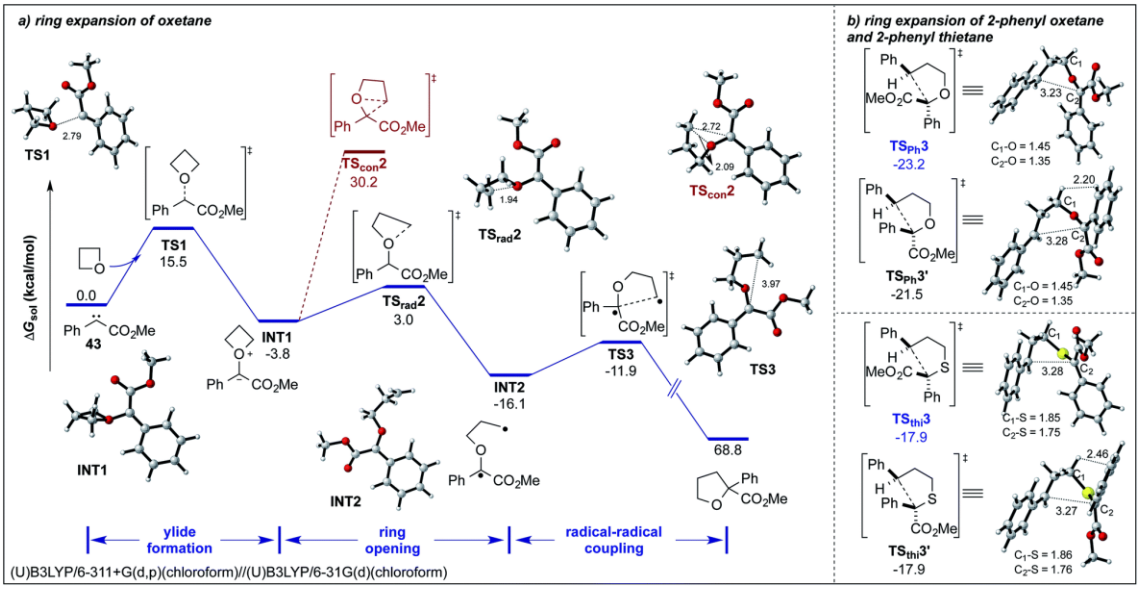

Figure 2.11 Energy surface for oxetane ring expansion by photochemical carbene transfer. Density functional theory calculations reveal diradical mechanistic pathway to ring expansion product. Adapted with permission from the Royal Society of Chemistry, Copyright 2019. S. Jana, Z. Yang, C. Pei, X. Xu and Rene M. Koenigs, *Chem. Sci.*, **2019**, *10*, 10129. DOI: 10.1039/C9SC04069B. Published by The Royal Society of Chemistry.

2.5 How To 'Cope' with Non-Statistical Dynamic Effects

Similar to ylide-formation/[2,3]-rearrangements, C–H activation/Cope rearrangements ([3,3]-sigmatropic shifts)[122,123] can be promoted by dirhodium catalysts.[124] Davies and coworkers, for

example, reported a joint experimental and theoretical study in which the mechanisms of these cascade processes were interrogated (Figure 2.12).[125] Results from DFT calculations (B3LYP/6-311+G(2d,2p)[Rh-RSC+4f]//B3LYP/6-31G(d)[Rh-RSC+4f]) support a pathway involving a concerted, yet highly asynchronous, hydride-transfer/C–C bond-forming process in which a post-transition state bifurcation (PTSB) is involved. Reactions that contain PTSBs involve a single (ambimodal) transition-state structure on the potential energy surface that leads to two products without intervening minima—a fork in the pathway downhill in energy toward the products.[54,126–130] Here, the ambimodal transition-state structure corresponded to the hydride-transfer process and the two products were related by a Cope rearrangement.

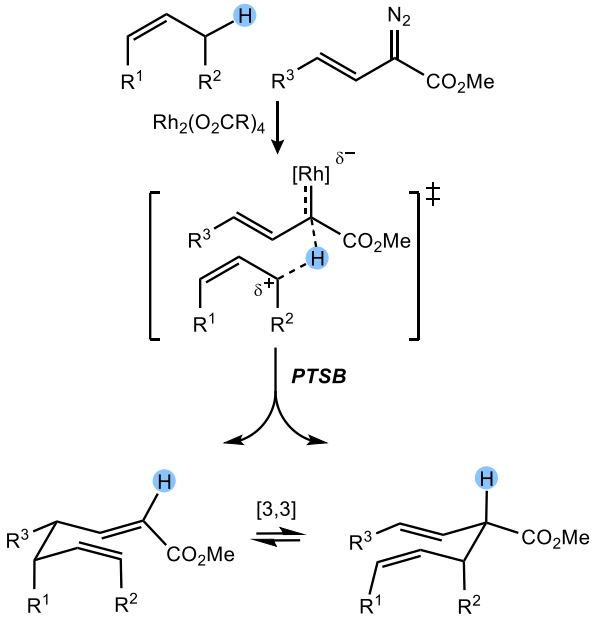

Figure 2.12 Post-transition state bifurcation is suggested in C-H activation/Cope rearrangement reaction by Davies and coworkers. If a PTSB exists, then nonstatistical dynamic effects determine product selectivity.

To predict product ratios for reactions with PTSBs, one generally needs to carry out AIMD simulations. Our group did this for a related $Rh_2(OAc)_4$-promoted reaction involving a transition state for hydride transfer to a Rh-carbene that we found (using B3LYP/LANL2DZ[6-31G(d)]

calculations) to be connected to both β-lactone and ketene/ketone products—the former arising from net C–H insertion and the latter from fragmentation (Figure 2.13).[131] Using AIMD simulations, we predicted that fragmentation should be preferred over the desired C–H insertion process, consistent with experimental results reported by Lee.[132] This study demonstrated that computational exploration of a reaction mechanism can lead to the proposal that unwanted side products might arise from PTSBs![133] Still, much has yet to be learned. Recent strides have been made in constructing bifurcating energy surfaces,[134] predicting major products of PTSBs without elaborate (and, admittedly, expensive AIMD) simulations,[135–137] exploring PTSBs important in biosynthetic pathways,[138–145] and mapping reaction pathways in phase space.[146]

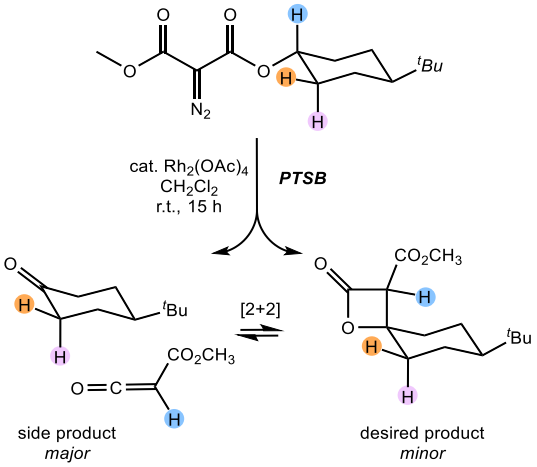

Figure 2.13 Accounting for non-statistical dynamic effects revealed a post-transition state bifurcation in our mechanistic study of C-H insertion reactions to β-lactone products.

2.6 Outlook

Electronic structure calculations are now ubiquitous in mechanistic chemistry due to significant leaps in modern computational power and reductions in barriers to entry for learning quantum chemistry software.[147,148] In this review, we have merely touched the tip of the iceberg when it comes to applied computational approaches for solving complex mechanistic problems. For

example, some are utilizing statistical tools to generate catalysts maps for dirhodium(II)[102] (and other) complexes to aid catalyst selection/design.[149,150] Others are harnessing the power of machine learning methods for accelerated reaction discovery and chemical space exploration.[151–153] Nonetheless, we hope that we have given readers a snapshot of the utility of current computational approaches through tales of transition-metal catalyzed sigmatropic rearrangements. We also hope that the caveats we describe are taken to heart. Both theory and experiment bring powerful insight to the table in designing reactions. The future of both fields seems bright, but the future when theory and experiment teams work together seems even brighter.

2.7 References

(1) Jones, A. C.; May, J. A.; Sarpong, R.; Stoltz, B. M. Toward a Symphony of Reactivity: Cascades Involving Catalysis and Sigmatropic Rearrangements. *Angew. Chem. Int. Ed.* **2014**, *53*, 2556–2591.

(2) Hoffmann, R. W. Stereochemistry of [2,3]Sigmatropic Rearrangements. *Angew. Chem. Int. Ed.* **1979**, *18*, 563–572.

(3) West, T. H.; Spoehrle, S. S. M.; Kasten, K.; Taylor, J. E.; Smith, A. D. Catalytic Stereoselective [2,3]-Rearrangement Reactions. *ACS Catal.* **2015**, *5*, 7446–7479.

(4) Doyle, M. P. Catalytic Methods for Metal Carbene Transformations. *Chem. Rev.* **1986**, *86*, 919–939.

(5) Moss, R. A.; Doyle, M. P. *Contemporary Carbene Chemistry. Wiley Series of Reactive Intermediates*; Moss, R. A., Doyle, M. P., Eds.; John Wiley & Sons, Inc.: Hoboken, New Jersey, 2014.

(6) Rao, S.; Prabhu, K. R. Gold-Catalyzed [2,3]-Sigmatropic Rearrangement: Reaction of Aryl Allyl Alcohols with Diazo Compounds. *Org. Lett.* **2017**, *19*, 846–849.

(7) He, F.; Jana, S.; Koenigs, R. M. Gold-Catalyzed Sigmatropic Rearrangement Reactions via Carbene Transfer Reactions. *J. Org. Chem.* **2020**, *85*, 11882–11891.

(8) Simonneaux, G.; Galardon, E.; Paul-Roth, C.; Gulea, M.; Masson, S. Ruthenium-Porphyrin-Catalyzed Carbenoid Addition to Allylic Compounds: Application to [2,3]-Sigmatropic Rearrangements of Ylides. *J. Organomet. Chem.* **2001**, *617–618*, 360–363.

(9) Zhou, C.-Y.; Huang, J.-S.; Che, C.-M. Ruthenium-Porphyrin-Catalyzed Carbenoid Transfer Reactions. *Synlett* **2010**, *2010*, 2681–2700.

(10) Jiang, J.; Ma, X.; Ji, C.; Guo, Z.; Shi, T.; Liu, S.; Hu, W. Ruthenium(II)/Chiral Brønsted Acid Co-Catalyzed Enantioselective Four-Component Reaction/Cascade Aza-Michael Addition for Efficient Construction of 1,3,4-Tetrasubstituted Tetrahydroisoquinolines. *Chem. Eur. J.* **2014**, *20*, 1505–1509.

(11) Viñas-Lóbez, J.; Levitre, G.; de Aguirre, A.; Besnard, C.; Poblador-Bahamonde, A. I.; Lacour, J. Enabling Cyclization Strategies through Carbonyl-Ylide-Mediated Synthesis of Malonate Enol Ethers. *ACS Org. Inorg. Au* **2021**, *1*, 11–17.

(12) Fukuda, T.; Katsuki, T. Co(III)-Salen Catalyzed Carbenoid Reaction: Stereoselective

[2,3]Sigmatropic Rearrangement of S-Ylides Derived from Allyl Aryl Sulfides. *Tetrahedron Lett.* **1997**, *38*, 3435–3438.
(13) Fukuda, T.; Irie, R.; Katsuki, T. Catalytic and Asymmetric [2,3]Sigmatropic Rearrangement: Co(III)-Salen Catalyzed S-Ylide Formation from Allyl Aryl Sulfides and Their Rearrangement. *Tetrahedron* **1999**, *55*, 649–664.
(14) Greenman, K. L.; Carter, D. S.; Van Vranken, D. L. Palladium-Catalyzed Insertion Reactions of Trimethylsilyldiazomethane. *Tetrahedron* **2001**, *57*, 5219–5225.
(15) Soheili, A.; Tambar, U. K. Tandem Catalytic Allylic Amination and [2,3]-Stevens Rearrangement of Tertiary Amines. *J. Am. Chem. Soc.* **2011**, *133*, 12956–12959.
(16) Kang, Z.; Zhang, D.; Hu, W. Regio- and Diastereoselective Three-Component Reactions via Trapping of Ammonium Ylides with N -Alkylquinolinium Salts: Synthesis of Multisubstituted Tetra- and Dihydroquinoline Derivatives. *Org. Lett.* **2017**, *19*, 3783–3786.
(17) Davies, P. W.; Albrecht, S. J. C.; Assanelli, G. Silver-Catalysed Doyle–Kirmse Reaction of Allyl and Propargyl Sulfides. *Org. Biomol. Chem.* **2009**, *7*, 1276.
(18) Lin, X.; Tang, Y.; Yang, W.; Tan, F.; Lin, L.; Liu, X.; Feng, X. Chiral Nickel(II) Complex Catalyzed Enantioselective Doyle–Kirmse Reaction of α-Diazo Pyrazoleamides. *J. Am. Chem. Soc.* **2018**, *140*, 3299–3305.
(19) Carter, D. S.; Van Vranken, D. L. Iron-Catalyzed Doyle−Kirmse Reaction of Allyl Sulfides with (Trimethylsilyl)Diazomethane. *Org. Lett.* **2000**, *2*, 1303–1305.
(20) Aviv, I.; Gross, Z. Iron(III) Corroles and Porphyrins as Superior Catalysts for the Reactions of Diazoacetates with Nitrogen- or Sulfur-Containing Nucleophilic Substrates: Synthetic Uses and Mechanistic Insights. *Chem. Eur. J.* **2008**, *14*, 3995–4005.
(21) Zhu, S.-F.; Zhou, Q.-L. Iron-Catalyzed Transformations of Diazo Compounds. *Natl. Sci. Rev.* **2014**, *1*, 580–603.
(22) Tyagi, V.; Sreenilayam, G.; Bajaj, P.; Tinoco, A.; Fasan, R. Biocatalytic Synthesis of Allylic and Allenyl Sulfides through a Myoglobin-Catalyzed Doyle-Kirmse Reaction. *Angew. Chem. Int. Ed.* **2016**, *55*, 13562–13566.
(23) Hock, K. J.; Mertens, L.; Hommelsheim, R.; Spitzner, R.; Koenigs, R. M. Enabling Iron Catalyzed Doyle–Kirmse Rearrangement Reactions with in Situ Generated Diazo Compounds. *Chem. Commun.* **2017**, *53*, 6577–6580.
(24) Batista, V. F.; Pinto, D. C. G. A.; Silva, A. M. S. Iron: A Worthy Contender in Metal Carbene Chemistry. *ACS Catal.* **2020**, *10*, 10096–10116.
(25) Carreras, V.; Tanbouza, N.; Ollevier, T. The Power of Iron Catalysis in Diazo Chemistry. *Synthesis* **2021**, *53*, 79–94.
(26) Solé, D.; Amenta, A.; Campos, C.; Fernández, I. Iron-Promoted Dealkylative Carbene Aminocyclization of δ-Arylamino-α-Diazoesters. *Dalt. Trans.* **2021**, 2167–2176.
(27) Doyle, M. P.; Tamblyn, W. H.; Bagheri, V. Highly Effective Catalytic Methods for Ylide Generation from Diazo Compounds. Mechanism of the Rhodium- and Copper-Catalyzed Reactions with Allylic Compounds. *J. Org. Chem.* **1981**, *46*, 5094–5102.
(28) Kirmse, W.; Kapps, M. Reaktionen Des Diazomethans Mit Diallylsulfid Und Allyläthern Unter Kupfersalz-Katalyse. *Chem. Ber.* **1968**, *101*, 994–1003.
(29) Nakai, T.; Mikami, K. [2,3]-Wittig Sigmatropic Rearrangements in Organic Synthesis. *Chem. Rev.* **1986**, *86*, 885–902.
(30) Mikami, K.; Nakai, T. Acyclic Stereocontrol via [2,3]-Wittig Sigmatropic Rearrangement. *Synthesis* **1991**, *1991*, 594–604.
(31) Clark, J. S. Nitrogen, Oxygen, and Sulfur Ylide Chemistry. A Practical Approach in Chemsitry; Oxford University Press: New York, 2002; pp 1–308.
(32) Sweeney, J. B. Sigmatropic Rearrangements of 'Onium' Ylids. *Chem. Soc. Rev.* **2009**, *38*, 1027.
(33) Li, Z.; Boyarskikh, V.; Hansen, J. H.; Autschbach, J.; Musaev, D. G.; Davies, H. M. L. Scope and Mechanistic Analysis of the Enantioselective Synthesis of Allenes by

Rhodium-Catalyzed Tandem Ylide Formation/[2,3]-Sigmatropic Rearrangement between Donor/Acceptor Carbenoids and Propargylic Alcohols. *J. Am. Chem. Soc.* **2012**, *134*, 15497–15504.
(34) Murphy, G. K.; Stewart, C.; West, F. G. Intramolecular Generation and Rearrangement of Oxonium Ylides: Methodology Studies and Their Application in Synthesis. *Tetrahedron* **2013**, *69*, 2667–2686.
(35) Bao, H.; Tambar, U. K. [2,3]-Rearrangements of Ammonium Zwitterions. In *Molecular Rearrangements in Organic Synthesis*; Rojas, C. M., Ed.; John Wiley & Sons, Inc.: New York, 2015; pp 459–496.
(36) Ford, A.; Miel, H.; Ring, A.; Slattery, C. N.; Maguire, A. R.; McKervey, M. A. Modern Organic Synthesis with α-Diazocarbonyl Compounds. *Chem. Rev.* **2015**, *115*, 9981–10080.
(37) Hommelsheim, R.; Guo, Y.; Yang, Z.; Empel, C.; Koenigs, R. M. Blue-Light-Induced Carbene-Transfer Reactions of Diazoalkanes. *Angew. Chem. Int. Ed.* **2019**, *58*, 1203–1207.
(38) Jana, S.; Guo, Y.; Koenigs, R. M. Recent Perspectives on Rearrangement Reactions of Ylides via Carbene Transfer Reactions. *Chem. Eur. J.* **2021**, *27*, 1270–1281.
(39) Empel, C.; Pei, C.; Koenigs, R. M. Unlocking Novel Reaction Pathways of Diazoalkanes with Visible Light. *Chem. Commun.* **2022**, *58*, 2788–2798.
(40) Dasgupta, A.; Richards, E.; Melen, R. L. Triarylborane Catalyzed Carbene Transfer Reactions Using Diazo Precursors. *ACS Catal.* **2022**, *12*, 442–452.
(41) Babaahmadi, R.; Dasgupta, A.; Hyland, C. J. T.; Yates, B. F.; Melen, R. L.; Ariafard, A. Understanding the Influence of Donor-Acceptor Diazo Compounds on the Catalyst Efficiency of B(C 6 F 5) 3 Towards Carbene Formation. *Chem. Eur. J.* **2022**, *28*.
(42) Wu, Y. D.; Houk, K. N.; Marshall, J. A. Transition Structure for the [2,3]-Wittig Rearrangement and Analysis of Stereoselectivities. *J. Org. Chem.* **1990**, *55*, 1421–1423.
(43) Hock, K. J.; Koenigs, R. M. Enantioselective [2,3]-Sigmatropic Rearrangements: Metal-Bound or Free Ylides as Reaction Intermediates? *Angew. Chem. Int. Ed.* **2017**, *56*, 13566–13568.
(44) Laconsay, C. J.; Tantillo, D. J. Metal Bound or Free Ylides as Reaction Intermediates in Metal-Catalyzed [2,3]-Sigmatropic Rearrangements? It Depends. *ACS Catal.* **2021**, *11*, 829–839.
(45) Meek, S. J.; Pitman, C. L.; Miller, A. J. M. Deducing Reaction Mechanism: A Guide for Students, Researchers, and Instructors. *J. Chem. Educ.* **2016**, *93*, 275–286.
(46) Eisenstein, O. Concluding Remarks for "Mechanistic Processes in Organometallic Chemistry": The Importance of a Multidisciplinary Approach. *Faraday Discuss.* **2019**, *220*, 489–495.
(47) Sperger, T.; Sanhueza, I. A.; Schoenebeck, F. Computation and Experiment: A Powerful Combination to Understand and Predict Reactivities. *Acc. Chem. Res.* **2016**, *49*, 1311–1319.
(48) McLarney, B. D.; Hanna, S.; Musaev, D. G.; France, S. Predictive Model for the [Rh 2(Esp)2]-Catalyzed Intermolecular C(Sp3)–H Bond Insertion of β-Carbonyl Ester Carbenes: Interplay between Theory and Experiment. *ACS Catal.* **2019**, *9*, 4526–4538.
(49) Wheeler, S. E.; Seguin, T. J.; Guan, Y.; Doney, A. C. Noncovalent Interactions in Organocatalysis and the Prospect of Computational Catalyst Design. *Acc. Chem. Res.* **2016**, *49*, 1061–1069.
(50) Wagner, J. P.; Schreiner, P. R. London Dispersion in Molecular Chemistry - Reconsidering Steric Effects. *Angew. Chem. Int. Ed.* **2015**, *54*, 12274–12296.
(51) Carpenter, B. K. Dynamic Behavior of Organic Reactive Intermediates. *Angew. Chem. Int. Ed.* **1998**, *37*, 3340–3350.
(52) Carpenter, B. K. Energy Disposition in Reactive Intermediates. *Chem. Rev.* **2013**, *113*, 7265–7286.
(53) Tantillo, D. J. *Dynamic Effects on Organic Reactions*; Reedijk, J., Ed.; Elsevier Inc.: Waltham, MA, 2018.

(54) Hare, S. R.; Tantillo, D. J. Post-Transition State Bifurcations Gain Momentum-Current State of the Field. *Pure Appl. Chem.* **2017**, *89*, 679–698.
(55) Vitek, A. K.; Jugovic, T. M. E.; Zimmerman, P. M. Revealing the Strong Relationships between Ligand Conformers and Activation Barriers: A Case Study of Bisphosphine Reductive Elimination. *ACS Catal.* **2020**, *10*, 7136–7145.
(56) Pracht, P.; Bohle, F.; Grimme, S. Automated Exploration of the Low-Energy Chemical Space with Fast Quantum Chemical Methods. *Phys. Chem. Chem. Phys.* **2020**, *22*, 7169–7192.
(57) Gorbachev, V.; Tsybizova, A.; Miloglyadova, L.; Chen, P. Increasing Complexity in a Conformer Space Step-by-Step: Weighing London Dispersion against Cation−π Interactions. *J. Am. Chem. Soc.* **2022**, *17*, 46.
(58) Shao, H.; Chakrabarty, S.; Qi, X.; Takacs, J. M.; Liu, P. Ligand Conformational Flexibility Enables Enantioselective Tertiary C − B Bond Formation in the Phosphonate-Directed Catalytic Asymmetric Alkene Hydroboration. *J. Am. Chem. Soc.* **2021**, *143*, 4801–4808.
(59) Davies, H. M. L.; Parr, B. T. Rhodium Carbenes. In *Contemporary Carbene Chemistry*; Moss, R. A., Doyle, M. P., Eds.; John Wiley & Sons, Inc., 2014; pp 363–403.
(60) Adly, F. G. On the Structure of Chiral Dirhodium(II) Carboxylate Catalysts: Stereoselectivity Relevance and Insights. *Catalysts* **2017**, *7*, 347.
(61) Hrdina, R. Dirhodium(II,II) Paddlewheel Complexes. *Eur. J. Inorg. Chem.* **2021**, *2021*, 501–528.
(62) Azcarate, I.; Costentin, C.; Robert, M.; Savéant, J.-M. Through-Space Charge Interaction Substituent Effects in Molecular Catalysis Leading to the Design of the Most Efficient Catalyst of CO 2 -to-CO Electrochemical Conversion. *J. Am. Chem. Soc.* **2016**, *138*, 16639–16644.
(63) Martin, D. J.; Mercado, B. Q.; Mayer, J. M. All Four Atropisomers of Iron Tetra(O-N,N,N-trimethylanilinium)Porphyrin in Both the Ferric and Ferrous States. *Inorg. Chem.* **2021**, *60*, 5240–5251.
(64) Harada, S.; Kono, M.; Nozaki, T.; Menjo, Y.; Nemoto, T.; Hamada, Y. General Approach to Nitrogen-Bridged Bicyclic Frameworks by Rh-Catalyzed Formal Carbenoid Insertion into an Amide C–N Bond. *J. Org. Chem.* **2015**, *80*, 10317–10333.
(65) Plata, R. E.; Singleton, D. A. A Case Study of the Mechanism of Alcohol-Mediated Morita Baylis–Hillman Reactions. The Importance of Experimental Observations. *J. Am. Chem. Soc.* **2015**, *137*, 3811–3826.
(66) Sure, R.; el Mahdali, M.; Plajer, A.; Deglmann, P. Towards a Converged Strategy for Including Microsolvation in Reaction Mechanism Calculations. *J. Comput. Aided. Mol. Des.* **2021**, *35*, 473–492.
(67) Eisenstein, O.; Ujaque, G.; Lledós, A. What Makes a Good (Computed) Energy Profile? In *New Directions in the Modeling of Organometallic Reactions. Topics in Organometallic Chemistry*; Lledós, A., Ujaque, G., Eds.; Springer, 2020; Vol. 67, pp 1–38.
(68) Yang, Z.; Guo, Y.; Koenigs, R. M. Solvent-Dependent, Rhodium Catalysed Rearrangement Reactions of Sulfur Ylides. *Chem. Commun.* **2019**, *55*, 8410–8413.
(69) Tomasi, J.; Mennucci, B.; Cammi, R. Quantum Mechanical Continuum Solvation Models. *Chem. Rev.* **2005**, *105*, 2999–3094.
(70) Marenich, A. V.; Cramer, C. J.; Truhlar, D. G. Universal Solvation Model Based on Solute Electron Density and on a Continuum Model of the Solvent Defined by the Bulk Dielectric Constant and Atomic Surface Tensions. *J. Phys. Chem. B* **2009**, *113*, 6378–6396.
(71) Miertuš, S.; Scrocco, E.; Tomasi, J. Electrostatic Interaction of a Solute with a Continuum. A Direct Utilizaion of Ab Initio Molecular Potentials for the Prevision of Solvent Effects. *Chem. Phys.* **1981**, *55*, 117–129.
(72) Klamt, A.; Mennucci, B.; Tomasi, J.; Barone, V.; Curutchet, C.; Orozco, M.; Luque, F. J. On the Performance of Continuum Solvation Methods. A Comment on "Universal

Approaches to Solvation Modeling." *Acc. Chem. Res.* **2009**, *42*, 489–492.
(73) Ho, J.; Klamt, A.; Coote, M. L. Comment on the Correct Use of Continuum Solvent Models. *J. Phys. Chem. A* **2010**, *114*, 13442–13444.
(74) Yu, H. S.; He, X.; Li, S. L.; Truhlar, D. G. MN15: A Kohn-Sham Global-Hybrid Exchange-Correlation Density Functional with Broad Accuracy for Multi-Reference and Single-Reference Systems and Noncovalent Interactions. *Chem. Sci.* **2016**, *7*, 5032–5051.
(75) Vogiatzis, K. D.; Polynski, M. V.; Kirkland, J. K.; Townsend, J.; Hashemi, A.; Liu, C.; Pidko, E. A. Computational Approach to Molecular Catalysis by 3d Transition Metals: Challenges and Opportunities. *Chem. Rev.* **2019**, *119*, 2453–2523.
(76) Nieves-Quinones, Y.; Singleton, D. A. Dynamics and the Regiochemistry of Nitration of Toluene. *J. Am. Chem. Soc.* **2016**, *138*, 15167–15176.
(77) Fu, Y.; Bernasconi, L.; Liu, P. Ab Initio Molecular Dynamics Simulations of the SN1/SN2 Mechanistic Continuum in Glycosylation Reactions. *J. Am. Chem. Soc.* **2021**, *143*, 1577–1589.
(78) Handgraaf, J.-W.; Meijer, E. J. Realistic Modeling of Ruthenium-Catalyzed Transfer Hydrogenation. *J. Am. Chem. Soc.* **2007**, *129*, 3099–3103.
(79) Carpenter, B. K.; Harvey, J. N.; Orr-Ewing, A. J. The Study of Reactive Intermediates in Condensed Phases. *J. Am. Chem. Soc.* **2016**, *138*, 4695–4705.
(80) Govindarajan, N.; Meijer, E. J. Elucidating Cation Effects in Homogeneously Catalyzed Formic Acid Dehydrogenation. *Faraday Discuss.* **2019**, *220*, 404–413.
(81) Ryu, H.; Park, J.; Kim, H. K.; Park, J. Y.; Kim, S.-T.; Baik, M.-H. Pitfalls in Computational Modeling of Chemical Reactions and How To Avoid Them. *Organometallics* **2018**, *37*, 3228–3239.
(82) Ahn, S.; Hong, M.; Sundararajan, M.; Ess, D. H.; Baik, M.-H. Design and Optimization of Catalysts Based on Mechanistic Insights Derived from Quantum Chemical Reaction Modeling. *Chem. Rev.* **2019**, *119*, 6509–6560.
(83) Laconsay, C. J.; Pla-Quintana, A.; Tantillo, D. J. Effects of Axial Solvent Coordination to Dirhodium Complexes on the Reactivity and Selectivity in C–H Insertion Reactions: A Computational Study. *Organometallics* **2021**, *40*, 4120–4132.
(84) Drago, R. S.; Long, J. R.; Cosmano, R. Metal Synergism in the Coordination Chemistry of a Metal-Metal Bonded System: $Rh_2(C_3H_7COO)_4$. *Inorg. Chem.* **1981**, *20*, 2920–2927.
(85) Warzecha, E.; Berto, T. C.; Berry, J. F. Axial Ligand Coordination to the C-H Amination. *Inorg. Chem.* **2015**, *54*, 8817–8824.
(86) Sheffield, W.; Abshire, A.; Darko, A. Effect of Tethered, Axial Thioether Coordination on Rhodium(II)-Catalyzed Silyl-Hydrogen Insertion. *Eur. J. Org. Chem.* **2019**, *2019*, 6347–6351.
(87) Cressy, D.; Zavala, C.; Abshire, A.; Sheffield, W.; Darko, A. Tuning Rh(II)-Catalysed Cyclopropanation with Tethered Thioether Ligands. *Dalt. Trans.* **2020**, *49*, 15779–15787.
(88) Rej, S.; Chatani, N. Effect of Sulfonamide and Carboxamide Ligands on the Structural Diversity of Bimetallic Rh. *Inorg. Chem.* **2021**, *60*, 3534–3538.
(89) Li, F.; Pei, C.; Koenigs, R. M. Rhodium-Catalyzed Cascade Reactions of Triazoles with Organoselenium Compounds – A Combined Experimental and Mechanistic Study. *Chem. Sci.* **2021**, *12*, 6362–6369.
(90) Nair, V. N.; Kojasoy, V.; Laconsay, C. J.; Kong, W. Y.; Tantillo, D. J.; Tambar, U. K. Catalyst-Controlled Regiodivergence in Rearrangements of Indole-Based Onium Ylides. *J. Am. Chem. Soc.* **2021**, *143*, 9016–9025.
(91) Roytman, V. A.; Singleton, D. A. Solvation Dynamics and the Nature of Reaction Barriers and Ion-Pair Intermediates in Carbocation Reactions. *J. Am. Chem. Soc.* **2020**, *142*, 12865–12877.
(92) Nakamura, E.; Yoshikai, N.; Yamanaka, M. Mechanism of C−H Bond Activation/C−C Bond Formation Reaction between Diazo Compound and Alkane Catalyzed by Dirhodium Tetracarboxylate. *J. Am. Chem. Soc.* **2002**, *124*, 7181–7192.
(93) Hansen, J.; Autschbach, J.; Davies, H. M. L. Computational Study on the Selectivity of Donor/Acceptor-Substituted Rhodium Carbenoids. *J. Org. Chem.* **2009**, *74*, 6555–6563.

(94) DeAngelis, A.; Panish, R.; Fox, J. M. Rh-Catalyzed Intermolecular Reactions of α-Alkyl-α-Diazo Carbonyl Compounds with Selectivity over β-Hydride Migration. *Acc. Chem. Res.* **2016**, *49*, 115–127.
(95) Lamb, K. N.; Squitieri, R. A.; Chintala, S. R.; Kwong, A. J.; Balmond, E. I.; Soldi, C.; Dmitrenko, O.; Castiñeira Reis, M.; Chung, R.; Addison, J. B.; Fettinger, J. C.; Hein, J. E.; Tantillo, D. J.; Fox, J. M.; Shaw, J. T. Synthesis of Benzodihydrofurans by Asymmetric C−H Insertion Reactions of Donor/Donor Rhodium Carbenes. *Chem. Eur. J.* **2017**, *23*, 11843–11855.
(96) Yang, L.-L.; Evans, D.; Xu, B.; Li, W.-T.; Li, M.-L.; Zhu, S.-F.; Houk, K. N.; Zhou, Q.-L. Enantioselective Diarylcarbene Insertion into Si–H Bonds Induced by Electronic Properties of the Carbenes. *J. Am. Chem. Soc.* **2020**, *142*, 12394–12399.
(97) Jagannathan, J. R.; Fettinger, J. C.; Shaw, J. T.; Franz, A. K. Enantioselective Si–H Insertion Reactions of Diarylcarbenes for the Synthesis of Silicon-Stereogenic Silanes. *J. Am. Chem. Soc.* **2020**, *142*, 11674–11679.
(98) Davies, H. M. L.; Bruzinski, P. R.; Lake, D. H.; Kong, N.; Fall, M. J. Asymmetric Cyclopropanations by Rhodium(II) N -(Arylsulfonyl)Prolinate Catalyzed Decomposition of Vinyldiazomethanes in the Presence of Alkenes. Practical Enantioselective Synthesis of the Four Stereoisomers of 2-Phenylcyclopropan-1-Amino Acid. *J. Am. Chem. Soc.* **1996**, *118*, 6897–6907.
(99) Doyle, M. P.; Forbes, D. C. Recent Advances in Asymmetric Catalytic Metal Carbene Transformations. *Chem. Rev.* **1998**, *98*, 911–935.
(100) Lebel, H.; Marcoux, J. F.; Molinaro, C.; Charette, A. B. Stereoselective Cyclopropanation Reactions. *Chem. Rev.* **2003**, *103* (4), 977–1050.
(101) Archambeau, A.; Miege, F.; Meyer, C.; Cossy, J. Intramolecular Cyclopropanation and C–H Insertion Reactions with Metal Carbenoids Generated from Cyclopropenes. *Acc. Chem. Res.* **2015**, *48*, 1021–1031.
(102) Green, A. I.; Tinworth, C. P.; Warriner, S.; Nelson, A.; Fey, N. Computational Mapping of Dirhodium(II) Catalysts. *Chem. Eur. J.* **2021**, *27*, 2402–2409.
(103) Clark, J. S.; Hansen, K. E. Intramolecular Reactions of Metal Carbenoids with Allylic Ethers: Is a Free Ylide Involved in Every Case? *Chem. Eur. J.* **2014**, *20*, 5454–5459.
(104) Zhang, Z.; Sheng, Z.; Yu, W.; Wu, G.; Zhang, R.; Chu, W. D.; Zhang, Y.; Wang, J. Catalytic Asymmetric Trifluoromethylthiolation via Enantioselective [2,3]-Sigmatropic Rearrangement of Sulfonium Ylides. *Nat. Chem.* **2017**, *9*, 970–976.
(105) Li, S.-S.; Wang, J. Cu(I)/Chiral Bisoxazoline-Catalyzed Enantioselective Sommelet–Hauser Rearrangement of Sulfonium Ylides. *J. Org. Chem.* **2020**, *85*, 12343–12358.
(106) Harrison, J. G.; Gutierrez, O.; Jana, N.; Driver, T. G.; Tantillo, D. J. Mechanism of Rh2(II)-Catalyzed Indole Formation: The Catalyst Does Not Control Product Selectivity. *J. Am. Chem. Soc.* **2016**, *138*, 487–490.
(107) Nickerson, L. A.; Bergstrom, B. D.; Gao, M.; Shiue, Y.-S.; Laconsay, C. J.; Culberson, M. R.; Knauss, W. A.; Fettinger, J. C.; Tantillo, D. J.; Shaw, J. T. Enantioselective Synthesis of Isochromans and Tetrahydroisoquinolines by C–H Insertion of Donor/Donor Carbenes. *Chem. Sci.* **2020**, *11*, 494–498.
(108) Jana, S.; Koenigs, R. M. Rhodium-Catalyzed Carbene Transfer Reactions for Sigmatropic Rearrangement Reactions of Selenium Ylides. *Org. Lett.* **2019**, *21*, 3653–3657.
(109) Liu, Z.; Jin, X.; Dang, Y. Mechanistic Studies of Copper(I)-Catalyzed Stereoselective [2,3]-Sigmatropic Rearrangements of Diazoesters with Allylic Iodides/Sulfides. *ACS Catal.* **2021**, *11*, 691–702.
(110) Xu, B.; Tambar, U. K. Copper-Catalyzed Enantio-, Diastereo-, and Regioselective [2,3]-Rearrangements of Iodonium Ylides. *Angew. Chem. Int. Ed.* **2017**, *56*, 9868–9871.
(111) Schmid, S. C.; Guzei, I. A.; Schomaker, J. M. A Stereoselective [3+1] Ring Expansion for the Synthesis of Highly Substituted Methylene Azetidines. *Angew. Chem. Int. Ed.* **2017**, *56*, 12229–12233.
(112) Schmid, S. C.; Guzei, I. A.; Fernández, I.; Schomaker, J. M. Ring Expansion of Bicyclic Methyleneaziridines via Concerted, Near-Barrierless [2,3]-Stevens Rearrangements of

Aziridinium Ylides. *ACS Catal.* **2018**, *8*, 7907–7914.
(113) Stevens, T. S.; Creighton, E. M.; Gordon, A. B.; MacNicol, M. Degradation of Quaternary Ammonium Salts. Part I. *J. Chem. Soc.* **1928**, 3193–3197.
(114) Vanecko, J. A.; Wan, H.; West, F. G. Recent Advances in the Stevens Rearrangement of Ammonium Ylides. Application to the Synthesis of Alkaloid Natural Products. *Tetrahedron* **2006**, *62*, 1043–1062.
(115) Baidilov, D. On the Mechanism of the Stevens Rearrangement. *Synth.* **2020**, *52*, 21–26.
(116) Empel, C.; Jana, S.; Koenigs, R. M. Advances in [1,2]-Sigmatropic Rearrangements of Onium Ylides via Carbene Transfer Reactions. *Synthesis* **2021**, *53*, 4567–4587.
(117) Cammarota, R. C.; Liu, W.; Bacsa, J.; Davies, H. M. L.; Sigman, M. S. Mechanistically Guided Workflow for Relating Complex Reactive Site Topologies to Catalyst Performance in C–H Functionalization Reactions. *J. Am. Chem. Soc.* **2022**, *144*, 1881–1898.
(118) DeAngelis, A.; Dmitrenko, O.; Yap, G. P. A.; Fox, J. M. Chiral Crown Conformation of Rh_2(S-PTTL)$_4$: Enantioselective Cyclopropanation with α-Alkyl-α-Diazoesters. *J. Am. Chem. Soc.* **2009**, *131*, 7230–7231.
(119) Ghanem, A.; Gardiner, M. G.; Williamson, R. M.; Müller, P. First X-Ray Structure of a N -Naphthaloyl-Tethered Chiral Dirhodium(II) Complex: Structural Basis for Tether Substitution Improving Asymmetric Control in Olefin Cyclopropanation. *Chem. Eur. J.* **2010**, *16*, 3291–3295.
(120) DeAngelis, A.; Boruta, D. T.; Lubin, J.-B.; Plampin, III, J. N.; Yap, G. P. A.; Fox, J. M. The Chiral Crown Conformation in Paddlewheel Complexes. *Chem. Commun.* **2010**, *46*, 4541.
(121) Jana, S.; Yang, Z.; Pei, C.; Xu, X.; Koenigs, R. M. Photochemical Ring Expansion Reactions: Synthesis of Tetrahydrofuran Derivatives and Mechanism Studies. *Chem. Sci.* **2019**, *10*, 10129–10134.
(122) Davies, H. M. L.; Manning, J. R. Catalytic C-H Functionalization by Metal Carbenoid and Nitrenoid Insertion. *Nature* **2008**, *451*, 417–424.
(123) Davies, H. M. L.; Lian, Y. The Combined C–H Functionalization/Cope Rearrangement: Discovery and Applications in Organic Synthesis. *Acc. Chem. Res.* **2012**, *45*, 923–935.
(124) Combs, J. R.; Lai, Y.; Vranken, D. L. Van. Tandem Insertion/[3,3]-Sigmatropic Rearrangement Involving the Formation of Silyl Ketene Acetals by Insertion of Rhodium Carbenes into S − Si Bonds. *Org. Lett.* **2021**, *23*, 2841–2845.
(125) Hansen, J. H.; Gregg, T. M.; Ovalles, S. R.; Lian, Y.; Autschbach, J.; Davies, H. M. L. On the Mechanism and Selectivity of the Combined C−H Activation/Cope Rearrangement. *J. Am. Chem. Soc.* **2011**, *133*, 5076–5085.
(126) Ess, D. H.; Wheeler, S. E.; Iafe, R. G.; Xu, L.; Çelebi-Ölçüm, N.; Houk, K. N. Bifurcations on Potential Energy Surfaces of Organic Reactions. *Angew. Chem. Int. Ed.* **2008**, *47*, 7592–7601.
(127) Caramella, P.; Quadrelli, P.; Toma, L. An Unexpected Bispericyclic Transition Structure Leading to 4+2 and 2+4 Cycloadducts in the Endo Dimerization of Cyclopentadiene. *J. Am. Chem. Soc.* **2002**, *124*, 1130–1131.
(128) Hare, S. R.; Tantillo, D. J. Dynamic Behavior of Rearranging Carbocations - Implications for Terpene Biosynthesis. *Beilstein J. Org. Chem.* **2016**, *12*, 377–390.
(129) Tantillo, D. J. Dynamic Effects on Organic Reactivity—Pathways to (and from) Discomfort. *J. Phys. Org. Chem.* **2021**, *34*, 1–9.
(130) Tantillo, D. J. *Beyond Transition State Theory—Non-Statistical Dynamic Effects for Organic Reactions*, 1st ed.; Elsevier Ltd., 2021.
(131) Hare, S. R.; Tantillo, D. J. Cryptic Post-Transition State Bifurcations That Reduce the Efficiency of Lactone-Forming Rh-Carbenoid C-H Insertions. *Chem. Sci.* **2017**, *8*, 1442–1449.
(132) Eun, L.; Kyung, W. J.; Yong, S. K. Selectivity in the Lactone Formation via C-H Insertion Reaction of Diazomalonates. *Tetrahedron Lett.* **1990**, *31*, 1023–1026.
(133) Watson, W. On Byproducts and Side Products. *Org. Process Res. Dev.* **2012**, *16*, 1877–

1877.
(134) Chuang, H.-H.; Tantillo, D. J.; Hsu, C.-P. Construction of Two-Dimensional Potential Energy Surfaces of Reactions with Post-Transition-State Bifurcations. *J. Chem. Theory Comput.* **2020**, *16*, 4050–4060.
(135) Lee, S.; Goodman, J. M. Rapid Route-Finding for Bifurcating Organic Reactions. *J. Am. Chem. Soc.* **2020**, *142*, 9210–9219.
(136) Lee, S.; Goodman, J. M. VRAI-Selectivity: Calculation of Selectivity beyond Transition State Theory†. *Org. Biomol. Chem.* **2021**, *19*, 3940–3947.
(137) Ang, S. J.; Wang, W.; Schwalbe-Koda, D.; Axelrod, S.; Gómez-Bombarelli, R. Active Learning Accelerates Ab Initio Molecular Dynamics on Reactive Energy Surfaces. *Chem* **2021**, *7*, 738–751.
(138) Hong, Y. J.; Tantillo, D. J. Biosynthetic Consequences of Multiple Sequential Post-Transition-State Bifurcations. *Nat. Chem.* **2014**, *6*, 104–111.
(139) Patel, A.; Chen, Z.; Yang, Z.; Gutiérrez, O.; Liu, H.-W.; Houk, K. N.; Singleton, D. A. Dynamically Complex [6+4] and [4+2] Cycloadditions in the Biosynthesis of Spinosyn A. *J. Am. Chem. Soc.* **2016**, *138*, 3631–3634.
(140) Yang, Z.; Dong, X.; Yu, Y.; Yu, P.; Li, Y.; Jamieson, C.; Houk, K. N. Relationships between Product Ratios in Ambimodal Pericyclic Reactions and Bond Lengths in Transition Structures. *J. Am. Chem. Soc.* **2018**, *140*, 3061–3067.
(141) Yang, Z.; Yang, S.; Yu, P.; Li, Y.; Doubleday, C.; Park, J.; Patel, A.; Jeon, B. sun; Russell, W. K.; Liu, H. wen; et al. Influence of Water and Enzyme SpnF on the Dynamics and Energetics of the Ambimodal [6+4]/[4+2] Cycloaddition. *Proc. Natl. Acad. Sci. U. S. A.* **2018**, *115*, E848–E855.
(142) Zhang, B.; Wang, K. B.; Wang, W.; Wang, X.; Liu, F.; Zhu, J.; Shi, J.; Li, L. Y.; Han, H.; Xu, K.; et al. Enzyme-Catalysed [6+4] Cycloadditions in the Biosynthesis of Natural Products. *Nature* **2019**, *568*, 122–126.
(143) Jamieson, C. S.; Ohashi, M.; Liu, F.; Tang, Y.; Houk, K. N. The Expanding World of Biosynthetic Pericyclases: Cooperation of Experiment and Theory for Discovery. *Nat. Prod. Rep.* **2019**, *36*, 698–713.
(144) Zhang, C.; Wang, X.; Chen, Y.; He, Z.; Yu, P.; Liang, Y. Dynamical Trajectory Study of the Transannular [6+4] and Ambimodal Cycloaddition in the Biosynthesis of Heronamides. *J. Org. Chem.* **2020**, *85*, 9440–9445.
(145) Wang, X.; Zhang, C.; Jiang, Y.; Wang, W.; Zhou, Y.; Chen, Y.; Zhang, B.; Tan, R. X.; Ge, H. M.; Yang, Z. J.; et al. Influence of Water and Enzyme on the Post-Transition State Bifurcation of NgnD-Catalyzed Ambimodal [6+4]/[4+2] Cycloaddition. *J. Am. Chem. Soc.* **2021**, *143*, 27.
(146) Hare, S.; Bratholm, L.; Glowacki, D.; Carpenter, B. Low Dimensional Representations Along Intrinsic Reaction Coordinates and Molecular Dynamics Trajectories Using Interatomic Distance Matrices. *Chem. Sci.* **2019**, *10*, 9954–9968.
(147) Grimme, S.; Schreiner, P. R. Computational Chemistry: The Fate of Current Methods and Future Challenges. *Angew. Chem. Int. Ed.* **2018**, *57*, 4170–4176.
(148) Neese, F.; Atanasov, M.; Bistoni, G.; Maganas, D.; Ye, S. Chemistry and Quantum Mechanics in 2019: Give Us Insight and Numbers. *J. Am. Chem. Soc.* **2019**, *141*, 2814–2824.
(149) Durand, D. J.; Fey, N. Computational Ligand Descriptors for Catalyst Design. *Chem. Rev.* **2019**, *119*, 6561–6594.
(150) Durand, D. J.; Fey, N. Building a Toolbox for the Analysis and Prediction of Ligand and Catalyst Effects in Organometallic Catalysis. *Acc. Chem. Res.* **2021**, *54*, 837–848.
(151) C. Gallegos, L.; Luchini, G.; C. St. John, P.; Kim, S.; S. Paton, R. Importance of Engineered and Learned Molecular Representations in Predicting Organic Reactivity, Selectivity, and Chemical Properties. *Acc. Chem. Res.* **2021**, *54*, 827–836.
(152) Janet, J. P.; Duan, C.; Nandy, A.; Liu, F.; Kulik, H. J. Navigating Transition-Metal Chemical Space: Artificial Intelligence for First-Principles Design. *Acc. Chem. Res.* **2021**, *54*, 532–545.

(153) dos Passos Gomes, G.; Pollice, R.; Aspuru-Guzik, A. Navigating through the Maze of Homogeneous Catalyst Design with Machine Learning. *Trends Chem.* **2021**, *3*, 96–110.

Chapter 3

Metal Bound or Free Ylides as Reaction Intermediates in Metal-Catalyzed [2,3]-Sigmatropic Rearrangements? It Depends*

Should I stay or should I go now? / If I go there will be trouble/ And if I stay it will be double / So you got to let me know / Should I stay or should I go?

- The Clash

3.1 Abstract

Density functional theory calculations were applied to study four previously published metal-catalyzed [2,3]-rearrangements from onium ylide intermediates, in pursuit of generalizations about when, during these types of reactions, catalysts dissociate. Our results corroborate past studies where free ylide mechanisms were proposed to be operative. Results of calculations on case studies indicate that the origin of metal-catalyst dissociation can be attributed primarily to the steric bulkiness of functional groups adjacent to the carbene carbon.

* This chapter is a modified version of the following published article: Laconsay, C. J.; Tantillo, D. J. Metal Bound or Free Ylides as Reaction Intermediates in Metal-Catalyzed [2,3]-Sigmatropic Rearrangements? It Depends, *ACS Catalysis* **2021**, *11*, 829-839 with permission from the American Chemical Society. Copyright 2021 American Chemical Society.

3.2 Introduction

3.2.1 Ylide Formation/[2,3]-Sigmatropic Rearrangements

Sigmatropic rearrangement reactions hold a privileged position in the synthetic organic chemist's toolbox for forming new carbon-carbon/carbon-heteroatom bonds. Ylide formation/[2,3]-sigmatropic rearrangement tandem reactions, or 'duets',[1] have gained attention as an important tool for synthesizing heteroatom-containing compounds with high stereochemical fidelity. Of the two main methodologies for generating ylide intermediates for these reactions, the transition-metal catalyzed variant is milder than base-promoted methodologies.[2,3] One question that remains unanswered for many transition-metal-catalyzed ylide formation/[2,3]-sigmatropic rearrangement reactions (from here on, just 'ylide rearrangements' for simplicity) is whether the catalyst is explicitly bound to the ylide during the [2,3]-rearrangement step.[2–5] Does the metal catalyst remain covalently bound (what we refer to as 'metal-bound') to the substrate or dissociate (what we refer to as a 'free-ylide' or 'metal-unbound' if the metal catalyst is nearby, but not covalently bonded to, the substrate) before the rearrangement step? This question has implications for stereoselectivity[6] and regioselectivity,[7] because whether the metal catalysts are able to effectively pass on chiral information depends on whether the catalyst is bound to its substrate during the stereodetermining step(s).[6,8] For example, in a selective Au(I)-catalyzed C-H functionalization reaction of *N*-heterocycles, Koenigs and coworkers demonstrated, using density functional theory (DFT) calculations and control experiments, that the key proton shuttle step in the mechanism likely does not involve a Au-complex—the catalyst likely dissociates before the rate-determining (last) step.[9]

3.2.2 The Role of Dirhodium Metal Carbenes

The combination of steps from reactant to product and concomitant regeneration of catalyst is called the catalytic cycle, and it is, often implicitly, assumed (at least in organometallic chemistry textbooks)[10,11] that the catalyst remains bound to its substrate until the end of the cycle, when it releases the product and binds another reactant. Although this may be true for many catalytic cycles, we focus here on cases in which this assumption is not valid—specifically, reactions promoted by dirhodium tetracarboxylate catalysts.

Chemists have made strides in stereoselective ylide rearrangements with electrophilic metal carbenes: not only are these reactions highly stereoselective, but they often show excellent chemo- and regioselectivities.[8,12–20] The focus on metal carbenes[21] for this reaction, and in particular, rhodium (Rh) carbenes generated *in situ* from diazo compounds and metal catalyst,[22–26] has in large part been motivated by the ability to control stereoselectivity by exploiting different chiral ligands. Rh carbenes[24] are now commonplace in organic synthesis and especially useful in C-H functionalization. They are often categorized into five main groups: i.e. (1) acceptor,[27,28] (2) acceptor/acceptor,[14,29] (3) donor/acceptor,[26,30,31] (4) donor,[32] and (5) donor/donor[33–38] (Scheme 3.1a), depending on the electron withdrawing or donating ability of substituents adjacent to the carbene center. This versatility in functional group discretion enables one to fine-tune the reactivity and selectivity of the carbene intermediate, which make Rh carbenes amenable to a wide range of chemical transformations. Due to the electrophilicity of the metal-carbene intermediates bearing electron-withdrawing substituents, acceptor, acceptor/acceptor and donor/acceptor compounds are typically used in ylide rearrangements.[20] Presumably safety factors, including thermal stability and ease of handling under desired reaction conditions, play a significant role as well—note the recent article by Green *et al.* on the thermal stability and explosive hazards of diazo compounds.[39]

Alternatives to metal catalysts and diazo compounds involve forming the ylide by deprotonation with a strong base—for instance, Tambar's palladium-catalyzed allylic substitution chemistry,[40] or Smith's isothiourea-catalyzed [2,3]-rearrangement.[41,42] Low-energy light induced carbene transfer reactions have also been explored by Koenigs's group as a viable method for ylide formations posed to undergo subsequent rearrangement[43,44] and other reactivity.[45] With exception to these examples, the use of metal carbenes from diazo precursors have generally guided much of the stereoselective ylide rearrangements—albeit, up until recently,[4] with only modest enantioselectivity. We focus our efforts herein, therefore, on Rh-catalyzed ylide rearrangements.

Scheme 3.1 (a) Five Major Classes of Rh Carbenes and (b) Rh Catalyst: Should It "Stay", or Should It "Go"?

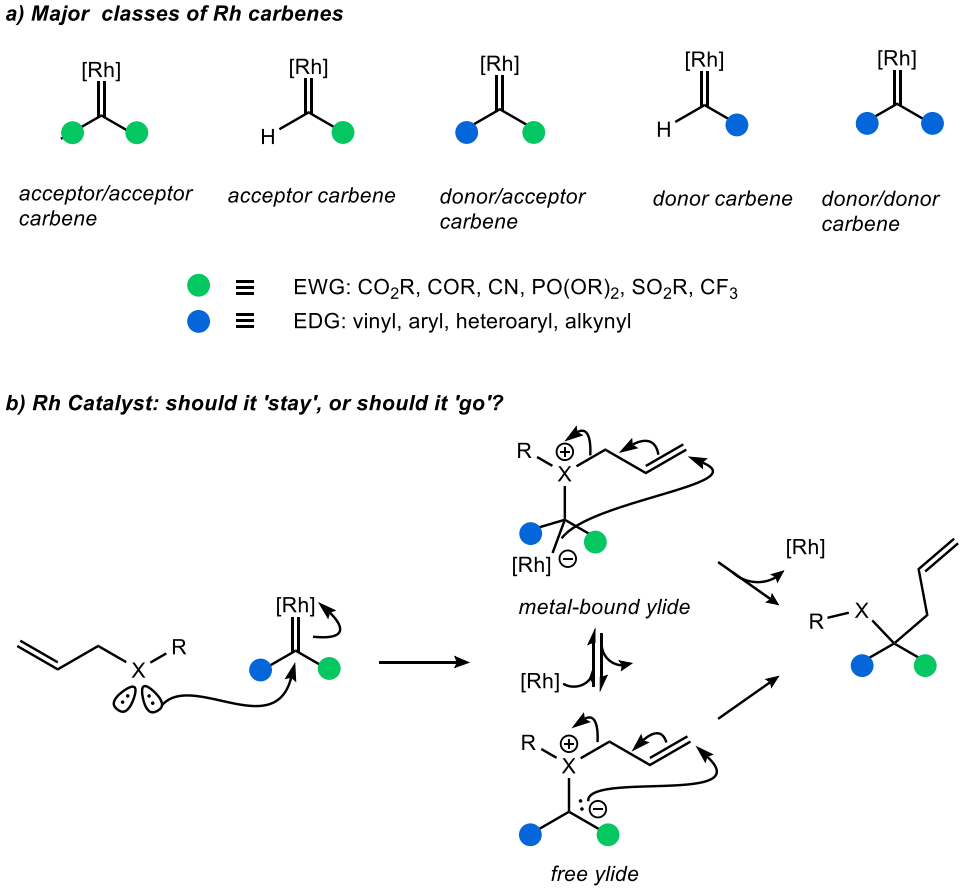

Metal-promoted ylide formation can occur between a metal-carbene and a Lewis-basic heteroatom such as nitrogen, oxygen, sulfur, selenium, and iodine to form ammonium,[46] oxonium,[18,47–57] sulfonium,[58–65] selenonium,[66–68] and iodonium ylides,[69] respectively (Scheme 3.1b).[70] Subsequent rearrangements from the onium ylide can ensue thereafter (or not[62]), and the type of rearrangement depends on the groups attached to the heteroatom.[*] Rearrangements that can occur from ylide intermediates include the Doyle-Kirmse rearrangement (i.e., [2,3]-rearrangement from ylides of allylic sulfides),[2,58,71–73] the Stevens rearrangement (i.e., [1,2]-rearrangement of onium ylides),[74–76] and the Sommelet-Hauser rearrangement (i.e., [2,3]-rearrangement with an aromatic ring as a π-component) rearrangements.[77–81]

Detailed understanding of the role of the metal catalyst in these types of reaction is needed for future design of new catalysts and for studies on origins of stereoselectivity.[82] This imperative applies not only to the onium ylide types mentioned above. For instance, the Schomaker group has reported that carbene-generated aziridinium ylides generate metal-free ylide intermediates after metal dissociation.[83] Experimental groups have expressed the need for quantum chemical studies to corroborate conclusions arrived at by control experiments that support free-ylide mechanisms for onium ylide [2,3]-sigmatropic rearrangement and [1,2]-sigmatropic rearrangement reactions.[2,4,5,60,67,84] Whether recently described selenonium ylide analogues are Rh-bound or 'free' has yet to be explored as well. Previously, our group demonstrated through DFT calculations that a free ylide pathway is energetically favored over a metal-bound ylide pathway in Rh(II)-promoted indole formation of vinyl/azidoarenes (Scheme 3.2a).[85] We also recently collaborated with the

[*] Non-statistical dynamic effects can complicate [1,2]- and [2,3]-rearrangement product selectivity, as Singleton demonstrated for ammonium ylides.[101]

Shaw group and discovered an unexpected concerted,* metal-unbound (or free-ylide) Stevens rearrangement resulting in an isoindoline product during attempts to synthesize tetrahydroisoquinolines with donor/donor Rh-carbenes (Scheme 3.2b).[33]

Scheme 3.2 Precedent for free ylide intermediates from computational studies.

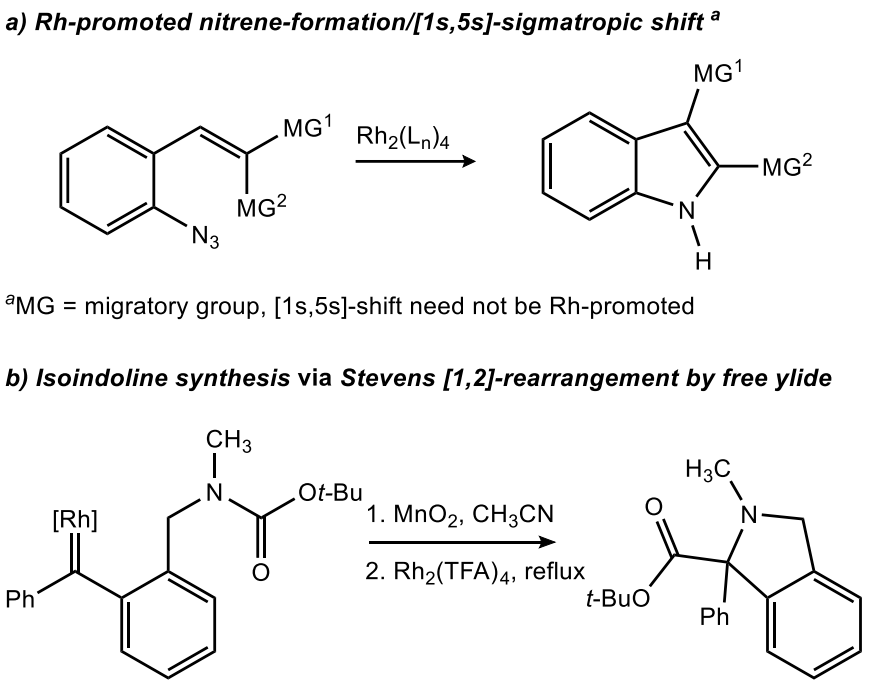

3.2.3 Aim of This Study

Against this backdrop, we investigate whether Rh catalysts remain covalently bound or heterolytically dissociate before the [2,3]-sigmatropic-rearrangement step in ylide rearrangements. We first discuss DFT calculations for three previously reported reactions as case studies. We begin

* Unexpected because Stevens rearrangements from quaternary ammonium ylides are typically discussed in the literature as going through stepwise, homolytic cleavage/recombination (radical-pair type) processes.[102,103]

with a reaction involving an oxonium ylide by Clark and Hansen[82] and "walk" down group 16 (the chalcogens) of the periodic table to a reaction involving a sulfonium ylide example by Wang and coworkers[4] and, finally, end with an example of a reaction by Jana and Koenigs involving a selenonium ylide.[68] Then, we discuss our designed study based on Jana and Koenigs's selenonium ylide intermediate: varying the electronic and steric nature of the ylide, we find under what conditions the Rh-catalyst remains bound in our computations. We close with a comparison to a recently reported Au-catalyzed [2,3]-rearrangement reaction.[86]

3.3 Computational Methods

DFT calculations were carried out in *Gaussian 09*.[87] Transition-state structures (TSSs) were verified with frequency calculations and by identifying one imaginary frequency. Minima were verified as such by the absence of imaginary frequencies. Intrinsic Reaction Coordinate (IRC) calculations[88,89] were used to further characterize TSSs.[88–90] We carried out geometry optimizations at the unrestricted B3LYP level of DFT with the LANL2DZ basis set for Rh and 6-31G(d) for all other atoms—i.e., uB3LYP/LANL2DZ[6-31G(d)] and one case in which we used a triple-zeta basis set (involving Se). The B3LYP functional has proven to be sufficient in successfully modeling experimentally relevant geometries and energies in past studies on related chemistry.[33,85,91,92] To ensure that relative free energies are reasonable, we conducted unrestricted single-point calculations at the B3LYP-D3(BJ) and ωB97X-D[93] level to account for dispersion.[94,95] These calculations also made use of a larger basis set (LANL2DZ[6-31+G(d,p)]). A data set

collection of computational results is available in the ioChem-BD repository[96] and can be accessed via https://doi.org/10.19061/iochem-bd-6-68.*

3.4 Results and Discussion

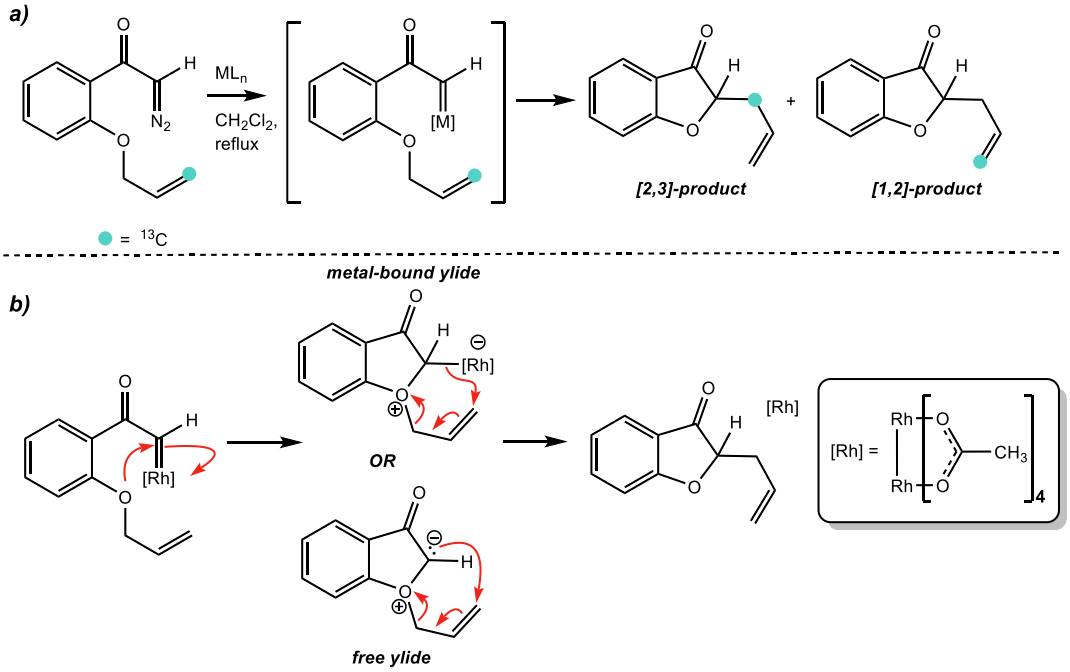

Figure 3.1 Metal-catalyzed oxonium-ylide rearrangement to benzofuranones by Clark and Hansen, [M] = Rh(II)- and Cu(II)-catalysts.[82] a) ^{13}C-labelled experiments predict that [2,3]- to [1,2]-product ratio is dependent on the nature of Rh catalyst, favoring the [2,3]-product b) system modeled here with DFT calculations, where [Rh] = $Rh_2(OAc)_4$.

3.4.1 Oxonium Ylide

Clark and Hansen performed ^{13}C-labelling studies to gain insight into the mechanism of a metal-catalyzed ylide rearrangement of diazo ketone substrates to benzofuranones, a reaction that had

* A discussion of computational benchmark tests is described in the Supporting Information of *ACS Catalysis* **2021**, *11*, 829-839. See p. S3-S7.

been previously studied by Pirrung and Werner using dirhodium(II) acetate[97] and similar to a reaction studied by Hashimoto and coworkers.[55] Expanding on this methodology, Clark and Hansen used Cu, Ir, and Rh complexes—[$Cu(acac)_2$] (acac = actetylacetonate), [{$Ir(cod)Cl\}_2$] and $Rh_2(OAc)_4$, among other similar catalysts (Figure 3.1).[82] Determining the ratio of the ^{13}C-labelled [1,2]- and [2,3]-products by ^1H and ^{13}C NMR spectroscopy, they observed a dependence of the ratio on the type of Rh-catalyst used. These results are inconsistent with a mechanism that forms a free oxonium ylide. Either the reaction undergoes a metal-bound ylide or alternative non-ylide pathway. Is the conclusion that the rhodium-catalyzed reaction involves a metal-bound ylide supported by DFT calculations?[5]

We modeled both the free ylide mechanism and the metal-bound mechanism with DFT calculations starting from the metal-bound ylide (Figure 3.2), where the metal catalyst here, and from here on in the manuscript, is $Rh_2(OAc)_4$. We predict that the free ylide mechanism is kinetically unfavorable compared to the metal-bound ylide mechanism by at least 2 kcal mol^{-1} ($\Delta\Delta G^{\ddagger}$ = 3.8 kcal mol^{-1}), which is consistent with the conclusions made by Clark and Hansen. Intrinsic reaction coordinate calculations confirm that the Rh catalyst remains bound to the substrate in the metal-bound pathway.[*]

[*] IRC data are described in the Supporting Information of *ACS Catalysis* **2021**, *11*, 829-839. See Figure S11, p. S16.

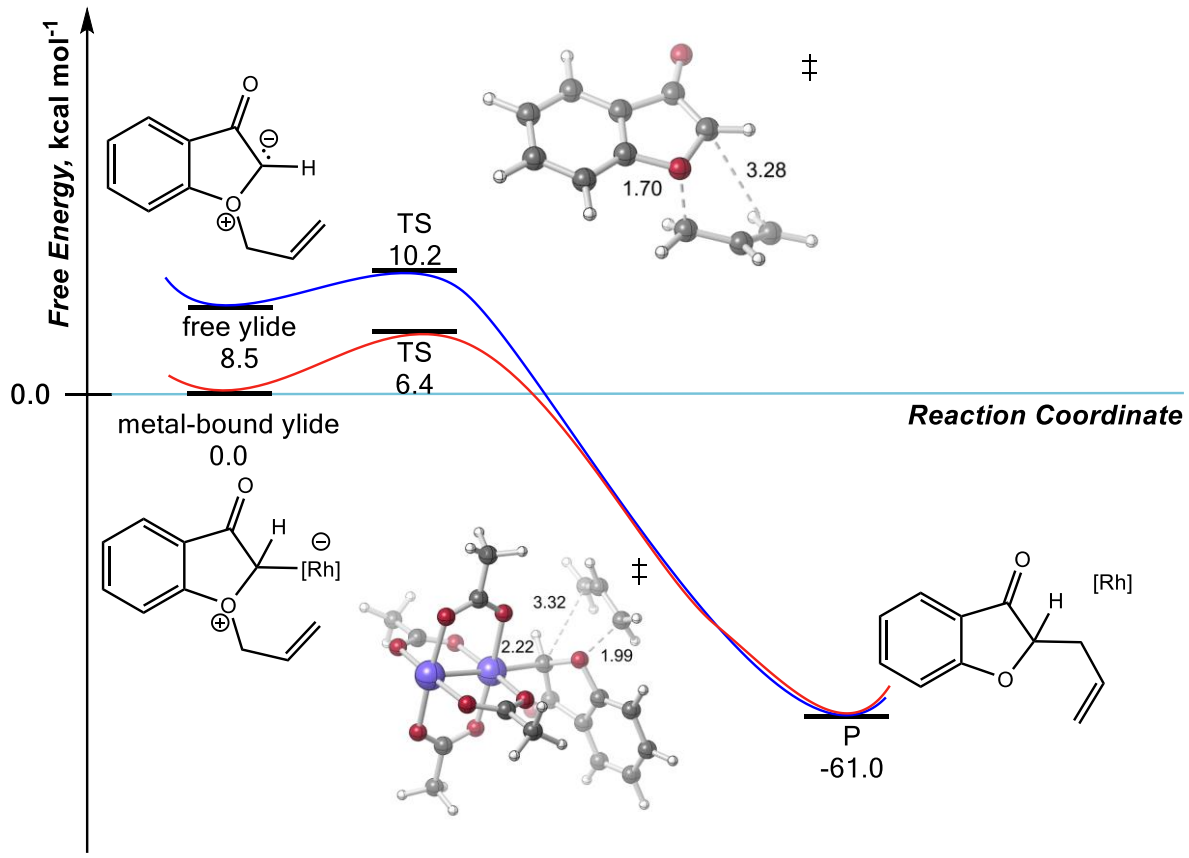

Figure 3.2 Energy profile for oxonium-ylide [2,3]-rearrangement step in the intramolecular cyclization to form benzofuranones (by Clark and Hansen).[82] Free energies (in kcal mol^{-1}) are reported at the B3LYP/LANL2DZ[6-31G(d)] level.

3.4.2 Sulfonium Ylide

The transition-metal catalyzed [Rh(II) or Cu(I)] reaction that generates a sulfonium ylide prior to a [2,3]-sigmatropic rearrangement is known as the Doyle-Kirmse reaction. Wang and coworkers[4] recently reported a highly enantioselective metal carbene-catalyzed Doyle-Kirmse reaction based on previous work by Uemura and coworkers.[98] Whether the [2,3]-sigmatropic rearrangement step in this mechanism involves the metal-catalyst bound to the substrate remains unclear. Wang and coworkers dedicated a substantial portion of their study to control experiments to address this

ambiguity. They concluded from experiments that their asymmetric trifluoromethylthiolation *via* an enantioselective Doyle-Kirmse reaction likely undergoes a free-ylide mechanism (Figure 3.3).

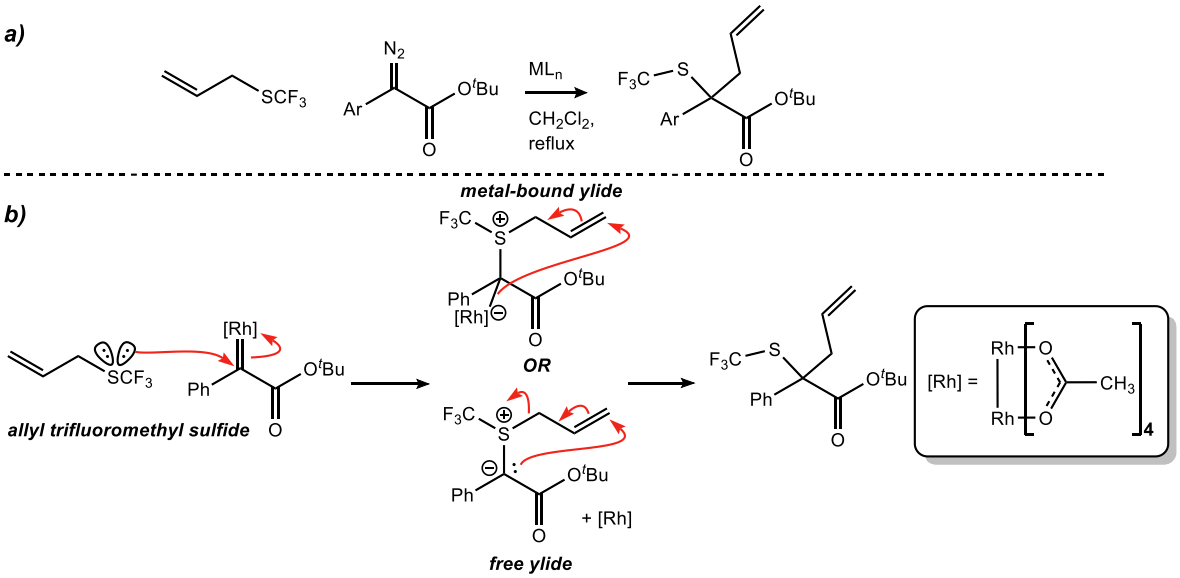

Figure 3.3 a) asymmetric Rh-catalyzed sulfonium-ylide rearrangement (Doyle-Kirmse reaction) by Wang and coworkers[4] where ML_n = Rh(II)- and Cu(I)-catalysts b) system modeled here with DFT calculations, where [Rh] = $Rh_2(OAc)_4$.

Our DFT results support a free ylide mechanism. Every attempt to locate a TSS that corresponds to a metal-bound structure failed. Specifically, potential energy scans resulted in the Rh catalyst dissociating from the ylide carbon and associating with a π-face of the aryl ring. It is unlikely that alternative Rh catalysts with bulkier ligands would diverge from this result. Attempts to find a [2,3]-rearrangement TSS with the Rh catalyst unbound resulted in the so-called "metal-unbound ylide" TSS shown in Figure 3.4. Intrinsic reaction coordinate calculations from this TSS led to a metal-unbound ylide.* Rh-catalyzed Doyle-Kirmse reactions using propargyl sulfides were also tested in the original experimental paper.[4] We modeled the [2,3]-rearrangement for these

* Ibid, S16 (see Figure S12).

substrates and find similar results to that of Figure 3.4—no Rh-bound rearrangement TSS could be located.*

Loss of Rh catalyst to form the free ylide is predicted to be energetically favorable by >20 kcal mol^{-1}. Activation barriers from either the free ylide (blue) or the metal-unbound ylide (red) are comparable (~10 kcal mol^{-1}), which can be attributed to the fact that the metal-unbound ylide is effectively a free ylide with the metal catalyst as a nearby spectator. Unlike the oxonium ylide system discussed earlier, however, these results suggest that this sulfonium ylide prefers to dissociate from the metal catalyst first, and then undergoes the rearrangement step.

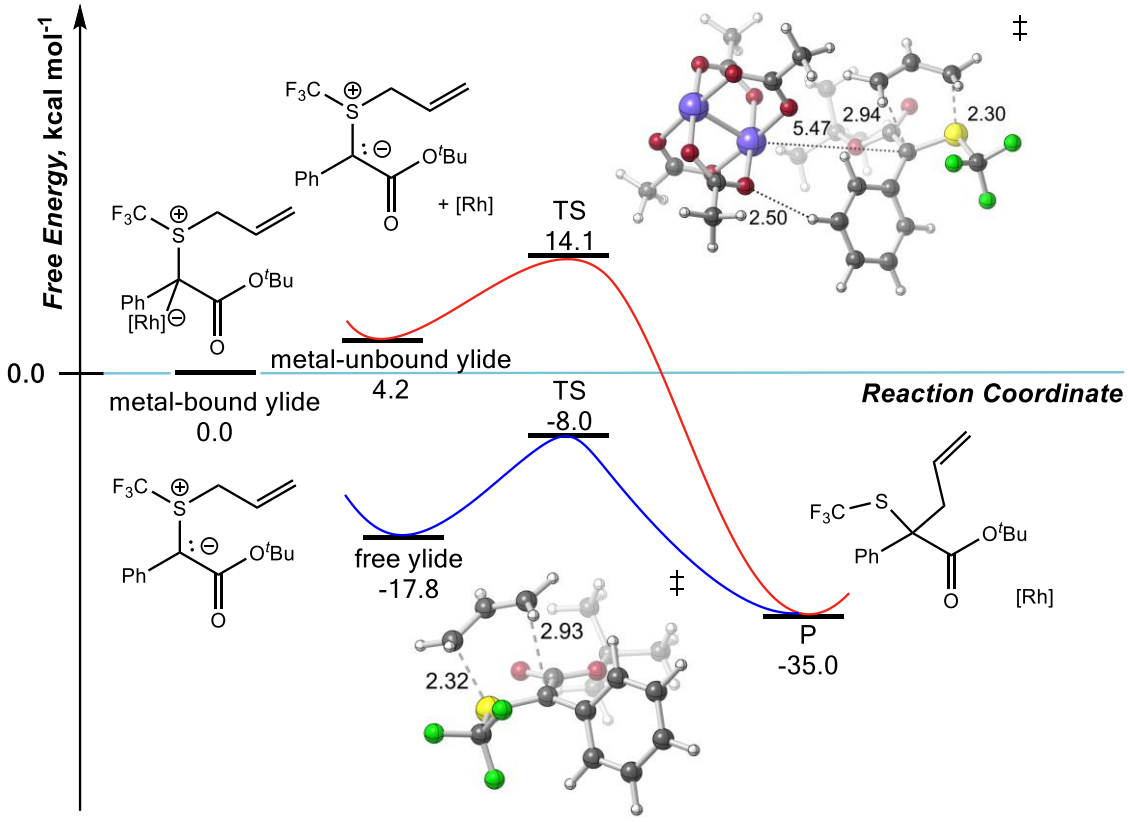

Figure 3.4. Energy profile for sulfonium-ylide [2,3]-rearrangement step in the Doyle-Kirmse reaction (by Wang and coworkers).[4] Free energies (in kcal mol^{-1}) are reported at the B3LYP/LANL2DZ[6-31G(d)] level.

* Ibid, S13 and S15 (see Figure S10 and Table S3).

3.4.3 Selenonium Ylide

Although discussed less frequently in the literature, selenonium ylides also can undergo rearrangements.[99] These are effectively Doyle-Kirmse rearrangements with selenium in place of sulfur. Jana and Koenigs demonstrated this reaction recently using diazoalkanes and allyl selenides to generate homoallyl selenides (Figure 3.5).[68]

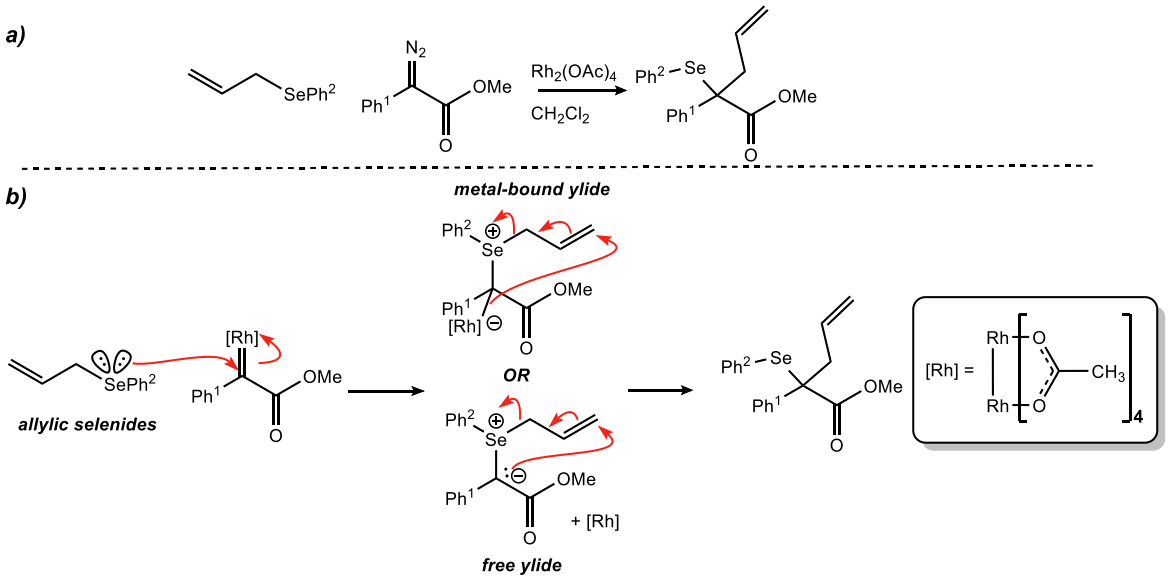

Figure 3.5 a) asymmetric Rh-catalyzed selenonium-ylide rearrangement (Doyle-Kirmse reaction) by Jana and Koenigs[68] where ML_n = $Rh_2(OAc)_4$ b) system modeled here with DFT calculations, where [Rh] = $Rh_2(OAc)_4$.

They observed that the selectivity is only slightly affected by the type of catalyst, lending support to the hypothesis that this reaction undergoes a free-ylide mechanism. Is this conclusion borne out in DFT calculations?

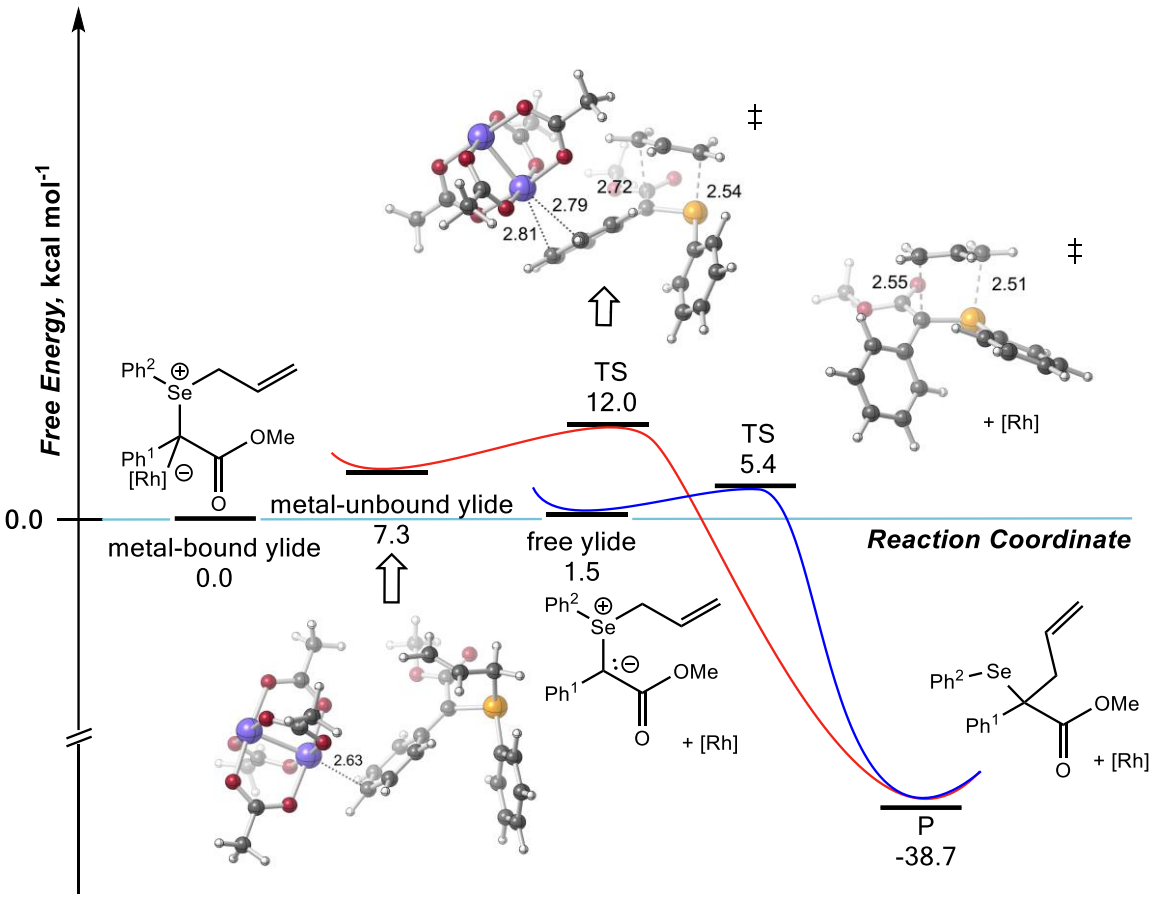

Figure 3.6 Energy profile for Rh-unbound and free ylide selenonium-ylide [2,3]-rearrangement step in the Doyle-Kirmse reaction (by Jana and Koenigs).[68] Free energies (in kcal mol^{-1}) are reported at the B3LYP/LANL2DZ[6-311G(d)]//B3LYP/LANL2DZ[6-31G(d)] level for structures including Rh and B3LYP/6-311G(d)//B3LYP/6-31G(d) without Rh.*

Yes. Only a metal-dissociated TSS for the [2,3]-sigmatropic rearrangement could be located and all attempts to find a TSS with the metal bound resulted in the metal catalyst dissociating before the TSS (Figure 3.6). The free ylide pathway is energetically viable (only a 5.4 kcal mol^{-1} barrier to product), supporting the conclusion the free ylide intermediates can undergo the rearrangement step.† As we observed in the sulfonium ylide system by Wang and coworkers

* Ibid, S6 (see Table S0).
† Ibid, S5 (further discussion on relative energies of Figure 3.6 is described in the SI).

(*vide supra*), TSS searches for a [2,3]-rearrangement TSSs with the Rh covalently bound resulted in only a catalyst-unbound TSS, with the Rh-catalyst associated to the aryl ring (Ph^1). On the surface, these results suggest that for both the sulfonium and selenonium cases, only free ylide mechanisms are energetically viable and something about these two cases prevents the Rh catalyst from remaining bound to its substrate prior to rearrangement.

These specific examples of rearrangement for each ylide type (oxonium, sulfonium, and selenonium) should not be generalized to all similar ylides undergoing [2,3]-rearrangements. However, our results support past experimental results that proposed free-ylide mechanisms based on cross-over experiments.

3.4.4 Beyond Donor-Acceptor Carbenes—Studies for Understanding the Origin of Dissociation

To understand why there is a preference for the Rh catalyst to remain covalently bound in the oxonium case, but heterolytically dissociate in the sulfonium and selenonium cases, we used the system studied by Jana and Koenigs (X = Se, Figures 3.5 and 3.6) as a case study. We explored how the electronic nature of the carbene center would influence the metal-bound ylide/free ylide equilibrium. In Koenigs's study,[68] an electrophilic carbene with at least one electron-withdrawing group (donor-acceptor) is used, and in most [2,3]-rearrangements from diazo compound-derived ylide intermediates, this is the case.[3,20] Although, to our knowledge, donor-donor and donor diazo compounds have not been used in these specific reactions, we can study the effects of such compounds computationally.

Of the five Rh carbene types (acceptor, acceptor/acceptor, donor/donor, donor/acceptor, and donor) studied here, which ones prefer to dissociate Rh catalyst prior to the [2,3]-sigmatropic

shift (Scheme 3.3)? We located a metal-bound [2,3]-rearrangement with the Rh catalyst explicitly bound to the carbene carbon in the acceptor and donor carbene cases only, and only for carbene intermediates in which one of the substituents adjacent to the carbene carbon was hydrogen (Table 3.1). However, even these systems exhibited lower-energy rearrangement pathways with Rh unbound (i.e., we predict free ylides are operative).

Scheme 3.3 Five types of Rh carbenes studied in [2,3]-sigmatropic rearrangement step.

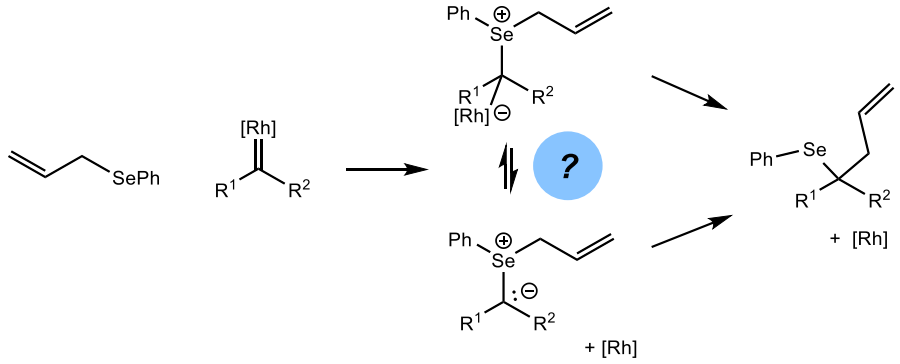

Acceptor-Acceptor (AA): $R^1 = CO_2Me$, $R^2 = CO_2Me$
Acceptor (A): $R^1 = H$, $R^2 = CO_2Me$ or CN
Donor-Acceptor (DA): $R^1 = Ph$, $R^2 = CO_2Me$
Donor (D): $R^1 = H$, $R^2 = Ph$
Donor-donor (DD): $R^1 = Ph$, $R^2 = Ph$

Table 3.1 Selenonium-ylide [2,3]-rearrangement step in the Doyle-Kirmse reaction (based on study by Jana and Koenigs[68] for donor, donor-donor, donor-acceptor, acceptor, and acceptor-acceptor Rh carbenes. Free energies (in kcal mol^{-1}) are reported at the B3LYP/LANL2DZ[6-31G(d)] level.

Rh-Carbene	Metal-bound [2,3] TSS?	$\Delta G^{\ddagger}_{\text{metal-bound}}$	$\Delta G^{\ddagger}_{\text{free-ylide}}$
Acceptor ($R^2 = CO_2Me$)	Yes	17.3	13.9
Acceptor ($R^2 = CN$)	Yes	19.1	10.0
Donor	Yes	18.3	1.6
Acceptor-Acceptor	No	-	10.2
Donor-Acceptor	No	-	11.7
Donor-Donor	No	-	5.8

Whether the Rh catalyst dissociates is sensitive to the identity of the substituents adjacent to the carbene carbon, which raises the question whether this sensitivity is a result of steric hindrance of the adjacent substituent or the electronic nature of the carbene. To address this question, we modeled the donor variant of Koenigs's system—that is, the two adjacent groups to the carbene being H and Ph—and varied the *para* substituent on both phenyl rings (phenyl of the 'donor' group or the phenyl attached to Se atom). We reasoned that any electronic variation induced by a *para* substituent might tip the balance in favor of a fully Rh-catalyst-dissociated [2,3]-sigmatropic rearrangement, as opposed to a Rh-bound one, by introducing a greater build-up or reduction in electron density at the benzylic carbon.

We find, however, that varying the electronic nature of either phenyl ring does not cause catalyst dissociation.* In all cases, we found a Rh-bound [2,3]-sigmatropic rearrangement. More importantly, any change to the electronic nature of the phenyl ring has only a small effect on barriers (< 1 kcal mol^{-1}). This observation led us to suspect that catalyst dissociation originates from a steric effect of substituents adjacent to the benzylic position.

We next varied the adjacent hydrogen substituent—keeping all else the same—to substituents with increasing steric bulk. In the first variation, when changing H to Me, we could no longer optimize a [2,3]-sigmatropic shift TSS with the Rh catalyst bound to the substrate. However, we did optimize a metal-unbound [2,3]-TSS with the catalyst dissociated. Failures to find metal-bound [2,3]-TSSs for even more sterically bulky groups, such as ethyl and isopropyl, and phenyl (i.e., the donor/donor variation, *vide supra*) led us to conclude that steric effects—specifically, those caused by groups adjacent to the carbene carbon—are primarily responsible for preventing the Rh catalyst from being bound to its substrate during the [2,3]-sigmatropic shift event.

3.4.5 All That Glitters is Not Gold—A Comparison to a Reaction with Gold-Catalyst Dissociation

Koenigs and coworkers reported a gold-catalyzed sigmatropic rearrangement from gold carbenes (Scheme 3.4).[86] The authors argued for a free ylide mechanism because the diastereoselectivity of their reactions is consistent with their past reactions of similar systems.[86] We sought to find out if this conclusion is also borne out in our DFT calculations.

* Ibid, S9-S11. Figures S6-S8 show a Hammett plot that relates the *para* substituent's Hammett constant to the free energy barrier of activation.

Scheme 3.4 a) Gold-catalyzed rearrangement reaction[86] b) proposed catalytic cycle (shown in gold color) to product.

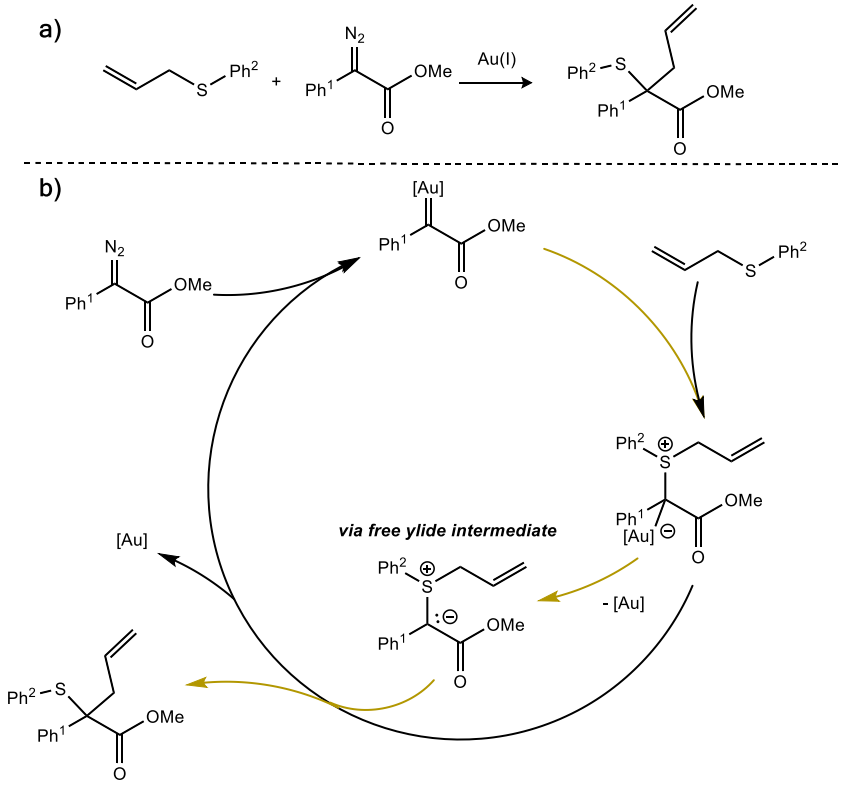

Reported optimized conditions involved a tris-*t*-butyl phosphine gold complex (*t*Bu$_3$P(AuCl)), which we simplified to [CH$_3$P(Au)]$^+$ in our modeling, given past precedent in modeling gold-catalyzed sigmatropic rearrangements.[100] Again, we could not successfully locate a metal-bound [2,3]-rearrangement TSS. Instead, we located a metal-unbound (or free) ylide that underwent the rearrangement step with a barrier of ~10 kcal mol^{-1} in free energy (Figure 3.7). This non-Rh example by Koenigs hints that this phenomenon could be more general and plague other transition-metal catalyzed rearrangements involving onium ylides.[100, *]

[*] Ibid, S7 (further discussion of these results).

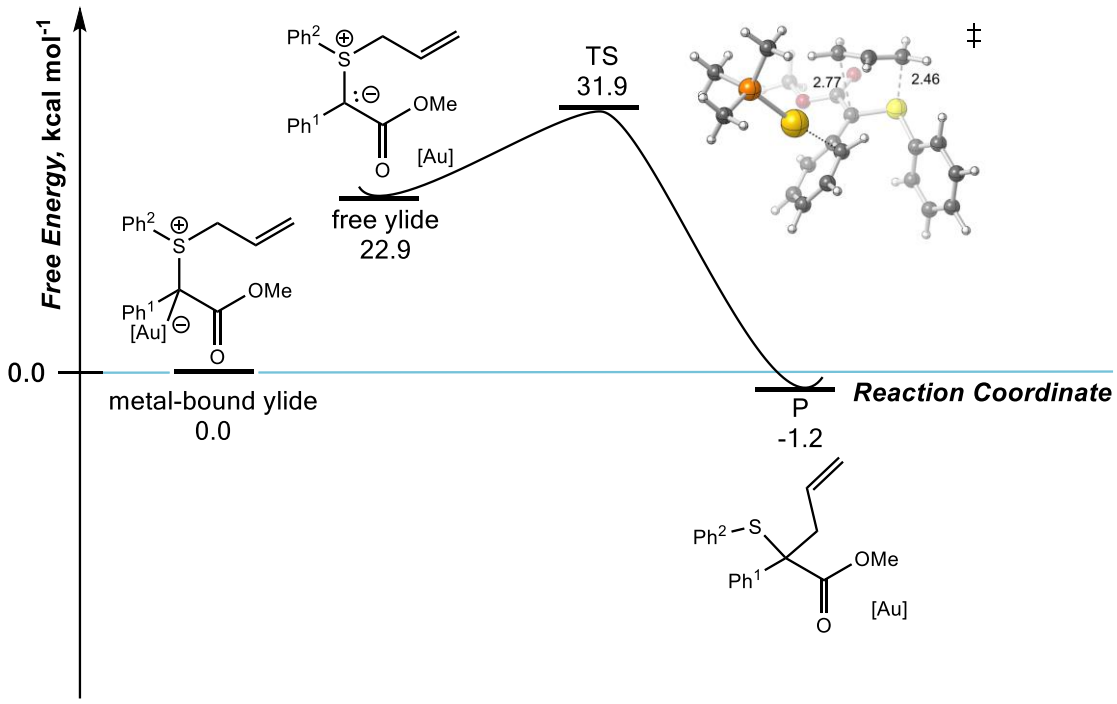

Figure 3.7 Energy profile for Au-catalyzed, metal-unbound sulfonium ylide [2,3]-rearrangement step.[86] Free energies (in kcal mol^{-1}) are reported at the B3LYP/LANL2DZ[6-31G(d)] level.

3.5 Conclusions

Do metal-promoted [2,3]-sigmatropic rearrangements involve metal-bound or free ylide reaction intermediates?[5] The answer is: *it depends on the system*. Specifically, it will depend on the metal catalyst used, the substituents attached to the carbene carbon, the type of onium ylide involved, and whether remote functional groups are present that can alter the electronic nature of the carbene center. All of these factors can have severe effects on whether the metal catalyst 'stays' or 'goes'. In this study, we sought to address which of these factors contribute most significantly to catalyst dissociation before rearrangement, here focused on experimentally reported ylide-formation/[2,3]-rearrangement reactions catalyzed by $Rh_2(OAc)_4$. We discovered that the most significant factor was the steric bulk of the neighboring functional groups at the carbene carbon. Bulkier groups

adjacent to the carbene favored free ylide mechanisms even when the electronic nature of the carbene carbon was changed significantly and the onium ylide (e.g., oxonium, sulfonium, and selenonium) kept the same. In sum, should the Rh catalyst 'stay' or 'go' in these reactions? *It depends* on the *steric clash* of substituents adjacent to the carbene carbon.*

3.6 References

(1) Jones, A. C.; May, J. A.; Sarpong, R.; Stoltz, B. M. Toward a Symphony of Reactivity: Cascades Involving Catalysis and Sigmatropic Rearrangements. *Angew. Chem. Int. Ed.* **2014**, *53*, 2556–2591.

(2) Doyle, M. P.; Tamblyn, W. H.; Bagheri, V. Highly Effective Catalytic Methods for Ylide Generation from Diazo Compounds. Mechanism of the Rhodium- and Copper-Catalyzed Reactions with Allylic Compounds. *J. Org. Chem.* **1981**, *46*, 5094–5102.

(3) Jana, S.; Guo, Y.; Koenigs, R. M. Recent Perspectives on Rearrangement Reactions of Ylides via Carbene Transfer Reactions. *Chem. Eur. J.* **2021**, *27*, 1270–1281.

(4) Zhang, Z.; Sheng, Z.; Yu, W.; Wu, G.; Zhang, R.; Chu, W. D.; Zhang, Y.; Wang, J. Catalytic Asymmetric Trifluoromethylthiolation via Enantioselective [2,3]-Sigmatropic Rearrangement of Sulfonium Ylides. *Nat. Chem.* **2017**, *9*, 970–976.

(5) Hock, K. J.; Koenigs, R. M. Enantioselective [2,3]-Sigmatropic Rearrangements: Metal-Bound or Free Ylides as Reaction Intermediates? *Angew. Chem. Int. Ed.* **2017**, *56*, 13566–13568.

(6) Doyle, M. P. Enantiocontrol in Catalytic Metal Carbene Reactions. *Russ. Chem. Bull.* **1999**, *48*, 16–20.

(7) Demonceau, A.; Noels, A. F.; Costa, J.-L. Rhodium(II) Carboxylate-Catalyzed Reactions of Diazoesters: Evidence for an Equilibrium between Free Carbene and a Metal-Carbene Complex. *J. Mol. Catal.* **1990**, *58*, 21–26.

(8) West, T. H.; Spoehrle, S. S. M.; Kasten, K.; Taylor, J. E.; Smith, A. D. Catalytic Stereoselective [2,3]-Rearrangement Reactions. *ACS Catal.* **2015**, *5*, 7446–7479.

(9) Jana, S.; Empel, C.; Pei, C.; Aseeva, P.; Nguyen, T. V.; Koenigs, R. M. C-H Functionalization Reactions of Unprotected N-Heterocycles by Gold-Catalyzed Carbene Transfer. *ACS Catal.* **2020**, *10*, 9925–9931.

(10) Hartwig, J. F. Organotransition Metal Chemistry: From Bonding to Catalysis; University Science Books, 2009; p 544.

(11) Crabtree, R. The Organometallic Chemistry of the Transition Metals; Wiley, 2009; pp 224–253.

(12) Hoffmann, R. W. Stereochemistry of [2,3]Sigmatropic Rearrangements. *Angew. Chem. Int. Ed. English* **1979**, *18*, 563–572.

(13) Nakai, T.; Mikami, K. [2,3]-Wittig Sigmatropic Rearrangements in Organic Synthesis. *Chem. Rev.* **1986**, *86*, 885–902.

* The conclusions in this chapter have been corroborated by further experimental studies since its publication.[104,105]

(14) Doyle, M. P.; Forbes, D. C. Recent Advances in Asymmetric Catalytic Metal Carbene Transformations. *Chem. Rev.* **1998**, *98*, 911–935.
(15) Mikami, K.; Nakai, T. Acyclic Stereocontrol via [2,3]-Wittig Sigmatropic Rearrangement. *Synthesis* **1991**, *1991*, 594–604.
(16) Clark, J. S. Nitrogen, Oxygen, and Sulfur Ylide Chemistry. A Practical Approach in Chemsitry; Oxford University Press: New York, 2002; pp 1–308.
(17) Sweeney, J. B. Sigmatropic Rearrangements of 'Onium' Ylids. *Chem. Soc. Rev.* **2009**, *38*, 1027.
(18) Murphy, G. K.; Stewart, C.; West, F. G. Intramolecular Generation and Rearrangement of Oxonium Ylides: Methodology Studies and Their Application in Synthesis. *Tetrahedron* **2013**, *69*, 2667–2686.
(19) Bao, H.; Tambar, U. K. [2,3]-Rearrangements of Ammonium Zwitterions. In *Molecular Rearrangements in Organic Synthesis*; Rojas, C. M., Ed.; John Wiley & Sons, Inc.: New York, 2015; pp 459–496.
(20) Sheng, Z.; Zhang, Z.; Chu, C.; Zhang, Y.; Wang, J. Transition Metal-Catalyzed [2,3]-Sigmatropic Rearrangements of Ylides: An Update of the Most Recent Advances. *Tetrahedron* **2017**, *73*, 4011–4022.
(21) Caballero, A.; Pérez, P. J. Dimensioning the Term Carbenoid. *Chem. Eur. J.* **2017**, *23*, 14389–14393.
(22) Doyle, M. P. Catalytic Methods for Metal Carbene Transformations. *Chem. Rev.* **1986**, *86*, 919–939.
(23) Davies, H. M. L.; Morton, D. Guiding Principles for Site Selective and Stereoselective Intermolecular C-H Functionalization by Donor/Acceptor Rhodium Carbenes. *Chem. Soc. Rev.* **2011**, *40*, 1857–1869.
(24) Davies, H. M. L.; Parr, B. T. Rhodium Carbenes. In *Contemporary Carbene Chemistry*; Moss, R. A., Doyle, M. P., Eds.; John Wiley & Sons, Inc., 2014; pp 363–403.
(25) Adly, F. G. On the Structure of Chiral Dirhodium(II) Carboxylate Catalysts: Stereoselectivity Relevance and Insights. *Catalysts* **2017**, *7*, 347.
(26) Davies, H. M. L.; Liao, K. Dirhodium Tetracarboxylates as Catalysts for Selective Intermolecular C–H Functionalization. *Nat. Rev. Chem.* **2019**, *3*, 347–360.
(27) Ford, A.; Miel, H.; Ring, A.; Slattery, C. N.; Maguire, A. R.; McKervey, M. A. Modern Organic Synthesis with α-Diazocarbonyl Compounds. *Chem. Rev.* **2015**, *115*, 9981–10080.
(28) Doyle, M. P.; McKervey, M. A.; Ye, T. *Modern Catalytic Methods for Organic Synthesis with Diazo Compounds: From Cyclopropanes to Ylides*; Doyle, M. P., McKervey, M. A., Ye, T., Eds.; John Wiley & Sons, Inc.: New York, NY, 1998.
(29) Doyle, M. P.; Duffy, R.; Ratnikov, M.; Zhou, L. Catalytic Carbene Insertion into C-H Bonds. *Chem. Rev.* **2010**, *110*, 704–724.
(30) Davies, H. M. L.; Beckwith, R. E. J. Catalytic Enantioselective C-H Activation by Means of Metal-Carbenoid-Induced C-H Insertion. *Chem. Rev.* **2003**, *103*, 2861–2903.
(31) Davies, H. M. L.; Manning, J. R. Catalytic C-H Functionalization by Metal Carbenoid and Nitrenoid Insertion. *Nature* **2008**, *451*, 417–424.
(32) Zhu, D.; Chen, L.; Fan, H.; Yao, Q.; Zhu, S. Recent Progress on Donor and Donor–Donor Carbenes. *Chem. Soc. Rev.* **2020**, *49*, 908–950.
(33) Nickerson, L. A.; Bergstrom, B. D.; Gao, M.; Shiue, Y.-S.; Laconsay, C. J.; Culberson, M. R.; Knauss, W. A.; Fettinger, J. C.; Tantillo, D. J.; Shaw, J. T. Enantioselective Synthesis

of Isochromans and Tetrahydroisoquinolines by C–H Insertion of Donor/Donor Carbenes. *Chem. Sci.* **2020**, *11*, 494–498.
(34) Soldi, C.; Lamb, K. N.; Squitieri, R. A.; González-López, M.; Di Maso, M. J.; Shaw, J. T. Enantioselective Intramolecular C–H Insertion Reactions of Donor–Donor Metal Carbenoids. *J. Am. Chem. Soc.* **2014**, *136*, 15142–15145.
(35) Shaw, J. T. C-H Insertion Reactions of Donor/Donor Carbenes: Inception, Investigation, and Insights. *Synlett* **2020**, *31*, 838–844.
(36) Werlé, C.; Goddard, R.; Philipps, P.; Farès, C.; Fürstner, A. Structures of Reactive Donor/Acceptor and Donor/Donor Rhodium Carbenes in the Solid State and Their Implications for Catalysis. *J. Am. Chem. Soc.* **2016**, *138*, 3797–3805.
(37) Lamb, K. N.; Squitieri, R. A.; Chintala, S. R.; Kwong, A. J.; Balmond, E. I.; Soldi, C.; Dmitrenko, O.; Castiñeira Reis, M.; Chung, R.; Addison, J. B.; ; Fettinger, J. C.; Hein, J. E.; Tantillo, D. J.; Fox, J. M.; Shaw, J. T. Synthesis of Benzodihydrofurans by Asymmetric C−H Insertion Reactions of Donor/Donor Rhodium Carbenes. *Chem. Eur. J.* **2017**, *23*, 11843–11855.
(38) Bergstrom, B. D.; Nickerson, L. A.; Shaw, J. T.; Souza, L. W. Transition Metal Catalyzed Insertion Reactions with Donor/Donor Carbenes. *Angew. Chem. Int. Ed.* **2021**, *60*, 6864–6878.
(39) Green, S. P.; Wheelhouse, K. M.; Payne, A. D.; Hallett, J. P.; Miller, P. W.; Bull, J. A. Thermal Stability and Explosive Hazard Assessment of Diazo Compounds and Diazo Transfer Reagents. *Org. Process Res. Dev.* **2020**, *24*, 67–84.
(40) Soheili, A.; Tambar, U. K. Tandem Catalytic Allylic Amination and [2,3]-Stevens Rearrangement of Tertiary Amines. *J. Am. Chem. Soc.* **2011**, *133*, 12956–12959.
(41) West, T. H.; Daniels, D. S. B.; Slawin, A. M. Z.; Smith, A. D. An Isothiourea-Catalyzed Asymmetric [2,3]-Rearrangement of Allylic Ammonium Ylides. *J. Am. Chem. Soc.* **2014**, *136*, 4476–4479.
(42) West, T. H.; Walden, D. M.; Taylor, J. E.; Brueckner, A. C.; Johnston, R. C.; Cheong, P. H.-Y.; Lloyd-Jones, G. C.; Smith, A. D. Catalytic Enantioselective [2,3]-Rearrangements of Allylic Ammonium Ylides: A Mechanistic and Computational Study. *J. Am. Chem. Soc.* **2017**, *139*, 4366–4375.
(43) Li, F.; He, F.; Koenigs, R. M. Catalyst-Free [2,3]-Sigmatropic Rearrangement Reactions of Photochemically Generated Ammonium Ylides. *Synthesis* **2019**, *51*, 4348–4358.
(44) Hommelsheim, R.; Guo, Y.; Yang, Z.; Empel, C.; Koenigs, R. M. Blue-Light-Induced Carbene-Transfer Reactions of Diazoalkanes. *Angew. Chem. Int. Ed.* **2019**, *58*, 1203–1207.
(45) Jana, S.; Pei, C.; Empel, C.; Koenigs, R. M. Photochemical Carbene Transfer Reactions of Aryl/Aryl Diazoalkanes—Experiment and Theory. *Angew. Chem. Int. Ed.* **2021**, *60*, 13271–13279.
(46) West, F. G. Rearrangement Processes of Oxonium and Ammonium Ylides Formed by Rhodium(II)-Catalyzed Carbene Transfer. In *Modern Rhodium-Catalyzed Organic Reactions*; Evans, P. A., Ed.; Wiley-VCH, 2005; pp 417–431.
(47) McCarthy, N.; McKervey, M. A.; Ye, T.; McCann, M.; Murphy, E.; Doyle, M. P. A New Rhodium(II) Phosphate Catalyst for Diazocarbonyl Reactions Including Asymmetric Synthesis. *Tetrahedron Lett.* **1992**, *33*, 5983–5986.
(48) Li, Z.; Boyarskikh, V.; Hansen, J. H.; Autschbach, J.; Musaev, D. G.; Davies, H. M. L. Scope and Mechanistic Analysis of the Enantioselective Synthesis of Allenes by

Rhodium-Catalyzed Tandem Ylide Formation/[2,3]-Sigmatropic Rearrangement between Donor/Acceptor Carbenoids and Propargylic Alcohols. *J. Am. Chem. Soc.* **2012**, *134*, 15497–15504.

(49) Li, Z.; Parr, B. T.; Davies, H. M. L. Highly Stereoselective C-C Bond Formation by Rhodium-Catalyzed Tandem Ylide Formation/[2,3]-Sigmatropic Rearrangement between Donor/Acceptor Carbenoids and Chiral Allylic Alcohols. *J. Am. Chem. Soc.* **2012**, *134* (26), 10942–10946.

(50) Ferris, L.; Haigh, D.; Moody, C. J. New Chiral Rhodium(II) Carboxylates and Their Use as Catalysts in Carbenoid Transformations. *Tetrahedron Lett.* **1996**, *37*, 107–110.

(51) Doyle, M. P.; Peterson, C. S. Macrocyclic Oxonium Ylide Formation and Internal [2,3]-Sigmatropic Rearrangement. Catalyst Influence on Selectivity. *Tetrahedron Lett.* **1997**, *38*, 5265–5268.

(52) Pierson, N.; Fernández-García, C.; McKervey, M. A. Catalytic Asymmetric Oxonium Ylide - [2,3] Sigmatropic Rearrangement with Diazocarbonyl Compounds: First Use of C2-Symmetry in Rh(II) Carboxylates. *Tetrahedron Lett.* **1997**, *38*, 4705–4708.

(53) Clark, J. S.; Fretwell, M.; Whitlock, G. A.; Burns, C. J.; Fox, D. N. A. Asymmetric Synthesis of Cyclic Ethers by Rearrangement of Oxonium Ylides Generated from Chiral Copper Carbenoids. *Tetrahedron Lett.* **1998**, *39*, 97–100.

(54) Hodgson, D. M.; Petroliagi, M. Rh(II)-Binaphthol Phosphate Catalysts in the Enantioselective Intramolecular Oxonium Ylide Formation–[3,2] Sigmatropic Rearrangement of α-Diazo-β-Ketoesters. *Tetrahedron: Asymmetry* **2001**, *12*, 877–881.

(55) Kitagaki, S.; Yanamoto, Y.; Tsutsui, H.; Anada, M.; Nakajima, M.; Hashimoto, S. Enantioselective [2,3]-Sigmatropic and [1,2]-Stevens Rearrangements via Intramolecular Formation of Allylic Oxonium Ylides Catalyzed by Chiral Dirhodium(II) Carboxylates. *Tetrahedron Lett.* **2001**, *42*, 6361–6364.

(56) Shimada, N.; Nakamura, S.; Anada, M.; Shiro, M.; Hashimoto, S. Enantioselective Construction of a 2,8-Dioxabicyclo[3.2.1]Octane Ring System via [2,3]-Sigmatropic Rearrangement of Oxonium Ylide Using Chiral Dirhodium(II) Carboxylates. *Chem. Lett.* **2009**, *38*, 488–489.

(57) Li, Z.; Davies, H. M. L. Enantioselective C−C Bond Formation by Rhodium-Catalyzed Tandem Ylide Formation/[2,3]-Sigmatropic Rearrangement between Donor/Acceptor Carbenoids and Allylic Alcohols. *J. Am. Chem. Soc.* **2010**, *132*, 396–401.

(58) Reggelin, M. [2,3]-Sigmatropic Rearrangements of Allylic Sulfur Compounds. *Top Curr Chem* **2007**, *275*, 1–65.

(59) Hock, K. J.; Mertens, L.; Hommelsheim, R.; Spitzner, R.; Koenigs, R. M. Enabling Iron Catalyzed Doyle–Kirmse Rearrangement Reactions with in Situ Generated Diazo Compounds. *Chem. Commun.* **2017**, *53*, 6577–6580.

(60) Yang, Z.; Guo, Y.; Koenigs, R. M. Solvent-Dependent, Rhodium Catalysed Rearrangement Reactions of Sulfur Ylides. *Chem. Commun.* **2019**, *55*, 8410–8413.

(61) Kaiser, D.; Klose, I.; Oost, R.; Neuhaus, J.; Maulide, N. Bond-Forming and -Breaking Reactions at Sulfur(IV): Sulfoxides, Sulfonium Salts, Sulfur Ylides, and Sulfinate Salts. *Chem. Rev.* **2019**, *119*, 8701–8780.

(62) Empel, C.; Hock, K. J.; Koenigs, R. M. Dealkylative Intercepted Rearrangement Reactions of Sulfur Ylides. *Chem. Commun.* **2019**, *55*, 338–341.

(63) Xu, X.; Li, C.; Tao, Z.; Pan, Y. Aqueous Hemin Catalyzed Sulfonium Ylide Formation and Subsequent [2,3]-Sigmatropic Rearrangements. *Green Chem.* **2017**, *19*, 1245–1249.

(64) Yan, X.; Li, C.; Xu, X.; Zhao, X.; Pan, Y.-J. Hemin Catalyzed Dealkylative Intercepted [2, 3]-Sigmatropic Rearrangement Reactions of Sulfonium Ylide with 2, 2, 2-Trifluorodiazoethane. *Adv. Synth. Catal.* **2020**, 1–8.
(65) Qin, H.; Jia, Y.; Wang, N.; Jiang, Z.-X.; Yang, Z. Practical and Regioselective Halo-Trifluoromethylthiolation of Sulfur Ylides. *Chem. Commun.* **2020**, *56*, 8265–8268.
(66) Reddy, A. C. S.; Anbarasan, P. Rhodium-Catalyzed Rearrangement of S/Se-Ylides for the Synthesis of Substituted Vinylogous Carbonates. *Org. Lett.* **2019**, *21*, 9965–9969.
(67) Jana, S.; Aseeva, P.; Koenigs, R. M. Rhodium Catalysed Synthesis of Seleno-Ketals via Carbene Transfer Reactions of Diazoesters. *Chem. Commun.* **2019**, *55*, 12825–12828.
(68) Jana, S.; Koenigs, R. M. Rhodium-Catalyzed Carbene Transfer Reactions for Sigmatropic Rearrangement Reactions of Selenium Ylides. *Org. Lett.* **2019**, *21*, 3653–3657.
(69) Xu, B.; Tambar, U. K. Copper-Catalyzed Enantio-, Diastereo-, and Regioselective [2,3]-Rearrangements of Iodonium Ylides. *Angew. Chem. Int. Ed.* **2017**, *56*, 9868–9871.
(70) Padwa, A.; Hornbuckle, S. F. Ylide Formation from the Reaction of Carbenes and Carbenoids with Heteroatom Lone Pairs. *Chem. Rev.* **1991**, *91*, 263–309.
(71) Kirmse, W.; Kapps, M. Reaktionen Des Diazomethans Mit Diallylsulfid Und Allyläthern Unter Kupfersalz-Katalyse. *Chem. Ber.* **1968**, *101*, 994–1003.
(72) Zhang, Y.; Wang, J. Catalytic [2,3]-Sigmatropic Rearrangement of Sulfur Ylide Derived from Metal Carbene. *Coord. Chem. Rev.* **2010**, *254*, 941–953.
(73) Li, Y.; Huang, Z.; Wu, X.; Xu, P.-F.; Jin, J.; Zhang, Y.; Wang, J. Rh(II)-Catalyzed [2,3]-Sigmatropic Rearrangement of Sulfur Ylides Derived from N-Tosylhydrazones and Sulfides. *Tetrahedron* **2012**, *68*, 5234–5240.
(74) Stevens, T. S.; Creighton, E. M.; Gordon, A. B.; MacNicol, M. Degradation of Quaternary Ammonium Salts. Part I. *J. Chem. Soc.* **1928**, 3193–3197.
(75) Empel, C.; Jana, S.; Koenigs, R. M. Advances in [1,2]-Sigmatropic Rearrangements of Onium Ylides via Carbene Transfer Reactions. *Synthesis* **2021**, *53*, 4567–4587.
(76) Baidilov, D. On the Mechanism of the Stevens Rearrangement. *Synthesis* **2020**, *52*, 21–26.
(77) Sommelet, M. On a Particular Mode of Intramolecular Rearrangement. *Hebd, CR Seances Acad. Sci* **1937**, *205*, 56.
(78) Kantor, S. W.; Hauser, C. R. Rearrangements of Benzyltrimethylammonium Ion and Related Quaternary Ammonium Ions by Sodium Amide Involving Migration into the Ring. *J. Am. Chem. Soc.* **1951**, *73*, 4122–4131.
(79) Hauser, C. R.; Kantor, S. W.; Brasen, W. R. Rearrangement of Benzyl Sulfides to Mercaptans and of Sulfonium Ions to Sulfides Involving the Aromatic Ring by Alkali Amides. *J. Am. Chem. Soc.* **1953**, *75*, 2660–2663.
(80) Liao, M.; Peng, L.; Wang, J. Rh(II)-Catalyzed Sommelet−Hauser Rearrangement. *Org. Lett.* **2008**, *10*, 693–696.
(81) Nair, V. N.; Tambar, U. K. Catalytic Rearrangements of Onium Ylides in Aromatic Systems. *Org. Biomol. Chem.* **2022**, *20*, 3427–3439.
(82) Clark, J. S.; Hansen, K. E. Intramolecular Reactions of Metal Carbenoids with Allylic Ethers: Is a Free Ylide Involved in Every Case? *Chem. Eur. J.* **2014**, *20*, 5454–5459.
(83) Dequina, H. J.; Schomaker, J. M. Aziridinium Ylides: Underused Intermediates for Complex Amine Synthesis. *Trends Chem.* **2020**, *2*, 874–887.
(84) Li, S.-S.; Wang, J. Cu(I)/Chiral Bisoxazoline-Catalyzed Enantioselective Sommelet–Hauser Rearrangement of Sulfonium Ylides. *J. Org. Chem.* **2020**, *85*, 12343–12358.
(85) Harrison, J. G.; Gutierrez, O.; Jana, N.; Driver, T. G.; Tantillo, D. J. Mechanism of

Rh2(II)-Catalyzed Indole Formation: The Catalyst Does Not Control Product Selectivity. *J. Am. Chem. Soc.* **2016**, *138*, 487–490.
(86) He, F.; Jana, S.; Koenigs, R. M. Gold-Catalyzed Sigmatropic Rearrangement Reactions via Carbene Transfer Reactions. *J. Org. Chem.* **2020**, *85*, 11882–11891.
(87) Frisch, M. J.; Trucks, G. W.; Schlegel, H. B.; Scuseria, G. E. .; Robb, G. E.; Cheeseman, J. R.; Scalmani, G.; Barone, V.; Mennucci, B. .; Petersson, G. A.; Nakatsuji, H.; Caricato, M.; Li, X.; Hratchian, H. P. .; Izmaylov, A. F.; Bloino, J.; Zheng, G.; Sonnenberg, J. L.; Hada, M. .; Ehara, M.; Toyota, K.; Fukuda, R.; Hasegawa, J.; Ishida, M.; Nakajima, T. .; Honda, Y.; Kitao, O.; Nakai, H.; Vreven, T.; Montgomery, Jr., J. A. . P.; J. E.; Ogliaro, F.; Bearpark, M.; Heyd, J. J.; Brothers, E. . K.; K. N.; Staroverov, V. N.; Keith, T.; Kobayashi, R.; Normand, J. . R.; K.; Rendell, A.; Burant, J. C.; Iyengar, S. S.; Tomasi, J. . C.; M.; Rega, N.; Millam, J. M.; Klene, M.; Knox, J. E.; Cross, J. B. .; Bakken, V.; Adamo, C.; Jaramillo, J.; Gomperts, R.; Stratmann, R. E.; Yazyev O.; Austin, A. J.; Cammi, R.; Pomelli, C.; Ochterski, J. W.; Martin R. L.; Morokuma, K.; Zakrzewski, V. G.; Voth, G. A.; Salvador, P.; Dannenberg, J. J.; Dapprich, S.; Daniels, A. D.; Farkas O.; Foresman, J. B.; Ortiz, J. V.; Cioslowski, J.; Fox, D. J. *Gaussian 09*, Revision D.01. Gaussian Inc. Wallingford, CT 2009.
(88) Fukui, K. The Path of Chemical Reactions -- The IRC Approach. *Acc. Chem. Res.* **1981**, *14*, 363–368.
(89) Gonzalez, C.; Schlegel, H. B. Reaction Path Following In Mass-Weighted Internal Coordinates Cartesians and with Internal Coordinates without Mass-Weighting. *J. Phys. Chem.* **1990**, *94*, 5523–5527.
(90) Maeda, S.; Harabuchi, Y.; Ono, Y.; Taketsugu, T.; Morokuma, K. Intrinsic Reaction Coordinate: Calculation, Bifurcation, and Automated Search. *Int. J. Quantum Chem.* **2015**, *115*, 258–269.
(91) Schmid, S. C.; Guzei, I. A.; Fernández, I.; Schomaker, J. M. Ring Expansion of Bicyclic Methyleneaziridines via Concerted, Near-Barrierless [2,3]-Stevens Rearrangements of Aziridinium Ylides. *ACS Catal.* **2018**, *8*, 7907–7914.
(92) Lee, M.; Ren, Z.; Musaev, D. G.; Davies, H. M. L. Rhodium-Stabilized Diarylcarbenes Behaving as Donor/Acceptor Carbenes. *ACS Catal.* **2020**, *10*, 6240–6247.
(93) Chai, J.-D.; Head-Gordon, M. Long-Range Corrected Hybrid Density Functionals with Damped Atom–Atom Dispersion Corrections. *Phys. Chem. Chem. Phys.* **2008**, *10*, 6615.
(94) Grimme, S.; Antony, J.; Ehrlich, S.; Krieg, H. A Consistent and Accurate Ab Initio Parametrization of Density Functional Dispersion Correction (DFT-D) for the 94 Elements H-Pu. *J. Chem. Phys.* **2010**, *132*, 154104.
(95) Grimme, S.; Ehrlich, S.; Goerigk, L. Effect of the Damping Function in Dispersion Corrected Density Functional Theory. *J. Comput. Chem.* **2011**, *32*, 1456–1465.
(96) Álvarez-Moreno, M.; de Graaf, C.; López, N.; Maseras, F.; Poblet, J. M.; Bo, C. Managing the Computational Chemistry Big Data Problem: The ioChem-BD Platform. *J. Chem. Inf. Model.* **2015**, *55*, 95–103.
(97) Pirrung, M. C.; Werner, J. A. Intramolecular Generation and [2,3]-Sigmatropic Rearrangement of Oxonium Ylides. *J. Am. Chem. Soc.* **1986**, *108*, 6060–6062.
(98) Nishibayashi, Y.; Ohe, K.; Uemura, S. The First Example of Enantioselective Carbenoid Addition to Organochalcogen Atoms: Application to [2,3]Sigmatropic Rearrangement of Allylic Chalcogen Ylides. *J. Chem. Soc. Chem. Commun.* **1995**, 1245.
(99) Drabowicz, J.; Rzewnicka, A.; Żurawiński, R. Selenonium Ylides: Syntheses, Structural

Aspects, and Synthetic Applications. *Molecules* **2020**, *25*, 2420.
(100) Felix, R. J.; Weber, D.; Gutierrez, O.; Tantillo, D. J.; Gagné, M. R. A Gold-Catalysed Enantioselective Cope Rearrangement of Achiral 1,5-Dienes. *Nat. Chem.* **2012**, *4*, 405–409.
(101) Biswas, B.; Singleton, D. A. Controlling Selectivity by Controlling the Path of Trajectories. *J. Am. Chem. Soc.* **2015**, *137*, 14244–14247.
(102) Pine, S. H. 1,2-Anionic Rearrangements. An Example of Mechanistic Evolution. *J. Chem. Educ.* **1971**, *48*, 99.
(103) Ghigo, G.; Cagnina, S.; Maranzana, A.; Tonachini, G. The Mechanism of the Stevens and Sommelet−Hauser Rearrangements. A Theoretical Study. *J. Org. Chem.* **2010**, *75*, 3608–3617.
(104) Nair, V. N.; Kojasoy, V.; Laconsay, C. J.; Kong, W. Y.; Tantillo, D. J.; Tambar, U. K. Catalyst-Controlled Regiodivergence in Rearrangements of Indole-Based Onium Ylides. *J. Am. Chem. Soc.* **2021**, *143*, 9016–9025.
(105) Kanchupalli, V.; Thorbole, L. A.; Kalepu, J.; Joseph, D.; Arshad, M.; Katukojvala, S. Rhodium-Catalyzed Enal Transfer with N-Methoxypyridazinium Salts. *Org. Lett.* **2022**, *24*, 3850-3854.

Chapter 4

Effects of Axial Solvent Coordination to Dirhodium Complexes on the Reactivity and Selectivity in C–H Insertion Reactions: A Computational Study*

The world is so complicated, tangled, and overloaded that to see into it with any clarity you must prune and prune.

- Italo Calvino

4.1 Abstract

Density functional theory calculations were used to systematically explore the effects of axial ligation by solvent molecules on the reactivity and selectivity of dirhodium tetracarboxylates with diazo compounds in the context of C–H insertion into propane. Insertions on three types of diazo compounds—acceptor/acceptor, donor/acceptor, and donor/donor—promoted by dirhodium tetraformate were tested with and without axial solvent ligation for no surrounding solvent, dichloromethane, isopropanol, and acetonitrile. Magnitudes, origins, and consequences of structural and electronic changes arising from axial ligation were characterized. The results suggest that axial ligation affects barriers for N_2 extrusion and C–H insertion, the former to a larger extent.

* This chapter is a modified version of the following published article: Laconsay, C. J.; Pla-Quintana, A.; Tantillo, D. J. Effects of Axial Solvent Coordination to Dirhodium Complexes on the Reactivity and Selectivity in C–H Insertion Reactions: A Computational Study, *Organometallics* **2021**, *40*, 4120-4132 with permission from the American Chemical Society. Copyright 2021 American Chemical Society. Anna Pla-Quintana carried out DFT calculations and contributed to the writing, editing, and revision of the final version of the manuscript.

4.2 Introduction

4.2.1 Overview and Historical Context

Dirhodium tetracarboxylate complexes (Scheme 4.1, left) are among the most commonly used catalysts in organometallic chemistry. These bimetallic complexes have a "paddle wheel" (sometimes called "lantern") structure, containing a Rh–Rh single bond, the details of which has been subject to experimental and theoretical interrogations for decades.[1–8] These complexes—which have applications spanning from catalysis[9,10] and biology[11–13] to supramolecular chemistry[14–17]—are potent catalysts in organic chemistry because of their ability to promote nitrogen extrusion from diazo compounds to generate transient rhodium carbene intermediates (Scheme 4.1, center, L = CR_2). These intermediates are capable of engaging in a wide range of chemical reactions including (2 + 1) cycloadditions (e.g., cyclopropanation, cyclopropenation, insertion into X–H bonds), various (n + 1) cycloaddition reactions where n > 2, and a diverse array of ylide reactions.[18–27] The efficiency and selectivity imparted by dirhodium tetracarboxylate catalysts, including enantioselectivity when chiral carboxylate (or related) ligands are used, makes them especially useful tools in the construction of complex organic molecules.[28–30] While one of the two rhodium atoms is involved directly in bond-making/breaking with substrates,[31] the other is crucial for the overall catalytic performance of the complex, as it is involved in compensating for electronic alterations during a reaction (a phenomenon referred to as the *trans* effect or *trans* influence).[32,33]

Scheme 4.1 Dirhodium "paddlewheel" complexes have four bidentate bridging ligands and two axial sites for additional ligands (L) to bind.

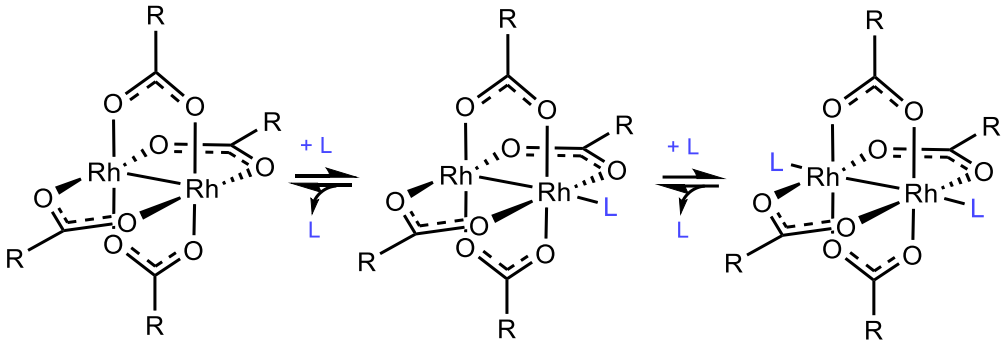

Each of the two rhodium atoms in a dirhodium tetracarboxylate is Lewis acidic and can complete an octahedral geometry by filling the coordination site along the axis of the Rh–Rh bond. In the bioinorganic realm, the availability of these labile axial sites is crucial for anti-tumor activity and DNA targeting.[34] In heterogenous catalysis, axial ligation to dirhodium(II) complexes has been used to immobilize complexes in silica (e.g., SBA-15) materials.[35,36] Davies et al., for example, used axial coordination of pyridine groups from polymeric resins as a means to reuse chiral dirhodium catalysts with low to no effect on catalyst activity.[37–40]

Most reported X-ray crystal structures of dirhodium complexes contain bound axial ligands, usually solvent but sometimes substrates, other ligands, or other complexes (i.e., in coordination polymers).[41–47] Even though dirhodium complexes have been known since the 1960s, it was not until 2002 that an X-ray crystal structure of a dirhodium complex *without* axial ligands was reported.[48] The few reported X-ray structures of dirhodium *carbenes* crystallize as coordination polymers: OMe or NMe_2 groups present in the carbene appendants coordinate to the rhodium not bearing the carbene carbon of the next unit.[49,50] These complexes require CH_2Cl_2 and toluene to be stable in crystalline form and their unit cells contain highly disordered solvent molecules.[49]

In solution, axial solvent coordination to dirhodium complexes is well known,[51–55] and even macroscopically evident due to its effect on the electronic structure of the complex. Coordination by solvent molecules is comparatively much weaker than carboxylate coordination. Nevertheless, as a result of populating a vacant Rh–Rh σ* orbital upon coordination (by solvent or other ligands), one will observe in color changes.[56–59] Triple resonance NMR experiments confirmed that axial ligand coordination changes the chemical environment at the Rh nuclei, and the donor strength of a labile ligand is observed in ^{103}Rh chemical shift "deshielding".[60] Several directions have been explored to effect changes on dirhodium complexes by way of axial ligation, some of which are summarized below.

4.2.2 Axial Ligands

Berry's three-center/four-electron (3c/4e) bonding model in the Rh–Rh–CR_2 fragment (Scheme 4.1, center, L = CR_2) helps rationalize the diverse reactivity of dirhodium carbenes.[58] As a result of the communication between these three atoms, dirhodium carbene reactivity is potentially "tunable" by axial ligation opposite to the Rh–C bond. For instance, many have designed dirhodium complexes with improved catalytic properties[54,61–65] by incorporating ligands with tethered axial donors (or ligands that shield the Rh core from axial coordination by external molecules[66]). However, this direction is still in its infancy compared to that of modifying electronic and steric properties of the bridging ligands.[7]

Some have explored *N*-heterocyclic carbenes (NHCs) as external axial coordinating ligands. In one example, Snyder et al. isolated a dirhodium carboxylate complex with tetramethylimidazolidene coordinated to the axial position in order to obtain a dirhodium carbene structure suitable for X-ray structure characterization.[67] No significant differences in activity or

selectivity were found with and without the NHC, which led the authors to conclude that an equilibrium was taking place that furnishes dirhodium carbene free of axial ligand as the active catalyst. Subsequently, Gois et al. utilized *N*,*N*-(2,6-diisopropylphenyl)imidazolidene, a more sterically hindered NHC, and obtained dirhodium dicarboxylates with axially coordinated NHCs to showcase different reactivity and selectivity.[68] These complexes catalyzed C–H insertion reactions of diazo compounds at considerably slower rates than the compounds without axial ligation and with substantial differences in selectivity. These observations were attributed to a "push-pull" mechanism, in which an axial NHC causes a weakening of the Rh–C_{NHC} bond in the presence of a bound diazo compound ("pull"), and the NHC weakens the Rh=$C_{carbene}$ partial double bond in the dirhodium carbene complex ("push").[68]

Axial complexation of groups that are not as strong σ-donors as NHCs have also been explored.[69–71] Darko et al., for example, reported a heteroleptic dirhodium complex that contained a bridging ligand with a tethered thioether that axially coordinates to rhodium.[70,71] Beneficial effects on the activity – and especially the selectivity – were observed upon using the heteroleptic complex as a catalyst for cyclopropanation. Further studies from the same group with mixed oxazolidinate/carboxylate dirhodium complexes confirmed the positive effect that the coordination of tethered thioether donors had on the catalytic activity of the complexes in Si–H insertion reactions and cyclopropanation reactions.[63,64] The authors argued that the enhanced selectivity they observed was related to an increase in the energy of the LUMO of the complex upon coordination of the axial ligand.[55]

Coordinating Lewis basic additives may also lead to divergent outcomes. For instance, Doyle and coworkers disclosed a dearomatizing formal [3+3]-cycloaddition of isoquinolinium/pyridinium methylides and enol diazoacetates whose chemo- and

enantioselectivity depended on Lewis base additives.[72] The main difficulty in this strategy is to find a suitable concentration of the additive that favors mono-coordination over di-coordination, since the latter would render the catalytic system inactive (Scheme 4.1, center and right). Additives such as tetramethyl urea, Hünig's base, *N*,*N*-diethylaniline, 2,4,6-trimethylpyridine, $TfNH_2$, DMAP, and 2-chloropyridine also have been used to modulate the reactivity and selectivity of dirhodium tetracarboxylate complexes through axial coordination.[73–77]

4.2.3 Solvent Effects

Solvent effects can be crucial in catalysis.[78] The effects of axial coordination by solvent on Rh-carbene reactivity and selectivity should be considered, since it has been shown that reaction outcome can highly depend on the solvent.[26,79–81] Weakly Lewis basic and non-polar/low-polarity solvents, expected to be poorly coordinating, such as dichloromethane or hexane, are generally considered the most efficient reaction media for C–H functionalization.[29] Still, there are examples reported of C–H insertion[82,83] and cyclopropanation[84] reactions in water, a highly coordinating, polar solvent. Though acetonitrile (CH_3CN), another Lewis basic solvent, sometimes works poorly in Rh-catalyzed reactions,[85,86] it has been shown to be an effective solvent for others.[87] Predicting an optimal solvent is not always trivial. For example, in a Rh-catalyzed C(sp^3)–H amination, *t*BuCN was identified as the optimal solvent because the lifetime of $Rh_2(esp)_2$ was prolonged in *t*BuCN compared to that in acetonitrile or CH_2Cl_2.[88]

Computational studies exploring the effects of axial solvent coordination on reactivity and selectivity are sparse, though some exist.[89–91] Davies and coworkers investigated one case (see Figure 6 of their study) of axially coordinated acetone on a dirhodium tetraformate catalyzed cyclopropanation of styrene by methyl phenyldiazoacetate, a donor acceptor carbene (at the

B3LYP/6-311G(2d,2p)[Rh-RSC+4f]//B3LYP/6-31G(d)[Rh-RSC+4f] level of theory).[89] Their results indicated that acetone coordination slows down the rate of nitrogen (N_2) extrusion (a barrier increase of 4.7 kcal mol^{-1}) and makes it less exothermic (ΔE = -3.1 kcal mol^{-1}) compared to that without acetone coordination (ΔE = -9.1 kcal mol^{-1}). This reactivity difference, captured by DFT calculations, better aligns with their experimental data.

Kisan and Sunoj reported a computational study (at the SMD($CHCl_3$)-M06/LANL2DZ[6-31G(d,p)]//B3LYP/LANL2DZ[6-31G(d)] level of theory) in which axial solvent ($CHCl_3$) coordination was shown to have minimal effects on all reaction steps except for the step responsible for the enantioselectivity in an asymmetric N–H insertion reaction with cooperative dual catalysts: a chiral SPINOL-phosphoric acid and a dirhodium tetracarboxylate.[90] In addition, axial coordination of the chiral SPINOL-phosphoric acid catalyst seemed to selectively stabilize the preferred transition state structure (TSS).[90] Additionally, with the exception of some experimental-computational studies wherein axial ligation is explicitly considered in the computational studies (and compared to the non-complexed states),[92–94] axial ligation is generally *not* considered in computational modeling of synthetically-relevant reactions (including our own work[95,96]).

4.2.4 Goals of This Work

If, for the most part, axial solvent ligation is ignored in computational studies of dirhodium catalyzed reactions, we ask '*should it be*'? The aim of the present work is to systematically evaluate the effects that coordination of single solvent molecules at the axial sites of dirhodium complexes has on C–H insertion reactions. Two main questions were the focus of our attention: (1) Is there a meaningful difference in reactivity and selectivity for such reactions when an implicit molecule is

axially coordinated? (2) Is it possible to rationally tune reactivity and selectivity by solvent? Our tool of choice for answering these questions is density functional theory (DFT), which has been used effectively to model related systems on many occasions.[97] For more information on approaches and caveats for modeling organometallic reactions see our recent review[97] (or see Chapter 2) and excellent reviews published by others.[98–106]

4.3 Computational Methods

DFT calculations were carried out with the *Gaussian 09* quantum chemistry package.[107] Stationary points were classified as either TSSs or minima on the potential energy surface (PES) by identification of one imaginary frequency for the former and the absence of imaginary frequencies for the latter. To confirm that TSSs are connected to particular minima, we employed intrinsic reaction coordinate (IRC calculations).[108–110] For geometry optimizations, we used the B3LYP[111] functional with the LANL2DZ[6-31G(d)] basis set, i.e., the LANL2DZ effective core potential (ECP)[112] for Rh and 6-31G(d) for all other atoms. Implicit solvent was treated with the conductor-like polarizable continuum model (CPCM).[113–115] Reported energies are from single points using CPCM with the M06[116] functional with a larger basis set, the SDD[117] ECP for Rh and the 6-311+G(d,p) basis set for all other atoms. Natural bond orbital (NBO) calculations were carried out in Gaussian with Gaussian NBO version 3.1.[118–121]

We and others have shown that the B3LYP functional is a reasonable choice for geometry optimizations of relatively small systems involving dirhodium carbenes.[98,101,122–125] In fact this level of theory provides good agreement with experiment for $\Delta H^{\ddagger}$ for N_2 extrusion, the step that contains the turnover-determining transition state,[126] for the reactions we describe below with the methyl diazoacetate-dirhodium formate adduct: we compute a $\Delta H^{\ddagger}$ = 15.1 kcal mol^{-1} with

B3LYP/LANL2DZ[6-31G(d)] versus an experimental $\Delta H^{\ddagger}$ of 15.0 kcal mol^{-1} for dirhodium tetraacetate-catalyzed cyclopropanation of ethyl diazoacetetate and styrene,[127] which can also be compared with $\Delta H^{\ddagger}$ of 13.3 kcal mol^{-1} for N_2 extrusion from diazoketones by Pirrung and coworkers.[31] Additionally, we tested other functionals and ECP basis sets: M06,[116] M06L,[128] and MN15[129] functionals with either the LANL2DZ or SDD basis set. Tracking the variation of relative electronic energies with respect to level of theory led us to conclude that M06/SDD[6-311+G(d,p)], which predicted the N_2 extrusion $\Delta E^{\ddagger}$ for the reaction mentioned above to be 16.4 kcal mol^{-1},[127] afforded a reasonable compromise of accuracy and computational cost.[116*] Optimized stationary points using dispersion-corrected B3LYP (i.e., B3LYP-D3(BJ))[130,131] had little to no effect on the relative free energies.[†] As a result of these tests, we utilized the M06/SDD[6-311+G(d,p)]//B3LYP/LANL2DZ[6-31G(d)] level of theory throughout this study. Similar levels of theory have been employed for DFT investigations of synthetically-relevant, Rh-catalyzed C–H insertions.[132,133] All computed structures are available on the ioChem-BD platform[134] and can be accessed *via* https://doi.org/10.19061/iochem-bd-6-111. Energies and lowest vibrational frequencies are summarized in the Supporting Information using the files names on the ioChem-BD database for ease of access.

[*] Data from this computational test are described in the Supporting Information of *Organometallics* **2021**, *40*, 4120-4132. See Figure S3 on p. S6.
[†] Ibid, S7 (see Table S3 and discussion thereof).

4.4 Results and Discussion

4.4.1 Overall Approach

For simplicity, we selected the C–H insertion of three representative diazo compounds **1a-c**—one each with acceptor/acceptor (A/A),[20,135,136] donor/acceptor (D/A),[21,22,28,137] and donor/donor (D/D)[25,27,138,139] substituents—into propane (**2**) catalyzed by the simplest dirhodium tetracarboxylate, dirhodium tetraformate ([Rh_2(formate)$_4$], **3**) (Scheme 4.2). We explored insertion both into the internal (CH_2) and terminal (CH_3) positions of propane, which lead to insertion products **4** and **5**, respectively. Our model system closely resembles that employed in the seminal computational study of Nakamura and coworkers,[140] in which propane and the same catalyst model was used. However, they only explored acceptor diazo compounds and did not consider the effects axial ligand binding might have on reactivity and selectivity.

Scheme 4.2 Rh-catalyzed transformation of A/A, D/A, and D/D diazo compounds and propane to C–H insertion products.

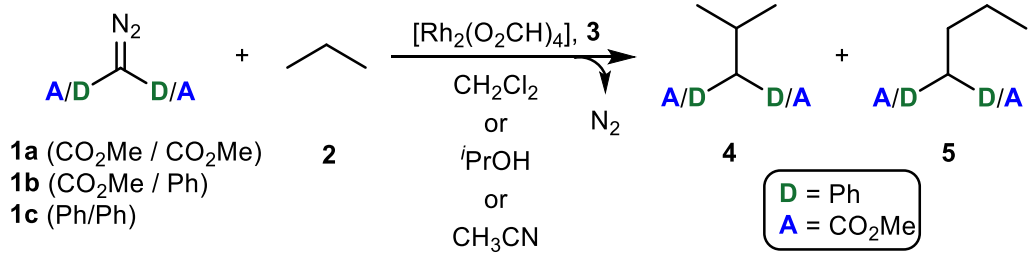

A schematic representation of the generally accepted mechanism for the C–H insertion process is shown in Figure 4.1 (blue inner ring). The reaction starts with nucleophilic attack of the diazo compound (**1**) on dirhodium tetraformate (**3**) to generate an ylide (**6**). Dirhodium carbene (**7**) is formed by N_2 extrusion from **6**. A weakly bound complex (**8**) is then formed, from which the carbene carbon inserts into a C–H bond of propane (**2**). Such C–H insertions are generally

concerted, but involve asynchronous formation of the new C–H and C–C bonds (with the former leading and the latter lagging).[140,141] However, Shaw and coworkers have found that donor/donor carbenes can undergo two-step, stepwise C–H insertions,[142] or exist at the borderlands[143] of concerted and stepwise.[144] Finally, dissociation of product **4** from weakly bound complex **9** regenerates catalyst **3**.

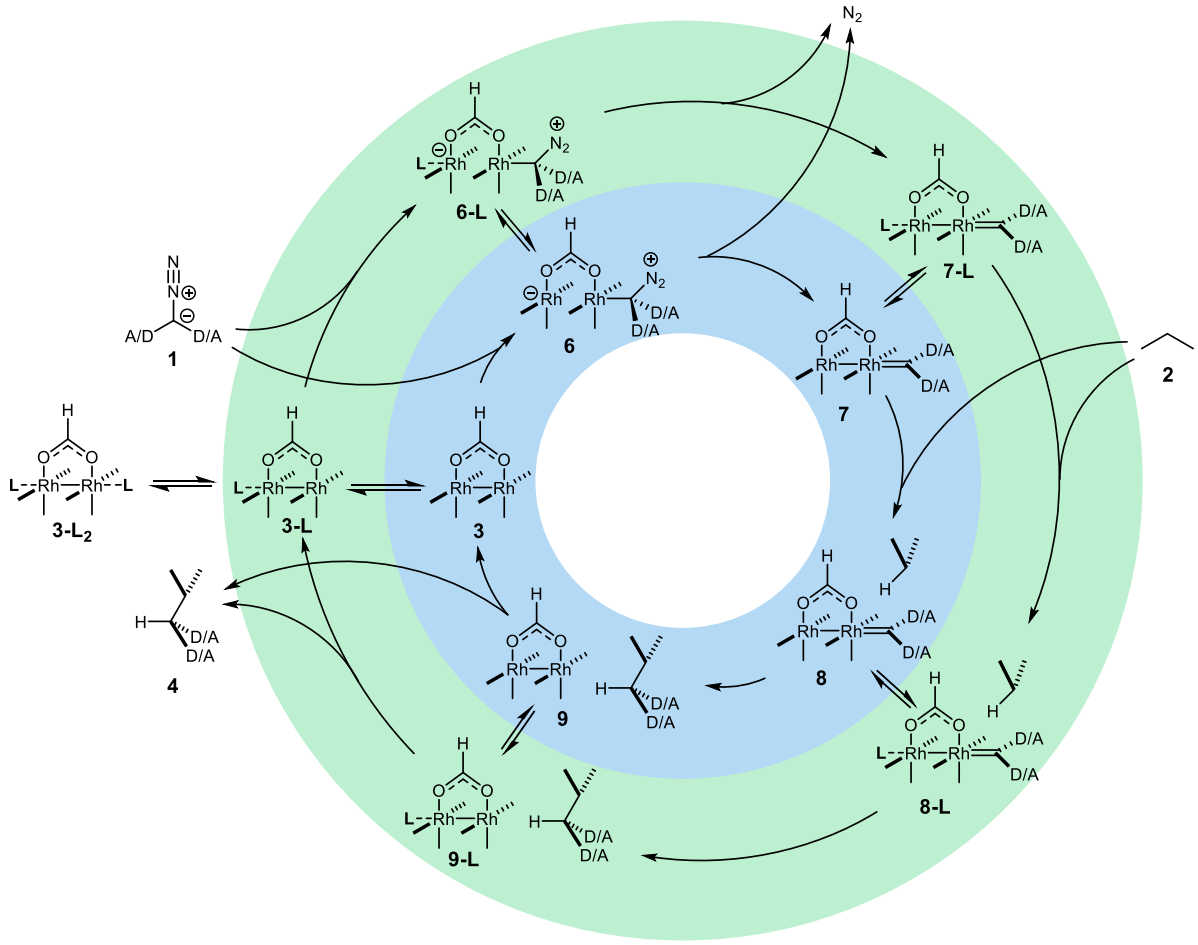

Figure 4.1 Mechanism postulated for the insertion of a diazo compound into propane catalyzed by dirhodium tetraformate (only one formate is shown explicitly). Blue inner ring: no axial ligand. Green outer ring: one axial ligand bound.

It is unclear whether axial solvent ligation is relevant at any point in this catalytic cycle (Figure 4.1, outer green circle versus inner blue circle). Solvent coordination may occur for some intermediates and not others (e.g., **3** to **3-L** equilibria) and when it coordinates, it may or may not

have a significant effect on structure or reactivity. These issues are addressed below. Reactions with and without explicit coordinated solvent molecules were first studied in the gas-phase and then in three common solvents using the CPCM model: dichloromethane ($\varepsilon = 8.9$), isopropanol ($\varepsilon = 19.9$) and acetonitrile ($\varepsilon = 37.5$). We selected these solvents because they are commonly used in dirhodium catalyzed reactions, and because they provide variety of dielectric constants and donating ability.

4.4.2 Effects of Solvent on Diazo Complexation: HOMO-LUMO Modulation

To investigate the effects afforded by an axial ligand on diazo complexation, we first assessed the frontier orbitals, the highest occupied molecular orbital (HOMO) and lowest unoccupied molecular orbital (LUMO), and their change in energetic splitting upon axial ligation. For this section, we narrow our attention on donor-acceptor (D/A) systems, a reasonable middle ground in terms of electrophilicity, selectivity, and functional group tolerance in the literature, but similar qualitative energetic trends were noted for D/D and A/A systems so the conclusions drawn from the D-A systems can reasonably be extended to those systems.[22*]

Berry demonstrated that axial ligand coordination raises the energy of the Rh–Rh σ^* LUMO, and alters the HOMO-LUMO energy splitting.[55,58,59] An examination of the frontier orbitals of solvent-unbound [Rh_2(formate)$_4$] (**3**) and solvent-bound compounds **3-L** demonstrates that the LUMO energy increases by 1.3 eV (~ 30 kcal mol^{-1}) from **3** to **3-ACN**. While HOMO energies also increase, they do not increase by as much, and thus the net effect is an increase in the HOMO-LUMO gap (by 0.62 eV from **3** to **3-ACN**; Figure 4.2). A similar effect is observed

[*] Ibid, S4-S5 (see Tables S1 and S2 for data on D/D and A/A systems).

for dirhodium carbene structures **7** and **7-L**, but the magnitudes of the changes are much smaller than those observed with free [Rh_2(formate)$_4$] (Figure 4.3). Darko and coworkers computed similar qualitative trends in the HOMO-LUMO gap for their tethered, axial thioether-coordinated dirhodium catalysts with DFT calculations (M06-2X/def2TZVPP level of theory).[63] Increases to LUMO energies should lead to greater difficulty in forming **6**/**6-L**. The results of our computations support this notion.

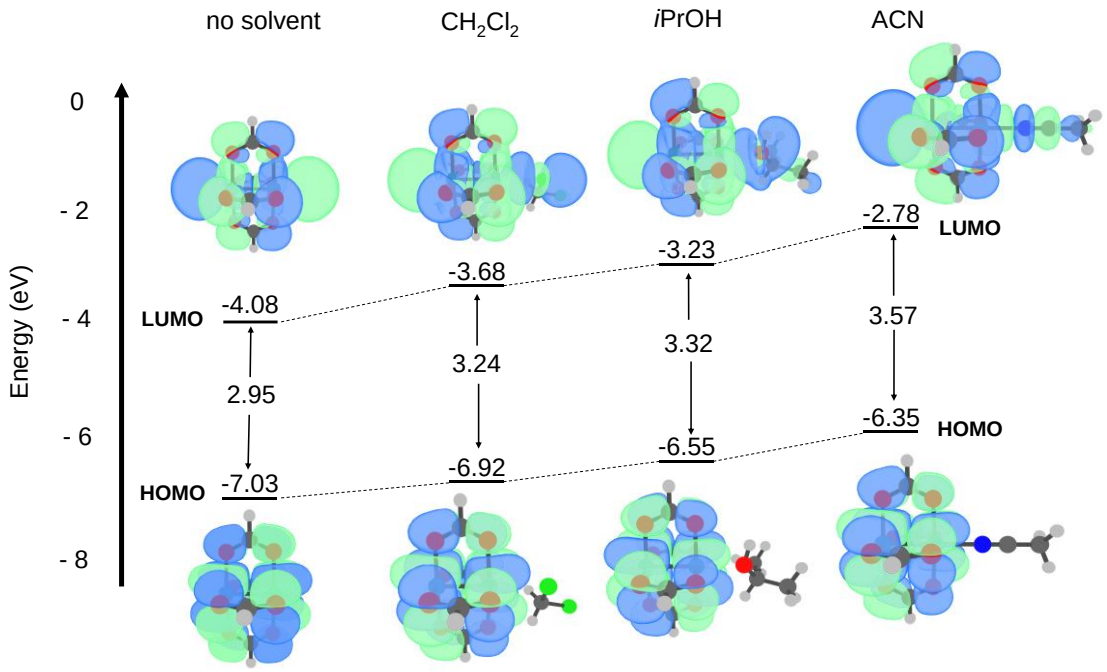

Figure 4.2 Frontier molecular orbitals (HOMO and LUMO) and HOMO-LUMO gaps (in eV) for **3** and **3-L** structures computed at the M06/SDD[6-311+G(d,p)]//B3LYP/LANL2DZ[6-31G(d)] level of theory.

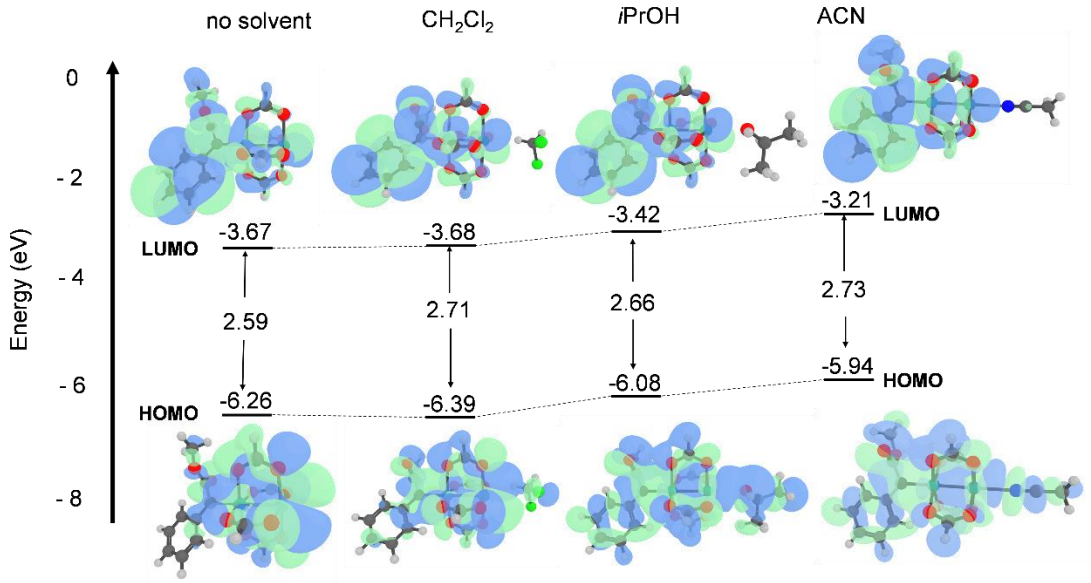

Figure 4.3 Frontier molecular orbitals (HOMO and LUMO) and HOMO-LUMO gaps (in eV) for **7** and **7-L** structures computed at the M06/SDD[6-311+G(d,p)]//B3LYP/LANL2DZ[6-31G(d)] level of theory.

4.4.3 Explicit Versus Implicit Solvent—An Acetonitrile Case Study

Next, we directed our attention towards whether including an explicit axial ligand changes predictions about mechanism and/or energetics compared to using an implicit solvent model. Of the three solvents studied, we expect acetonitrile to have the most significant effects on reactivity, since it is the strongest σ-donor,[53,55,60] so we focus on it here first.

Four approaches for modeling solvent were compared for the reaction of D/A diazo compound **1b** and propane to form C–H insertion products (Figure 4.4): (1) neither implicit nor explicit solvent included ("no coord. / gas"), (2) implicit solvent, but no explicit solvent included ("no coord. / acetonitrile"), (3) explicit solvent, but no implicit solvent included ("acetonitrile / gas"), (4) both implicit and explicit solvent included ("acetonitrile / acetonitrile"). Free energy barriers ($\Delta G^{\ddagger}$'s, relative to the minimum immediately preceding the TSS in each case) for carbene

formation and C–H insertion at both the CH_2 ("Internal") and CH_3 ("Terminal") positions of propane were computed using all four approaches. Free energy barriers varied within 3 kcal mol^{-1} for each reaction, a small change, but barriers for N_2 extrusion increased upon explicit solvent coordination and barriers for C–H insertion decreased upon solvent coordination to a lesser degree. *In summary, predicted effects are not large, but, if borne out in a flask, could alter rates by an order of magnitude or more.*

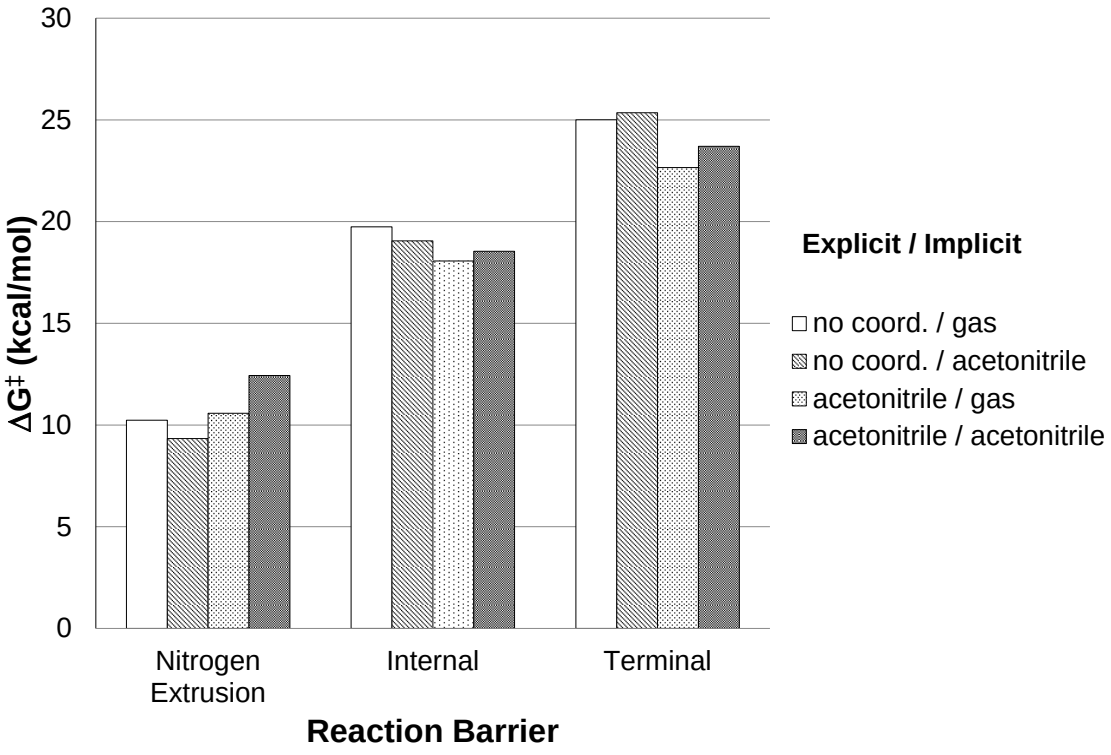

Figure 4.4 Variation of computed free energy barriers ($\Delta G^{\ddagger}$) for N_2 extrusion (left), insertion at CH_2 internal position (center), and insertion at CH_3 terminal position (right) due to solvent model on donor-acceptor diazo compound (**1b**). All barriers are relative to the preceding minimum to each TSS.

4.4.4 Effects of Solvent on N_2 Extrusion Barriers

Once it was clear that axial solvent coordination affected frontier molecular orbital energies of diazo complex (Figures 4.2 and 4.3) and energetic barriers (Figure 4.4), we proceeded to compare barriers for N_2 extrusion in other solvents (Figure 4.5). Here, all solvents are modeled with both implicit solvent and one explicit solvent molecule. Independent of carbene type, the barriers for N_2 extrusion increase with stronger σ-donor ligands. The absence of a barrier for the D/D system without a coordinated solvent is notable – a caution for those modeling N_2 extrusion in such systems.

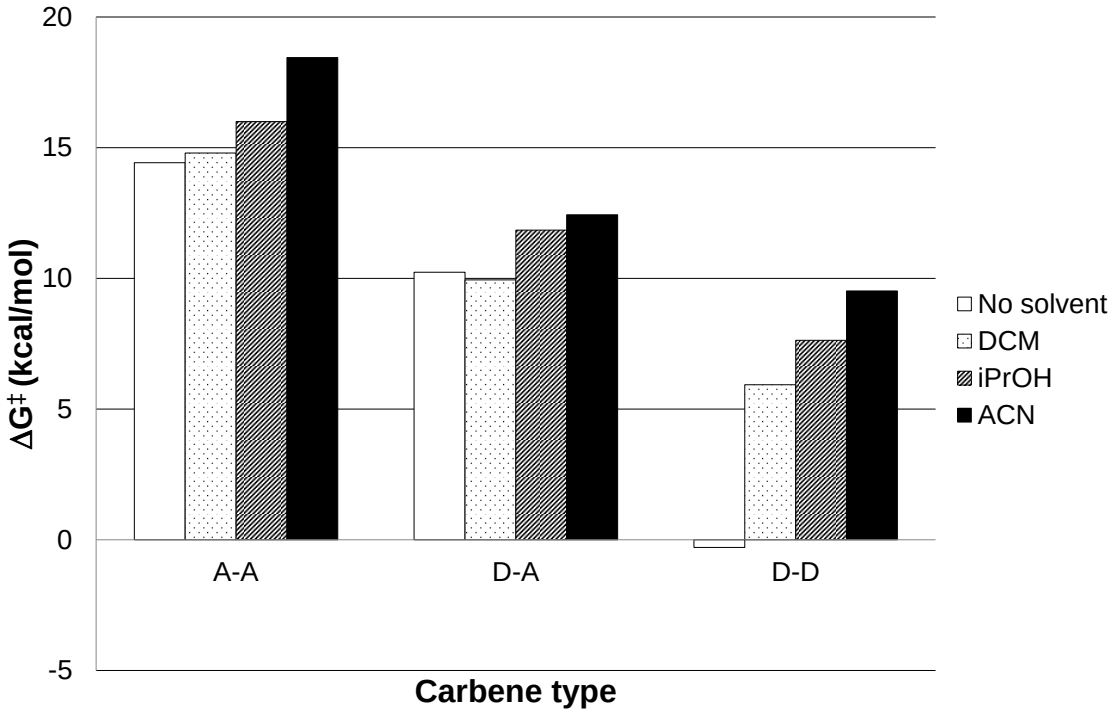

Figure 4.5 Comparison of the Gibbs free energy barriers of N_2 extrusion for acceptor/acceptor (A/A), donor/acceptor (D/A) and donor/donor (D/D) diazo compounds in gas-phase (No solvent) and dichloromethane (DCM), isopropanol (^{i}PrOH) and acetonitrile (ACN) solution. All barriers are relative to the preceding minimum to each TSS.

Gas-phase calculations with explicit solvent were used to isolate the effects of axial solvent on the N_2 extrusion barrier. Our results demonstrate that increasingly Lewis-basic axial ligands

raise the energies of the (1) tetrahedral complex **6**/(**6-L**), (2) the N_2 extrusion TSS, and (3) dirhodium carbene **7**/(**7-L**) relative to the sum of the free energies of **1-3** (Figure 4.6). An increase in N_2 extrusion barriers (**6**/**6-L** → **7**/**7-L**) is observed for more strongly donating axial ligands; a similar qualitative trend is observed when implicit *and* explicit solvent are modeled.[*] Why? Structures **6-*i*PrOH** and **6-ACN**, when optimized in the gas-phase from the endpoints of IRC paths originating from TSSs for N_2 extrusion, are not bound tetrahedral minima (Rh–C bonds are ~3.8 Å, C–N bonds are ~1.3 Å, and natural charges are redistributed); donation from the distal axial ligand appears to be sufficient to promote diazo dissociation., which, of course, hinders N_2 loss. As described by Fürstner and coworkers, Rh d-orbital back-bonding promotes N_2 extrusion and dirhodium carbene formation (Figure 4.6, inset),[45] an orbital interaction that is not fully expressed until the diazo carbon binds rhodium. The situation observed for **6-*i*PrOH** and **6-ACN** in the gas-phase is extreme, but a weaker version of the same effect is observed with any axial donor.

[*] Ibid, S3 (see Figure S1 for data resulting from calculations resulting from inclusion of both implicit continuum solvent *and* explicit solvent.

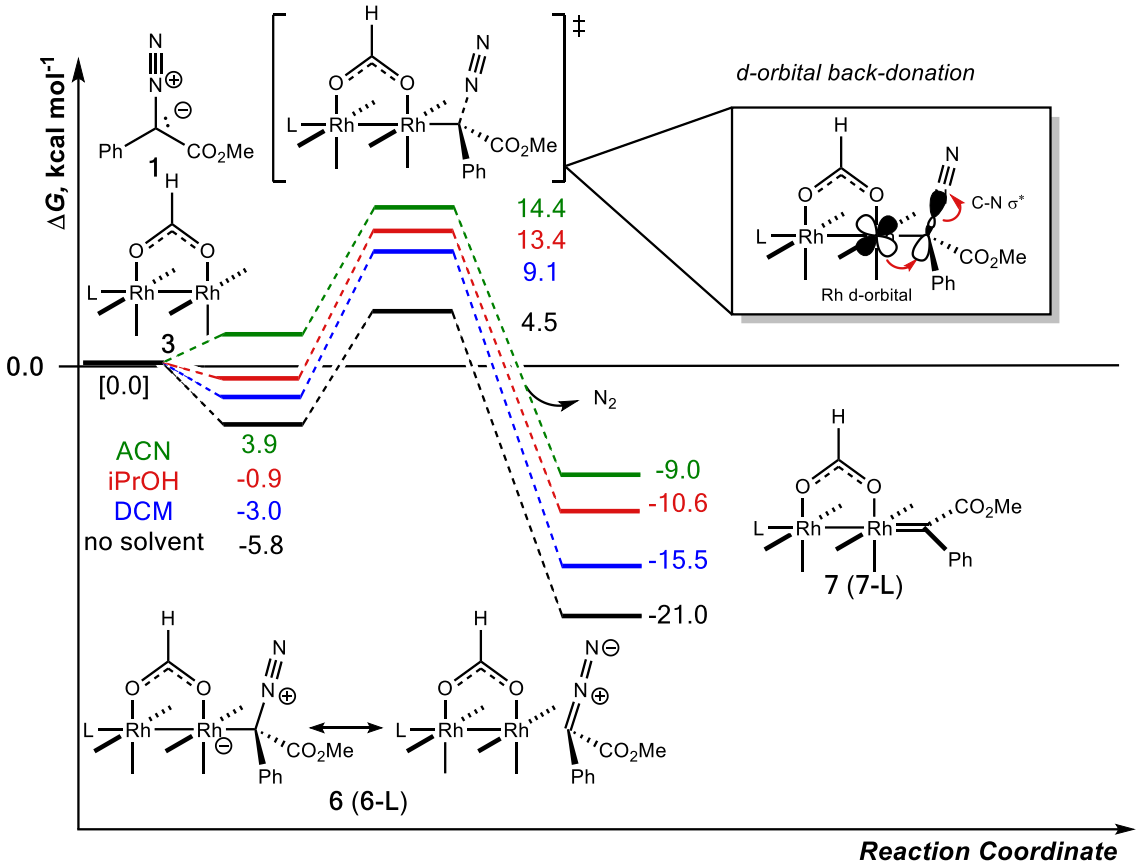

Figure 4.6 Formation and decomposition of **6**/**6-L** with and without solvent bound computed at the M06/SDD[6-311+G(d,p)]//B3LYP/LANL2DZ[6-31G(d)] level of theory for D/A diazo compounds (**1b**).

4.4.5 Effects of Solvent on CH_2/CH_3 Insertion Selectivity

While the overall barriers for C–H insertion did not change much with solvent coordination, selectivity can be greatly affected by small changes in relative energies of transition states. The order of inherent reactivity for insertion into differently substituted alkyl C–H bonds is well-established—primary << secondary < tertiary C–H bonds—so we would expect our computed barriers for insertion into the internal position of propane to be lower than those for insertion into the terminal position.[140,145,146]

Kisan and Sunoj highlighted the effect that axial ligation can have on the selectivity of asymmetric N–H insertion reactions catalyzed by dirhodium tetracarboxylates with a chiral SPINOL-phosphoric acid bound.[90] In a similar manner, we can compute free energy differences ($\Delta\Delta G^{\ddagger}$) between transition states for insertion into internal versus terminal positions of propane. As shown in Figure 4.7, we computed synthetically meaningful differences in insertion barriers.[*] For A/A carbenes, strongly donating solvents decrease selectivity. For D/A and D/D carbenes, however, *iso*-propanol coordination leads to the best selectivity (i.e., the greatest magnitude in $\Delta\Delta G^{\ddagger}$). Though we are unaware of experimental studies where *iso*-propanol leads to optimal selectivity, past studies show that selectivity can be solvent-dependent.[147] Given the magnitude of our predicted effects, decomposing their origins with current theoretical methods would not be reliable;[79,148] Nonetheless, Darko and co-workers observed an increase in product yield for Si–H insertion reactions when dirhodium catalysts with tethered, axial coordinating ligands were used.[63] Results in Figure 4.7 suggest that perhaps tethered, axial coordinating ligands might also enhance regioselectivity.

[*] Ibid, S4 (see SI Figure S2 for $\Delta G^{\ddagger}$'s from which the $\Delta\Delta G^{\ddagger}$ are derived).

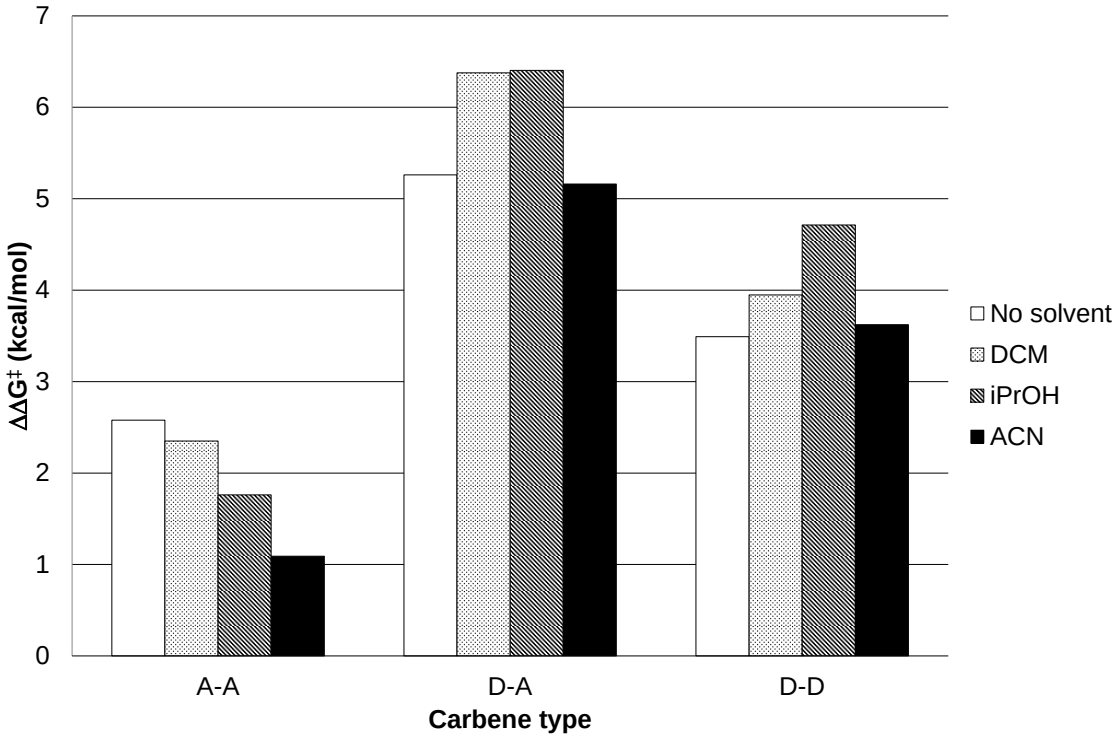

Figure 4.7 Comparison of the Gibbs free energy barriers difference for insertion of the carbene into the CH_2 and CH_3 of propane for acceptor/acceptor (A-A), donor/acceptor (D-A) and donor/donor (D-D) carbenes in gas phase and dichloromethane (DCM), isopropanol (^{i}PrOH) and acetonitrile (ACN) solution.

4.4.6 Structural Changes Upon Axial Ligand Binding

How strong is the interaction between the axial ligand and the dirhodium complex? One classic, although debated,[149–151] means of characterizing bond strength is to use bond length as a measure for a series of related compounds. For the Rh–L interaction, where L is the atom of the axial solvent in contact with Rh, we compared *d*(Rh•••L) to the sum of the van der Waals radii of Rh and the bond atom of L ($\Sigma(r_{vdW})$), assuming a covalent interaction exists if *d*(Rh•••L) < $\Sigma(r_{vdW})$ (Scheme 4.3a).[152] We also computed Wiberg bond indices (WBIs)[153] for gas-phase geometries of **3**, **3-L**, **6**, **6-L**, **7**, and **7-L**. These data are shown in Table 4.1. For all cases, *d*(Rh•••L) magnitudes are less

than $\Sigma(r_{vdW})$, however WBIs for Rh–L bonds are low: 0.1-0.4. WBIs are greatest for acetonitrile, as expected, but similar for *iso*-propanol and dicholoromethane.

Scheme 4.3 a) key parameters collected in Table 4.1 b) representation of d_z^2 orbitals that contribute to the donor-acceptor interactions between Rh_2X_4 fragments that make up the Rh-Rh single bond c) orbital representation of donor-acceptor interaction and d) d-orbitals of Rh-Rh bond.

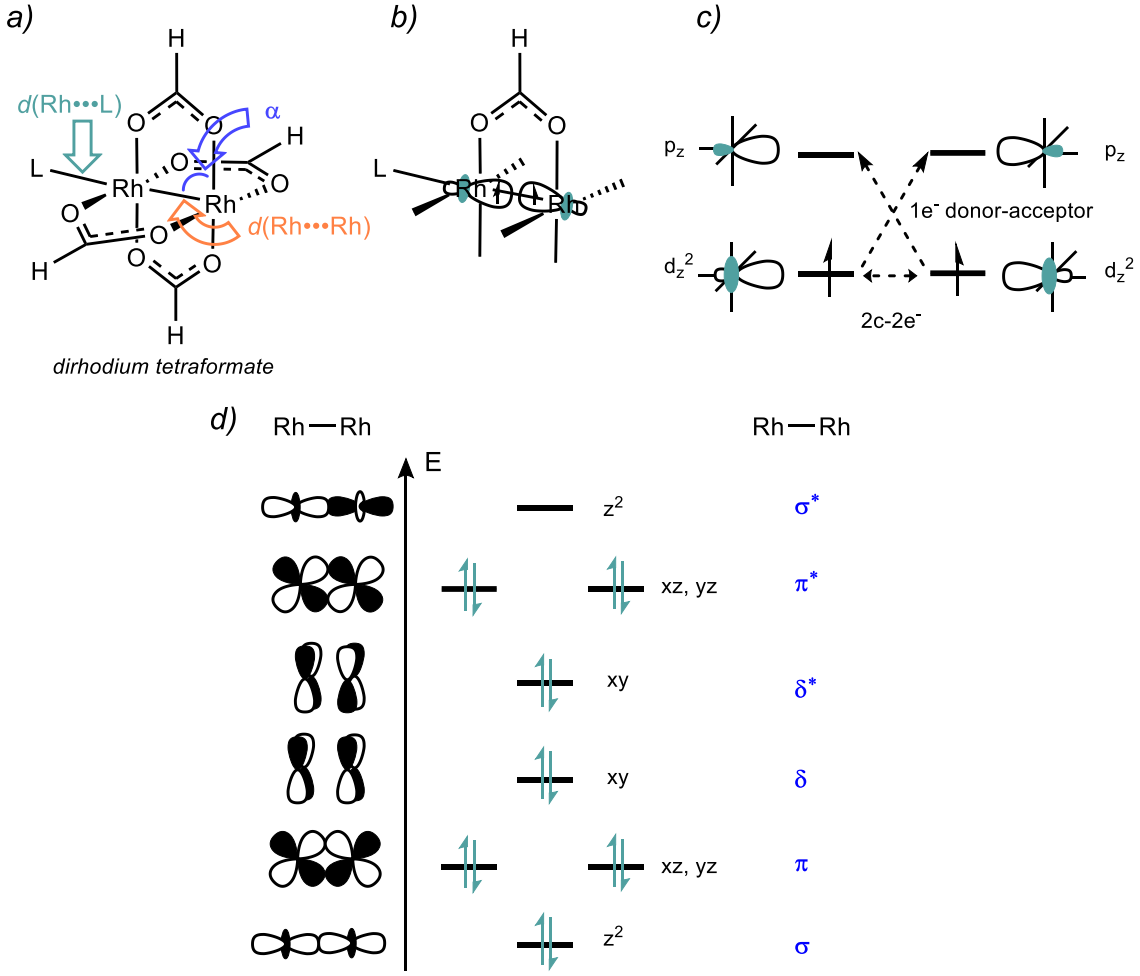

Table 4.1 Key distances (*d*(Rh•••Rh) and *d*(Rh•••L)), pyramidality angles (α), Wiberg bond indices (WBIs), and global electrophilicity index values (ω) for dirhodium complexes with axial ligands: DCM (L = Cl), ^{i}PrOH (L = O), and ACN (L = N). All complexes bound to diazo substrates are D-A substrates. Distance and orbital energies were measured from gas-phase M06/SDD[6-311+G(d,p)]//B3LYP/LANL2DZ[6-31G(d)] structures.

Rh_2 Complex	*d*(Rh•••Rh) (Å)	α	*d*(Rh•••L) (Å)	Rh-L $\Sigma(r_{vdW})$ (Å)[a]	Rh-Rh WBI	Rh-L WBI	ω (eV)
3	2.40	88.3	-	-	0.89	-	5.23
3-DCM	2.41	88.1	2.73	3.94	0.84	0.28	4.34
3-^{i}PrOH	2.42	88.2	2.27	4.26	0.83	0.23	3.59
3-ACN	2.43	88.2	2.20	4.10	0.81	0.36	2.91
6	2.43	88.0	-	-	0.77	-	3.82
6-DCM	2.43	87.7	2.84	3.94	0.78	0.23	3.59
6-^{i}PrOH	2.43	87.7	2.32	4.26	0.81	0.21	2.48
6-ACN	2.43	87.9	2.23	4.10	0.82	0.37	2.22
7	2.48	87.9	-	-	0.59	-	4.64
7-DCM	2.49	87.6	3.21	3.94	0.57	0.10	4.68
7-^{i}PrOH	2.49	87.7	2.51	4.26	0.64	0.14	4.23
7-ACN	2.49	87.5	2.49	4.10	0.63	0.23	3.84

Changes in Rh–Rh bond distances (*d*(Rh•••Rh)) are small with solvent coordination (Table 4.1). Pyramidality angle (α) (Scheme 4.3a) deviations from 90° are also small (Table 4.1), consistent with conclusions arrived at by Aullón and Alvarez.[154] While distortions of α might be expected since an axial ligand donates electron density into the Rh-Rh σ^* orbital, the bridging ligands, along with other orbital interactions, resist major deformation: (1) a 2c-2e$^-$ bond between the two d_z^2 orbitals of individual Rh_2X_4 fragments and (2) a 1e$^-$ donor-acceptor interaction between a d_z^2 of one Rh and the empty p_z of the other Rh (Scheme 4.3b-d).[55,154]

While small increases in *d*(Rh•••Rh) for **3**/**3-L** are accompanied by decreases in the Rh-Rh WBI, the Rh-L WBI increases in the series from no solvent to acetonitrile (Table 4.1). For **6**/**6-L** and **7**/**7-L**, changes in *d*(Rh•••Rh) (at most a 0.1 Å change) and Rh-Rh WBI are not as large (e.g., ΔWBI = 0.05 for **6-ACN** vs. ΔWBI = 0.08 for **3-ACN**), which suggests that the effects of axial solvent coordination on the Rh-Rh bond are not as potent compared to that of **3**. We suggest that the strong structural changes observed for **3**/**3-L** and diminished structural changes in **6**/**6-L** and **7**/**7-L** might be a result of a competition between L and the diazo compound to engage in 3c/4e bonding. Berry rationalized minor changes to the Rh-Rh bond distance upon axial complexation of increasing sigma-donor capacity in his 3c/4e bond model by observing that axial ligand binding mostly impacts the unoccupied LUMO orbital (Scheme 4.3d); in other words, the Rh-Rh bond length 4.is generally insensitive to axial ligation.[58] The results in Table 4.1 for Rh-Rh distances that match crystallographically determined Rh-Rh bond distances (distances fall within a narrow window of ranging from 2.35-2.45 Å)[2,50,154]—and the minor, almost negligible, changes in WBIs—support this model.

Electrophilicity of the dirhodium core can be investigated by computing the global electrophilicity index (GEI, ω, equation 1,[66,155–158] wherein χ is electronegativity[159] and η is chemical hardness).[160] The GEI can be derived from HOMO and LUMO energies with equations 2 and 3.

$$\omega = \chi^2 / 2\eta \quad (1)$$

$$\chi = - (E_{HOMO} + E_{LUMO}) / 2 \quad (2)$$

$$\eta = E_{LUMO} - E_{HOMO} \quad (3)$$

Computed GEI values for **3/3-L**, **6**/**6-L**, and **7**/**7-L** (Table 4.1, the greater the value of ω, the greater the electrophilicity) suggest that axial ligation generally makes these structures less electrophilic and increasingly so from DCM to ACN.

4.5 Summary and Outlook

In this study, we used DFT calculations to compute energetic barriers for N_2 extrusion and C–H insertion of A/A, D/A, and D/D carbenes with and without axial solvent ligation. Our attention centered around two main questions: (1) Is there a meaningful difference in reactivity and selectivity for such reactions when an implicit molecule is axially coordinated? (2) Is it possible to rationally tune reactivity and selectivity by solvent? In short, our study revealed that the answer to questions 1 and 2 are both "yes". While the predicted effects are not large, they are not negligible.

What do our results imply for future computational studies of dirhodium-catalyzed reactions, an increasingly important tool in aiding organic synthesis? We conclude that it is worth seriously considering axial solvent ligation in such studies. In some cases, the changes in relative energies will be small, in which case one can deduce that axial solvent might not play an important role. In some cases, however, including axial solvent may be essential to accurately capture reactivity and selectivity—e.g., in computationally modeling stereoselective reactions,[161] in which case, accurately predicting $\Delta\Delta G^{\ddagger}$ may hinge on incorporating axial solvent in one's model—and missing the opportunity to do so due to axial solvent neglect would be an unfortunate oversight.

4.6 Acknowledgements

Support from the US National Science Foundation (CHE-1856416 and XSEDE) and the Ministerio de Educación, Cultura y Deporte, Programa Estatal de Promoción del Talento y su Empleabilidad en I+D+i, Subprograma Estatal de Movilidad del Plan Estatal de I+D+I (PRX19/00533) is gratefully acknowledged. We thank Prof. Jared T. Shaw (UC Davis) for encouragement, helpful discussion, and advice.

4.7 References

(1) Porai-Koshits, M. A.; Antsuskhima, A. S. The Structure of Rhodium Acetate Complexes. *Dokl. Akad. Nauk SSSR* **1962**, *146*, 1102–1105.
(2) Chifotides, H. T.; Dunbar, K. R. Rhodium Compounds. In *Multiple Bonds Between Metal Atoms*; Cotton, F. A., Murillo, C. A., Walton, R. A., Eds.; Springer: Boston, MA, 1982; pp 465–589.
(3) Hansen, J.; Davies, H. M. L. High Symmetry Dirhodium(II) Paddlewheel Complexes as Chiral Catalysts. *Coord. Chem. Rev.* **2008**, *252*, 545–555.
(4) Adly, F. G. On the Structure of Chiral Dirhodium(II) Carboxylate Catalysts: Stereoselectivity Relevance and Insights. *Catalysts* **2017**, *7*, 347.
(5) Berry, J. F.; Lu, C. C. Metal-Metal Bonds: From Fundamentals to Applications. *Inorg. Chem.* **2017**, *56*, 7577–7581.
(6) Farley, C. M.; Uyeda, C. Organic Reactions Enabled by Catalytically Active Metal–Metal Bonds. *Trends Chem.* **2019**, *1*, 497–509.
(7) Hrdina, R. Dirhodium(II,II) Paddlewheel Complexes. *Eur. J. Inorg. Chem.* **2021**, *2021*, 501–528.
(8) Abshire, A.; Moore, D.; Courtney, J.; Darko, A. Heteroleptic Dirhodium(II,II) Paddlewheel Complexes as Carbene Transfer Catalysts. *Org. Biomol. Chem.* **2021**, *19*, 8886–8905.
(9) Doyle, M. P. Electrophilic Metal Carbenes as Reaction Intermediates in Catalytic Reactions. *Acc. Chem. Res.* **1986**, *19*, 348–356.
(10) Doyle, M. P. Catalytic Methods for Metal Carbene Transformations. *Chem. Rev.* **1986**, *86*, 919–939.
(11) Chifotides, H. T.; Dunbar, K. R. Interactions of Metal-Metal-Bonded Antitumor Active Complexes with DNA Fragments and DNA. *Acc. Chem. Res.* **2005**, *38*, 146–156.
(12) Ohata, J.; Ball, Z. T. Rhodium at the Chemistry-Biology Interface. *Dalt. Trans.* **2018**, *47*, 14855–14860.
(13) Sohrabi, M.; Saeedi, M.; Larijani, B.; Mahdavi, M. Recent Advances in Biological Activities of Rhodium Complexes: Their Applications in Drug Discovery Research. *Eur.*

J. Med. Chem. **2021**, *216*, 113308.
(14) Cotton, F. A.; Lin, C.; Murillo, C. A. Supramolecular Arrays Based on Dimetal Building Units. *Acc. Chem. Res.* **2001**, *34*, 759–771.
(15) Reger, D. L.; Debreczeni, A.; Smith, M. D. Rhodium Paddlewheel Dimers Containing the π···π Stacking, 1,8-Naphthalimide Supramolecular Synthon. *Inorganica Chim. Acta* **2011**, *378*, 42–48.
(16) Furukawa, S.; Horike, N.; Kondo, M.; Hijikata, Y.; Carné-Sánchez, A.; Larpent, P.; Louvain, N.; Diring, S.; Sato, H.; Matsuda, R.; et al. Rhodium-Organic Cuboctahedra as Porous Solids with Strong Binding Sites. *Inorg. Chem.* **2016**, *55*, 10843–10846.
(17) Pirillo, J.; Hijikata, Y. Trans Influence across a Metal-Metal Bond of a Paddle-Wheel Unit on Interaction with Gases in a Metal-Organic Framework. *Inorg. Chem.* **2020**, *59*, 1193–1203.
(18) Padwa, A.; Weingarten, M. D. Cascade Processes of Metallo Carbenoids. *Chem. Rev.* **1996**, *96*, 223–269.
(19) Doyle, M. P.; Forbes, D. C. Recent Advances in Asymmetric Catalytic Metal Carbene Transformations. *Chem. Rev.* **1998**, *98*, 911–935.
(20) Doyle, M. P.; McKervey, M. A.; Ye, T. *Modern Catalytic Methods for Organic Synthesis with Diazo Compounds: From Cyclopropanes to Ylides*; Doyle, M. P., McKervey, M. A., Ye, T., Eds.; John Wiley & Sons, Inc.: New York, NY, 1998.
(21) Davies, H. M. L.; Manning, J. R. Catalytic C-H Functionalization by Metal Carbenoid and Nitrenoid Insertion. *Nature* **2008**, *451*, 417–424.
(22) Davies, H. M. L.; Denton, J. R. Application of Donor/Acceptor-Carbenoids to the Synthesis of Natural Products. *Chem. Soc. Rev.* **2009**, *38*, 3061–3071.
(23) Davies, H. M. L.; Parr, B. T. Rhodium Carbenes. In *Contemporary Carbene Chemistry*; Moss, R. A., Doyle, M. P., Eds.; John Wiley & Sons, Inc., 2014; pp 363–403.
(24) Jana, S.; Guo, Y.; Koenigs, R. M. Recent Perspectives on Rearrangement Reactions of Ylides via Carbene Transfer Reactions. *Chem. Eur. J.* **2021**, *27*, 1270–1281.
(25) Zhu, D.; Chen, L.; Fan, H.; Yao, Q.; Zhu, S. Recent Progress on Donor and Donor–Donor Carbenes. *Chem. Soc. Rev.* **2020**, *49*, 908–950.
(26) Wei, B.; Sharland, J. C.; Lin, P.; Wilkerson-Hill, S. M.; Fullilove, F. A.; McKinnon, S.; Blackmond, D. G.; Davies, H. M. L. In Situ Kinetic Studies of Rh(II)-Catalyzed Asymmetric Cyclopropanation with Low Catalyst Loadings. *ACS Catal.* **2020**, *10*, 1161–1170.
(27) Bergstrom, B. D.; Nickerson, L. A.; Shaw, J. T.; Souza, L. W. Transition Metal Catalyzed Insertion Reactions with Donor/Donor Carbenes. *Angew. Chem. Int. Ed.* **2021**, *60*, 6864–6878.
(28) Davies, H. M. L.; Morton, D. Guiding Principles for Site Selective and Stereoselective Intermolecular C-H Functionalization by Donor/Acceptor Rhodium Carbenes. *Chem. Soc. Rev.* **2011**, *40*, 1857–1869.
(29) Davies, H. M. L.; Liao, K. Dirhodium Tetracarboxylates as Catalysts for Selective Intermolecular C–H Functionalization. *Nat. Rev. Chem.* **2019**, *3*, 347–360.
(30) Adly, F. G.; Gardiner, M. G.; Ghanem, A. Design and Synthesis of Novel Chiral Dirhodium(II) Carboxylate Complexes for Asymmetric Cyclopropanation Reactions. *Chem. Eur. J.* **2016**, *22*, 3447–3461.
(31) Pirrung, M. C.; Liu, H.; Morehead, A. T. Rhodium Chemzymes: Michaelis-Menten Kinetics in Dirhodium(II) Carboxylate-Catalyzed Carbenoid Reactions. *J. Am. Chem. Soc.*

2002, *124*, 1014–1023.
(32) Norman, J. G.; Kolari, H. J. Strength and Trans Influence of the Rh-Rh Bond in Rhodium(II) Carboxylate Dimers. *J. Am. Chem. Soc.* **1978**, *100*, 791–799.
(33) Christoph, G. G.; Koh, Y. B. Metal-Metal Bonding in Dirhodium Tetracarboxylates. Trans Influence and Dependence of the Rh-Rh Bond Distance upon the Nature of the Axial Ligands. *J. Am. Chem. Soc.* **1979**, *101*, 1422–1434.
(34) Aguirre, J. D.; Lutterman, D. A.; Angeles-Boza, A. M.; Dunbar, K. R.; Turro, C. Effect of Axial Coordination on the Electronic Structure and Biological Activity of Dirhodium(II,II) Complexes. *Inorg. Chem.* **2007**, *46*, 7494–7502.
(35) Liu, J.; Groszewicz, P. B.; Wen, Q.; Thankamony, A. S. L.; Zhang, B.; Kunz, U.; Sauer, G.; Xu, Y.; Gutmann, T.; Buntkowsky, G. Revealing Structure Reactivity Relationships in Heterogenized Dirhodium Catalysts by Solid-State NMR Techniques. *J. Phys. Chem. C* **2017**, *121*, 17409–17416.
(36) Pietruschka, D. S.; Kumari, B.; Buntkowsky, G.; Gutmann, T.; Mollenhauer, D. Mechanism of Heterogenization of Dirhodium Catalysts: Insights from DFT Calculations. *Inorg. Chem.* **2021**, *60*, 6239–6248.
(37) Nagashima, T.; Davies, H. M. L. Catalytic Asymmetric Cyclopropanation Using Bridged Dirhodium Tetraprolinates on Solid Support. *Org. Lett.* **2002**, *4*, 1989–1992.
(38) Davies, H. M. L.; Walji, A. M. Asymmetric Intermolecular C-H Activation, Using Immobilized Dirhodium Tetrakis((S)-N-(Dodecylbenzenesulfonyl)-Prolinate) as a Recoverable Catalyst. *Org. Lett.* **2003**, *5*, 479–482.
(39) Davies, H. M. L.; Walji, A. M.; Nagashima, T. Simple Strategy for the Immobilization of Dirhodium Tetraprolinate Catalysts Using a Pyridine-Linked Solid Support. *J. Am. Chem. Soc.* **2004**, *126*, 4271–4280.
(40) Davies, H. M. L.; Walji, A. M. Universal Strategy for the Immobilization of Chiral Dirhodium Catalysts Huw. *Org. Lett.* **2005**, *7*, 2941–2944.
(41) Kataoka, Y.; Fukumoto, R.; Yano, N.; Atarashi, D.; Tanaka, H.; Kawamoto, T.; Handa, M. Synthesis, Characterization, Absorption Properties, and Electronic Structures of Paddlewheel-Type Dirhodium(II) Tetra-μ-(n-Naphthoate) Complexes: An Experimental and Theoretical Study. *Molecules* **2019**, *24*, 447.
(42) Fussell, E. D.; Darko, A. Adducts of Rhodium(II) Acetate and Rhodium(II) Pivalate with 1,8-Diazabicyclo[5.4.0]Undec-7-Ene. *Crystals* **2021**, *11*, 517.
(43) Das, A.; Wang, C.-H.; Van Trieste, G.; Sun, C.-J.; Chen, Y.-S.; Reibenspies, J.; Powers, D. In Crystallo Snapshots of Rh_2-Catalyzed C–H Amination. *J. Am. Chem. Soc.* **2020**, *142*, 19862–19867.
(44) Lu, W.; Zhu, X.; Yang, L.; Wu, X.; Xie, X.; Zhang, Z. Distinct Catalytic Performance of Dirhodium(II) Complexes with Ortho-Metalated DPPP in Dehydrosilylation of Styrene Derivatives with Alkoxysilanes. *ACS Catal.* **2021**, *11*, 10190–10197.
(45) Löffler, L. E.; Buchsteiner, M.; Collins, L. R.; Caló, F. P.; Singha, S.; Fürstner, A. $[Rh_2(MEPY)_4]$ and $[BiRh(MEPY)_4]$: Convenient Syntheses and Computational Analysis of Strikingly Dissimilar Siblings. *Helv. Chim. Acta* **2021**, *104*, e2100042.
(46) Wu, R.; Lu, J.; Cao, T.; Ma, J.; Chen, K.; Zhu, S. Enantioselective Rh(II)-Catalyzed Desymmetric Cycloisomerization of Diynes: Constructing Furan-Fused Dihydropiperidines with an Alkyne-Substituted Aza-Quaternary Stereocenter. *J. Am. Chem. Soc.* **2021**, *143*, 14916–14925.
(47) Vosáhlo, P.; Harmach, P.; Císařová, I.; Štěpnička, P. Synthesis and Characterisation of

Dirhodium(II) Tetraacetates Bearing Axial Ferrocene Ligands. *J. Organomet. Chem.* **2021**, *953*, 122065.
(48) Cotton, F. A.; Hillard, E. A.; Murillo, C. A. The First Dirhodium Tetracarboxylate Molecule without Axial Ligation: New Insight into the Electronic Structures of Molecules with Importance in Catalysis and Other Reactions. *J. Am. Chem. Soc.* **2002**, *124*, 5658–5660.
(49) Werlé, C.; Goddard, R.; Fürstner, A. The First Crystal Structure of a Reactive Dirhodium Carbene Complex and a Versatile Method for the Preparation of Gold Carbenes by Rhodium-to-Gold Transmetalation. *Angew. Chem. Int. Ed.* **2015**, *54*, 15452–15456.
(50) Werlé, C.; Goddard, R.; Philipps, P.; Farès, C.; Fürstner, A. Structures of Reactive Donor/Acceptor and Donor/Donor Rhodium Carbenes in the Solid State and Their Implications for Catalysis. *J. Am. Chem. Soc.* **2016**, *138*, 3797–3805.
(51) Drago, R. S.; Tanner, S. P.; Richman, R. M.; Long, J. R. Quantitative Studies of Chemical Reactivity of Tetra-μ-Butyrato-Dirhodium(II) Complexes. *J. Am. Chem. Soc.* **1979**, *101*, 2897–2903.
(52) Drago, R. S.; Long, J. R.; Cosmano, R. Metal Synergism in the Coordination Chemistry of a Metal-Metal Bonded System: $Rh_2(C_3H_7COO)_4$. *Inorg. Chem.* **1981**, *20*, 2920–2927.
(53) Drago, R. S.; Long, J. R.; Cosmano, R. Comparison of the Coordination Chemistry and Inductive Transfer through the Metal—Metal Bond in Adducts of Dirhodium and Dimolybdenum Carboxylates. *Inorg. Chem.* **1982**, *21*, 2196–2202.
(54) Trindade, A. F.; Coelho, J. A. S. T.; Afonso, C. A. M.; Veiros, L. F.; Gois, P. M. P. Fine Tuning of Dirhodium(II) Complexes: Exploring the Axial Modification. *ACS Catal.* **2012**, *2*, 370–383.
(55) Warzecha, E.; Berto, T. C.; Berry, J. F. Axial Ligand Coordination to the C-H Amination Catalyst $Rh_2(esp)_2$: A Structural and Spectroscopic Study. *Inorg. Chem.* **2015**, *54*, 8817–8824.
(56) Johnson, S. A.; Hunt, H. R.; Neumann, H. M. Preparation and Properties of Anhydrous Rhodium(II) Acetate and Some Adducts Thereof. *Inorg. Chem.* **1963**, *2*, 960–962.
(57) Antos, J. M.; McFarland, J. M.; Iavarone, A. T.; Francis, M. B. Chemoselective Tryptophan Labeling with Rhodium Carbenoids at Mild pH. *J. Am. Chem. Soc.* **2009**, *131*, 6301–6308.
(58) Berry, J. F. The Role of Three-Center/Four-Electron Bonds in Superelectrophilic Dirhodium Carbene and Nitrene Catalytic Intermediates. *Dalt. Trans.* **2012**, *41*, 700–713.
(59) Warzecha, E.; Berto, T. C.; Wilkinson, C. C.; Berry, J. F. Rhodium Rainbow: A Colorful Laboratory Experiment Highlighting Ligand Field Effects of Dirhodium Tetraacetate. *J. Chem. Educ.* **2019**, *96*, 571–576.
(60) Caló, F. P.; Bistoni, G.; Auer, A. A.; Leutzsch, M.; Fürstner, A. Triple Resonance Experiments for the Rapid Detection of ^{103}Rh NMR Shifts: A Combined Experimental and Theoretical Study into Dirhodium and Bismuth−Rhodium Paddlewheel Complexes. *J. Am. Chem. Soc.* **2021**, *143*, 12473–12479.
(61) Sarkar, M.; Daw, P.; Ghatak, T.; Bera, J. K. Amide-Functionalized Naphthyridines on a RhII –RhII Platform: Effect of Steric Crowding, Hemilability, and Hydrogen-Bonding Interactions on the Structural Diversity and Catalytic Activity of Dirhodium(II) Complexes. *Chem. Eur. J.* **2014**, *20*, 16537–16549.
(62) Sambasivan, R.; Zheng, W.; Burya, S. J.; Popp, B. V.; Turro, C.; Clementi, C.; Ball, Z. T. A Tripodal Peptide Ligand for Asymmetric Rh(II) Catalysis Highlights Unique Features

of on-Bead Catalyst Development. *Chem. Sci.* **2014**, *5*, 1401–1407.
(63) Sheffield, W.; Abshire, A.; Darko, A. Effect of Tethered, Axial Thioether Coordination on Rhodium(II)-Catalyzed Silyl-Hydrogen Insertion. *Eur. J. Org. Chem.* **2019**, *2019*, 6347–6351.
(64) Cressy, D.; Zavala, C.; Abshire, A.; Sheffield, W.; Darko, A. Tuning Rh(II)-Catalysed Cyclopropanation with Tethered Thioether Ligands. *Dalt. Trans.* **2020**, *49*, 15779–15787.
(65) Cressy, D. *Fine Tuning RhII Complexes with Tethered, Axial Coordination: Structural Studies and Application to Diazo-Mediated Cyclopropanation Reactions. PhD Diss., University of Tennessee*; 2021.
(66) Ohnishi, R.; Ohta, H.; Mori, S.; Hayashi, M. Cationic Dirhodium Complexes Bridged by 2-Phosphinopyridines Having an Exquisitely Positioned Axial Shielding Group: A Molecular Design for Enhancing the Catalytic Activity of the Dirhodium Core. *Organometallics* **2021**, *40*, 2678–2690.
(67) Snyder, J. P.; Padwa, A.; Stengel, T.; Arduengo III, A. J.; Jockisch, A.; Kim, H.-J. A Stable Dirhodium Tetracarboxylate Carbenoid: Crystal Structure, Bonding Analysis, and Catalysis. *J. Am. Chem. Soc.* **2001**, *123*, 11318–11319.
(68) Gomes, L. F. R.; Trindade, A. F.; Candeias, N. R.; Veiros, L. F.; Gois, P. M. P.; Afonso, C. A. M. Cyclization of Diazoacetamides Catalyzed by N-Heterocyclic Carbene Dirhodium(II). *Synthesis* **2009**, *20*, 3519–3526.
(69) Rej, S.; Chatani, N. Effect of Sulfonamide and Carboxamide Ligands on the Structural Diversity of Bimetallic Rh. *Inorg. Chem.* **2021**, *60*, 3534–3538.
(70) Anderson, B. G.; Cressy, D.; Patel, J. J.; Harris, C. F.; Yap, G. P. A.; Berry, J. F.; Darko, A. Synthesis and Catalytic Properties of Dirhodium Paddlewheel Complexes with Tethered, Axially Coordinating Thioether Ligands. *Inorg. Chem.* **2019**, *58*, 1728–1732.
(71) Zavala, C.; Darko, A. Effect of Tethered, Axially Coordinated Ligands (TACLs) on Dirhodium(II,II) Catalyzed Cyclopropanation: A Linear Free Energy Relationship Study. *J. Org. Chem.* **2022**, *87*, 6910–6917.
(72) Xu, X.; Zavalij, P. Y.; Doyle, M. P. Catalytic Asymmetric Syntheses of Quinolizidines by Dirhodium-Catalyzed Dearomatization of Isoquinolinium/Pyridinium Methylides−The Role of Catalyst and Carbene Source. *J. Am. Chem. Soc.* **2013**, *135*, 12439–12447.
(73) Nelson, T. D.; Song, Z. J.; Thompson, A. S.; Zhao, M.; DeMarco, A.; Reamer, R. A.; Huntington, M. F.; Grabowski, E. J. J.; Reider, P. J. Rhodium-Carbenoid-Mediated Intermolecular O–H Insertion Reactions: A Dramatic Additive Effect. Application in the Synthesis of an Ascomycin Derivative. *Tetrahedron Lett.* **2000**, *41*, 1877–1881.
(74) Marcoux, D.; Azzi, S.; Charette, A. B. TfNH2 as Achiral Hydrogen-Bond Donor Additive to Enhance the Selectivity of a Transition Metal Catalyzed Reaction. Highly Enantio- And Diastereoselective Rhodium-Catalyzed Cyclopropanation of Alkenes Using α-Cyano Diazoacetamide. *J. Am. Chem. Soc.* **2009**, *131*, 6970–6972.
(75) Marcoux, D.; Lindsay, V. N. G.; Charette, A. B. Use of Achiral Additives to Increase the Stereoselectivity in Rh(II)-Catalyzed Cyclopropanations. *Chem. Commun.* **2010**, *46*, 910–912.
(76) Lindsay, V. N. G.; Nicolas, C.; Charette, A. B. Asymmetric Rh(II)-Catalyzed Cyclopropanation of Alkenes with Diacceptor Diazo Compounds: P-Methoxyphenyl Ketone as a General Stereoselectivity Controlling Group. *J. Am. Chem. Soc.* **2011**, *133*, 8972–8981.
(77) Sharland, J. C.; Wei, B.; Hardee, D. J.; Hodges, T. R.; Gong, W.; Voight, E. A.; Davies,

H. M. L. Role of Additives to Overcome Limitations of Intermolecular Rhodium-Catalyzed Asymmetric Cyclopropanation. *ChemRxiv* **2021**, doi: 10.26434/chemrxiv.14479593.v1.

(78) Varghese, J. J.; Mushrif, S. H. Origins of Complex Solvent Effects on Chemical Reactivity and Computational Tools to Investigate Them: A Review. *React. Chem. Eng.* **2019**, *4*, 165–206.

(79) Wynne, D. C.; Olmstead, M. M.; Jessop, P. G. Supercritical and Liquid Solvent Effects on the Enantioselectivity of Asymmetric Cyclopropanation with Tetrakis[1-[(4-Tert-Butylphenyl)- Sulfonyl]-(2S)-Pyrrolidinecarboxylate]Dirhodium(II). *J. Am. Chem. Soc.* **2000**, *122*, 7638–7647.

(80) Rosales, A.; Rodríguez-García, I.; López-Sánchez, C.; Álvarez-Corral, M.; Muñoz-Dorado, M. Solvent Influence in the Rh-Catalyzed Intramolecular 1,6 C-H Insertions: A General Approach to the Chromane and Flavanone Skeletons. *Tetrahedron* **2011**, *67*, 3071–3075.

(81) Yang, Z.; Guo, Y.; Koenigs, R. M. Solvent-Dependent, Rhodium Catalysed Rearrangement Reactions of Sulfur Ylides. *Chem. Commun.* **2019**, *55*, 8410–8413.

(82) Candeias, N. R.; Gois, P. M. P.; Afonso, C. A. M. Rh(II) Catalysed Intramolecular C-H Insertion of Diazo Substrates in Water: A Simple and Efficient Approach to Catalyst Reuse. *Chem. Commun.* **2005**, 391–393.

(83) Candeias, N. R.; Gois, P. M. P.; Afonso, C. A. M. Rh(II)-Catalyzed Intramolecular C-H Insertion of Diazo Substrates in Water: Scope and Limitations. *J. Org. Chem.* **2006**, *71*, 5489–5497.

(84) Wurz, R. P.; Charette, A. B. Transition Metal-Catalyzed Cyclopropanation of Alkenes in Water: Catalyst Efficiency and in Situ Generation of the Diazo Reagent. *Org. Lett.* **2002**, *4*, 4531–4533.

(85) Zhu, C.-Z.; Wei, Y.; Shi, M. Rhodium(II)-Catalyzed Intramolecular Transannulation of 4-Methoxycyclohexa-2,5-Dienone Tethered 1-Sulfonyl-1,2,3-Triazoles: Synthesis of Azaspiro[5.5]Undecane Derivatives. *Adv. Synth. Catal.* **2019**, *361*, 3430–3435.

(86) Zhu, C.-Z.; Wei, Y.; Shi, M. Rhodium(II)-Catalyzed Divergent Intramolecular Tandem Cyclization of N-or O-Tethered Cyclohexa-2,5-Dienones with 1-Sulfonyl-1,2,3- Triazole: Synthesis of Cyclopropa[Cd]Indole and Benzofuran Derivatives. *Org. Chem. Front.* **2019**, *6*, 2884–2891.

(87) Nickerson, L. A.; Bergstrom, B. D.; Gao, M.; Shiue, Y. S.; Laconsay, C. J.; Culberson, M. R.; Knauss, W. A.; Fettinger, J. C.; Tantillo, D. J.; Shaw, J. T. Enantioselective Synthesis of Isochromans and Tetrahydroisoquinolines by C-H Insertion of Donor/Donor Carbenes. *Chem. Sci.* **2020**, *11*, 494–498.

(88) Chiappini, N. D.; Mack, J. B. C.; Du Bois, J. Intermolecular C(sp^3)−H Amination of Complex Molecules. *Angew. Chem. Int. Ed.* **2018**, *57*, 4956–4959.

(89) Hansen, J.; Li, B.; Dikarev, E.; Autschbach, J.; Davies, H. M. L. Combined Experimental and Computational Studies of Heterobimetallic Bi-Rh Paddlewheel Carboxylates as Catalysts for Metal Carbenoid Transformations. *J. Org. Chem.* **2009**, *74*, 6564–6571.

(90) Kisan, H. K.; Sunoj, R. B. Axial Coordination Dichotomy in Dirhodium Carbenoid Catalysis: A Curious Case of Cooperative Asymmetric Dual-Catalytic Approach toward Amino Esters. *J. Org. Chem.* **2015**, *80*, 2192–2197.

(91) Azek, E.; Lai, C.; Ernzerhof, M.; Lebel, H. Rhodium-Catalyzed Sulfimidation Reactions: A Computational Study. *Organometallics* **2021**, *40*, 3267–3275.

(92) Mato, M.; Montesinos-Magraner, M.; Sugranyes, A. R.; Echavarren, A. M. Rh(II)-Catalyzed Alkynylcyclopropanation of Alkenes by Decarbenation of Alkynylcycloheptatrienes. *J. Am. Chem. Soc.* **2021**, *143*, 10760–10769.
(93) Li, F.; Pei, C.; Koenigs, R. M. Rhodium-Catalyzed Cascade Reactions of Triazoles with Organoselenium Compounds – A Combined Experimental and Mechanistic Study. *Chem. Sci.* **2021**, *12*, 6362–6369.
(94) Zhao, Y.-T.; Su, Y.-X.; Li, X.-Y.; Yang, L.-L.; Huang, M.-Y.; Zhu, S.-F. Dirhodium-Catalyzed Enantioselective B–H Bond Insertion of Gem-Diaryl Carbenes: Efficient Access to Gem-Diarylmethine Boranes. *Angew. Chem. Int. Ed.* **2021**, *60*, 24214–24219.
(95) Harrison, J. G.; Gutierrez, O.; Jana, N.; Driver, T. G.; Tantillo, D. J. Mechanism of Rh_2(II)-Catalyzed Indole Formation: The Catalyst Does Not Control Product Selectivity. *J. Am. Chem. Soc.* **2016**, *138*, 487–490.
(96) Laconsay, C. J.; Tantillo, D. J. Metal Bound or Free Ylides as Reaction Intermediates in Metal-Catalyzed [2,3]-Sigmatropic Rearrangements? It Depends. *ACS Catal.* **2021**, *11*, 829–839.
(97) Laconsay, C. J.; Tantillo, D. J. Melding of Experiment and Theory Illuminates Mechanisms of Metal-Catalyzed Rearrangements: Computational Approaches and Caveats. *Synthesis* **2021**, *53*, 3639–3652.
(98) Sperger, T.; Sanhueza, I. A.; Kalvet, I.; Schoenebeck, F. Computational Studies of Synthetically Relevant Homogeneous Organometallic Catalysis Involving Ni, Pd, Ir, and Rh: An Overview of Commonly Employed DFT Methods and Mechanistic Insights. *Chem. Rev.* **2015**, *115*, 9532–9586.
(99) Sperger, T.; Sanhueza, I. A.; Schoenebeck, F. Computation and Experiment: A Powerful Combination to Understand and Predict Reactivities. *Acc. Chem. Res.* **2016**, *49*, 1311–1319.
(100) Ryu, H.; Park, J.; Kim, H. K.; Park, J. Y.; Kim, S.-T.; Baik, M.-H. Pitfalls in Computational Modeling of Chemical Reactions and How To Avoid Them. *Organometallics* **2018**, *37*, 3228–3239.
(101) Ahn, S.; Hong, M.; Sundararajan, M.; Ess, D. H.; Baik, M.-H. Design and Optimization of Catalysts Based on Mechanistic Insights Derived from Quantum Chemical Reaction Modeling. *Chem. Rev.* **2019**, *119*, 6509–6560.
(102) Harvey, J. N.; Himo, F.; Maseras, F.; Perrin, L. Scope and Challenge of Computational Methods for Studying Mechanism and Reactivity in Homogeneous Catalysis. *ACS Catal.* **2019**, *9*, 6803–6813.
(103) Eisenstein, O.; Ujaque, G.; Lledós, A. What Makes a Good (Computed) Energy Profile? In *New Directions in the Modeling of Organometallic Reactions. Topics in Organometallic Chemistry*; Lledós, A., Ujaque, G., Eds.; Springer, 2020; Vol. 67, pp 1–38.
(104) Morgante, P.; Peverati, R. The Devil in the Details: A Tutorial Review on Some Undervalued Aspects of Density Functional Theory Calculations. *Int. J. Quantum Chem.* **2020**, *120*, e26332.
(105) Qi, X.; Lan, Y. Recent Advances in Theoretical Studies on Transition-Metal- Catalyzed Carbene Transformations. *Acc. Chem. Res.* **2021**, *54*, 2905–2915.
(106) Matsuzawa, A.; Harvey, J. N.; Himo, F. On the Importance of Considering Multinuclear Metal Sites in Homogeneous Catalysis Modeling. *Top. Catal.* **2022**, *65*, 96–104.
(107) Frisch, M. J.; Trucks, G. W.; Schlegel, H. B.; Scuseria, G. E. .; Robb, G. E.; Cheeseman,

J. R.; Scalmani, G.; Barone, V.; Mennucci, B. .; Petersson, G. A.; Nakatsuji, H.; Caricato, M.; Li, X.; Hratchian, H. P. .; Izmaylov, A. F.; Bloino, J.; Zheng, G.; Sonnenberg, J. L.; Hada, M. .; Ehara, M.; Toyota, K.; Fukuda, R.; Hasegawa, J.; Ishida, M.; Nakajima, T. .; Honda, Y.; Kitao, O.; Nakai, H.; Vreven, T.; Montgomery, Jr., J. A. . P.; J. E.; Ogliaro, F.; Bearpark, M.; Heyd, J. J.; Brothers, E. . K.; K. N.; Staroverov, V. N.; Keith, T.; Kobayashi, R.; Normand, J. . R.; K.; Rendell, A.; Burant, J. C.; Iyengar, S. S.; Tomasi, J. . C.; M.; Rega, N.; Millam, J. M.; Klene, M.; Knox, J. E.; Cross, J. B. .; Bakken, V.; Adamo, C.; Jaramillo, J.; Gomperts, R.; Stratmann, R. E.; Yazyev O.; Austin, A. J.; Cammi, R.; Pomelli, C.; Ochterski, J. W.; Martin R. L.; Morokuma, K.; Zakrzewski, V. G.; Voth, G. A.; Salvador, P.; Dannenberg, J. J.; Dapprich, S.; Daniels, A. D.; Farkas O.; Foresman, J. B.; Ortiz, J. V.; Cioslowski, J.; Fox, D. J. *Gaussian 09*, Revision D.01. Gaussian Inc. Wallingford, CT 2009.

(108) Fukui, K. The Path of Chemical Reactions -- The IRC Approach. *Acc. Chem. Res.* **1981**, *14*, 363–368.

(109) Gonzalez, C.; Schlegel, H. B. Reaction Path Following In Mass-Weighted Internal Coordinates Cartesians and with Internal Coordinates without Mass-Weighting. *J. Phys. Chem.* **1990**, *94*, 5523–5527.

(110) Maeda, S.; Harabuchi, Y.; Ono, Y.; Taketsugu, T.; Morokuma, K. Intrinsic Reaction Coordinate: Calculation, Bifurcation, and Automated Search. *Int. J. Quantum Chem.* **2015**, *115*, 258–269.

(111) Becke, A. D. Density-Functional Thermochemistry. III. The Role of Exact Exchange. *J. Chem. Phys.* **1993**, *98*, 5648–5652.

(112) Hay, P. J.; Wadt, W. R. Ab Initio Effective Core Potentials for Molecular Calculations. Potentials for the Transition Metal Atoms Sc to Hg. *J. Chem. Phys.* **1985**, *82*, 270–283.

(113) Barone, V.; Cossi, M. Quantum Calculation of Molecular Energies and Energy Gradients in Solution by a Conductor Solvent Model. *J. Phys. Chem. A* **1998**, *102*, 1995–2001.

(114) Cossi, M.; Rega, N.; Scalmani, G.; Barone, V. Energies, Structures, and Electronic Properties of Molecules in Solution with the C-PCM Solvation Model. *J. Comput. Chem.* **2003**, *24*, 669–681.

(115) Takano, Y.; Houk, K. N. Benchmarking the Conductor-like Polarizable Continuum Model (CPCM) for Aqueous Solvation Free Energies of Neutral and Ionic Organic Molecules. *J. Chem. Theory Comput.* **2005**, *1*, 70–77.

(116) Zhao, Y.; Truhlar, D. G. The M06 Suite of Density Functionals for Main Group Thermochemistry, Thermochemical Kinetics, Noncovalent Interactions, Excited States, and Transition Elements: Two New Functionals and Systematic Testing of Four M06-Class Functionals and 12 Other Function. *Theor. Chem. Acc.* **2008**, *120*, 215–241.

(117) Fuentealba, P.; Preuss, H.; Stoll, H.; Von Szentpály, L. A Proper Account of Core-Polarization with Pseudopotentials: Single Valence-Electron Alkali Compounds. *Chem. Phys. Lett.* **1982**, *89*, 418–422.

(118) Weinhold, F.; Carpenter, J. E. The Natural Bond Orbital Lewis Structure Concept for Molecules, Radicals, and Radical Ions. In *The Structure of Small Molecules and Ions*; Naaman, R., Vager, Z., Eds.; Springer: Boston, MA, 1988; pp 227–236.

(119) Foster, J. P.; Weinhold, F. Natural Hybrid Orbitals. *J. Am. Chem. Soc.* **1980**, *102*, 7211–7218.

(120) Weinhold, F.; Landis, C. R.; Glendening, E. D. What Is NBO Analysis and How Is It Useful? *Int. Rev. Phys. Chem.* **2016**, *35*, 399–440.

(121) Glendening, E. D.; Reed, A. E.; Carpenter, J. E.; Weinhold, F. NBO Version 3.1 Gaussian Inc. Pittsburgh 2003.
(122) Nowlan III, D. T.; Gregg, T. M.; Davies, H. M. L.; Singleton, D. A. Isotope Effects and the Nature of Selectivity in Rhodium-Catalyzed Cyclopropanations. *J. Am. Chem. Soc.* **2003**, *125*, 15902–15911.
(123) Kisan, H. K.; Sunoj, R. B. Deciphering the Origin of Cooperative Catalysis by Dirhodium Acetate and Chiral Spiro Phosphoric Acid in an Asymmetric Amination Reaction. *Chem. Commun.* **2014**, *50*, 14639–14642.
(124) Lee, M.; Ren, Z.; Musaev, D. G.; Davies, H. M. L. Rhodium-Stabilized Diarylcarbenes Behaving as Donor/Acceptor Carbenes. *ACS Catal.* **2020**, *10*, 6240–6247.
(125) Nair, V. N.; Kojasoy, V.; Laconsay, C. J.; Kong, W. Y.; Tantillo, D. J.; Tambar, U. K. Catalyst-Controlled Regiodivergence in Rearrangements of Indole-Based Onium Ylides. *J. Am. Chem. Soc.* **2021**, *143*, 9016–9025.
(126) Kozuch, S.; Shaik, S. How to Conceptualize Catalytic Cycles? The Energetic Span Model. *Acc. Chem. Res.* **2011**, *44*, 101–110.
(127) Anciaux, A. J.; Hubert, A. J.; Noels, A. F.; Petiniot, N.; Teyssié, P. Transition-Metal-Catalyzed Reactions of Diazo Compounds. 1. Cyclopropanation of Double Bonds. *J. Org. Chem.* **1980**, *45*, 695–702.
(128) Zhao, Y.; Truhlar, D. G. A New Local Density Functional for Main-Group Thermochemistry, Transition Metal Bonding, Thermochemical Kinetics, and Noncovalent Interactions. *J. Chem. Phys.* **2006**, *125*, 194101.
(129) Yu, H. S.; He, X.; Li, S. L.; Truhlar, D. G. MN15: A Kohn-Sham Global-Hybrid Exchange-Correlation Density Functional with Broad Accuracy for Multi-Reference and Single-Reference Systems and Noncovalent Interactions. *Chem. Sci.* **2016**, *7*, 5032–5051.
(130) Grimme, S.; Antony, J.; Ehrlich, S.; Krieg, H. A Consistent and Accurate Ab Initio Parametrization of Density Functional Dispersion Correction (DFT-D) for the 94 Elements H-Pu. *J. Chem. Phys.* **2010**, *132*, 154104.
(131) Grimme, S.; Ehrlich, S.; Goerigk, L. Effect of the Damping Function in Dispersion Corrected Density Functional Theory. *J. Comput. Chem.* **2011**, *32*, 1456–1465.
(132) Liao, K.; Pickel, T. C.; Boyarskikh, V.; Bacsa, J.; Musaev, D. G.; Davies, H. M. L. Site-Selective and Stereoselective Functionalization of Non-Activated Tertiary C-H Bonds. *Nature* **2017**, *551*, 609–613.
(133) Zhou, M.; Springborg, M. Theoretical Study of the Mechanism behind the Site- and Enantio-Selectivity of C-H Functionalization Catalysed by Chiral Dirhodium Catalyst. *Phys. Chem. Chem. Phys.* **2020**, *22*, 9561–9572.
(134) Álvarez-Moreno, M.; de Graaf, C.; López, N.; Maseras, F.; Poblet, J. M.; Bo, C. Managing the Computational Chemistry Big Data Problem: The ioChem-BD Platform. *J. Chem. Inf. Model.* **2015**, *55*, 95–103.
(135) Ford, A.; Miel, H.; Ring, A.; Slattery, C. N.; Maguire, A. R.; McKervey, M. A. Modern Organic Synthesis with α-Diazocarbonyl Compounds. *Chem. Rev.* **2015**, *115*, 9981–10080.
(136) Medvedev, J. J.; Nikolaev, V. A. Recent Advances in the Chemistry of Rh Carbenoids: Multicomponent Reactions of Diazocarbonyl Compounds. *Russ. Chem. Rev.* **2015**, *84*, 737–757.
(137) Davies, H. M. L.; Beckwith, R. E. J. Catalytic Enantioselective C-H Activation by Means of Metal-Carbenoid-Induced C-H Insertion. *Chem. Rev.* **2003**, *103*, 2861–2903.

(138) Staudinger, H.; Endle, R. Über Reaktionen Des Methylens. IV: Über Die Zersetzung Der Ketene Bei Hoher Temperatur. *Ber. Chem.* **1913**, *46*, 1437–1442.
(139) Shaw, J. T. C-H Insertion Reactions of Donor/Donor Carbenes: Inception, Investigation, and Insights. *Synlett* **2020**, *31*, 838–844.
(140) Nakamura, E.; Yoshikai, N.; Yamanaka, M. Mechanism of C−H Bond Activation/C−C Bond Formation Reaction between Diazo Compound and Alkane Catalyzed by Dirhodium Tetracarboxylate. *J. Am. Chem. Soc.* **2002**, *124*, 7181–7192.
(141) Hare, S. R.; Tantillo, D. J. Cryptic Post-Transition State Bifurcations That Reduce the Efficiency of Lactone-Forming Rh-Carbenoid C-H Insertions. *Chem. Sci.* **2017**, *8*, 1442–1449.
(142) Lamb, K. N.; Squitieri, R. A.; Chintala, S. R.; Kwong, A. J.; Balmond, E. I.; Soldi, C.; Dmitrenko, O.; Castiñeira Reis, M.; Chung, R.; Addison, J. B.; Fettinger, J. C.; Hein, J. E.; Tantillo, D. J.; Fox, J. M.; Shaw, J. T. Synthesis of Benzodihydrofurans by Asymmetric C−H Insertion Reactions of Donor/Donor Rhodium Carbenes. *Chem. Eur. J.* **2017**, *23*, 11843–11855.
(143) Tantillo, D. J. Recent Excursions to the Borderlands between the Realms of Concerted and Stepwise: Carbocation Cascades in Natural Products Biosynthesis. *J. Phys. Org. Chem.* **2008**, *21*, 561–570.
(144) Dishman, S. N.; Laconsay, C. J.; Fettinger, J. C.; Tantillo, D. J.; Shaw, J. T. Divergent Stereochemical Outcomes in the Insertion of Donor/Donor Carbenes into the C–H Bonds of Stereogenic Centers. *Chem. Sci.* **2022**, *13*, 1030–1036.
(145) Taber, D. F.; Ruckle Jr., R. E. Cyclopentane Construction by $Rh_2(OAc)_4$-Mediated Intramolecular C-H Insertion: Steric and Electronic Effects. *J. Am. Chem. Soc.* **1986**, *108*, 7686–7693.
(146) Doyle, M. P.; Westrum, L. J.; Wolthuis, W. N. E.; See, M. M.; Boone, W. P.; Bagheri, V.; Pearson, M. M. Electronic and Steric Control in Carbon-Hydrogen Insertion Reactions of Diazoacetoacetates Catalyzed by Dirhodium(II) Carboxylates and Carboxamides. *J. Am. Chem. Soc.* **1993**, *115*, 958–964.
(147) Zakrzewska, M. E.; Cal, P. M. S. D.; Candeias, N. R.; Bogel-Łukasik, R.; Afonso, C. A. M.; Ponte, M. N.; Gois, P. M. P. Intramolecular C–H Insertion Catalyzed by Dirhodium(II) Complexes Using CO_2 as the Reaction Media. *Green Chem. Lett. Rev.* **2012**, *5*, 211–240.
(148) Mu, L.; Drago, R. S.; Richardson, D. E. A Model Based QSPR Analysis of the Unified Non-Specific Solvent Polarity Scale. *J. Chem. Soc. Perkin Trans. 2* **1998**, *2*, 159–167.
(149) Badger, R. M. A Relation Between Internuclear Distances and Bond Force Constants. *J. Chem. Phys.* **1934**, *2*, 128–131.
(150) Huggins, M. L. Atomic Radii. IV. Dependence of Interatomic Distance on Bond Energy. *J. Am. Chem. Soc.* **1953**, *75*, 4126–4133.
(151) Kaupp, M.; Metz, B.; Stoll, H. Breakdown of Bond Length-Bond Strength Correlation: A Case Study. *Angew. Chem. Int. Ed.* **2000**, *39*, 4607–4609.
(152) Alvarez, S. A Cartography of the van Der Waals Territories. *Dalt. Trans.* **2013**, *42*, 8617–8636.
(153) Wiberg, K. B. Application of the Pople-Santry-Segal CNDO Method to the Cyclopropylcarbinyl and Cyclobutyl Cation and to Bicyclobutane. *Tetrahedron* **1968**, *24*, 1083–1096.
(154) Aullón, G.; Alvarez, S. Pyramidality Effect on Rh(II)-Rh(II) Single Bonds. *Inorg. Chem.*

1993, *32*, 3712–3719.
(155) Parr, R. G.; Szentpály, L. v.; Liu, S. Electrophilicity Index. *J. Am. Chem. Soc.* **1999**, *121*, 1922–1924.
(156) Chattaraj, P. K.; Sarkar, U.; Roy, D. R. Electrophilicity Index. *Chem. Rev.* **2006**, *106*, 2065–2091.
(157) Domingo, L. R.; Ríos-Gutiérrez, M.; Pérez, P. Applications of the Conceptual Density Functional Theory Indices to Organic Chemistry Reactivity. *Molecules* **2016**, *21*, 748.
(158) Jupp, A. R.; Johnstone, T. C.; Stephan, D. W. Improving the Global Electrophilicity Index (GEI) as a Measure of Lewis Acidity. *Inorg. Chem.* **2018**, *57*, 14764–14771.
(159) Parr, R. G.; Donnelly, R. A.; Levy, M.; Palke, W. E. Electronegativity: The Density Functional Viewpoint. *J. Chem. Phys.* **1978**, *68*, 3801–3807.
(160) Parr, R. G.; Pearson, R. G. Absolute Hardness: Companion Parameter to Absolute Electronegativity. *J. Am. Chem. Soc.* **1983**, *105*, 7512–7516.
(161) Peng, Q.; Duarte, F.; Paton, R. S. Computing Organic Stereoselectivity-from Concepts to Quantitative Calculations and Predictions. *Chem. Soc. Rev.* **2016**, *45*, 6093–6107.

Chapter 5

A Stepwise S_E2 Mechanism in the Insertion of Donor/Donor Carbenes into the C–H Bonds of Stereogenic Centers*

While differing widely in the various little bits we know, in our infinite ignorance we are all equal.

- Karl R. Popper

5.1 Abstract

A stepwise S_E2 mechanism was discovered in a computational study of an experimentally observed C-H insertion reaction of a donor/donor Rh carbene. Collaboration with experiment (with Sarah Dishman and Jared Shaw) helped elucidate the mechanistic origin of stereoselectivity in this dirhodium(II)-promoted C-H insertion reaction into a stereocenter to benzodihydrofurans with two contiguous stereocenters.

5.2 Introduction

The activation of C-H bonds has transformed organic chemists' ability to forge new chemical bonds. Metal-carbene intermediates play an indispensable role towards the development of

* Portions of this chapter are reproduced or adapted from Dishman, S. N.; Laconsay, C. J.; Fettinger, J. C.; Tantillo, D. J.; Shaw, J. T. Divergent stereochemical outcomes in the insertion of donor/donor carbenes into the C–H bonds of stereogenic centers, *Chem. Sci.* **2022**, *13*, 1030-1036 with permission from the Royal Society of Chemistry. Sarah Dishman (of Prof. Jared Shaw's group) completed the experimental portions of this chapter.

efficient C-H activation methods. Indeed, while much is understood regarding metal-carbenes with one (or more)—so called "donor/acceptor" or "acceptor/acceptor" carbenes—less is understood about metal-carbenes with two electron-donating groups, or "donor/donor" carbenes. In particular, the general mechanism and origins of stereoselectivity of these reactions lack clarity. Herein lies the knowledge gap we aim to fill in part by studying an example system.

What is the stereochemical impact of the stereogenic insertion center in C-H insertions of donor/donor carbenes? Can chiral metal catalysts control diastereoselectivity? And is the transformation concerted, or is it stepwise? This study illustrates the structural features of C-H insertion centers that drive experimentally observed stereochemical outcomes. Based on data gleaned from the laboratory, we propose a mechanistic model (derived from our computations) which describes a stepwise S_E2 mechanism for a C-H insertion reaction to trisubstituted benzodihydrofurans.

The current paradigm for acceptor carbene mechanisms is one based on concerted C-H insertions: both hydride transfer and C-C bond formation steps occur in one step. For example, studies by Taber[1] and Doyle[2] established stereochemical models for the C-H insertions of acceptor carbenes, models rationalized by the retained stereochemistry at the C-H insertion center. To our knowledge, no mechanistic studies on donor/donor carbenes exist to date. A fundamental understanding of the mechanism, and the stereochemical impact of C-H insertion centers, would therefore aid in the design of future studies involving donor/donor carbenes.

Scheme 5.1 a) Prior work: tertiary C–H insertion centers with acceptor carbenes. b) This work: donor/donor carbenes with chiral tertiary C–H insertion centers.

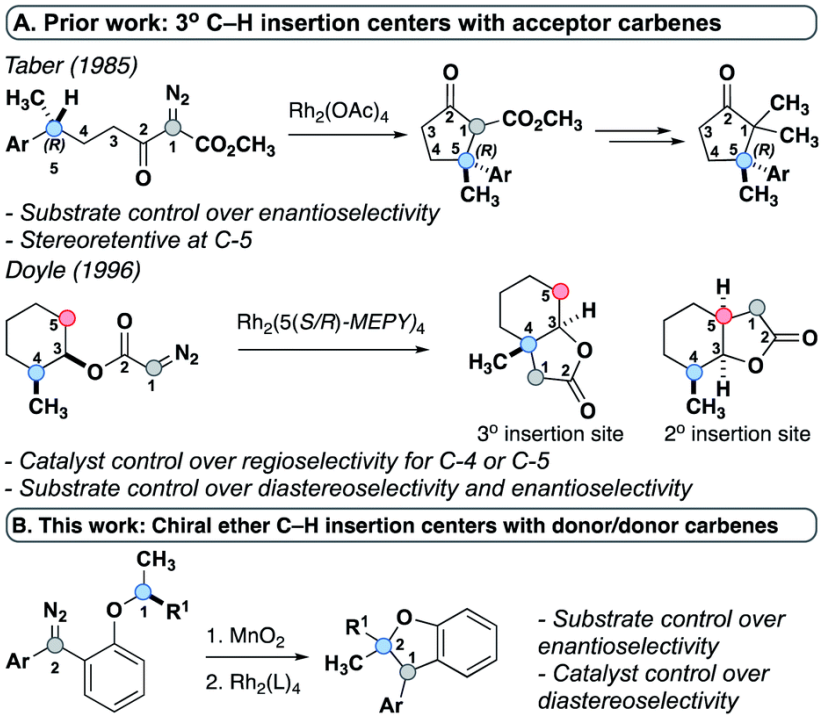

5.3 Experimental Results

Ethers **1** and **2** (Tables 5.1 and 5.2) were studied within this context to elucidate the effects of varying C-H insertion sites on the degree of stereocontrol from substrate and catalyst. Ether **1** has a benzylic C-H insertion center and is highly reactive, relative to a C-H insertion site which lacks a group that can stabilize the buildup of positive charge through resonance, such as ether **2**, substituted with a methyl and homoallylic group. Tables 5.1 and 5.2 show the results of the C-H insertion reactions of **1** and **2**, respectively, with chiral (Figure 5.1, **3**) or achiral catalysts (**4**). A full discussion of the experimental details can be found in the original publication and supporting information of Dishman, S. N. *et al. Chem. Sci.* **2022**, *13*, 1030-1036.

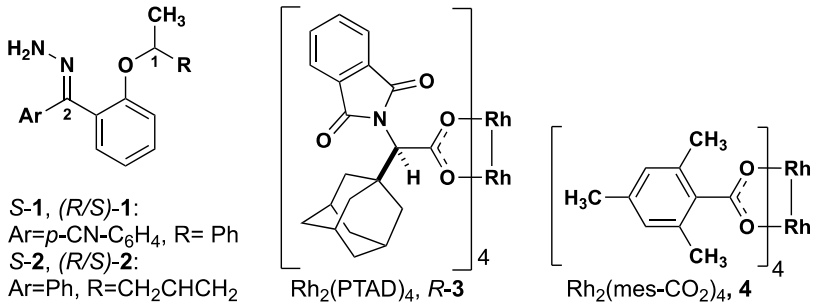

Figure 5.1 Structures of hydrazone precursors and commonly used dirhodium catalysts with donor/donor carbene C–H insertion systems.

For the purposes of this dissertation, however, which focuses solely on the computational results, we summarize some key experimental takeaways.

Table 5.1 Alkyl/Aryl Stereogenic Insertion Centers.

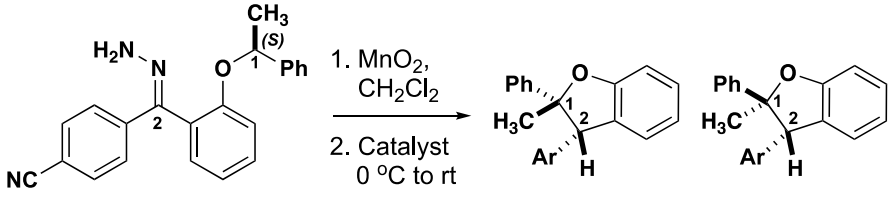

1 5a 5b

Entry	SM	Catalyst	dr[a] 5a:5b	er[b] (5a) (*R*,*S*):(*S*,*R*)	Yield (%)
1	(*R*/*S*)-**1**	*R*-**3**	>95:5	49:51	68
2	(*R*/*S*)-**1**	*S*-**3**	>95:5	49:51	65
3	(*R*/*S*)-**1**	4	>95:5	49:51	65
4[c]	(*S*)-**1**	*R*-**3**	>95:5	97:03	82
5	(*S*)-**1**	*S*-**3**	>95:5	97:03	71
6	(*S*)-**1**	4	>95:5	97:03	76

[a] dr determined by 1H NMR analysis of unpurified reaction mixtures. [b] er determined by chiral HPLC. [c] Absolute stereochemistry confirmed by X-ray crystallography.

Table 5.2 Alkyl/Aryl Stereogenic Insertion Centers.

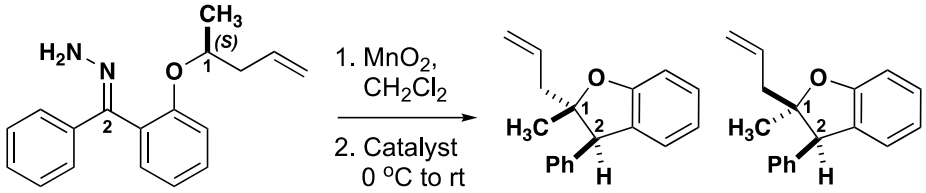

2 6a 6b

Entry	SM	Catalyst	dr[a] 6a:6b	er[b]-6a (*S*,*R*): (*R*,*S*)	er[b]-6b (*R*,*R*): (*S*,*S*)	Yield (%)
1	(*R*/*S*)-**2**	*R*-**3**	47:53	91:09	86:14	70
2	(*R*/*S*)-**2**	*S*-**3**	48:52	11:89	16:84	68
3	(*R*/*S*)-**2**	4	57:43	49:51	50:50	91
4[c]	(*S*)-**2**	*R*-**3**	86:14	99:01	99:01	77
5	(*S*)-**2**	*S*-**3**	10:90	74:26	99:01	75
6	(*S*)-**2**	4	53:47	98:02	99:01	58

[a] dr determined by 1H NMR analysis of unpurified reaction mixtures. [b] er determined by chiral HPLC. [c] Absolute stereochemistry confirmed by X-ray crystallography

Each C-H insertion reaction can yield two diastereomers and their enantiomers (four possible products) in a reaction that starts with either racemic or enantiopure substrate in the presence of either chiral (e.g., Rh_2(*R*-PTAD)$_4$, *R*-**3**) or achiral catalysts (e.g., Rh_2(mes-CO)$_4$, **4**). Both racemic **1** and enantiopure **1** yielded the benzodihydrofuran product as a single *cis* diastereomer (**5a**, Table 5.1, entries 1-3) irrespective of which catalyst was used. The enantioselectivity followed a similar trend where racemic **1** provided racemic **5a** and enantiopure **1** gave a single enantiomer of **5a** in 97:03 er (Table 5.1, entries 4-6) regardless of the catalyst employed in the reaction. Therefore, these substrates with highly activated benzylic C–H elicit highly stereoselective substrate-controlled C–H insertion reactions.

To investigate the influence of the C-H insertion center on the diastereo- and enantioselectivity, we subjected **2** to the same reaction conditions in the presence the same chiral and achiral catalysts. While racemic **2** led to racemic mixtures of **6a** : **6b** in the presence of chiral catalysts (47 : 53 and 48 : 52 for *R*-3 and *S*-3, respectively) and slight enhancement of dr with achiral catalyst (57 : 43), we observe high er in the presence of chiral catalysts (Table 5.2, 1-2). This observation suggests that chiral catalysts may steer racemic 2 to enantio-enriched products. The results with (*S*)-**2** were even more striking. Treatment of this substrate with *R*-**3** resulted in preferential formation of *trans* benzodihydrofuran **6a** (Table 5.2, entry 4) with high enantioselectivity. Use of the same substrate with *S*-**3** resulted in inverted diastereoselectivity with the same enantiomeric preference as the reaction with *R*-**3** (Table 5.2, entry 5)! The eroded enantioselectivity for the formation of **6a** in this case highlights the mismatch in stereochemical preference between the substrate and the catalyst. Finally, the insertion of (*S*)-**2** with achiral catalyst (**4**) showed little diastereoselectivity while retaining the high substrate-induced enantioselectivity (Table 5.2, entry 6). On one hand, these results demonstrate that the stereocenter undergoing insertion controls the magnitude and orientation of enantioselectivity for both newly formed stereocenters in the product. The catalyst, on the other hand, can have a strong influence on the diastereoselectivity, and (*R/S*)-**3** is a privileged catalyst scaffold for this system.[3] These results are consistent with a highly stereoselective hydride transfer step that is followed by a diastereoselective ring closure that can be controlled by the configuration of the catalyst.

5.4 Computational Details

Density functional theory (DFT) calculations were carried out using the *Gaussian 16* suite of programs.[4] DFT methods were chosen because of the size of the molecules involved in this study

and their reliability to perform well in similar mechanistic studies. DFT methods (similar to those used here) have been successfully implemented in past computational mechanistic studies of C-H insertion reactions of dirhodium carbenes and other transition-metal catalyzed reactions in the field of homogeneous catalysis.[5–10] Geometries of transition state structures (TSSs) and minima along the reaction pathway were optimized using the B3LYP[11] functional with Grimme's D3 correction with Becke-Johnson (BJ) damping (i.e., B3LYP-D3(BJ)) to correct for the lack of adequate dispersion treatment in B3LYP.[12,13] Harmonic vibrational frequencies were computed at the same level, from which we extracted free energy correction values (*vide infra*) to compute relative free energies (ΔG); imaginary vibrational modes were visualized to confirm we identified true TSSs; one imaginary frequency confirmed we computed first-order saddle points for TSSs and the lack of any imaginary frequencies confirmed we computed energy minima. Intrinsic reaction coordinate (IRC) calculations were carried out from each TSS to identify flanking minima on the potential energy surface.[14–16]

All computations were carried out with an ultrafine integration grid (99 radial shells and 590 angular points per shell), the default in *Gaussian 16* and recommended minimum-sized integration grid to achieve quantitative accuracy.[17] We employed a Pople-type double-ζ basis set, 6-31G(d) basis set[18] for C, H, O, and N and the LANL2DZ[19] basis set and effective core potential (ECP) for Rh (i.e., B3LYP-D3(BJ)/LANL2DZ[6-31G(d)]) for geometry optimizations. Single-point calculations were subsequently carried out on the above-mentioned optimized geometries with the same functional, B3LYP-D3(BJ), using a larger, more flexible basis set and ECP—the Stuttgart/Dresden SDD ECP[20] for Rh, and 6-31+G(d,p) for C, H, O, and N, which includes diffuse and polarization functions—to more-accurately account for the charged-minima and TSSs in this reaction (i.e., PCM(CH_2Cl_2)-B3LYP-D3(BJ)/SDD[6-31+G(d,p)]//PCM(CH_2Cl_2)-B3LYP-

D3(BJ)/LANL2DZ[6-31G(d)]).[21] We observed that increasing the basis set size from double-ζ to triple-ζ (i.e., 6-31G to 6-311G) was too costly to be practical given the size of the system studied here and the computational resources at our disposal. Adding additional diffuse and/or polarization basis functions, too, can be harmful—not to mention increase the cost—so we reasoned that a minimally-augmented 6-31+G(d,p) basis set would suffice.[22]

All optimized structure coordinates are reported on the ioChem-BD database for ease of access.[23] The reader may find these structures at the following DOI: https://doi.org/10.19061/iochem-bd-6-94

5.5 Mechanistic Model for Observed Stereoselectivity

To investigate the C–H insertion mechanism leading to **6** and delve further into the origins of the observed stereocontrol, we turned our attention to computational studies. Density functional theory (DFT) calculations have previously aided our (i.e., a previous Shaw-Tantillo collaboration) study of C–H insertion mechanisms of donor/donor carbenes.[24] However, unlike previous DFT explorations of similar reactions in which the Rh catalyst can be reasonably modeled with $Rh_2(OAc)_4$, or even $Rh_2(HCO_2)_4$,[22] we could only reasonably investigate the current mechanistic question by modeling the insertion reaction of **6** within the chiral cavity[23,24] of either Rh_2(*R*-PTAD)$_4$ or Rh_2(*S*-PTAD)$_4$. Given the size of the *N*-phthalimido and adamantyl ligands on Rh_2(*R*-PTAD)$_4$ (weighing in at 219 atoms and 940 electrons), and its concomitant computational cost, we reasoned that truncating the

adamantyl groups to methyl groups struck a sensible balance between mechanistic insight and cost with the modeling capabilities at our disposal.[23,24*]

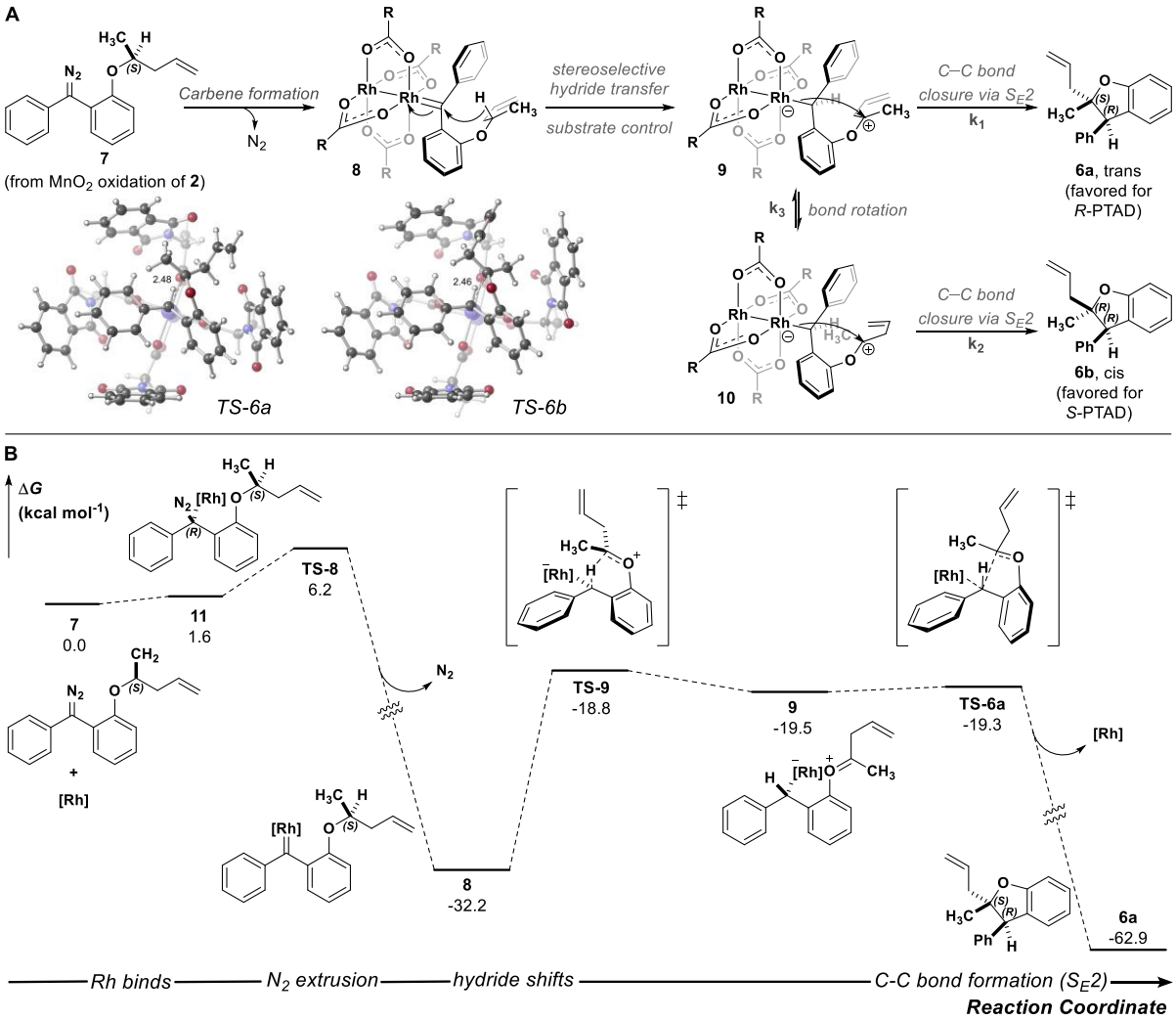

Figure 5.2 a) Arrow pushing mechanism and S_E2 transition-state structures leading to **6a** and **6b**.[†] b) Reaction energy profile computed with DFT at the PCM(CH_2Cl_2)-B3LYP-D3(BJ)/SDD[6-31+G(d,p)]//PCM(CH_2Cl_2)-B3LYP-D3(BJ)/LANL2DZ[6-31G(d)] level of theory; [Rh] = Rh_2(R-PTAD)$_4$.

[*] One (perhaps significant) drawback of this truncation is the loss of fidelity with respect to the size and shape, or "entry surface area", of the 3D chiral pocket shape.[37] One of the possible roles of the adamantyl groups is to decrease the 3D pocket shape and pre-distort the substrate. With the computational cost associated with this study, however, it's impractical to model with the adamantyl groups. So, we add a note of caution to the reader that, considering this tradeoff, the level of resolution of our conclusions may indeed *approach*, but not *exactly reflect*, that of reality. Faster machine learning tools may eliminate the need for this tradeoff.[37]

[†] Full potential energy surfaces for formation of 6a/6b is described in the Computational Supporting Information of *Chem. Sci.* **2022**, *13*, 1030-1036. See SI Figure 4 for TS-6b.

A stepwise mechanism containing a short lived zwitterionic intermediate was found for the reactions of substrate **2**, similar to that previously proposed for C–H insertions of donor/donor carbenes with primary, achiral insertion sites[24] (see computational SI for details; all computed structures can be found in the ioChem-BD repository[25]). For clarity, the mechanism for formation of one enantiomer of the major diastereomer from diazo compound **7** is shown in Figure 5.2.[*] First, addition of the chiral catalyst results in a tetrahedral intermediate (**11**) with N_2 poised to leave. The free energy barrier to extrude nitrogen is low (overall, a 6.3 kcal mol^{-1} barrier from **7**) and this process is predicted to be highly exergonic (ΔG = -32.2 kcal mol^{-1}), forming one major rotamer of Rh carbene (**8**). From **8**, an initial hydride-shift from C-1 to C-2 is followed by an S_E2 C–C bond closure step to yield the major product (**6a**).[26] The hydride transfer occurs with high stereochemical fidelity, accounting for the high selectivity for the newly formed stereogenic center at C-2. The diastereomeric ratio observed is hypothesized to be due to the major oxocarbenium ion intermediate (**9**) rotating about the C_{aryl}–O bond to expose one prochiral face, preferentially exposing one prochiral face based on the configuration of the catalyst. Although our computed mechanism is formally stepwise, the C–H insertion event can be considered to border the realm of a concerted, highly asynchronous mechanism (see Figure 5.3).[27]

Although, we successfully identified transition states leading from **9** to **6a** and from **10** to **6b**,[†] the transition state for **9** to **10** remains elusive. The observed 85:15 ratio results from the relative energy of these two transition states, as well as the interconversion of **9** to **10**. While it is difficult to disentangle the exact influence of these three transition states on diastereoselectivity, the data are consistent with an oxocarbenium ion whose stereochemical fate is determined by the catalyst. Small perturbations resulting from

[*] Ibid, see SI Figures 4-5 for detailed reaction profiles for formation of the other diastereomer and its enantiomer.
[†] Ibid, SI Figures 4-5.

factors not explicitly modeled here, e.g., explicit solvent effects, deviations in the chiral crown structure, or non-statistical dynamic effects, could account for issues in delineating these three steps' effect on the diastereoselectivity.[28-33] Results in the supporting information* corroborate the experimental enantioselectivity: specifically formation of pro-chiral *R*-**3** bound Rh-carbene intermediate (**SI-23**) leading to (*R*,*S*)-**6a** is kinetically and thermodynamically unfavorable ($\Delta\Delta G^{\ddagger}$ = 4.3 kcal/mol and $\Delta\Delta G$ = 3.9 kcal/mol relative to **7**) compared to that leading to (*S*,*R*)-**6a**, consistent with an er of 99:1 at 0°C (Table 5.2, entry 4).

5.6 Discussion of Computational Results

The robustness of our chosen level of theory was tested by employing a series of various functionals and computing the $\Delta\Delta E^{\ddagger}$ for TSS's **TS-6b** and **TS-6a** (Table 5.3). Different functionals resulted in varying quantitative results in predicting $\Delta\Delta E^{\ddagger}$'s—the free energy differences fall within ~1-2 kcal/mol, all within typical DFT error. This result suggests that we are unable to accurately predict the experimentally observed diastereoselectivity with our employed DFT methods. *However, these results do not diminish the validity and value of our main conclusions that the C-H insertion mechanisms with R-PTAD catalyst is stepwise.* After all, the conclusions drawn from our studies are qualitative, not quantitative.

* Ibid, SI Figures 4-5

Table 5.3 Single-point energy comparison of $\Delta\Delta E^{\ddagger}$ with various DFT functionals. $\Delta\Delta E^{\ddagger}$'s are computed as the difference between **TS-6b** and **TS-6a**. All single-points were carried out with the SDD basis set and ECP for Rh and 6-31+G(d,p) for all other atoms, unless stated otherwise (in one case we employ the def2-SVP basis set). Single-point calculations were computed at the B3LYP-D3(BJ)/LANL2DZ[6-31G(d)]-optimized geometry.

Functional	$\Delta\Delta E^{\ddagger}$ (kcal mol^{-1})
B3LYP-D3(BJ)	1.1
B3LYP-D3(BJ)/def2-SVP	0.3
PW6B95-D3(BJ)	-0.1
ωB97X-D	0.2
PBE0-D3	0.1
M06-D3	-0.6
M06	-0.4
MN15	-1.2

The key advance that emerges out of our computational studies regards the nature of the bond-making and –breaking events in the C-H insertions event: that the C-H insertion event involves a formally stepwise mechanism with hydride transfer-S_E2 C-C bond formation events. S_E2 mechanisms are unusual and sparsely reported in the literature. As far as we know, they have not been reported for systems involving Rh. Electrophilic cleavages of organomercurial compounds usually exhibit S_E2 retention of configuration at carbon mechanisms; while S_E2 inversion has been reported for some organotin compounds, it is much more rare (as far as we know).[30] Concerted (sometimes asynchronous) C-H insertion mechanisms have been invoked frequently for donor/acceptor and acceptor carbenes and these have involved retention of configuration at the C-H insertion carbon, but previously-reported intramolecular C-H insertions

with donor/donor carbenes catalyzed by $Rh_2(OAc)_4$ also involve *stepwise* mechanisms. All of these mechanistic possibilities for hydride shift and C-C bond closure events are depicted on a More O'Ferrall-Jencks plot[31,32] of the sort shown in Figure 5.3.[33,34] The stepwise mechanism we report exists very close to (but not within) the border area (light blue) of concerted, and we suspect that this is the case due to the distortion the substrate must adopt in the chiral catalyst cavity (and this distortion may even be *stronger* with inclusion of adamantane groups at the methyl positions where we needed to truncate our *R*-PTAD catalyst model due to computational cost, as noted in the footnote above[†]). We hope that future work may validate this claim.

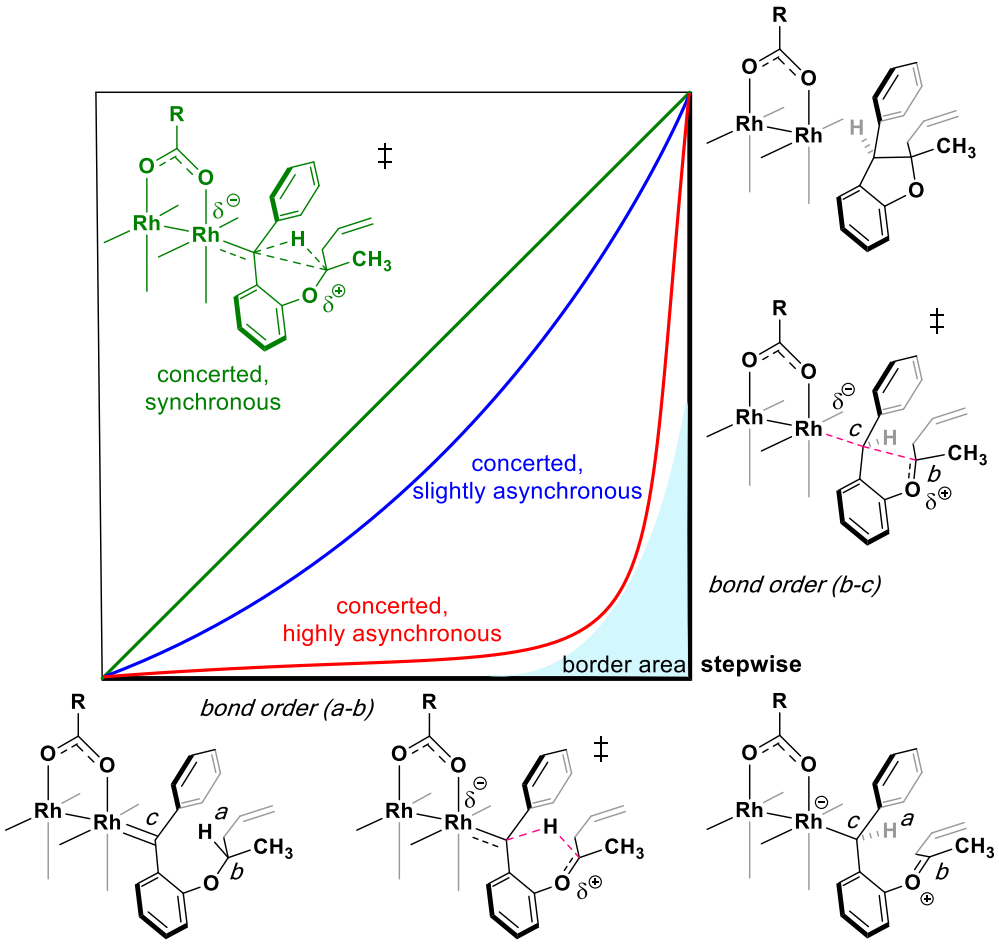

Figure 5.3 Qualitative More O'Ferrall-Jencks plot for Rh-catalyzed C-H insertion of donor/donor carbenes. Past studies have either found clearly stepwise or concerted asynchronous mechanisms, whereas the mechanism discovered here borders the two.

5.7 Notable Limitations of Current Study

That our current model is limited with respect to the origin of diastereoselectivity presents ample opportunity for future experimental and/or theoretical studies to update the current model. Variations in energies emerging out of the DFT functionals in Table 5.3 leave the origin of diastereoselectivity hanging in the balance and suggests that the use of much higher levels of theory and/or running dynamics simulations—an as-yet impractical task with currently available tools given the size of the system studied here—might aid in future studies.

The relatively flat surface connecting the hydride-shift and S_E2 TSSs on the PES also indicates caution when drawing conclusions based solely on stationary point analysis. A great deal of literature discusses dynamic effects that may govern selectivity of reactive species on broad, plateau-like regions of potential energy surfaces (PESs).[35] Our model may be further updated by considering the effects of explicit solvent. As we mentioned above, truncating the catalyst may have had a significant effect on the chiral cavity shape, which poses an additional limitation on our model, but we do not believe this truncation compromises the evidence in favor of a stepwise mechanism. So, we are left with a "thin" mechanistic model, which is still valuable for the purposes of this study.[36]

In sum, we have gathered strong evidence that supports a stepwise C-H insertion mechanism involving an S_E2 C-C bond closure step. Though the qualitative structure of our mechanism is championed by our results, the *details* about the origin of diastereoselectivity remain elusive. These limitations, however, should inspire future experimental or computational studies. We foresee in the future *ab initio* molecular dynamics and/or a fuller treatment of explicit solvent effects elucidating a clearer origin of stereoselectivity.

5.8 References

(1) Taber, D. F.; Petty, E. H.; Raman, K. Enantioselective Ring Construction: Synthesis of (+)-.Alpha.-Cuparenone. *J. Am. Chem. Soc.* **1985**, *107*, 196–199.

(2) Doyle, M. P.; Kalinin, A. V.; Ene, D. G. Chiral Catalyst Controlled Diastereoselection and Regioselection in Intramolecular Carbon−Hydrogen Insertion Reactions of Diazoacetates. *J. Am. Chem. Soc.* **1996**, *118*, 8837–8846.

(3) Lamb, K. N.; Squitieri, R. A.; Chintala, S. R.; Kwong, A. J.; Balmond, E. I.; Soldi, C.; Dmitrenko, O.; Castiñeira Reis, M.; Chung, R.; Addison, J. B.; Fettinger, J. C.; Hein, J. E.; Tantillo, D. J.; Fox, J. M.; Shaw, J. T. Synthesis of Benzodihydrofurans by Asymmetric C−H Insertion Reactions of Donor/Donor Rhodium Carbenes. *Chem. Eur. J.* **2017**, *23*, 11843–11855.

(4) Frisch, M. J.; Trucks, G. W.; Schlegel, H. B.; Scuseria, G. E.; Robb, M. A.; Cheeseman, J. R.; Scalmani, G.; Barone, V.; Petersson, G. A.; Nakatsuji, H.; Li, X.; Caricato, M.; Marenich, A. V.; Bloino, J.; Janesko, B. G.; Gomperts, R.; Mennucci, B.; Hratchian, H. P.; Ortiz, J. V.; Izmaylov, A. F.; Sonnenberg, J. L.; Williams-Young, D.; Ding, F.; Lipparini, F.; Egidi, F.; Goings, J.; Peng, B.; Petrone, A.; Henderson, T.; Ranasinghe, D.; Zakrzewski, V. G.; Gao, J.; Rega, N.; Zheng, G.; Liang, W.; Hada, M.; Ehara, M.; Toyota, K.; Fukuda, R.; Hasegawa, J.; Ishida, M.; Nakajima, T.; Honda, Y.; Kitao, O.; Nakai, H.; Vreven, T.; Throssell, K.; Montgomery, J. A., Jr.; Peralta, J. E.; Ogliaro, F.; Bearpark, M. J.; Heyd, J. J.; Brothers, E. N.; Kudin, K. N.; Staroverov, V. N.; Keith, T. A.; Kobayashi, R.; Normand, J.; Raghavachari, K.; Rendell, A. P.; Burant, J. C.; Iyengar, S. S.; Tomasi, J.; Cossi, M.; Millam, J. M.; Klene, M.; Adamo, C.; Cammi, R.; Ochterski, J. W.; Martin, R. L.; Morokuma, K.; Farkas, O.; Foresman, J. B.; Fox, D. J Gaussian 16, Revision A.03. Gaussian, Inc.: Willingford, CT 2016.

(5) Pidko, E. A. Toward the Balance between the Reductionist and Systems Approaches in Computational Catalysis: Model versus Method Accuracy for the Description of Catalytic Systems. *ACS Catal.* **2017**, *7*, 4230–4234.

(6) Vogiatzis, K. D.; Polynski, M. V.; Kirkland, J. K.; Townsend, J.; Hashemi, A.; Liu, C.; Pidko, E. A. Computational Approach to Molecular Catalysis by 3d Transition Metals: Challenges and Opportunities. *Chem. Rev.* **2019**, *119*, 2453–2523.

(7) Sperger, T.; Sanhueza, I. A.; Kalvet, I.; Schoenebeck, F. Computational Studies of Synthetically Relevant Homogeneous Organometallic Catalysis Involving Ni, Pd, Ir, and Rh: An Overview of Commonly Employed DFT Methods and Mechanistic Insights. *Chem. Rev.* **2015**, *115*, 9532–9586.

(8) Sperger, T.; Sanhueza, I. A.; Schoenebeck, F. Computation and Experiment: A Powerful Combination to Understand and Predict Reactivities. *Acc. Chem. Res.* **2016**, *49*, 1311–1319.

(9) Funes-Ardoiz, I.; Schoenebeck, F. Established and Emerging Computational Tools to Study Homogeneous Catalysis—From Quantum Mechanics to Machine Learning. *Chem* **2020**, *6*, 1904–1913.

(10) Ahn, S.; Hong, M.; Sundararajan, M.; Ess, D. H.; Baik, M.-H. Design and Optimization of Catalysts Based on Mechanistic Insights Derived from Quantum Chemical Reaction Modeling. *Chem. Rev.* **2019**, *119*, 6509–6560.

(11) Becke, A. D. Density-Functional Thermochemistry. III. The Role of Exact Exchange. *J.*

Chem. Phys. **1993**, *98*, 5648–5652.
(12) Grimme, S.; Antony, J.; Ehrlich, S.; Krieg, H. A Consistent and Accurate Ab Initio Parametrization of Density Functional Dispersion Correction (DFT-D) for the 94 Elements H-Pu. *J. Chem. Phys.* **2010**, *132*, 154104.
(13) Grimme, S.; Ehrlich, S.; Goerigk, L. Effect of the Damping Function in Dispersion Corrected Density Functional Theory. *J. Comput. Chem.* **2011**, *32*, 1456–1465.
(14) Fukui, K. The Path of Chemical Reactions -- The IRC Approach. *Acc. Chem. Res.* **1981**, *14*, 363–368.
(15) Gonzalez, C.; Schlegel, H. B. Reaction Path Following In Mass-Weighted Internal Coordinates Cartesians and with Internal Coordinates without Mass-Weighting. *J. Phys. Chem.* **1990**, *94*, 5523–5527.
(16) Maeda, S.; Harabuchi, Y.; Ono, Y.; Taketsugu, T.; Morokuma, K. Intrinsic Reaction Coordinate: Calculation, Bifurcation, and Automated Search. *Int. J. Quantum Chem.* **2015**, *115*, 258–269.
(17) Bootsma, A. N.; Wheeler, S. E. Popular Integration Grids Can Result in Large Errors in DFT-Computed Free Energies. *ChemRxiv* **2019**, 1–20.
(18) Hariharan, P. C.; Pople, J. A. The Influence of Polarization Functions on Molecular Orbital Hydrogenation Energies. *Theor. Chim. Acta* **1973**, *28*, 213–222.
(19) Hay, P. J.; Wadt, W. R. Ab Initio Effective Core Potentials for Molecular Calculations. Potentials for the Transition Metal Atoms Sc to Hg. *J. Chem. Phys.* **1985**, *82*, 270–283.
(20) Dunning, T. H.; Hay, P. J. Gaussian Basis Sets for Molecular Calculations. In *Methods of Electronic Structure Theory*; Schaefer, H. F., Ed.; Springer: Boston, MA, 1977; pp 1–27.
(21) Hansen, J.; Autschbach, J.; Davies, H. M. L. Computational Study on the Selectivity of Donor/Acceptor-Substituted Rhodium Carbenoids. *J. Org. Chem.* **2009**, *74*, 6555–6563.
(22) Papajak, E.; Truhlar, D. G. Efficient Diffuse Basis Sets for Density Functional Theory. *J. Chem. Theory Comput.* **2010**, *6*, 597–601.
(23) Álvarez-Moreno, M.; de Graaf, C.; López, N.; Maseras, F.; Poblet, J. M.; Bo, C. Managing the Computational Chemistry Big Data Problem: The IoChem-BD Platform. *J. Chem. Inf. Model.* **2015**, *55*, 95–103.
(24) Lamb, K. N.; Squitieri, R. A.; Chintala, S. R.; Kwong, A. J.; Balmond, E. I.; Soldi, C.; Dmitrenko, O.; Castiñeira Reis, M.; Chung, R.; Addison, J. B.; ; Fettinger, J. C.; Hein, J. E.; Tantillo, D. J.; Fox, J. M.; Shaw, J. T. Synthesis of Benzodihydrofurans by Asymmetric C−H Insertion Reactions of Donor/Donor Rhodium Carbenes. *Chem. Eur. J.* **2017**, *23*, 11843–11855.
(25) Nakamura, E.; Yoshikai, N.; Yamanaka, M. Mechanism of C-H Bond Activation/C-C Bond Formation Reaction between Diazo Compound and Alkane Catalyzed by Dirhodium Tetracarboxylate. *J. Am. Chem. Soc.* **2002**, *124*, 7181–7192.
(26) Singha, S.; Buchsteiner, M.; Bistoni, G.; Goddard, R.; Furstner, A. A New Ligand Design Based on London Dispersion Empowers Chiral Bismuth − Rhodium Paddlewheel Catalysts. *J. Am. Chem. Soc.* **2021**, *143*, 5666–5673.
(27) Kong, L.; Han, X.; Chen, H.; Sun, H.; Lan, Y.; Li, X. Rhodium(II)-Catalyzed Regioselective Remote C − H Alkylation of Protic Indoles. *ACS Catal.* **2021**, *11*, 4929-4935.
(28) Wang, J.; Chen, B.; Bao, J. Electronic Effects of Rh(II)-Mediated Carbenoid Intramolecular C-H Insertion: A Linear Free Energy Correlation Study. *J. Org. Chem.* **1998**, *63*, 1853–1862.

(29) Drago, R. S.; Tanner, S. P.; Richman, R. M.; Long, J. R. Quantitative Studies of Chemical Reactivity of Tetra-Yu-Butyrato-Dirhodium(II) Complexes. *J. Am. Chem. Soc.* **1979**, *101*, 2897–2903.
(30) Fukuto, J. M.; Jensen, F. R. Mechanisms of SE2 Reactions: Emphasis on Organotin Compounds. *Acc. Chem. Res.* **1983**, *16*, 177–184.
(31) More O'Ferrall, R. A. Relationships between E2 and E1cB Mechanisms of β-Elimination. *J. Chem. Soc. B Phys. Org.* **1970**, 274–277.
(32) Jencks, W. P. General Acid-Base Catalysis of Complex Reactions in Water. *Chem. Rev.* **1972**, *72*, 705–718.
(33) Tantillo, D. J. Recent Excursions to the Borderlands between the Realms of Concerted and Stepwise: Carbocation Cascades in Natural Products Biosynthesis. *J. Phys. Org. Chem.* **2008**, *21*, 561–570.
(34) Nakamura, E.; Yoshikai, N.; Yamanaka, M. Mechanism of C−H Bond Activation/C−C Bond Formation Reaction between Diazo Compound and Alkane Catalyzed by Dirhodium Tetracarboxylate. *J. Am. Chem. Soc.* **2002**, *124*, 7181–7192.
(35) Carpenter, B. K. Energy Disposition in Reactive Intermediates. *Chem. Rev.* **2013**, *113*, 7265–7286.
(36) Plata, R. E.; Singleton, D. A. A Case Study of the Mechanism of Alcohol-Mediated Morita Baylis–Hillman Reactions. The Importance of Experimental Observations. *J. Am. Chem. Soc.* **2015**, *137*, 3811–3826.
(37) Cammarota, R. C.; Liu, W.; Bacsa, J.; Davies, H. M. L.; Sigman, M. S. Mechanistically Guided Workflow for Relating Complex Reactive Site Topologies to Catalyst Performance in C–H Functionalization Reactions. *J. Am. Chem. Soc.* **2022**, *144*, 1881–1898.

Chapter 6

Can Dirhodium Complexes Catalyze Cyclopropanation of Cycloheptatriene Diazo Compounds to Synthesize Substituted-Semibullvalenes?

While it is mutually advantageous to tie theory with experiment, I still feel that theory should lead, rather than follow experiment in exploring chemistry.

Paul Schleyer, *J. Comp. Chem.* **2001**, *13*, ix-xi

6.1 Abstract

In theory, yes.

6.2 Introduction

In 1966, Zimmerman and Grunewald introduced semibullvalene (SBV) to the world of chemistry, a fortunate stroke of serendipity. Upon photolysis of barrelene they discovered that they had synthesized SBV and its closely related C_8H_8 isomer, cyclooctatetraene (Scheme 6.1a).[1] In 1972, Zimmerman and Sousa then synthesized cycloheptatrienyldiazomethane and studied its thermal and photochemical rearrangement to products resulting from nitrogen loss and subsequent rearrangement of the carbene intermediate, thinking they might observe SBV among other C_8H_8 products.[2] They did *not*. Instead, they isolated benzene, cyclooctatetraene, and heptafulvene, and acetylene. Considering advanced methods for "taming" carbene reactivity with transition metals (e.g., Rh) to make metal carbenes,[3] one wonders whether metal carbenes might, in theory, pave the way to SBV à la Zimmerman. Indeed, more than 50 years later, SBV still remains a physical

organic chemist's playground[4,5] and finding ways to SBV would be synthetically useful. Here, we offer a theoretical prediction for a synthetic route to SBV *via* a cyclopropanation of dirhodium carbenes derived from cycloheptatrienyl diazo compounds.

Synthetic and theoretical chemists have studied SBV from many angles. Some have studied its rapid, degenerate Cope rearrangement[6,7] and fluxional[8] (or locked[9]) behavior. Others leveraged the fluxionality of related carbon cage molecules, such as bullvalene and barbaralane, for applications in materials and sensing, sparking new interest in shapeshifting molecules.[10–16] The Maimone group used shapeshifting anions in a total synthesis Ocellatusone C, highlighting that "the barbaralyl nucleus remains an outstanding synthetic challenge".[17] The synthesis of related fluxional carbon cages, such as SBV, apply to this statement as well.[18] Past work on SBV investigated its electronic structure,[19–21] heavy-atom tunneling capabilities (a theoretical prediction[22] borne out by experiment),[22–26] and Cope rearrangement barrier height[27] with quantum calculations. Some have even introduced ways to reduce,[19] eliminate,[28] interrupt,[29] and invert the activation barrier for its rearrangement to a homoaromatic minimum (Scheme 6.1b).[30–36] Its bromination mechanism[37] has been examined in detail, as has its dynamic behavior associated with its formation via a reaction with a post-transition state bifurcation (PTSB).[38–40]

Efforts to synthesize SBV and its analogue, 2,6-diazasemibullvalene, abound (Scheme 6.1c).[41–47] One might think that chemists have exhausted ways to synthesize SBV, but with the continuous emergence and discovery of new reactions in organic chemistry, there remains room for breathing new life into SBV synthesis and that of other fluxional molecules. Using quantum chemical computations, we explore the viability of a new approach to synthesize monosubstituted SBVs via a dirhodium(II)-catalyzed cyclopropanation (CP) through a metal carbene intermediate (Scheme 6.1f).

Metal-carbene mediated chemistry has a long and winding history.[3] Our group has collaborated closely with experimental groups to understand mechanisms of Rh-carbene mediated transformations, including C-H insertion[48–50] and ylide formation reactions[51–54] with the aim of developing synthetically-useful models of reactivity and selectivity. This chemistry has proven to be a playground of its own, a family of synthetically relevant organometallic reactions that display behaviors considered by some to be esoteric. For example, our groups has shown that some C-H insertion reactions involve cryptic post-transition state bifurcations (PTSBs) that provide facile routes to unwanted side products.[55–57] Tandem processes[58] from Rh-carbene intermediates—such as CP/Cope rearrangements,[59–62] which have been applied in total syntheses to access (otherwise difficult to synthesize) seven-membered rings, or C-H insertion/Cope rearrangements[63]—may also involve PTSBs.[56,57] Given this precedent, we additionally ask whether SBV can be generated by a CP that would involve a PTSB (Scheme 6.1f).

Scheme 6.1. Select examples of semibullvalene and barbaralone syntheses (a-e). This work (f).

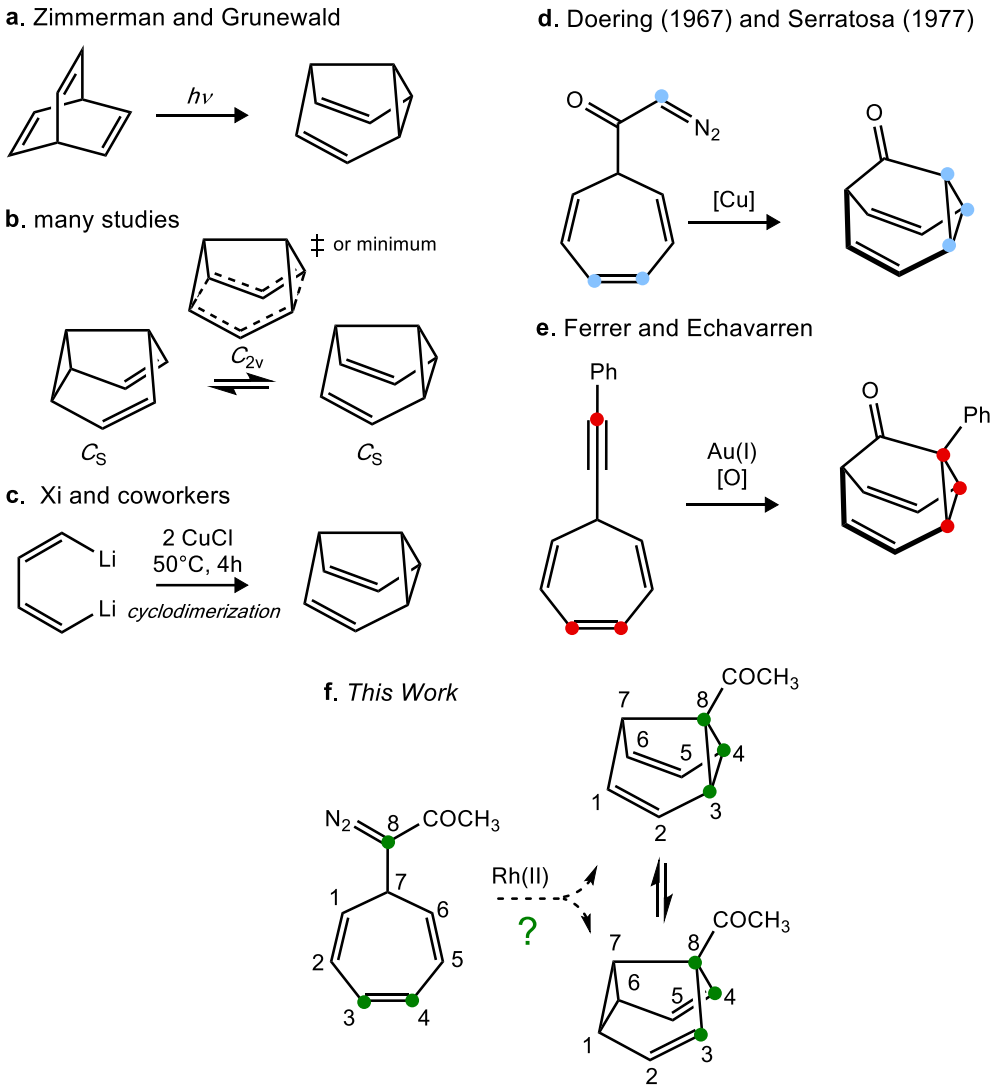

We are not the first group to suggest a transition metal-catalyzed synthesis of fluxional molecules from cycloheptatrienes. In 1967, the Doering group discovered a synthetic route to barbaralone from a cyclohepatrien-7-yl diazomethyl ketone.[64] Building on that work in 1977, Casas and Serratosa synthesized barbaralone with a Cu-carbene mediated CP in their synthesis of bullvalene (Scheme 6.1d).[65] Both methods result in products that are net cyclopropanations of the diazomethyl ketone with the transannular bond of the cycloheptatriene.

Recently, Ferrer and Echavarren synthesized barbaralones by gold(I)-catalyzed intramolecular oxidative cyclization of 7-ethynyl-1,3,5-cycloheptatrienes (Scheme 6.1e).[66] The same group also reported generation of closely related and highly fluxional barbaralyl cations from 7-alkynyl cycloheptatrienes by gold catalysis.[67] Could Rh(II)-catalysts assist in this type of transformation? When the Echavarren group expanded on this work in 2021 they discovered that the use of Rh(II)-catalysts led to a decarbenation to alkynylcyclopropanes from 7-alkynyl cycloheptatrienes and attributed the result to a lower barrier for decarbenation ($\Delta G^{\ddagger}$ = 21.9 kcal mol^{-1}) than the 6-*endo*-dig cyclization ($\Delta G^{\ddagger}$ = 24.4 kcal mol^{-1}) with the use of Rh(II) catalysts.[68] Cu(I) catalysts have similarly been shown to work in a synthesis of barabaralyl-substituted allenyl acid esters from terminal alkynes and tropylium tetrafluoroborate.[69]

May cycloheptatrienyl diazo compounds be a reasonable starting point to synthesize semibullvalenes using Rh(II)-catalysts through an intramolecular cyclopropanation, analogous to Echavarren's intramolecular oxidative cyclization? Our explorations lead us to predict[70,71] that regardless if this approach succeeds in the lab, unusual rearrangement chemistry will likely reveal itself from the metal carbene intermediate.

6.3 Computational Methods

Due to their low barriers for rearrangement, fluxional molecules are challenging to model—and so it is no surprise that the barrier and reaction energies for the Cope rearrangement of SBV has historically been challenging to accurately model. Many have considered the B3LYP[72] functional reliable for obtaining reasonable geometries, and to a certain extent, reaction barriers that are consistent with experiment.[29,73,74] In some cases, however, spurious intermediates and/or

significant deviation from experimentally-derived activation barriers have clouded the consensus on the reliability of B3LYP for Cope rearrangements.[31,75,76] Karton reported three functionals (BMK, PW6B95, and MN12-SX) outperformed other functionals in predicting accurate Cope barrier heights and reaction energies when compared to CCSD(T)/CBS benchmark calculations and experiment.[77] Based on Karton's benchmark work showing that PW6B95 performs accurately for systems involving SBV and Rh,[78] we settled on PW6B95[79] as a functional with the def2-SVP basis set (i.e., PW6B95/def2-SVP), a reasonable level of theory for qualitative investigations of this kind which have no experimental precedent to compare data against.[80] Additional tests to make sure our chosen level of theory is reasonable bolstered our confidence in our chosen level: specifically, we tested our chosen level's ability to predict known experimental free energy barriers, such as the Cope rearrangement of SBV (5.5[81] to 6.2[82] kcal mol^{-1}) and the isomerization barrier of cycloheptatriene to norcaradiene (7.2 kcal mol^{-1}).[83] Our results of 6.8 and 7.1 kcal mol^{-1} for the Cope and isomerization barriers, respectively, are well within chemical accuracy (<1 kcal mol^{-1}). Data from benchmark studies are summarized in Tables 1 and 2 below.

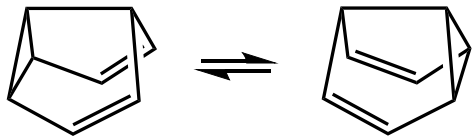

Table 1. Computed Cope Rearrangement barriers of SBV, compared with experimental barriers.

Reference	$\Delta G^{\ddagger}$, TSS_{Cope}
81 and 82 (experiment)	5.5[81] - 6.2[82]
This work (PW6B95/def2-SVP)	6.8
27 (theoretical benchmark study)[a]	6.7[27]

[a] CCSDT(Q)/cc-pVDZ//B3LYP-D3(BJ)/def2-TZVPP

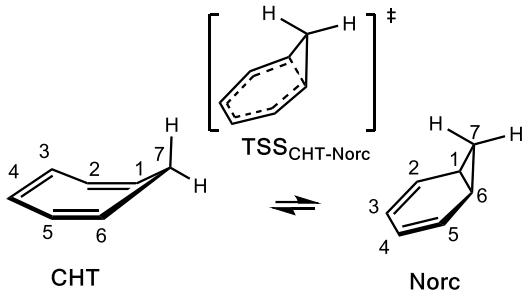

Table 2. Computed 6-electron electrocyclic ring closing of cycloheptatriene to norcaradiene, compared with experimental barriers.

Reference	$\Delta G^{‡}$, TSS_{Cope}	ΔG, Norc
83 (experiment)	7.2[83]	4.0
This work (PW6B95/def2-SVP)	7.1	2.4
84 (theoretical)[a]	8.2[84]	4.1

[a] ωB97X-D/def2-TZVPP-SMD(acetone)//ωB97X-D/def2-SVP

Geometry optimizations and frequency calculations were carried out with Gaussian 16.[85] Transition state structures (TSSs) were identified by the presence of one imaginary vibrational frequency and subsequent intrinsic reaction coordinate (IRC) calculations identified the minima on the potential energy surface to which TSSs are connected.[86–88]

6.4 Results and Discussion

6.4.1 Acetyl-SBV

The simplest reaction that we envisioned could be within reach experimentally was the transformation of diazo compound **A** to acetyl-SBV **D**/**E** (Figure 6.1, path II in green). We chose R to be a simple acetyl (Ac = $COCH_3$) group, given the body of literature on acceptor and donor-

acceptor carbenes.[89] In addition, structures similar to (diazocarbonylmethyl)cycloheptatriene (**A**), have been described in the literature.[90]

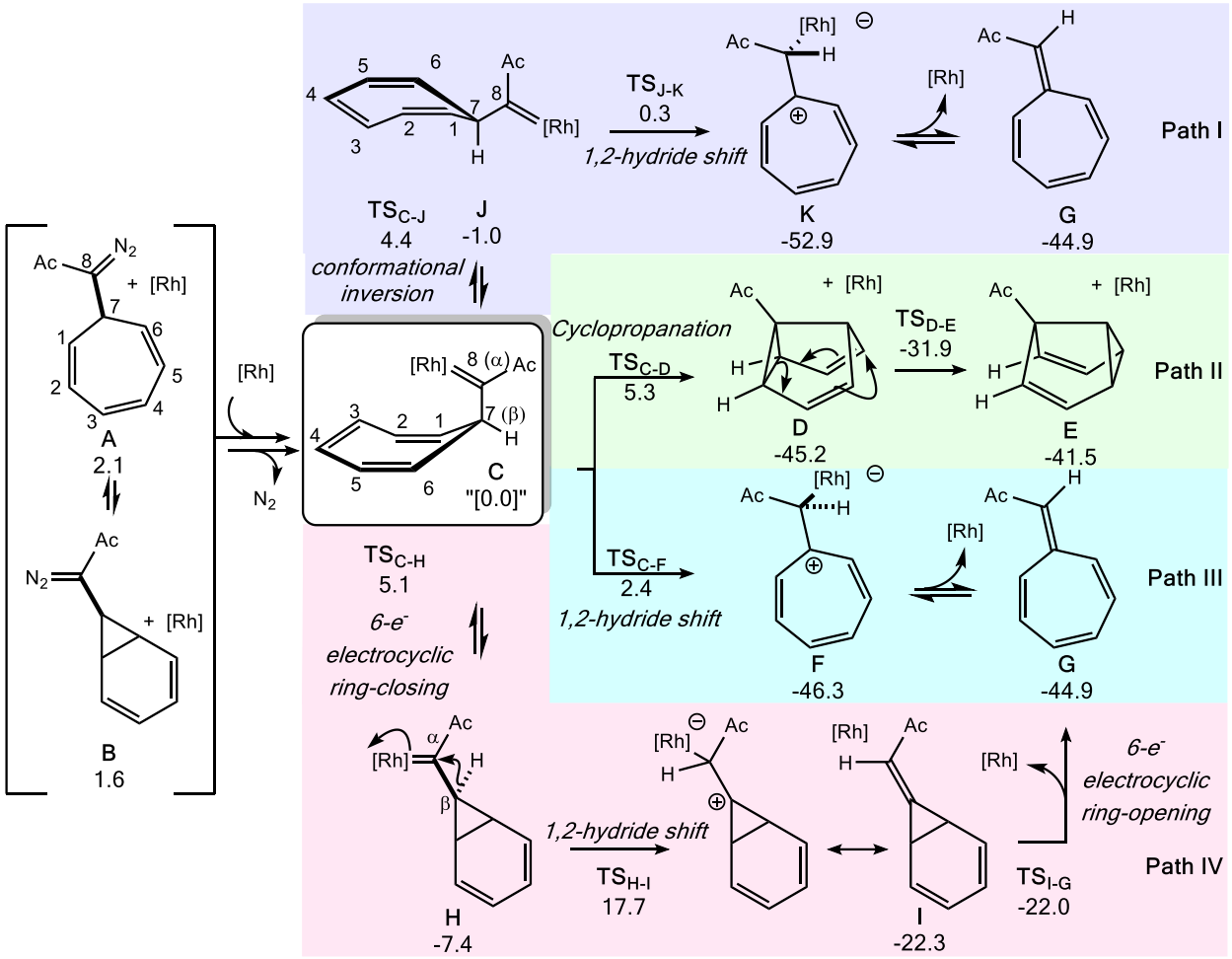

Figure 6.1 Possible mechanistic pathways explored. All relative free energies (PW6B95/def2-SVP, $\Delta G^{\ddagger}$) are in units of kcal mol^{-1}. (1) top, purple: conformational inversion followed by 1,2-hydride shift; (2) second to top, green: SBV formation by CP; (3) second to bottom, blue: 1,2-hydride shift; (4) bottom, red: norcaradiene formation followed by 1,2-hydride shift and electrocyclic ring-opening.

Exposure of **A** to a Rh catalyst (here, we model $Rh_2(OAc)_4$ for simplicity) should lead to nitrogen extrusion to form Rh-carbene species **C**. The barrier for intramolecular CP of **C** (via (**TS$_{C\text{-}D}$**)) is predicted to be very low (5.3 kcal mol^{-1}). Formation of Ac-SBV **D** is highly exergonic (-45.2 kcal mol^{-1}), and its Cope rearrangement is predicted to require a 13.3 kcal mol^{-1} barrier (**TS$_{D\text{-}E}$**) to form the slightly less-favorable **E** (-41.5 kcal mol^{-1}). While these results indicate that Ac-SBV

would not face a large barrier, possible competing reactions must be considered. For instance: (i) the cycloheptatriene–norcaradiene equilibrium (**C** ⇌ **H**) favors the norcaradiene **H** by ~7 kcal mol^{-1}, (ii) conformational isomerization slightly favors the isomer wherein the hydrogen at the C7, instead of the Rh-carbene, is positioned on the concave face of the cycloheptatriene (Scheme 6.2), and (iii) once the Rh-carbene is formed, side-reactions (such as *β*-hydride migration to heptafulvenes, e.g., **C** → **F** → **G** or **C** → **J** → **K** → **G**)[91,92] can occur. We are unable to ignore the of kinetic instability of intermediate **C**.[93] The variety of escape channels that can result is abundant—these possibilities were investigated in detail.[94]

Scheme 6.2 Cycloheptatriene-norcaradiene equilibrium. Three-dimensional depictions. highlight the boat conformation of cycloheptatriene with “concave” and “convex” faces.

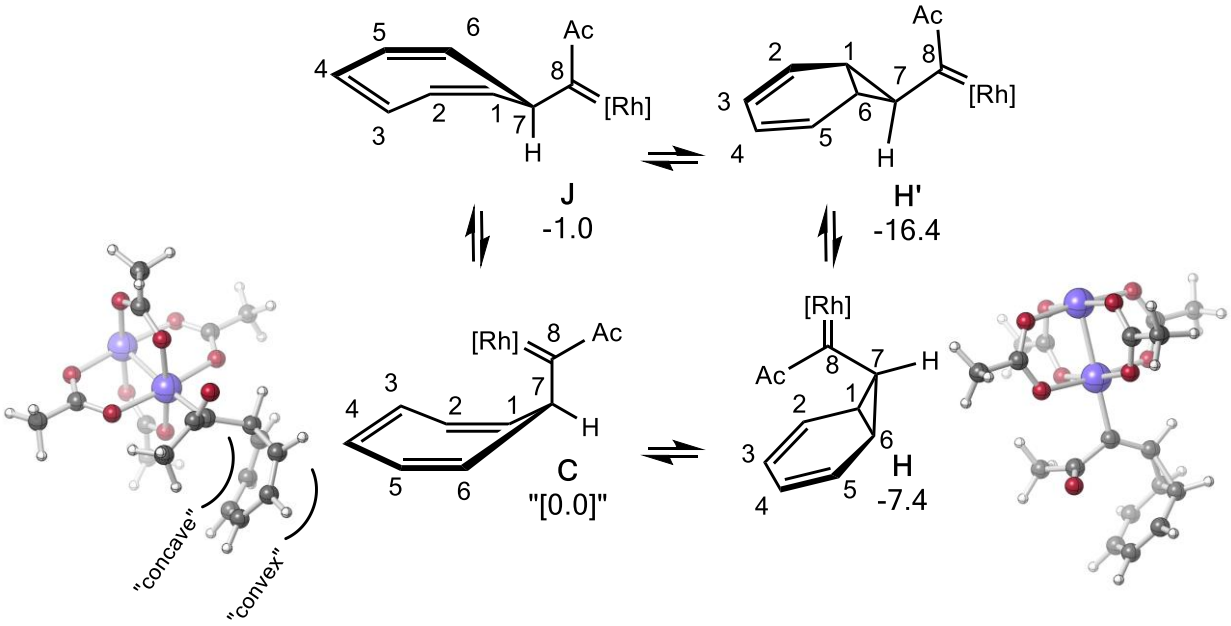

Complications I – Electrocyclization. Cycloheptatrienes[95–97] are generally in rapid equilibrium with norcaradienes (Scheme 6.2).[98–101] If our desired CP reaction is to predominate, either its barrier must be lower than that for **C**/**H** equilibration or that equilibration must not lead

to an undesired reaction that serves as a kinetic trap. In our system, the 7-position (C7) sports a π-electron acceptor – the metal carbene group[102] – which tends to favor norcaradiene formation.[100] **H** is predicted to be much lower in energy than **C** (and the **C** → **H** barrier is predicted to be 5.1 kcal mol^{-1}, lower than the CP barrier to **D**; Figure 6.1). However, the subsequent 1,2-hydride migration that would lead to catalyst dissociation is associated with a TSS that is much higher in energy than that for CP (17.7 kcal mol^{-1}; $TSS_{H\text{-}I}$). Consequently, the **C** → **H** → **I**… path does not appear to threaten our desired reaction.

Complications II – Conformational Bias. Cycloheptatrienes are not geometrically flat in three-dimensions—instead, their sp^3 carbon is bent out of plane in a boat conformation (cf. Scheme 6.2).[103] Parent tropilidene (i.e., hydrogens at C7) has a ring-inversion barrier of approximately 6 kcal mol^{-1} by low temperature ^{1}H NMR.[104–106] As a result, the environments of the two groups on this carbon are different: one sits over the cycloheptatriene π-system, while the other points "outside". For CP to occur, the carbene center must reside over the π-system. The carbene center prefers to reside outside (by 1 kcal mol^{-1}; compare **C** vs. **J**). When the carbene center is outside, a 1,2-hydride shift (a *β*-hydride migration) can occur (**J** → **K**) that is predicted to be rapid and exergonic.[107] Our computed ring-inversion barrier ($TSS_{C\text{-}J}$) is 4.4 kcal mol^{-1}, which suggests the *β*-hydride migration might indeed be a dead-end kinetic trap (Path I).

Complications III – Another β-Hydride Migration. A *β*-hydride migration also can occur directly from conformer **C** (Figure 6.1, Path III). While the TSS for this 1,2-hydride migration is predicted to be higher in energy than that for **J** (2.4 vs. 0.3 kcal mol^{-1}), it is predicted to be lower than the desired CP step (5.3 kcal mol^{-1}). Tendency to migrate hydride is increased for *α*-diazocarbonyl compounds—precursors to (donor-acceptor metal-carbenes)—due to their higher electrophilicity compared to donor and donor-donor metal-carbenes.[48] Indeed, in Path C, we find

that the barrier for *β*-hydride migration directly from **C** is increased upon swapping out the carbonyl acyl group for a phenyl group, thereby making the donor-acceptor carbene into a donor-donor carbene (Path C, 2.4 kcal mol^{-1} vs. 5.2 kcal mol^{-1}).* However, though the barrier for *β*-hydride migration increases upon changing the carbene from donor-acceptor to donor-donor, so does the CP barrier (Path II, 5.3 kcal mol^{-1} vs. 8.9 kcal mol^{-1}). Swapping the acyl group for a phenyl group does not easily tip the selectivity in favor of CP to SBV—the data tell us (with a $\Delta\Delta G^{\ddagger}$ = 3.7 kcal mol^{-1}) that the reaction would still favor *β*-hydride migration over CP.

Our metal-carbene may escape our desired reaction through *β*-hydride migration escape channels to heptafulvene, **G**. Recall that heptafulvene was one product Zimmerman isolated in their original report.[2] Additionally, in 1993, Tomioka et al. reported heptafulvene products in the gas-phase rearrangement of phenyl carbenes, presumably through 7-membered ring intermediates.[108] Heptafulvene **G** can additionally undergo a 10-π electrocyclic ring closing to **M** because of the acetyl group attached to C8, similar to that of the acetyl-heptafulvene reported by Houk.[109†] We computed the barrier to do so and the barrier is 15 kcal mol^{-1} from **G** to **M**, and downhill in energy.

6.4.2 A Potential Antidote to β-hydride Migration

One way around *β*-hydride migration complications is to introduce a different functional group at C7 in place of the hydrogen, a group with a lower migratory aptitude (e.g., CH_3 for H). Though making this substitution in a computational study is trivial, implementing it in a synthetic campaign could be challenging. Our calculations indicate, however, that swapping out the H for a CH_3 group

* Data for donor/donor carbene is described in the Appendix, I-A.
† Ibid, Appendix 1-A.

would switch the selectivity in favor of CP over a possible concerted, intramolecular C-H insertion ($TS_{C\text{-}F}$; $\Delta\Delta G^{\ddagger}$ = 0.8 kcal mol^{-1}; Figure 6.2) to a spirononatriene: a direct result of our attempts to locate a 1,2-methyl shift (not found). Though small-ring spiro compounds have precedent in the literature,[110] to our knowledge, relatively few papers report structures resembling spirononatriene.[111–114] Conformational inversion of CHT is energetically more favorable than CP (by 0.7 kcal mol^{-1}), which can then undergo a 1,2-methyl shift to cycloheptafulvene (**G**). Isomerization to norcaradiene, **H**, is also possible. But the high barrier out of **H** to spironorcaradiene compound, **I**, relative to that for reverting to **C** does not necessarily make **Path IV** to **I** a probable escape route. Tricyclic spiro compounds like **I** have some literature precedent, but to our knowledge, spironorcaradienes of the sort we describe have not been reported, though some structures resemble it.[115] Therefore, although C7 methyl substitution makes CP to SBV more likely than in the C7 hydrogen substituted case (Figure 6.1), methyl migration (Path I) could still preclude the desired chemoselectivity. Despite the lower barrier to isomerize to the other CHT boat ($TS_{C\text{-}H}$; 4.9 kcal mol^{-1}), $TS_{C\text{-}H}$ and $TS_{C\text{-}D}$ energies are close enough where SBV formation could be competitive with heptafulvene formation. So far, the C7-methylated system provides the most promising substrate for SBV synthesis from cycloheptatrienyl diazo compounds. Similar qualitative conclusions are realized for the donor Rh-carbene system (a $\Delta\Delta G^{\ddagger}$ = 1.4 kcal mol^{-1} when Ac = Ph).[*]

[*] Ibid, Appendix I-A (see Figure A.4).

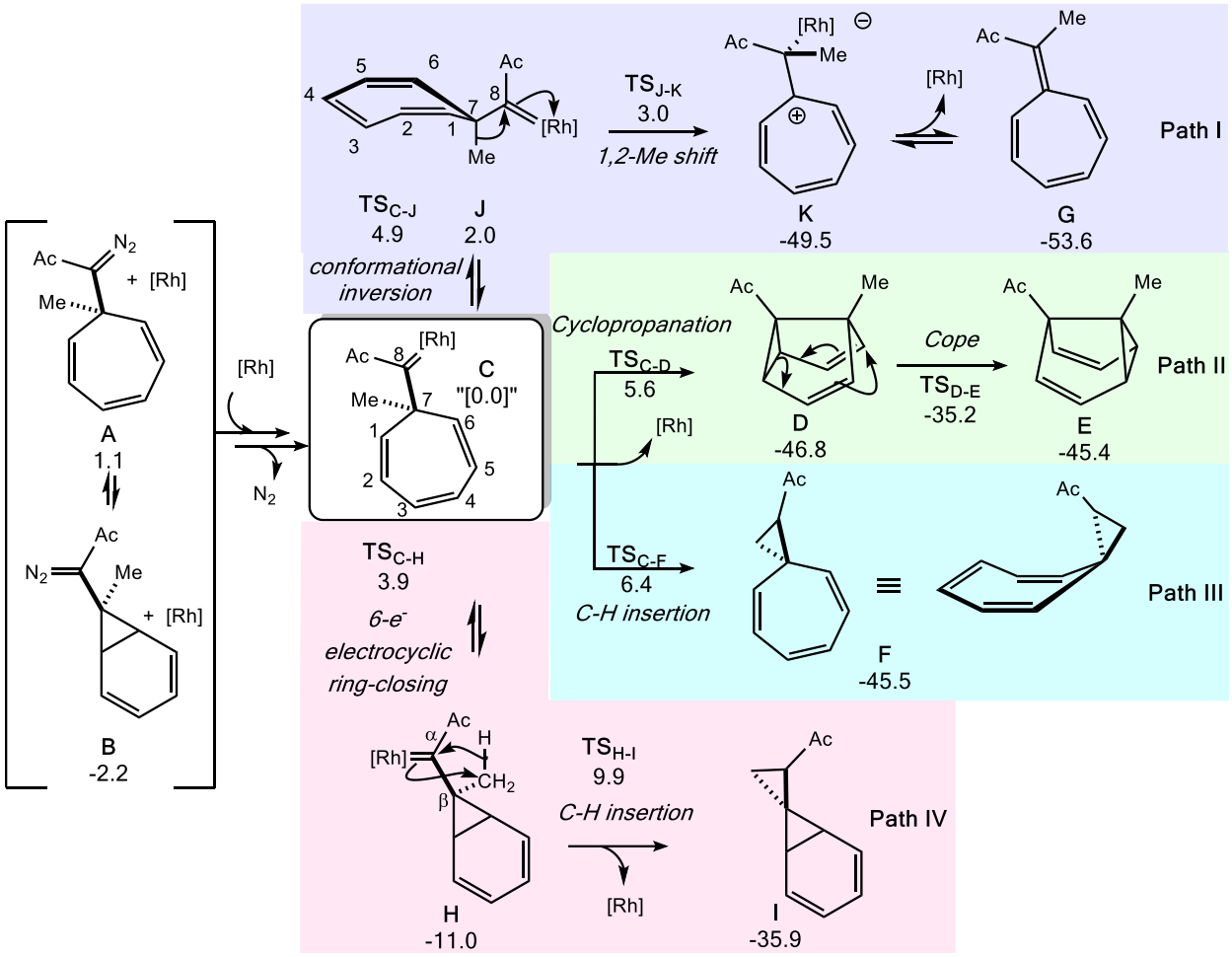

Figure 6.2 Methyl substitution at C7 tips the chemoselectivity to CP over β-hydride migration, but simultaneously introduces the possibility of concerted, intramolecular C-H insertion to generate a spirononatriene (**F**).

6.4.3 Gold(I)-catalyzed synthesis of barbaralones

For comparison, we examined Ferrer and Echavarren's gold(I)-catalyzed oxidative cyclizations[66,116] to barbaralones (Scheme 6.1e). In their 2016 study, Ferrer and Echavarren proposed two pathways to barbarlones—specifically, 6-*endo*-dig[117] cyclization then oxidation or *vice versa*. We computed both possible pathways (Figure 6.3 and 6.4). The predicted barrier for cyclization in the unoxidized system is higher than that for the oxidized system. The oxidized system also has a significant energetic driving force (ΔG = -37.8 kcal mol^{-1}) that the unoxidized

system lacks.[68] The results in Figure 6.4 resemble our computed CP path (Path II, Figure 6.1), but do not necessarily provide evidence for or against Ferrer and Echavarren's proposal that oxidation takes place on barbaralyl gold(I) intermediates after cyclization—further calculations would be needed.[66] Unlike their reaction, however, questions about oxidation state are irrelevant here with [Rh].

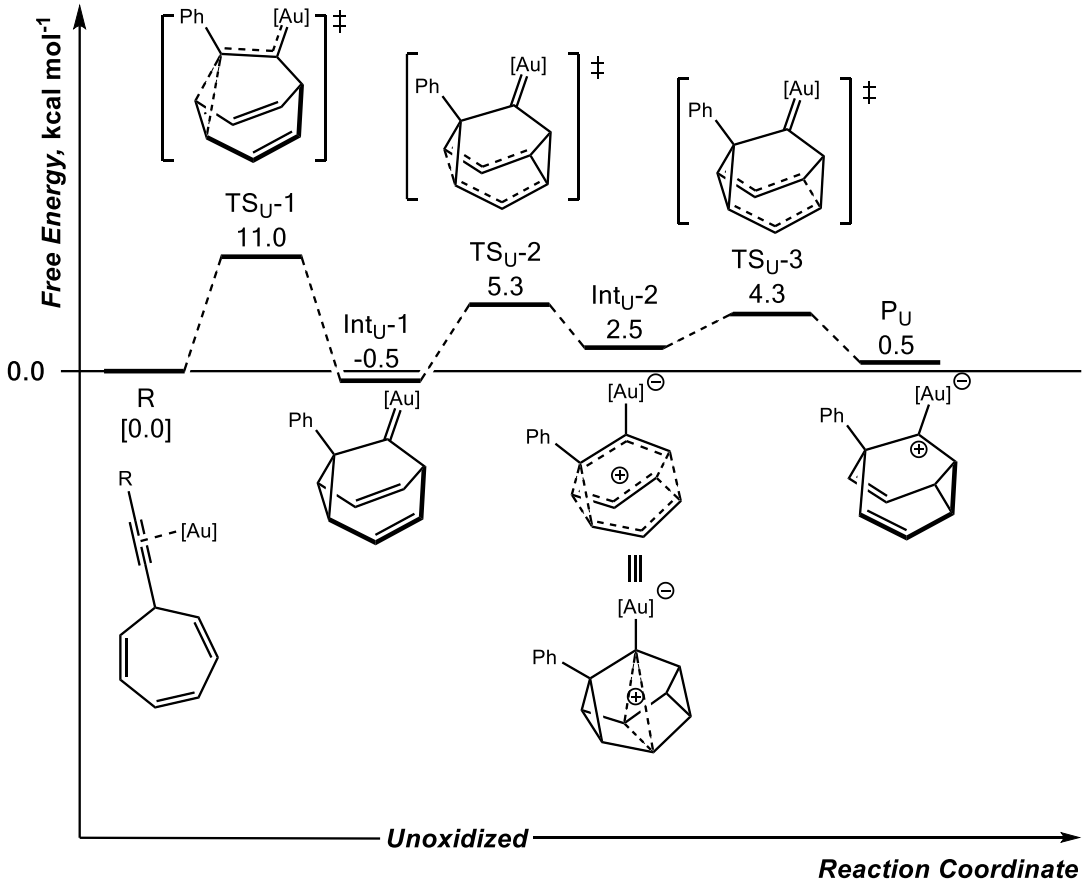

Figure 6.3 Potential energy surface of barbaryl cation formation and sequential Cope rearrangements. Relative free energies (PW6B95/def2-SVP) shown are in kcal mol^{-1} and are relative to their respective reactants, R.

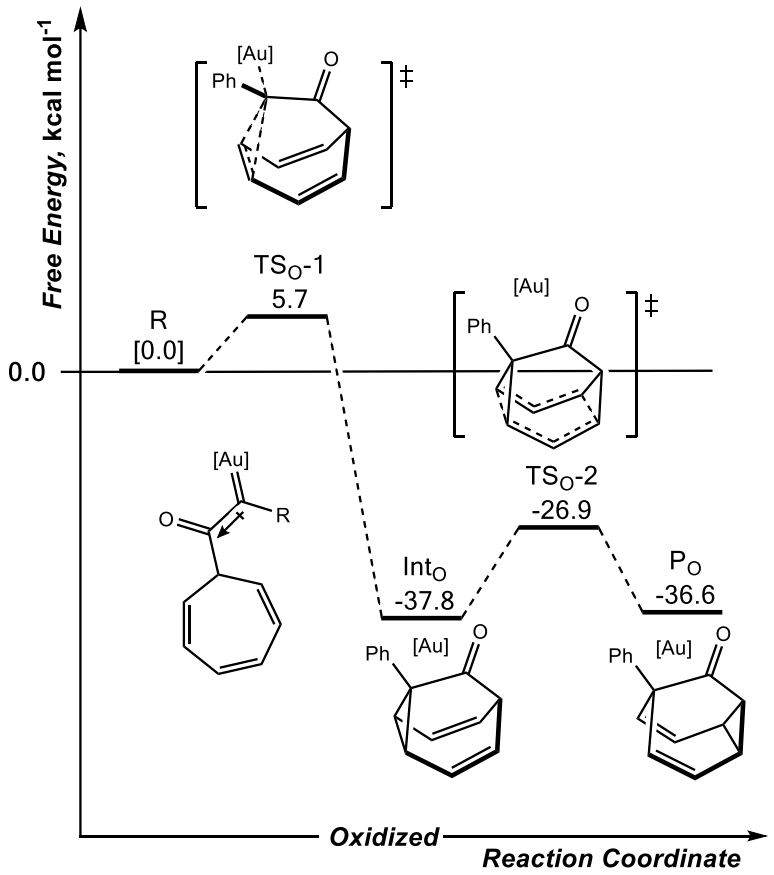

Figure 6.4 Potential energy surface of barbaralone cation formation and sequential Cope rearrangements. Relative free energies (PW6B95/def2-SVP) shown are in kcal mol^{-1} and are relative to their respective reactants, R.

We compute that the [3,3]-sigmatropic rearrangement for the unoxidized system is stepwise (not surprising given the copious studies that have reported interrupted, and aborted pathways for Au-catalyzed pericyclic reactions, in addition to concerted ones).[118–120] The intermediate that interrupts the rearrangement (Int_U-2) can be described as a metal-stabilized 9-barbaralyl cation.[121,122] Free of catalyst and substituents, the 9-barbaralyl cation exhibits D_{3h} symmetry and has been the focus of several studies since its description by Schleyer and coworkers.[123]

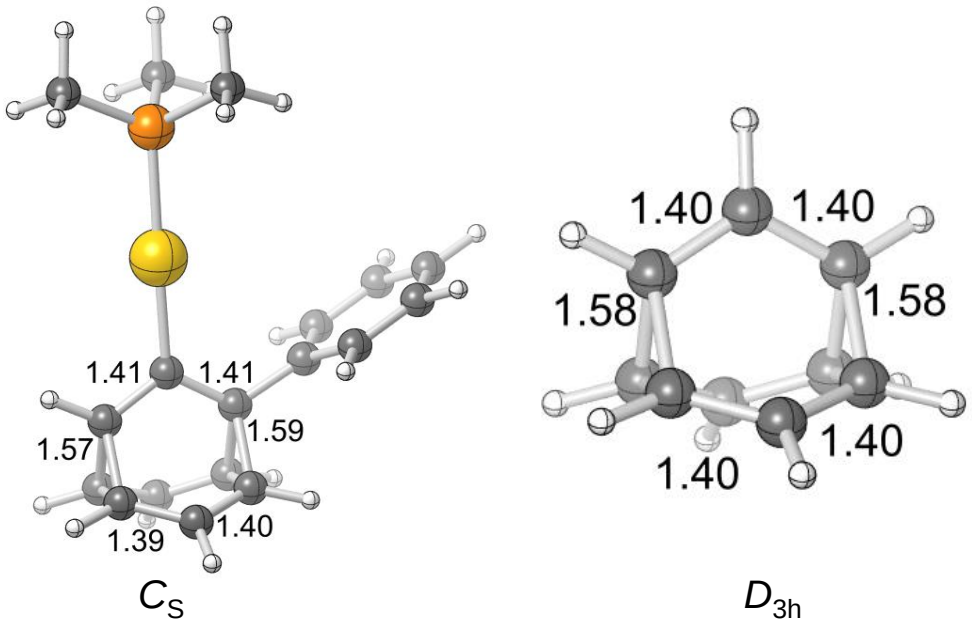

Figure 6.5 Comparison of C_s (Int_U-2, Figure 6.3) and D_{3h} (9-barbaralyl cation). Bond lengths (C-C bonds) are angstrom (Å).

6.5 Conclusions and Future Work

We have provided a prediction of a Rh(II)-catalyzed CP strategy for potential application to synthesize monofunctionalized semibullvalenes from cycloheptatriene diazo compounds. The potential CP step is investigated by DFT calculations, the results of which indicate that CP is energetically feasible from the Rh-carbene intermediate generated after decomposition of diazo compound. Potential side reactions and isomerizations were explored. *β*-hydride migration is computed to be lower in energy than CP, leading to substituted heptafulvenes, a useful product that can be evolved further to other products—undesired side reactions can potentially be prevented by introducing a methyl group at C7 in place of hydrogen, though notably, spirononatrienes may also result.[*] Dynamics studies are underway to test for the possibility of a

[*] Though not our aims here, such a side reaction might provide an interesting way to synthesize spirononatrienes, which, to our knowledge, only have few reports (< 10 studies)—see ref. 104-108.

post-transition state bifurcation in our system. We also look forward to the possibility that our prediction will be tested in the laboratory one day and (hopefully) validated. Work is currently being carried out in the lab of Prof. Jared Shaw to test our predictions.

6.6 Acknowledgements

Support from the US National Science Foundation (CHE- 1856416 and XSEDE) is gratefully acknowledged. The authors also thank Dr. Eric Ashley (Merck) for fruitful discussion and advice during the 2021 Bay Area Chemical Symposium poster session.

6.7 References

(1) Zimmerman, H. E.; Grunewald, G. L. The Chemistry of Barrelene. III. A Unique Photoisomerization to Semibullvalene. *J. Am. Chem. Soc.* **1966**, *88*, 183–184.
(2) Zimmerman, H. E.; Sousa, L. R. Cyclohepatrienyldiazomethane. Its Synthesis and Behavior. C8H8 Chemistry. X. Correlation Diagrams and Nodal Properties. *J. Am. Chem. Soc.* **1972**, *94*, 834–842.
(3) Doyle, M. P. Catalytic Methods for Metal Carbene Transformations. *Chem. Rev.* **1986**, *86*, 919–939.
(4) Laszlo, P. Playing with Molecular Models. *Hyle* **2000**, *6*, 85–97.
(5) Parrish, S. Learning Through Play https://fs.blog/2020/11/learning-through-play/ (accessed Jul 22, 2021).
(6) Cope, A. C.; Hardy, E. M. The Introduction of Substituted Vinyl Groups. V. A Rearrangement Involving the Migration of an Allyl Group in a Three-Carbon System 1. *J. Am. Chem. Soc.* **1940**, *62*, 441–444.
(7) Graulich, N. The Cope Rearrangement—the First Born of a Great Family. *WIREs Comput. Mol. Sci.* **2011**, *1*, 172–190.
(8) Ma, Y.-Y.; Yan, M.; Li, H.-R.; Wu, Y.-B.; Tian, X.-X.; Lu, H.-G.; Li, S.-D. Probing the Fluxional Bonding Nature of Rapid Cope Rearrangements in Bullvalene $C_{10}H_{10}$ and Its Analogs C_8H_8, C_9H_{10}, and C_8BH_9. *Sci. Rep.* **2019**, *9*, 17074.
(9) Williams, R. V.; Aring, A. J.; Bonifacio, M. C.; Blumenfeld, A. 4,6-Barbaralanedicarboxy-2,8-Dicarboxylic Anhydride and 1,5-Dimethyl-4,6-Semibullvalenedicarboxy-2,8-Dicarboxylic Anhydride: Examples of Unusual Barbaralanes and Semibullvalenes That Do Not Undergo the Cope Rearrangement. They Are Locked as the Closed Tau. *J. Phys. Org. Chem.* **2017**, *30*, e3622.
(10) von E. Doering, W.; Roth, W. R. Thermal Rearrangements. *Angew. Chem. Int. Ed.* **1963**, *2*, 115–122.

(11) Lippert, A. R.; Naganawa, A.; Keleshian, V. L.; Bode, J. W. Synthesis of Phototrappable Shape-Shifting Molecules for Adaptive Guest Binding. *J. Am. Chem. Soc.* **2010**, *132*, 15790–15799.
(12) McKee, M. L. Fluctional Molecules. *WIREs Comput. Mol. Sci.* **2011**, *1* (6), 943–951.
(13) Larson, K. K.; He, M.; Teichert, J. F.; Naganawa, A.; Bode, J. W. Chemical Sensing with Shapeshifting Organic Molecules. *Chem. Sci.* **2012**, *3*, 1825.
(14) Teichert, J. F.; Mazunin, D.; Bode, J. W. Chemical Sensing of Polyols with Shapeshifting Boronic Acids As a Self-Contained Sensor Array. *J. Am. Chem. Soc.* **2013**, *135*, 11314–11321.
(15) Bismillah, A. N.; Sturala, J.; Chapin, B. M.; Yufit, D. S.; Hodgkinson, P.; McGonigal, P. R. Shape-Selective Crystallisation of Fluxional Carbon Cages. *Chem. Sci.* **2018**, *9*, 8631–8636.
(16) Bismillah, A. N.; Chapin, B. M.; Hussein, B. A.; McGonigal, P. R. Shapeshifting Molecules : The Story so Far and the Shape of Things to Come. *Chem. Sci.* **2020**, *11*, 324–332.
(17) Sanchez, A.; Maimone, T. J. Taming Shapeshifting Anions: Total Synthesis of Ocellatusone C. *J. Am. Chem. Soc.* **2022**, *144*, 7594–7599.
(18) Ferrer, S.; Echavarren, A. Synthesis of Bullvalenes: Classical Approaches and Recent Developments. *Synthesis* **2019**, *51*, 1037–1048.
(19) Hoffmann, R.; Stohrer, W. D. Cope Rearrangement Revisited. *J. Am. Chem. Soc.* **1971**, *93*, 6941–6948.
(20) Iyengar, R.; Piña, R.; Grohmann, K. Semibullvalenes IV: 2,6- and 2,8-Trapping of the Bicyclo[3.3.0]Octadienyl Diradical with Oxygen. *J. Am. Chem. Soc.* **1988**, *110*, 2643–2644.
(21) Zilberg, S.; Haas, Y.; Danovich, D.; Shaik, S. The Twin-Excited State as a Probe for the Transition State in Concerted Unimolecular Reactions: The Semibullvalene Rearrangement. *Angew. Chem. Int. Ed.* **1998**, *37*, 1394–1397.
(22) Zhang, X.; Hrovat, D. A.; Borden, W. T. Calculations Predict That Carbon Tunneling Allows the Degenerate Cope Rearrangement of Semibullvalene to Occur Rapidly at Cryogenic Temperatures. *Org. Lett.* **2010**, *12*, 2798–2801.
(23) Schleif, T.; Mieres-Perez, J.; Henkel, S.; Ertelt, M.; Borden, W. T.; Sander, W. The Cope Rearrangement of 1,5-Dimethylsemibullvalene-2(4)-D1: Experimental Evidence for Heavy-Atom Tunneling. *Angew. Chem. Int. Ed.* **2017**, *56*, 10746–10749.
(24) Greer, E. M.; Kwon, K.; Greer, A.; Doubleday, C. Thermally Activated Tunneling in Organic Reactions. *Tetrahedron* **2016**, *72*, 7357–7373.
(25) Schreiner, P. R. Tunneling Control of Chemical Reactions: The Third Reactivity Paradigm. *J. Am. Chem. Soc.* **2017**, *139*, 15276–15283.
(26) Schleif, T.; Tatchen, J.; Rowen, J. F.; Beyer, F.; Sanchez-Garcia, E.; Sander, W. Heavy Atom Tunneling in Semibullvalenes: How Driving Force, Substituents, and Environment Influence the Tunneling Rates. *Chem. Eur. J.* **2020**, *26*, 10452–10458.
(27) Karton, A. Cope Rearrangements in Shapeshifting Molecules Re-Examined by Means of High-Level CCSDT(Q) Composite Ab Initio Methods. *Chem. Phys. Lett.* **2020**, *759*, 138018.
(28) Jiao, H.; Schleyer, P. Elimination of the Barrier to Cope Rearrangement in Semibullvalene by Li+ Complexation. *Angew. Chem. Int. Ed.* **1993**, *32*, 1760–1763.
(29) Laconsay, C. J.; Mallick, D.; Shaik, S. External Electric Fields Interrupt the Concerted

Cope Rearrangement of Semibullvalene. *J. Org. Chem.* **2021**, *86*, 731–738.
(30) Jiao, H.; Nagelkerke, R.; Kurtz, H. A.; Williams, R. V.; Borden, W. T.; Von Ragué Schleyer, P. Annelated Semibullvalenes: A Theoretical Study of How They "cope" with Strain. *J. Am. Chem. Soc.* **1997**, *119*, 5921–5929.
(31) Hrovat, D. A.; Williams, R. V.; Goren, A. C.; Borden, W. T. B3LYP Calculations on Bishomoaromaticity in Substituted Semibullvalenes. *J. Comput. Chem.* **2001**, *22*, 1565–1573.
(32) Williams, R. V. Homoaromaticity. *Chem. Rev.* **2001**, *101*, 1185–1204.
(33) Wu, H.-S.; Jiao, H.; Wang, Z.-X.; Schleyer, P. V. R. Neutral Bishomoaromatic Semibullvalenes. *J. Am. Chem. Soc.* **2003**, *125*, 10524–10525.
(34) Seefelder, M.; Heubes, M.; Quast, H.; Edwards, W. D.; Armantrout, J. R.; Williams, R. V.; Cramer, C. J.; Goren, A. C.; Hrovat, D. A.; Borden, W. T. Experimental and Theoretical Study of Stabilization of Delocalized Forms of Semibullvalenes and Barbaralanes by Dipolar and Polarizable Solvents. Observation of a Delocalized Structure That Is Lower in Free Energy than the Localized Form. *J. Org. Chem.* **2005**, *70*, 3437–3449.
(35) Griffiths, P. R.; Pivonka, D. E.; Williams, R. V. The Experimental Realization of a Neutral Homoaromatic Carbocycle. *Chem. Eur. J.* **2011**, *17*, 9193–9199.
(36) Williams, R. V.; Al-Sehemi, A. G.; Meier, A. K.; Brown, Z. Z.; Armantrout, J. R. The Role of Strain in the Homoaromatization of Semibullvalenes. *J. Org. Chem.* **2017**, *82*, 4136–4147.
(37) Wang, S. C.; Tantillo, D. J. The Mechanism of Semibullvalene Bromination. *European J. Org. Chem.* **2006**, *2006*, 738–745.
(38) Ess, D. H.; Wheeler, S. E.; Iafe, R. G.; Xu, L.; Çelebi-Ölçüm, N.; Houk, K. N. Bifurcations on Potential Energy Surfaces of Organic Reactions. *Angew. Chem. Int. Ed.* **2008**, *47*, 7592–7601.
(39) Hare, S. R.; Tantillo, D. J. Post-Transition State Bifurcations Gain Momentum-Current State of the Field. *Pure Appl. Chem.* **2017**, *89*, 679–698.
(40) Mandal, N.; Datta, A. Dynamical Effects along the Bifurcation Pathway Control Semibullvalene Formation in Deazetization Reactions. *J. Phys. Chem. B* **2018**, *122*, 1239–1244.
(41) Paquette, L. A. Silver(I) Ion Catalyzed Rearrangements of Strained Sigma Bonds. II. Application of the Synthesis of Semibullvalene. *J. Am. Chem. Soc.* **1970**, *92*, 5765–5767.
(42) Turro, N. J.; Liu, J.-M.; Zimmerman, H. E.; Factor, R. E. Practical Synthesis of Semibullvalene. *J. Am. Chem. Soc.* **1980**, *45*, 3511–3512.
(43) Miller, L. S.; Grohmann, K.; Dannenberg, J. J. Semibullvalenes. 1. Synthesis and Crystal Structure of 1,5-Dimethyl-2,4,6,8-Tetrakis(Carbomethoxy)Tricyclo[3.3.0.02,8]Octa-3,6-Diene a Donor-Acceptor-Substituted Semibullvalene. *J. Am. Chem. Soc.* **1981**, *103*, 6249–6251.
(44) Mehta, G.; Ravikrishna, C. A New Synthesis of Semibullvalenes via Photodecarbonylation of Norsnoutanones. *Tetrahedron Lett.* **1998**, *39*, 4899–4900.
(45) Sauer, J.; Bäuerlein, P.; Ebenbeck, W.; Schuster, J.; Sellner, I.; Sichert, H.; Stimmelmayr, H. An One-Pot Synthesis of Semibullvalenes and Its Mechanism. *European J. Org. Chem.* **2002**, *2002*, 791–801.
(46) Zhang, S.; Zhan, M.; Wang, Q.; Wang, C.; Zhang, W.-X.; Xi, Z. Synthesis of Semibullvalene Derivatives via $Co_2(CO)_8$-Mediated Cyclodimerization of 1,4-Dilithio-

1,3-Butadienes. *Org. Chem. Front.* **2014**, *1*, 130–134.
(47) Zhang, S.; Zhang, W.-X.; Xi, Z. Semibullvalene and Diazasemibullvalene: Recent Advances in the Synthesis, Reaction Chemistry, and Synthetic Applications. *Acc. Chem. Res.* **2015**, *48*, 1823–1831.
(48) Bergstrom, B. D.; Nickerson, L. A.; Shaw, J. T.; Souza, L. W. Transition Metal Catalyzed Insertion Reactions with Donor/Donor Carbenes. *Angew. Chem. Int. Ed.* **2021**, *60*, 6864–6878.
(49) Nickerson, L. A.; Bergstrom, B. D.; Gao, M.; Shiue, Y.-S.; Laconsay, C. J.; Culberson, M. R.; Knauss, W. A.; Fettinger, J. C.; Tantillo, D. J.; Shaw, J. T. Enantioselective Synthesis of Isochromans and Tetrahydroisoquinolines by C–H Insertion of Donor/Donor Carbenes. *Chem. Sci.* **2020**, *11*, 494–498.
(50) Dishman, S. N.; Laconsay, C. J.; Fettinger, J. C.; Tantillo, D. J.; Shaw, J. T. Divergent Stereochemical Outcomes in the Insertion of Donor/Donor Carbenes into the C–H Bonds of Stereogenic Centers. *Chem. Sci.* **2022**, *13*, 1030–1036.
(51) Jana, S.; Guo, Y.; Koenigs, R. M. Recent Perspectives on Rearrangement Reactions of Ylides via Carbene Transfer Reactions. *Chem. Eur. J.* **2021**, *27*, 1270–1281.
(52) Laconsay, C. J.; Tantillo, D. J. Metal Bound or Free Ylides as Reaction Intermediates in Metal-Catalyzed [2,3]-Sigmatropic Rearrangements? It Depends. *ACS Catal.* **2021**, *11*, 829–839.
(53) Nair, V. N.; Kojasoy, V.; Laconsay, C. J.; Kong, W. Y.; Tantillo, D. J.; Tambar, U. K. Catalyst-Controlled Regiodivergence in Rearrangements of Indole-Based Onium Ylides. *J. Am. Chem. Soc.* **2021**, *143*, 9016–9025.
(54) Laconsay, C. J.; Tantillo, D. J. Melding of Experiment and Theory Illuminates Mechanisms of Metal-Catalyzed Rearrangements: Computational Approaches and Caveats. *Synthesis* **2021**, *53*, 3639–3652.
(55) Hare, S. R.; Tantillo, D. J. Cryptic Post-Transition State Bifurcations That Reduce the Efficiency of Lactone-Forming Rh-Carbenoid C-H Insertions. *Chem. Sci.* **2017**, *8*, 1442–1449.
(56) Hansen, J. H.; Gregg, T. M.; Ovalles, S. R.; Lian, Y.; Autschbach, J.; Davies, H. M. L. On the Mechanism and Selectivity of the Combined C−H Activation/Cope Rearrangement. *J. Am. Chem. Soc.* **2011**, *133*, 5076–5085.
(57) Rehbein, J.; Carpenter, B. K. Do We Fully Understand What Controls Chemical Selectivity? *Phys. Chem. Chem. Phys.* **2011**, *13*, 20906.
(58) Jones, A. C.; May, J. A.; Sarpong, R.; Stoltz, B. M. Toward a Symphony of Reactivity: Cascades Involving Catalysis and Sigmatropic Rearrangements. *Angew. Chem. Int. Ed.* **2014**, *53*, 2556–2591.
(59) Davies, H. M. L.; Smith, H. D.; Korkor, O. Tandem Cyclopropanation/Cope Rearrangement Sequence. Stereospecific [3 + 4] Cycloaddition Reaction of Vinylcarbenoids with Cyclopentadiene. *Tetrahedron Lett.* **1987**, *28*, 1853–1856.
(60) Padwa, A.; Krumpe, K. E.; Gareau, Y.; Chiacchio, U. Rhodium(II)-Catalyzed Cyclization Reactions of Alkynyl-Substituted .Alpha.-Diazo Ketones. *J. Org. Chem.* **1991**, *56*, 2523–2530.
(61) Schwartz, B. D.; Denton, J. R.; Lian, Y.; Davies, H. M. L.; Williams, C. M. Asymmetric [4 + 3] Cycloadditions between Vinylcarbenoids and Dienes: Application to the Total Synthesis of the Natural Product (−)-5- Epi -Vibsanin E. *J. Am. Chem. Soc.* **2009**, *131*, 8329–8332.

(62) Miller, L. C.; Ndungu, J. M.; Sarpong, R. Parallel Kinetic Resolution Approach to the Cyathane and Cyanthiwigin Diterpenes Using a Cyclopropanation/Cope Rearrangement. *Angew. Chem. Int. Ed.* **2009**, *48*, 2398–2402.
(63) Davies, H. M. L.; Lian, Y. The Combined C–H Functionalization/Cope Rearrangement: Discovery and Applications in Organic Synthesis. *Acc. Chem. Res.* **2012**, *45*, 923–935.
(64) von E. Doering, W.; Ferrier, B. M.; Fossel, E. T.; Hartenstein, J. H.; Jones, M.; Klumpp, G.; Rubin, R. M.; Saunders, M. A Rational Synthesis of Bullvalene Barbaralone and Derivatives; Bullvalone. *Tetrahedron* **1967**, *23*, 3943–3963.
(65) Casas, J.; Serratosa, F. An Alternative Synthesis of Bullvalene Through a Double Rearrangement. *An. Quim.* **1977**, *73*, 300–302.
(66) Ferrer, S.; Echavarren, A. M. Synthesis of Barbaralones and Bullvalenes Made Easy by Gold Catalysis. *Angew. Chem. Int. Ed.* **2016**, *55*, 11178–11182.
(67) McGonigal, P. R.; de León, C.; Wang, Y.; Homs, A.; Solorio-Alvarado, C. R.; Echavarren, A. M. Gold for the Generation and Control of Fluxional Barbaralyl Cations. *Angew. Chem. Int. Ed.* **2012**, *51*, 13093–13096.
(68) Mato, M.; Montesinos-Magraner, M.; Sugranyes, A. R.; Echavarren, A. M. Rh(II)-Catalyzed Alkynylcyclopropanation of Alkenes by Decarbenation of Alkynylcycloheptatrienes. *J. Am. Chem. Soc.* **2021**, *143*, 10760–10769.
(69) Fan, Z.; Ni, S.; Pang, J.; Guo, L.; Yang, H.; Li, K.; Ma, C.; Liu, J.; Wu, B.; Yang, J. Cu(I)-Catalyzed Cross-Coupling Rearrangements of Terminal Alkynes with Tropylium Tetrafluoroborate: Facile Access to Barbaralyl-Substituted Allenyl Acid Esters and 7-Alkynyl Cycloheptatrienes. *J. Org. Chem.* **2022**, *87*, 3066–3078.
(70) Dauenhauer, P. J. "I Guess What I Am Saying Is That I Would like a Computational Chemist to Approach Me with an Idea That I Could Test for Them Rather than the Other Way around...." *Twitter* **2022**, https://twitter.com/pauldauenhauer/status/14810933.
(71) Schleyer, P. von R. An Appreciation. *J. Comput. Chem.* **2001**, *22*, ix–xi.
(72) Lee, C.; Yang, W.; Parr, R. G. Development of the Colle-Salvetti Correlation-Energy Formula into a Functional of the Electron Density. *Phys. Rev. B* **1988**, *37*, 785–789.
(73) Wang, S. C.; Tantillo, D. J. Selective Stabilization of Transition State Structures for Cope Rearrangements of Semibullvalene and Barbaralane through Interactions with Halogens. *J. Phys. Chem. A* **2007**, *111*, 7149–7153.
(74) Greer, E. M.; Hoffmann, R. Metalla-Cope Rearrangements: Bridging Organic and Inorganic Chemistry †. *J. Phys. Chem. A* **2010**, *114*, 8618–8624.
(75) Staroverov, V. N.; Davidson, E. R. Transition Regions in the Cope Rearrangement of 1,5-Hexadiene and Its Cyano Derivatives. *J. Am. Chem. Soc.* **2000**, *122*, 7377–7385.
(76) Staroverov, V. N.; Davidson, E. R. The Cope Rearrangement in Theoretical Retrospect. *J. Mol. Struct. THEOCHEM* **2001**, *573*, 81–89.
(77) Karton, A. Can Density Functional Theory 'Cope' with Highly Fluxional Shapeshifting Molecules? *Chem. Phys.* **2021**, *540*, 111013.
(78) Quintal, M. M.; Karton, A.; Iron, M. A.; Daniel Boese, A.; Martin, J. M. L. Benchmark Study of DFT Functionals for Late-Transition-Metal Reactions. *J. Phys. Chem. A* **2006**, *110*, 709–716.
(79) Zhao, Y.; Truhlar, D. G. Design of Density Functionals That Are Broadly Accurate for Thermochemistry, Thermochemical Kinetics, and Nonbonded Interactions. *J. Phys. Chem. A* **2005**, *109*, 5656–5667.
(80) Schäfer, A.; Horn, H.; Ahlrichs, R. Fully Optimized Contracted Gaussian Basis Sets for

Atoms Li to Kr. *J. Chem. Phys.* **1992**, *97*, 2571–2577.
(81) Cheng, A. K.; Anet, F. A. L.; Mioduski, J.; Meinwald, J. Determination of the Fluxional Barrier in Semibullvalene by Proton and Carbon-13 Nuclear Magnetic Resonance Spectroscopy. *J. Am. Chem. Soc.* **1974**, *96*, 2887–2891.
(82) Moskau, D.; Aydin, R.; Leber, W.; Günther, H.; Quast, H.; Martin, H. -D; Hassenrück, K.; Miller, L. S.; Grohmann, K. Anwendungen Der ^{13}C-NMR-Spektroskopie, XXVII. Die Aktivierungsparameter Der Cope-Umlagerung von Semibullvalen, 1,5-Dimethylsemibullvalen Und 2,6-Dibrom-1,5-dimethylsemibullvalen. *Chem. Ber.* **1989**, *122*, 925–931.
(83) Rubin, M. B. Photolysis of Two Tricyclic Nonenediones. Direct Observation of Norcaradiene. *J. Am. Chem. Soc.* **1981**, *103*, 7791–7792.
(84) Chen, P.; Seeman, J. I.; Houk, K. N. Rolf Huisgen's Classic Studies of Cyclic Triene Diels–Alder Reactions Elaborated by Modern Computational Analysis. *Angew. Chem. Int. Ed.* **2020**, *59*, 12506–12519.
(85) Frisch, M. J.; Trucks, G. W.; Schlegel, H. B.; Scuseria, G. E.; Robb, M. A.; Cheeseman, J. R.; Scalmani, G.; Barone, V.; Petersson, G. A.; Nakatsuji, H.; Li, X.; Caricato, M.; Marenich, A. V.; Bloino, J.; Janesko, B. G.; Gomperts, R.; Mennucci, B.; Hratchian, H. P.; Ortiz, J. V.; Izmaylov, A. F.; Sonnenberg, J. L.; Williams-Young, D.; Ding, F.; Lipparini, F.; Egidi, F.; Goings, J.; Peng, B.; Petrone, A.; Henderson, T.; Ranasinghe, D.; Zakrzewski, V. G.; Gao, J.; Rega, N.; Zheng, G.; Liang, W.; Hada, M.; Ehara, M.; Toyota, K.; Fukuda, R.; Hasegawa, J.; Ishida, M.; Nakajima, T.; Honda, Y.; Kitao, O.; Nakai, H.; Vreven, T.; Throssell, K.; Montgomery, J. A., Jr.; Peralta, J. E.; Ogliaro, F.; Bearpark, M. J.; Heyd, J. J.; Brothers, E. N.; Kudin, K. N.; Staroverov, V. N.; Keith, T. A.; Kobayashi, R.; Normand, J.; Raghavachari, K.; Rendell, A. P.; Burant, J. C.; Iyengar, S. S.; Tomasi, J.; Cossi, M.; Millam, J. M.; Klene, M.; Adamo, C.; Cammi, R.; Ochterski, J. W.; Martin, R. L.; Morokuma, K.; Farkas, O.; Foresman, J. B.; Fox, D. J Gaussian 16, Revision A.03. Gaussian, Inc.: Willingford, CT 2016.
(86) Fukui, K. The Path of Chemical Reactions -- The IRC Approach. *Acc. Chem. Res.* **1981**, *14*, 363–368.
(87) Gonzalez, C.; Schlegel, H. B. Reaction Path Following In Mass-Weighted Internal Coordinates Cartesians and with Internal Coordinates without Mass-Weighting. *J. Phys. Chem.* **1990**, *94*, 5523–5527.
(88) Maeda, S.; Harabuchi, Y.; Ono, Y.; Taketsugu, T.; Morokuma, K. Intrinsic Reaction Coordinate: Calculation, Bifurcation, and Automated Search. *Int. J. Quantum Chem.* **2015**, *115*, 258–269.
(89) Davies, H. M. L.; Liao, K. Dirhodium Tetracarboxylates as Catalysts for Selective Intermolecular C–H Functionalization. *Nat. Rev. Chem.* **2019**, *3*, 347–360.
(90) Bethäuser, W.; Weber, B.; Heydt, H.; Regitz, M. Untersuchungen an Diazoverbindungen Und Aziden, LV. 7-(Diazomethyl)Cycloheptatriene Durch Elektrophile Diazoalkansubstitution. *Chem. Ber.* **1985**, *118*, 1315–1328.
(91) von E. Doering, W.; Wiley, D. W. Heptafulvene (Methylenecycloheptatriene). *Tetrahedron* **1960**, *11*, 183–198.
(92) Stępień, B. T.; Krygowski, T. M.; Cyrański, M. K. Variation of the π-Electron Delocalization in Exocyclically Substituted Heptafulvene Derivatives. *J. Phys. Org. Chem.* **2003**, *16*, 426–430.
(93) Hoffmann, R.; Schleyer, P. von R.; Schaefer, H. F. Predicting Molecules-More Realism,

Please! *Angew. Chem. Int. Ed.* **2008**, *47*, 7164–7167.
(94) Parambil, P. C.; Hoffmann, R. Alkyl Isosteres. *J. Am. Chem. Soc.* **2018**, *140*, 12844–12852.
(95) Chen, Z.; Jiao, H.; Wu, J. I.; Herges, R.; Zhang, S. B.; Schleyer, P. von R. Homobenzene: Homoaromaticity and Homoantiaromaticity in Cycloheptatrienes. *J. Phys. Chem. A* **2008**, *112*, 10586–10594.
(96) Williams, R. V.; Edwards, W. D.; Zhang, P.; Berg, D. J.; Mitchell, R. H. Experimental Verification of the Homoaromaticity of 1,3,5-Cycloheptatriene and Evaluation of the Aromaticity of Tropone and the Tropylium Cation by Use of the Dimethyldihydropyrene Probe. *J. Am. Chem. Soc.* **2012**, *134*, 16742–16752.
(97) Jorner, K.; Jahn, B. O.; Bultinck, P.; Ottosson, H. Triplet State Homoaromaticity: Concept, Computational Validation and Experimental Relevance. *Chem. Sci.* **2018**, *9*, 3165–3176.
(98) Ciganek, E. The Direct Observation of a Norcaradiene-Cycloheptatriene Equilibrium. *J. Am. Chem. Soc.* **1965**, *87*, 1149–1150.
(99) Maier, G. The Norcaradiene Problem. *Angew. Chem. Int. Ed.* **1967**, *6*, 402–413.
(100) Hoffmann, R. The Norcaradiene - Cycloheptatriene Equilibrium. *Tetrahedron Lett.* **1970**, *11*, 2907–2909.
(101) Ciganek, E. The Cycloheptatriene-Norcaradiene System. III. Dependence of the Ground-State Enthalpy Difference on Substituents in the 7 Position. *J. Am. Chem. Soc.* **1971**, *93*, 2207–2215.
(102) Berry, J. F. The Role of Three-Center/Four-Electron Bonds in Superelectrophilic Dirhodium Carbene and Nitrene Catalytic Intermediates. *Dalt. Trans.* **2012**, *41*, 700–713.
(103) Berson, J. A.; Willcott, III, M. R. Thermally Induced Skeletal Rearrangements of Tropilidenes. *J. Am. Chem. Soc.* **1966**, *88*, 2494–2502.
(104) Anet, F. A. L. Ring Inversion in Cycloheptatriene. *J. Am. Chem. Soc.* **1964**, *86*, 458–460.
(105) Jensen, F. R.; Smith, L. A. The Structure and Interconversion of Cycloheptatriene. *J. Am. Chem. Soc.* **1964**, *86*, 956–957.
(106) Freedberg, D. I.; Kopelevich, M.; Anet, F. A. L. Deuterium Conformational Equilibrium Isotope Effects in 1,3,5-Cycloheptatriene-7-D. *J. Phys. Org. Chem.* **2001**, *14*, 625–635.
(107) DeAngelis, A.; Panish, R.; Fox, J. M. Rh-Catalyzed Intermolecular Reactions of α-Alkyl-α-Diazo Carbonyl Compounds with Selectivity over β-Hydride Migration. *Acc. Chem. Res.* **2016**, *49*, 115–127.
(108) Tomioka, H.; Taketsuji, K. Formation of Heptafulvene in Reactions of [(Methoxycarbonyl)Methyl]Phenylcarbene in the Gas Phases. *J. Org. Chem.* **1993**, *58*, 4196–4197.
(109) Liu, C.-Y.; Houk, K. N. Intramolecular [8+2] Cycloaddition and 10π-Electron Electrocyclization Reactions of an 8-Acylheptafulvene. *Tetrahedron Lett.* **1987**, *28*, 1367–1370.
(110) Liebman, J. F.; Greenberg, A. A Survey of Strained Organic Molecules. *Chem. Rev.* **1976**, *76*, 311–365.
(111) Mukai, T.; Nakazawa, T.; Isobe, T. Thermal Decomposition of Troponetosylhydrazone. *Tetrahedron Lett.* **1968**, *9*, 565–569.
(112) Rostek, C. J.; Jones, W. M. Synthesis and Diels-Alder Reactions of Spiro(2.6)Nona-4,6,8-Triene. *Tetrahedron Lett.* **1969**, *10*, 3957–3960.
(113) Jones, W. M.; Ennis, C. L. Cycloheptatrienylidene. *J. Am. Chem. Soc.* **1969**, *91*, 6391–

6397.
(114) Waali, E. E.; Jones, W. M. An Improved Synthesis of Spiro[2.6]Nonatriene. The Addition of Cycloheptatrienylidene to Ethylene. *Synth. Commun.* **1973**, *3*, 49–52.
(115) Li, C.; Yang, Y.; Zhou, Y.; Yu, Z. A Formal [3+3+1] Reaction of Enyne-Methylenecyclopropanes through Au(I)-Catalyzed Enyne Cycloisomerization and Rh(I)-Catalyzed [6+1] Reaction of Vinylspiropentanes and CO. *Asian J. Org. Chem.* **2022**, *11*, e202100571.
(116) Zheng, Z.; Wang, Z.; Wang, Y.; Zhang, L. Au-Catalysed Oxidative Cyclisation. *Chem. Soc. Rev.* **2016**, *45*, 4448–4458.
(117) Alabugin, I. V; Gilmore, K. Finding the Right Path: Baldwin "Rules for Ring Closure" and Stereoelectronic Control of Cyclizations. *Chem. Commun.* **2013**, *49*, 11246–11250.
(118) Felix, R. J.; Weber, D.; Gutierrez, O.; Tantillo, D. J.; Gagné, M. R. A Gold-Catalysed Enantioselective Cope Rearrangement of Achiral 1,5-Dienes. *Nat. Chem.* **2012**, *4*, 405–409.
(119) Vidhani, D. V.; Krafft, M. E.; Alabugin, I. V. Gold(I)-Catalyzed Allenyl Cope Rearrangement: Evolution from Asynchronicity to Trappable Intermediates Assisted by Stereoelectronic Switching. *J. Am. Chem. Soc.* **2016**, *138*, 2769–2779.
(120) dos Passos Gomes, G.; Alabugin, I. V. Drawing Catalytic Power from Charge Separation: Stereoelectronic and Zwitterionic Assistance in the Au(I)-Catalyzed Bergman Cyclization. *J. Am. Chem. Soc.* **2017**, *139*, 3406–3416.
(121) Hoffmann, R.; Stohrer, W.-D.; Goldstein, M. J. The 9-Barbaralyl Cation. *Bull. Chem. Soc. Jpn.* **1972**, *45*, 2513–2514.
(122) Cremer, D.; Svensson, P.; Kraka, E.; Ahlberg, P. Exploration of the Potential Energy Surface of C9H9+ by Ab Initio Methods. 1. The Barbaralyl Cation. *J. Am. Chem. Soc.* **1993**, *115*, 7445–7456.
(123) Barborak, J. C.; Daub, J.; Follweiler, D. M.; Schleyer, P. von R. Degenerate Rearrangements of the 9-Barbarayl Cation. *J. Am. Chem. Soc.* **1969**, *91*, 7760–7761.

Part II

Theoretical Models of Divergent Heterolytic Fragmentations

Chapter 7

Tipping the Balance: Theoretical Interrogation of Divergent Extended Heterolytic Fragmentations*

The hardest thing of all to see is what is really there.

- John A. Baker, *The Peregrine* (1967)

7.1 Abstract

Herein we interrogate a type of heterolytic fragmentation reaction called a 'divergent fragmentation' using density functional theory (DFT), natural bond orbital (NBO) analysis, *ab initio* molecular dynamics (AIMD), and external electric field (EEF) calculations. We demonstrate that substituents, electrostatic environment and non-statistical dynamic effects all influence product selectivity in reactions that involve divergent fragmentation pathways. Direct dynamics simulations reveal an unexpected post-transition state bifurcation (PTSB), and EEF calculations suggest that divergent pathways can, in principle, be selectively stabilized if an electric field of the correct magnitude is oriented appropriately.

* This chapter is a slightly modified version of the following published article: Laconsay, C. J.; Tsui K. Y.; Tantillo, D. J. Tipping the balance: theoretical interrogation of divergent extended heterolytic fragmentations, *Chem. Sci.* **2020**, *11*, 2231-2242 with permission from the Royal Society of Chemistry. Ka Yi Tsui contributed key DFT calculations for elucidating the crucial role of substituents (including Wiberg bond orders), and contributed to the writing, editing, and revision of the final manuscript.

7.2 Introduction

While complex molecular architectures are usually constructed using key bond-making reactions, destructive reactions, in which key bonds are broken, can also be used to advantage. Here we examine the mechanism and consequences of a particular type of molecular destruction – divergent extended heterolytic fragmentation. Carbon-carbon (C-C), carbon-heteroatom (C-X), and heteroatom-heteroatom (X-Y) heterolytic fragmentation reactions offer methods for synthesizing structural motifs (some found in complex natural products) that might be difficult to synthesize using methods focused on bond formation.[1–7] Despite their continued use in organic synthesis[8–16] and their relevance to reactions occurring in mass spectrometers,[17] the application of heterolytic fragmentations in which multiple σ-bonds are cleaved in synthetic campaigns is limited by putative strict conformational requirements (e.g., an *anti*-periplanar conformation for the bonds that cleave during fragmentation; Scheme 7.1).[4,18] Few theoretical and mechanistic studies[19–23] have provided insight into the physical underpinnings for this class of reaction since the seminal work of Grob.[2] Our aim in this arena is to increase the understanding of underlying mechanistic factors that govern these transformations to facilitate recognition of key patterns associated with fragmentation reactivity and thereby help guide syntheses of compounds whose construction remains a challenge.

Scheme 7.1 General heterolytic fragmentation

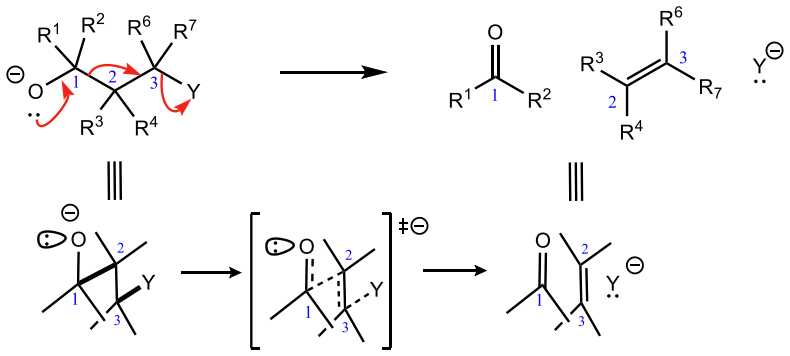

Two types of heterolytic fragmentations that have been reported in the literature but have received little theoretical attention are (1) extended fragmentations – heterolytic fragmentations that involve a chain of more than five atoms – and (2) divergent fragmentations – heterolytic fragmentations that involve the formation of two (or more) distinct products from a single substrate.[4] Extended fragmentations are unsurprisingly rare due to the complexity of orchestrating many bond-breaking events in one transformation.[24] Some experimental examples are shown in Figure 7.1a-b[25–27] Highlighted in bold are the bonds involved in each fragmentation. Here we focus on designing systems where these sorts of cage-supported extended fragmentations can have divergent outcomes (Figure 7.1d; inspired by reaction in Figure 7.1c).

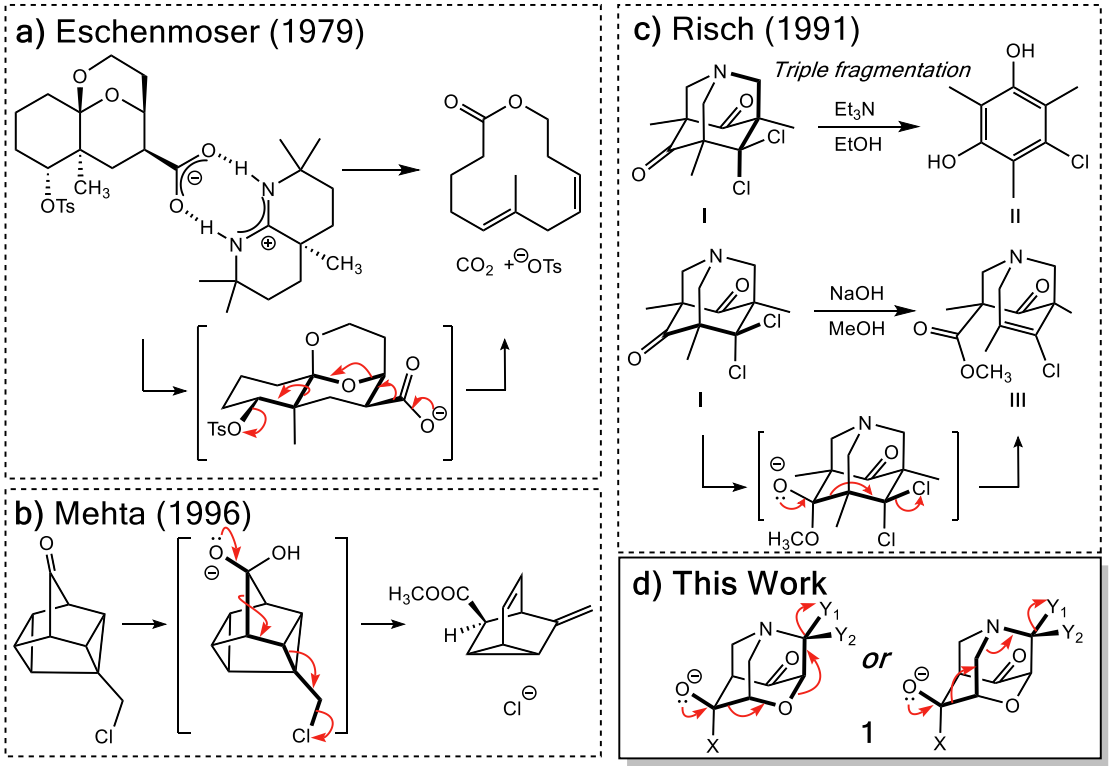

Figure 7.1 Previous extended heterolytic fragmentations.[26-28]

Initially, our objective was to find the length limit for a concerted extended fragmentation, but we encountered unexpected divergent fragmentations en route to this goal; our work on this length limit will be reported elsewhere. Using model systems inspired by experimentally relevant molecules,[27] we show that the outcome of divergent fragmentations can be substituent dependent, is sensitive to external electrostatic environments (i.e., in external electric fields (EEFs)), and can involve unusual potential energy surfaces (PES's) with features such as plateaus and post-transition state bifurcations (PTSBs,[28–33] which make these reactions subject to non-statistical dynamic effects).[34–37] The particular systems we examine (Figure 7.1d) involve divergence *after* the first σ-bond has broken, complicating the issue of where along the fragmentation reaction coordinate product selectivity is determined.

7.3 Methods

All density functional theory (DFT) calculations were carried out using the *Gaussian 09* suite of programs.[38] Transition-state structures (TSSs) and minima were verified as such by frequency calculations. Intrinsic Reaction Coordinate (IRC) calculations were used to further characterize TSSs.[39–41] Eight different functionals were tested against B3LYP-D3(BJ) for Table 7.1, Entry 1 to verify that geometries of TSSs and minima were reasonably consistent among various methods.[*] However, the difference in free energy barriers identified by these functionals ranged over more than 10 kcal mol^{-1}. Thus, B3LYP-D3(BJ) and M06-2X, each with the 6-31G(d) basis set, were tested against each other for entries 1-12 in Table 7.1, since, together, these two functionals covered the range of activation barriers. Employing these two functionals provided a check that

[*] Data from benchmark studies is described in the Supporting Information of *Chem. Sci.* **2020**, *11*, 2231-2242. See Table S1 on p. S3 and discussion thereof.

DFT reasonably captured the qualitative product selectivity trends with which this study is concerned. Employing a larger basis set (that includes diffuse functions), 6-31+G(d), did not change the overall qualitative conclusions, therefore we only report 6-31G(d) results from here on.[*] Quasi-classical *ab initio* direct dynamics simulations for entries 3 and 4 in Table 7.1 were initiated from optimized TSSs using the Progdyn script package provided by Singleton.[42] Trajectories were propagated in time in both the reactant and product directions until they reached product or reactant wells on the PES: trajectories were allowed to propagate until either the C^1–C^2 bond (Scheme 7.2) distance dropped below 1.58 Å, for which we report the trajectory as forming reactant **1**, until the O^3–C^4 bond distance exceeded 3.2 Å and the C^5–Y^1 bond distance exceeded 3.0 Å (while the C^5–Y^1 remained below 5.5 Å), for which we report the trajectory as forming product **A**, or until the C^7–N^6 bond distance exceeded 3.2 Å and the C^5–Y^1 bond distance exceeded 3.0 Å (while the C^5–Y^1 remained below 5.5 Å), for which we report the trajectory as forming product **B**. External Electric Field (EEF) calculations[43] were implemented using the "field" keyword in *Gaussian 09*.[39†] A recent study, in the form of the TITAN code, expands the various types of EEFs that can be generated.[44]

[*] Ibid, S4 (see Table S1-A for data resulting from basis set test).
[†] Ibid, S15. Detailed protocol of how EEF calculations were run are described in section S4 of SI.

7.4 Results and Discussion

7.4.1 Substituent Effects on Product Selectivity

In the course of our search for the length limit in concerted fragmentation, we found inspiration in Risch's 1-aza-adamantane (**I** in Figure 7.1c).[27,45] These 1-aza-adamantane structures have played a significant role in work done by the Castellano group in studying donor-acceptor through-bond interactions for crystal and materials design.[46–48] A simplified model system was designed such that it satisfied the expected structural and stereoelectronic requirements[49] for concerted fragmentation (**1**, Scheme 7.2). We hypothesized that this model system would undergo one of two possible concerted 7-atom fragmentations (red and blue arrows in Scheme 7.2). We successfully found a TSS, **TSS(A)**‡, that connects **1** to a product of extended fragmentation (**A**), where X = OCH_3, Y^1 = Cl and Y^2 = Cl (red arrows, Scheme 7.2).[27*] We also postulated that changing Y^1 to chloroformate (OC(=O)Cl) with Y^2 = H might lead to a TSS that involves a concerted 9-atom fragmentation, given that chloroformate could decarboxylate to form CO_2 and Cl^-, which would break one additional bond (C–Cl). However, following multiple relaxed potential energy surface scans, candidate TSSs only optimized to **TSS(B)**‡ (for breaking the C^7–N^6 bond; blue arrows in Scheme 7.2) instead of **TSS(A)**‡ (for breaking the O^3–C^4 bond), i.e., **TSS(B)**‡ connects **1** to **B**.

[*] Ibid, S35-S54. All IRCs of computed transition state structures can be found in section S8 of the Supporting Information.

Scheme 7.2 Divergent Fragmentation Pathways of **1**.

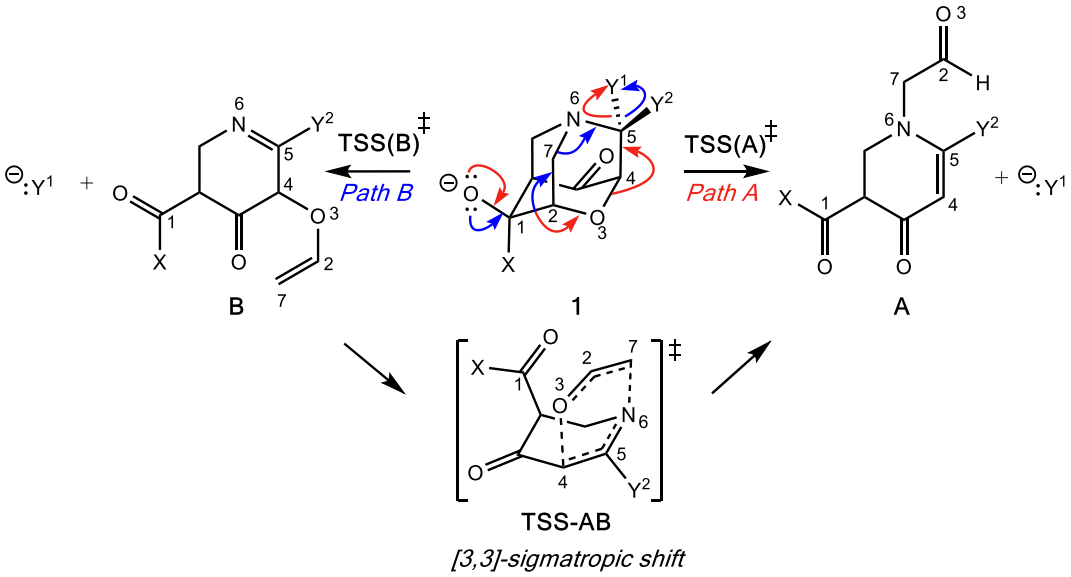

Calculations at the B3LYP-D3(BJ)/6-31G(d) and M06-2X/6-31G(d) levels reveal that the outcome of this divergent fragmentation (**1** can form **A** or **B)** is dependent on substituents X, Y^1 and Y^2 (Table 7.1). For example, changing the leaving group (or nucleofuge[1]), Y^1, from chloroformate (O(CO)Cl) to chlorine (Cl) and Y^2 = hydrogen (H) to chlorine (Cl) switched the energetically preferred fragmentation pathway from Path A to Path B. Additionally, some entries (entries 4, 6, 8, 10, and 12) in Table 7.1 have competing pathways, i.e. we could identify two TSSs on the PES that either lead to products **A** or **B** (products that are kinetically favored are bolded). Attempts to identify competing TSSs for entries including chloroformate at the Y^1 position (odd numbered entries in Table 7.1) proved unfruitful, as **TSS(A)**‡ was the only TSS we could identify. We suspect that different through-space and through-bond electronic effects are the cause of different energetically preferred fragmentation mechanisms—this possibility will be discussed further below.[50–52] Products **A** and **B** can be interconverted by a [3,3]-sigmatropic shift (TSS-AB), but the TSS for this interconversion consistently lies >30 kcal mol^{-1} uphill in free energy relative

to the less thermodynamically stable product.[*] Therefore, the influence of this interconversion on product selectivity is presumably negligible at reasonable experimental temperatures. Products **A** and **B** could be of synthetic utility, although synthesis of **1** presents its own challenges. DFT calculations predicted inconsistent results for entries 3 and 4 (*vide infra*). Worth noting here, too, is the effect of polar solvent on product selectivity when entries 1-12 are modeled in solvent: in all entries at the M06-2X level in an implicit conductor solvent model (CPCM)[53,54] of water, no change in product selectivity was observed; at the B3LYP-D3(BJ) level in the same solvent, entries 2, 6, and 8, switched from B to A as the predicted kinetic product. One of the possible reasons for this inconsistency between DFT methods for these systems when modeled in solvent is that they treat dispersion differently—in this case, solvent results are inconclusive, and we report gas-phase results from here on.

Table 7.1 Substituent Effect on Divergent Fragmentation Pathway. Free energy barriers ($\Delta G^{\ddagger}$) are reported in kcal mol^{-1}.

Entry	**X**	**Y^1**	**Y^2**	**$\Delta G^{\ddagger}_{B3LYP\text{-}D3(BJ)}$, A**	**$\Delta G^{\ddagger}_{M06\text{-}2X}$, A**	**$\Delta G^{\ddagger}_{B3LYP\text{-}D3(BJ)}$, B**	**$\Delta G^{\ddagger}_{M06\text{-}2X}$, B**	**Predicted Kinetic Product(s)**
1	$N(CH_3)_2$	O(CO)Cl	H	**33.8**	**46.9**	-	-	**A**
2	$N(CH_3)_2$	Cl	Cl	-	-	**32.9**	**44.1**	**B**
3	NH_2	O(CO)Cl	H	**28.5**	**39.4**	-	-	**A**
4[a]	NH_2	Cl	Cl	**28.2**	41.5	-	**38.8**	**A** & **B**
5	OCH_3	O(CO)Cl	H	**34.4**	**46.8**	-	-	**A**
6	OCH_3	Cl	Cl	-	48.2	**33.6**	**43.8**	**B**
7	$OCH(CH_3)_2$	O(CO)Cl	H	**36.7**	**47.9**	-	-	**A**

[*] Ibid, S8 (see Figure S1 for representative example of [3,3]-sigmatropic shift).

8	$OCH(CH_3)_2$	Cl	Cl	37.3	51.1	**35.9**	**47.0**	**B**
9	H	O(CO)Cl	H	**35.2**	**47.5**	**-**	**-**	**A**
10	H	Cl	Cl	36.4	49.4	**34.6**	**44.6**	**B**
11	F	O(CO)Cl	H	**38.1**	**50.6**	**-**	**-**	**A**
12	F	Cl	Cl	39.2	52.7	**37.6**	**47.7**	**B**

[a]The TSS computed at B3LYP-D3(BJ) leads to product A only and the TSS computed at M06-2X leads to B by an IRC. A TSS that leads to A at M06-2X was also identified, but it doesn't connect to **1** minimum by an IRC.

The behavior of the system in entry 4 proved to be sensitive to the theoretical method used. M06-2X calculations predict that product **B** formation is kinetically preferred over product **A**, which means that the C^4–O^3 bond stays intact while the other key bonds fragment. A representative plot of bond length changes along the reaction coordinate (Figure 7.2) reveals that this concerted fragmentation reaction is asynchronous: the C^1–C^2 bond cleaves before the C^4–O^3 or C^7–N^6 bonds.[55–57] However, a search for **TSS(B)**‡ at the B3LYP-D3(BJ) level only yielded a TSS connected to product **A**, **TSS(A)**‡; after re-optimizing this **TSS(A)**‡ at the M06-2X level, we identified a product-A-forming TSS that does not directly connect to reactant **1** as a minimum by an IRC. Instead, this **TSS(A)**‡ connected to an enolate structure that is similar to, but lower in energy than, **1**, i.e., a potential precursor to the reactant. Thus, we do not directly compare barriers for two TSS's at the M06-2X level, but we note that **TSS(A)**‡ is 2.7 kcal mol^{-1} higher in energy than is **TSS(B)**‡ if we compare the two TSSs free energies to that of **1**. The peculiarities of the system in entry 4 will be discussed in more detail below.

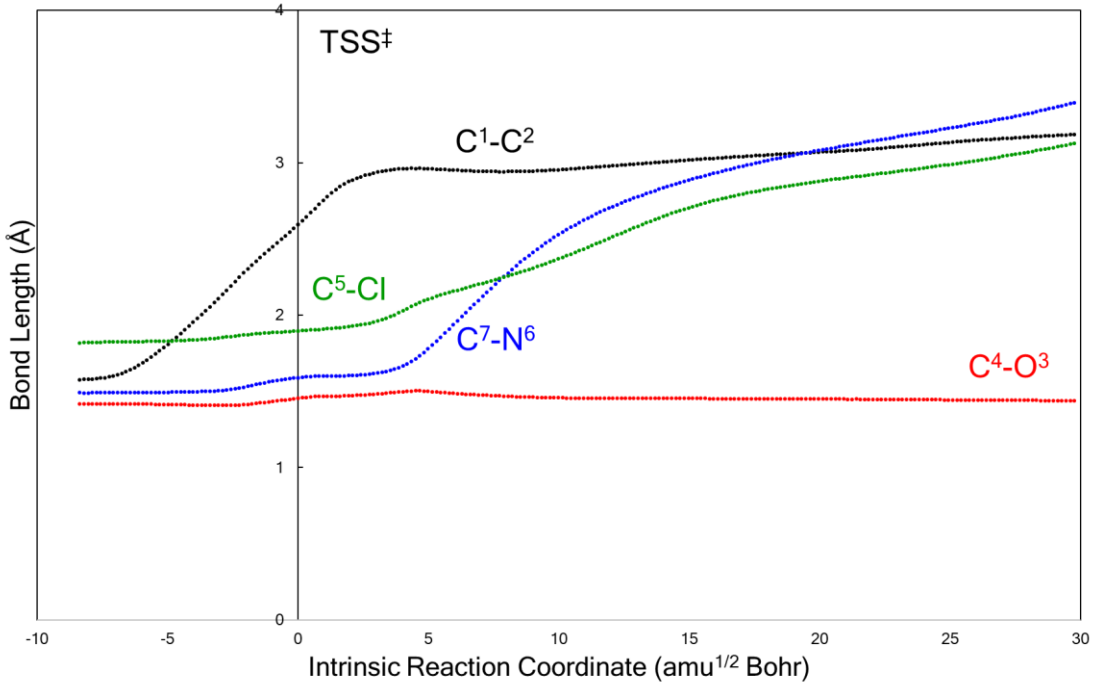

Figure 7.2 A representative example (from entry 4 of Table 7.1, M06-2X/6-31G(d)) of the evolution of key bond lengths involved in the fragmentation as the reaction progresses along the IRC. The transition state structure is at Reaction Coordinate = 0.

7.4.2 Stereoelectronic Effects

Why do different substituents have such a strong influence on which product is favored? We initially hypothesized that what drives the fragmentation towards one product or another is the net sum of stereoelectronic effects within the molecule that would favor breaking either the C^4–O^3 or the N^6–C^7 bond. We postulated that the change of one or two substituents would result in a tip in the delicate balance of donor-acceptor interactions and drive reactivity toward one product versus the other. Alabugin previously discussed fragmentation reactions in the context of donor-acceptor interactions (see "Remote Stereoelectronic Effects", Chapter 8).[49] For example, the concept of double hyperconjugation was introduced to explain the extra stabilization (δ-effect) from substituents in δ-cyclohexyl cations.[58–60] We hypothesized that the geometric restrictions in our 1-

aza-adamantane structure would enforce through-bond, 'double-hyperconjugation-like' communication through the σ-bond framework (Scheme 7.3). However, in our case, strong double hyperconjugation is not present, since the $\sigma_{C1\text{-}C2}$ orbital is not parallel with respect to the $\sigma^*_{C7\text{-}N6}$ and $\sigma^*_{C4\text{-}O3}$ orbitals.

Scheme 7.3 (a) Double hyperconjugation. (b) The $\sigma_{C\text{-}H}$ orbital is parallel with respect to antibonding molecular orbitals ($\sigma^*_{C\text{-}N}$ and $\sigma^*_{C\text{-}O}$) of **1.**

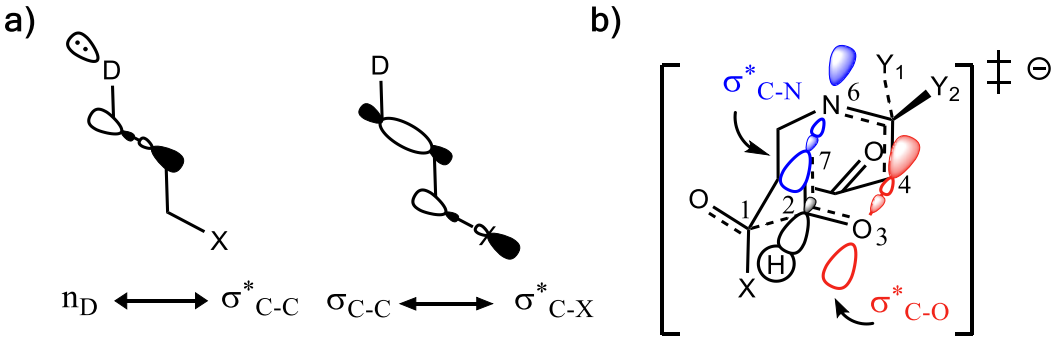

To elucidate the stereoelectronic effects that might lead to a change in product selectivity, we used NBO calculations, a standard approach for quantifying the magnitude of donor-acceptor orbital interactions.[49,61,62] A sum of second-order perturbation energies *E*(2) for TSSs for entries 1, 2 and 4 (Table 7.1), at the M06-2X/6-31G(d) level, are shown in Table 7.2.* The *E*(2) energies are qualitatively consistent with what is observed in the DFT calculations. For instance, the greater donation of electron density into $\sigma^*_{C4\text{-}O3}$ for entry 1 is consistent with formation of product **A**. The opposite is true for entry 2. Entry 4's TSS has a similar amount of donation into the σ* orbitals of both C^4–O^3 and C^7–N^6 bonds, which is consistent with different preferred products at different levels of theory (*vide supra*). It is difficult to assign responsibility to any one donor-acceptor interaction that favors cleavage of either the C^4–O^3 or C^7–N^6 bonds (acceptors), when in fact, it is

* Ibid, S11-S13, for the source of these values and discussion of NBO calculations.

a multitude of donors that donate electron density into these σ^* (acceptor) orbitals. One of the major factors contributing to this challenge is the difficulty delineating inductive and field effects in remote stereoelectronic effects.[49] This is especially prevalent in **1**, which as a cage-supported molecule has many through-bond and through-space interactions.

Table 7.2 *E*(2) values corresponding to the magnitude of donor-acceptor interactions involving σ^* orbitals of C–O and C–N bonds (kcal mol^{-1}; interactions involving all donors are summed).

Entry	$\sigma^*_{C4\text{-}O3}$	$\sigma^*_{C7\text{-}N6}$	**Predicted Kinetic Product(s)**
1	80.9	16.5	**A**
2	16.8	430.3	**B**
4	21.6	29.8	**A** & **B**

The results above are mirrored by computed Wiberg bond indices, or 'bond orders' (BO).[63,64] Wiberg BOs (computed in an NBO calculation) for the C^4–O^3 or C^7–N^6 bonds of the reactants alone are not predictive of which bond will break, consistent with a "dilution" of delocalization between the O^- lone pair and the bonds that will break due to the intermediacy of another σ-bond that must break.* We also computed the change in the Wiberg BO, ΔBO, which gives us insight into the perturbation each bond experiences upon reaching the TSS (Table 7.3). Not surprisingly, for most cases, the product formed can be predicted by which bond has the larger ΔBO (i.e., smaller BO in the fragmentation TSS; Table 7.3). For the system in entry 4 (Table 7.1), the ΔBO values are relatively close, however, precluding a clear prediction (*vide infra*).

* Ibid, S14 (see Tables S3-S4). All range from 0.91-0.94, with only slightly lower BOs for the bond that breaks.

Table 7.3. Wiberg bond order at the TS and bond order change (ΔBO) of the C^4-O^3 and C^7-N^6 bonds that break in forming products **A** and **B**, respectively. Wiberg BOs of reactants are omitted for clarity. Values are computed for M06-2X/6-31G(d) structures. Bold values correspond to products identified by an IRC calculation.

Entry	Wiberg BO, Reactant^{C-O}	Wiberg BO, Reactant^{C-N}	Wiberg BO, TSS^{C-O}	Wiberg BO, TSS^{C-N}	ΔBO^{C-O}	ΔBO^{C-N}	Predicted Kinetic Product(s)
1	0.92	0.95	**0.53**	0.92	**0.39**	0.03	**A**
2	0.92	0.92	0.89	**0.48**	0.03	**0.44**	**B**
3	0.91	0.94	**0.55**	0.92	**0.36**	0.02	**A**
4	0.92	0.93	0.87	0.77	0.04	0.16	**A** & **B**
5	0.92	0.94	**0.49**	0.92	**0.43**	0.02	**A**
6	0.93	0.93	0.89	**0.44**	0.04	**0.49**	**B**
7	0.92	0.94	**0.48**	0.92	**0.44**	0.02	**A**
8	0.92	0.93	0.89	**0.46**	0.03	**0.47**	**B**
9	0.91	0.94	**0.45**	0.93	**0.46**	0.01	**A**
10	0.92	0.93	0.88	**0.40**	0.04	**0.53**	**B**
11	0.92	0.93	**0.51**	0.93	**0.41**	0.00	**A**
12	0.92	0.93	0.88	**0.37**	0.04	**0.56**	**B**

7.4.3 Post-Transition State Bifurcations?

The inconsistency between the B3LYP-D3(BJ) and M06-2X results in entries 3 and 4 in Table 7.1 prompted us to explore the potential energy surfaces for these two systems using *ab initio* molecular dynamics (AIMD) simulations.[32,65–67] Previous work suggests that IRCs obtained with two different theoretical methods that lead to different products despite originating at ostensibly the same TSS could indicate that a PTSB follows this TSS.[68–70] In all dynamics simulations,

trajectories were initiated from the DFT-optimized TSSs and propagated in reactant and product directions until structures were reached that closely resembled minima on the PES (see Methods section for details).[30,32,71–73]

For the system in entry 3 (Table 7.1), downhill trajectories from **TSS(A)**‡ predominantly form **A**, with a small number forming **B** (Figure 7.3) at the M06-2X level. Product **A** can also originate from a shallow carbanion intermediate, **Int**, through **TSS(i)**‡. **Int** is not found on the B3LYP-D3(BJ) PES.[74,75*] Mandal and Datta reported a similarly shaped PES in a gold(I)-catalyzed Diels-Alder reaction with a single intermediate well leading to two different products where the product selectivity is steered by dynamic effects.[76] Trajectories originating from **TSS(i)**‡ also predominantly form **A**, with a slightly larger number forming **B**. Product **A** is thermodynamically favored, which may manifest in lower energy exit channels from both TSSs on the relatively flat energy surface in the vicinity of **TSS(i-A)**‡, **Int** and **TSS(i)**‡. No downhill trajectories from **TSS(A)**‡ result in formation of the imine product (**B**) when using B3LYP-D3(BJ) (Figure 7.3a). While the formation of some product **B** is consistent with the presence of a PTSB, the product distribution for this system is probably better described as arising from molecular motion on a flat energy surface.

* Ibid, S38-S39, for IRCs.

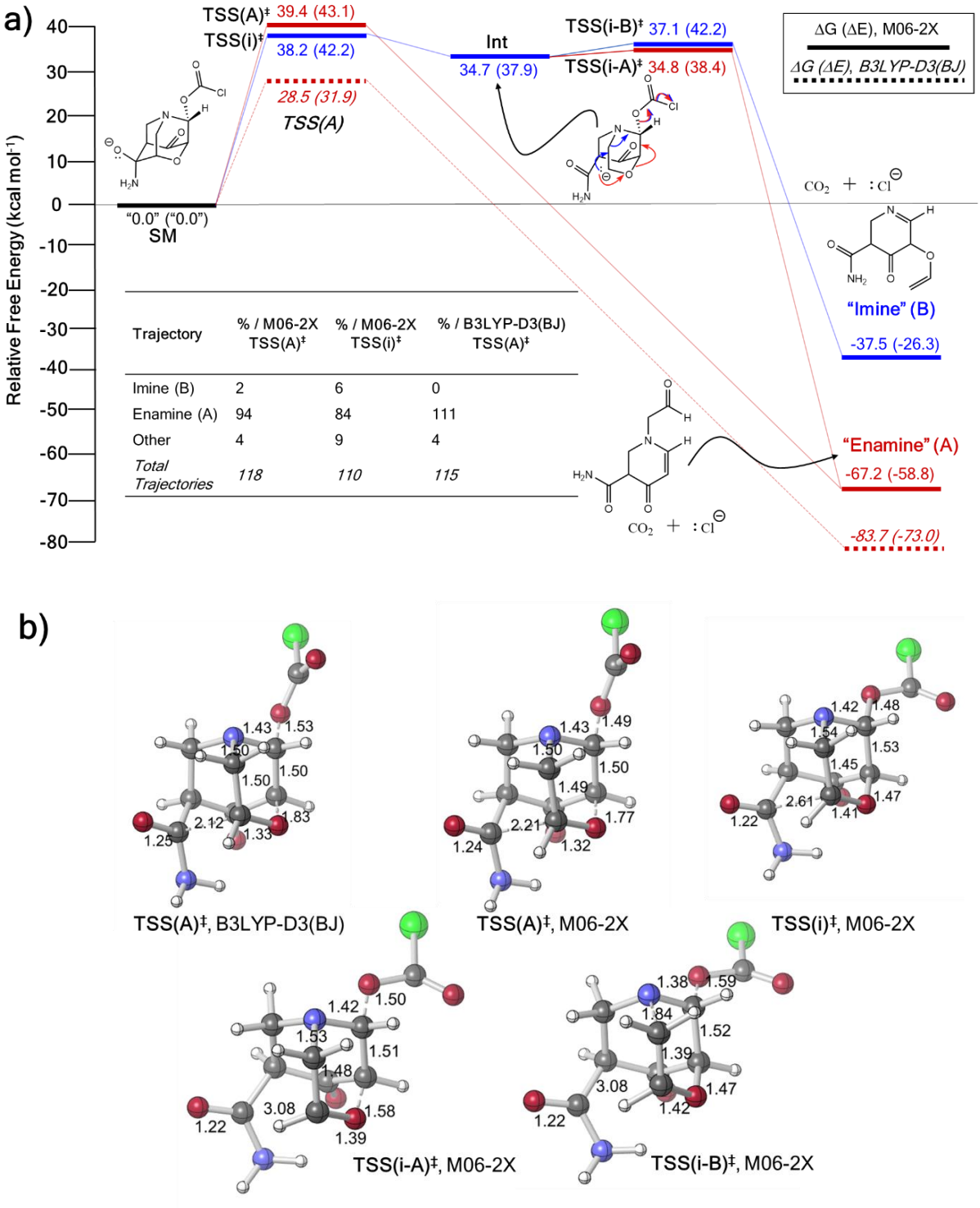

Figure 7.3 (a) Free energy profile (electronic energies in parentheses) and "downhill" dynamics results for entry 3 (Table 7.1). Product distributions from AIMD simulations originate from either **TSS(A)**‡ or **TSS(i)**‡. (b) *CYLview* images[77] of key TSSs on the PES for entry 3. Bond lengths in units of Å.

For the system in entry 4, no intermediate was found at either level of theory (Figure 7.4). Again, product **A** is much more favorable in free energy than product **B**. However, our AIMD calculations predict that products **A** and **B** are produced in comparable amounts using either functional. These results are consistent with a PTSB on the PES and non-statistical dynamic control of product distribution.[30]

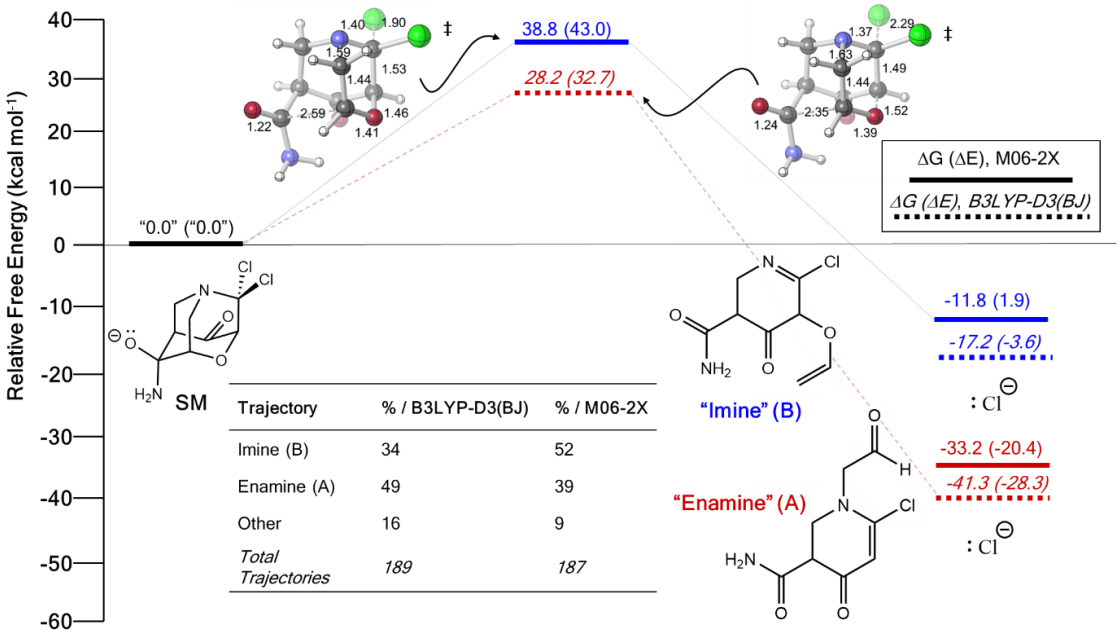

Figure 7.4 Free energy profile (electronic energies in parentheses) and "downhill" dynamics results from B3LYP-D3(BJ) and M06-2X PES's for entry 4 (Table 7.1). Products that are connected by a solid or dotted line to the TSS indicate that they are connected by an IRC to the reactant.

7.4.4 External Electric Fields

Since changing substituents X, Y^1, and Y^2 altered the outcome of divergent fragmentations of **1**, we questioned what might happen under the influence of an external perturbation like an external electric field (EEF). EEFs have recently received considerable attention, being referred to as "smart reagents" for catalysis because of their ability to control reactivity and selectivity.[43,78–80] A

seminal study by Shaik and co-workers demonstrated that not only can an EEF lower or raise the barrier for a Diels-Alder reaction when oriented in one direction or the other along the "reaction axis"—that is, the (approximate) axis along which electrons reorganize to make and break bonds—but an electric field oriented perpendicular to the reaction axis can induce *endo*/*exo* selectivity.[81] The potential for EEFs to control chemical transformations has captured the curiosity of many groups[82–90] since Coote and co-workers experimentally demonstrated electrostatic catalysis of a Diels-Alder reaction in 2016.[91] For example, a recent experimental study demonstrated EEF-induced selective catalysis in a two-step reaction.[92]

Effects on Reaction Rate

Do electric fields oriented in different directions have accelerating/decelerating effects on the rate of fragmentation of **1**? We selected entries 5 and 6 (Table 7.1) for our case studies because these entries are structurally similar, except for the identity of Y^1 and Y^2. To start any EEF study, the field's orientation must be carefully defined (see SI).[43] Figure 7.5 depicts the axis orientations employed here for EEF calculations and the effect of varying EEFs on the free energy barrier.[*] These results indicate that orienting the electric field down the "reaction-axis" (z) leads to an approximately linear change in activation barrier, which is consistent with what is known so far of EEF effects on reactivity.[43] Orienting an electric field in other directions has a weaker effect, as expected.[93]

[*] Ibid, S13. See Figure S6 and Figure S9 in the SI for representative examples of similar results with different axis orientations.

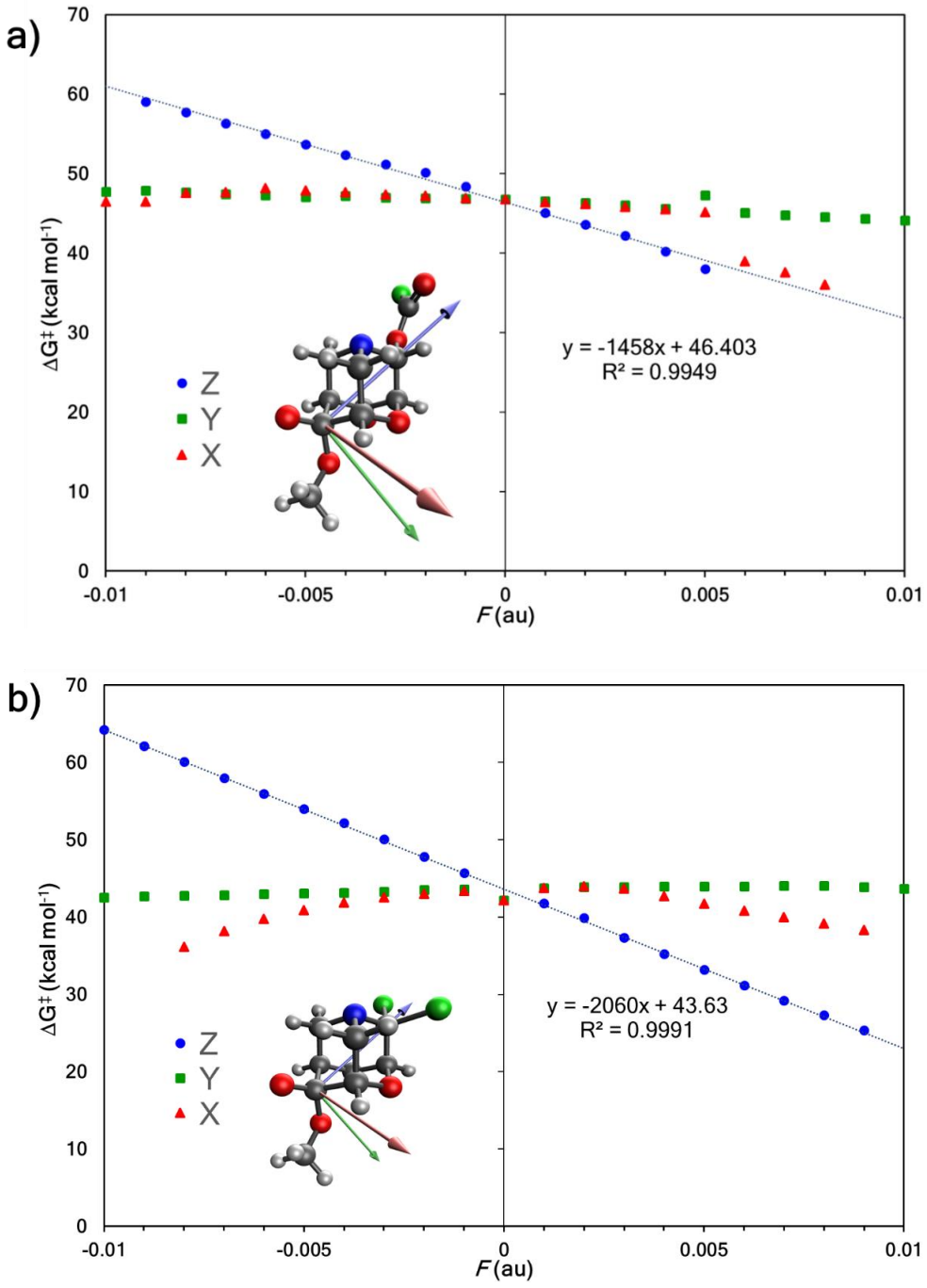

Figure 7.5 (a) External electric field effects on divergent fragmentation of **1** (entry 5, TSS for formation of **A** from Table 7.1). The high green data point at F_y = +0.005 results from a change in the reactant structure geometry in the presence of an EEF.[*] (b) Effects on divergent fragmentation of **1** (entry 6, TSS for formation of **B** from Table 7.1).

Effects on Product Selectivity—Divergent Outcomes from a Single Reactant

[*] Ibid, S9. Reactant structures optimized in EEFs of $F_y \geq 0.005$ au result in a structure shown in Figure S3.

How is product selectivity impacted in divergent heterolytic fragmentations in the presence of an EEF? To test this idea, we turned to a previous study that examined a simpler divergent fragmentation using both experiment and theory. While examining a C–C bond fragmentation approach to synthesize allenes (Figure 7.6), Williams and co-workers observed that both alkyne and allene products were formed initially, in a >20:1 ratio.[93] Over time, they observed that this ratio decreased to 3:1 favoring the allene. Our computed enthalpies and free energies agree qualitatively with their reported computational results and are consistent with experimental observations that initial allene formation is faster than alkyne formation: the predicted $\Delta\Delta G^{\ddagger}$ between **TS-II** and **TS-I** is 2.6 kcal mol^{-1} with B3LYP-D3(BJ) and 1.9 kcal mol^{-1} with M06-2X.[*] We envisioned that, since EEFs have a rate accelerating/decelerating effect, they also may have the ability to induce product selectivity in divergent fragmentations.

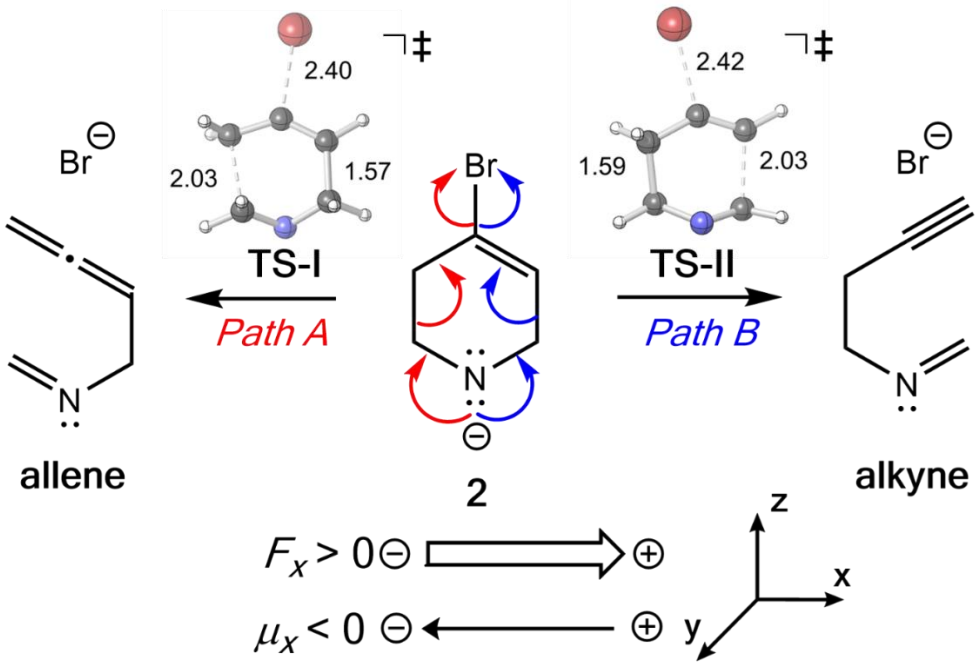

Figure 7.6 Fragmentation reaction of Williams and co-workers examined in the presence of EEFs. M06-2X/6-31G(d) optimized **TS-I** and **TS-II** are shown with key bond lengths in Å.

[*] Ibid, S21 (see Table S5).

The directional flow of electrons (or "reaction axis"[43]) in this system is assumed to point from the N atom to the Br atom down the +z axis (Figure 7.6). We postulated that, perpendicular to that axis, along the ±x axis, electron flow would be polarized to favor either Path A or Path B, i.e., one of **TS-I** and **TS-II** would be selectively stabilized while the other would be destabilized. This prediction is borne out in our computations (Figure 7.7). With a field of magnitude 0.004 au oriented in the –x direction, the free energy barriers for formation of the allene and alkyne are predicted to be equal, but different products are favored at higher or lower field strengths, i.e., there exists a mechanistic crossover point somewhere along the EEF spectrum. While the crossover point might occur at a different field strength with a different level of theory, this example serves as a proof-of-concept that one might be able to selectively produce either product of a divergent fragmentation with an appropriately oriented electric field.

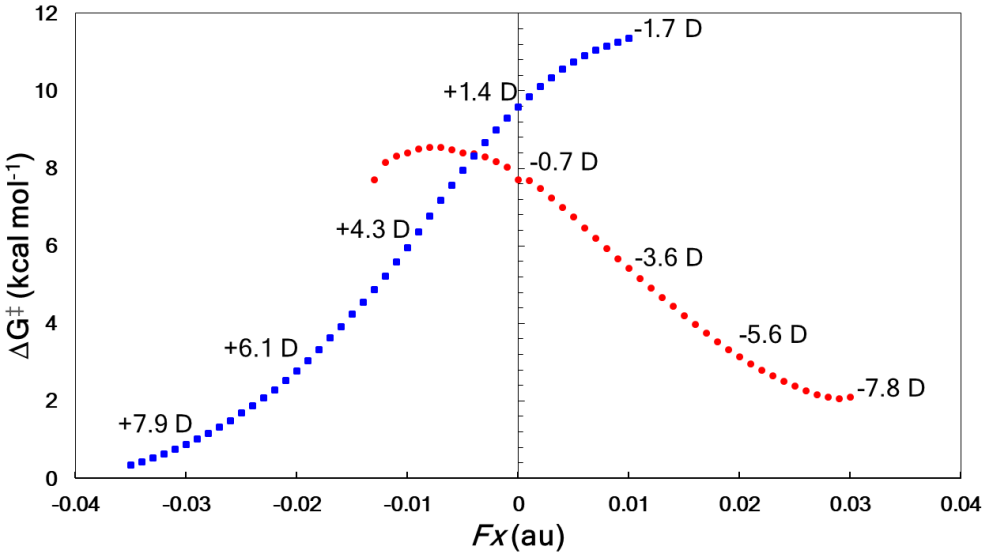

Figure 7.7 EEF effects on divergent fragmentation of **2**, examined using M06-2X/6-31G(d)). The x component of the molecular dipole moment (μ_x in Debye) is shown at each hundredth of an atomic unit (au) representing the magnitude of the electric field oriented in the in the ±x direction. Red circles correspond to Path A in Figure 7.6 and blue squares correspond to Path B. At points where the trendline falls off, we find that either the reactant structure and/or the TSS are not stationary points on the PES.

Do EEF's have a similar product selectivity effect on the fragmentation of **1**? To answer this question, we selected entries 6 and 10 (from Table 7.1) for our case studies because these entries each have two TSSs—one leading to product **A** (**TSS(A)**‡) and one leading to product **B** (**TSS(B)**‡). In both cases, product **B** is kinetically preferred in the absence of an EEF (with both B3LYP-D3(BJ) and M06-2X). The results of the EEF calculations in Figure 7.5 indicate that the z axis induces the most significant change to the free energy barrier. We hypothesized that an EEF along the ±z axis might have a significant (de)stabilizing effect on the free energy barriers, enough to switch product selectivity. Figure 7.8 displays the results of the calculations. Both **TSS(A)**‡ and **TSS(B)**‡ experience a linear change in the free energy barrier, however, only the barrier for formation of **B** is lowered in the presence of positive z ($+F_z$) fields. Attempts to optimize **TSS(A)**‡ in the presence of EEFs of $+F_z > 0.001$ au for entry 6 and $+F_z > 0.003$ for entry 10 led to **TSS(B)**‡. This result suggests that fields oriented in that direction might completely shut down the pathway to form product **A.** We note that we also carried out a test calculation, in which an EEF is oriented along the ±x and ±y axes, to test for switches in product selectivity, but observed no crossing of the free energy barriers for **TSS(A)**‡ and **TSS(B)**‡.[*] This means that there is no switch in selectivity for the divergent fragmentation of **1** in the presence of EEFs oriented in the x or y directions within the -0.01 au to +0.01 au magnitude range.[94] Nevertheless, as EEFs in the $-F_z$ direction increase in magnitude, the $\Delta\Delta G^{\ddagger}$ between **TSS(A)**‡ and **TSS(B)**‡ decreases (making the path to form A more competitive), and at some field, the selectivity switches. This, in principle, means that EEFs oriented down the ±z axis can alter product selectivity.

[*] Ibid, S17-S18 (see Figures S7 and S8).

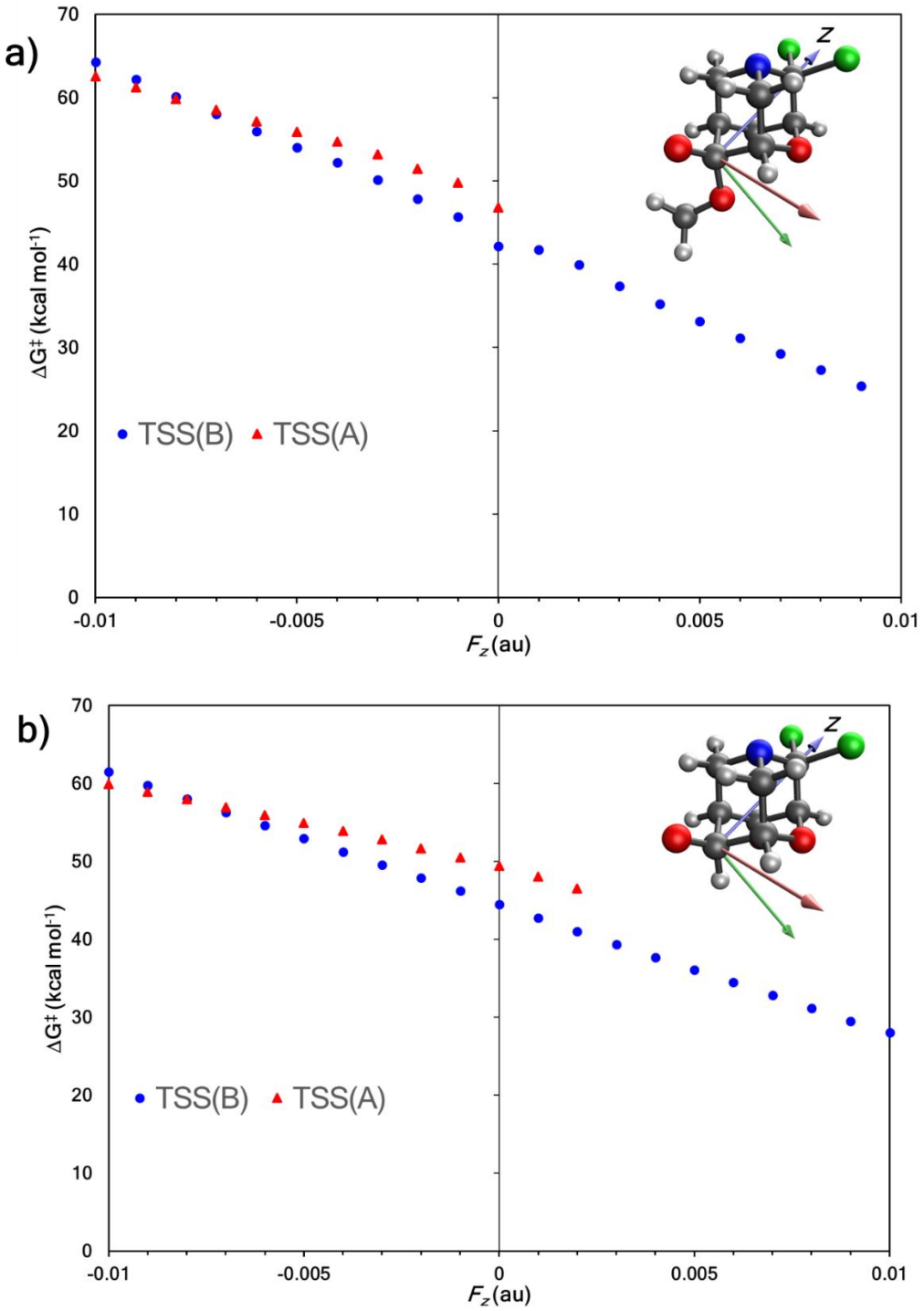

Figure 7.8 (a) External electric field effects ($\pm F_z$) on divergent fragmentation of **1** (entry 6, TSSs for formation of **A** and **B** from Table 7.1). (b) Effects on divergent fragmentation of **1** (entry 10, TSSs for formation of **A** and **B** from Table 7.1).

7.5 Conclusions

Since the 1950s, with the identification and categorization of fragmentations as a class of organic reaction by Eschenmoser[94] and its further development by Grob (with "…glaring disregard of the earlier contributions"[3]),[1-2] the heterolytic fragmentation has become a useful tool in organic synthesis. Nonetheless, we believe that additional interesting chemistry remains to be discovered in this area. In this study, we have expanded the concept of heterolytic fragmentation by exploring a model fragmentation in which a single substrate can fragment via two distinct pathways to different products after an initial σ-bond cleavage – a divergent extended fragmentation.[4] We demonstrated that substituents, electrostatic environment and dynamic effects can influence pathways to competing products. Direct dynamics simulations on some systems reveal flat regions of energy surfaces where selectivity is determined and yet another unexpected PTSB in a reaction of a complex organic molecule.[33] Finally, EEF calculations suggest that divergent pathways can, in principle, be selected between if an electric field is oriented appropriately.[*]

7.6 Acknowledgements

This work was inspired in part by a competition between the groups of DJT and Roald Hoffmann

[*] Altogether, these EEF results may have implications for fragmentation reactions that occur in a variety of environments, for example, in the active sites of enzymes or in solvent in a synthetic laboratory. It is important to recognize that our EEF analysis suffers from some limitations: (1) electric fields are not always homogenous EEFs, (for example in enzymes) and (2) gas-phase quantum calculations can only elucidate EEF effects on static electronic structure and energies of stationary points on our potential energy surface. Perhaps in solution, other significant effects, such as solvent effects, might induce other phenomena that cannot be modeled here. Solvent– solute dynamic effects modeled by explicit solvent were not considered in this study, but it has been discussed recently that local electric field effects due to explicit solvent molecules can alter the PES of the Claisen rearrangement of cis-2-vinylcyclopropanecarboxaldehyde, changing the concerted mechanism into a stepwise one (*J. Phys. Chem. Lett.* **2019**, *10*, 2991–2997). However, as a proof-of-concept, we have demonstrated that electrostatic effects have significant impacts on fragmentation reaction barriers. These conclusions lead to interesting questions on the effect of EEFs and more generally, local electrostatic environment, on dynamic effects such as dynamic matching and PTSBs. Work in our group is currently being carried out to answer these questions.

(Cornell) to find the limit for combining substitution events into concerted processes. Financial and computational (XSEDE) support from NSF is gratefully acknowledged.

7.7 References

(1) Grob, C. A.; Schiess, P. W. Heterolytic Fragmentation. A Class of Organic Reactions. *Angew. Chem. Int. Ed.* **1967**, *6*, 1–106.
(2) Grob, C. A. Mechanisms and Stereochemistry of Heterolytic Fragmentation. *Angew. Chem. Int. Ed.* **1969**, *8*, 535–546.
(3) Prantz, K.; Mulzer, J. Synthetic Applications of the Carbonyl Generating Grob Fragmentation. *Chem. Rev.* **2010**, *110*, 3741–3766.
(4) Drahl, M. A.; Manpadi, M.; Williams, L. J. C-C Fragmentation: Origins and Recent Applications. *Angew. Chem. Int. Ed.* **2013**, *52*, 11222–11251.
(5) Weyerstahl, P.; Marschall, H. Fragmentation Reactions. In *Comprehensive Organic Synthesis*; 1991; pp 1041–1070.
(6) Hoang, T. T.; Dudley, G. B.; Williams, L. J. Fragmentation Reactions. In *Comprehensive Organic Synthesis: Second Edition*; Elsevier Ltd., 2014; Vol. 6, pp 842–860.
(7) Yang, J.; Hoang, T. T.; Dudley, G. B. Alkynogenic Fragmentation. *Org. Chem. Front.* **2019**, *6*, 2560–2569.
(8) Corey, E. J.; Mitra, R. B.; Uda, H. Total Synthesis of d,l -Caryophyllene and d,l -Isocaryophyllene. *J. Am. Chem. Soc.* **1964**, *86*, 485–492.
(9) Hoang, T. T.; Birepinte, M.; Kramer, N. J.; Dudley, G. B. Six-Step Synthesis of Alcyopterosin A, a Bioactive Illudalane Sesquiterpene with a Gem -Dimethylcyclopentane Ring. *Org. Lett.* **2016**, *18*, 3470–3473.
(10) Uteuliyev, M. M.; Nguyen, T. T.; Coltart, D. M. Diastereoselective Addition of Grignard Reagents to α-Epoxy N-Sulfonyl Hydrazones. *Nat. Chem.* **2015**, *7*, 1024–1027.
(11) Shi, J.; Xu, H.; Qiu, D.; He, J.; Li, Y. Selective Aryne Formation via Grob Fragmentation from the [2+2] Cycloadducts of 3-Triflyloxyarynes. *J. Am. Chem. Soc.* **2016**, *139*, 623–626.
(12) Rastelli, E. J.; Bolinger, A. A.; Coltart, D. M. Stereodivergent Synthesis of β,γ-Fused Bicyclic γ-Lactones via a Multicomponent Ring-Expansion Cascade. *Chem* **2018**, *4*, 2228–2238.
(13) Donald, J. R.; Unsworth, W. P. Ring-Expansion Reactions in the Synthesis of Macrocycles and Medium-Sized Rings. *Chem. Eur. J.* **2017**, *23*, 8780–8799.
(14) Cao, L.; Wang, C.; Wipf, P. Grob-Type Fragmentation Releases Paracyclophane Ring Strain in a Late-Stage Precursor of Haouamine A. *Org. Lett.* **2019**, *21*, 1538–1541.
(15) Ma, B.; Zhao, Y.; He, C.; Ding, H. Total Synthesis of an Atropisomer of the Schisandra Triterpenoid Schiglautone A. *Angew. Chem. Int. Ed.* **2018**, *57*, 15567–15571.
(16) Gu, Q.; Wang, X.; Sun, B.; Lin, G. Grob-Fragmentation-Enabled Approach to Clavulactone Analogues. *Org. Lett.* **2019**, *21*, 5082–5085.
(17) Demarque, D. P.; Crotti, A. E. M.; Vessecchi, R.; Lopes, J. L. C.; Lopes, N. P. Fragmentation Reactions Using Electrospray Ionization Mass Spectrometry: An Important

Tool for the Structural Elucidation and Characterization of Synthetic and Natural Products. *Nat. Prod. Rep.* **2016**, *33*, 432–455.
(18) Wilson, R. M.; Danishefsky, S. J. Pattern Recognition in Retrosynthetic Analysis: Snapshots in Total Synthesis. *J. Org. Chem.* **2007**, *72*, 4293–4305.
(19) Davis, R. L.; Leverett, C. A.; Romo, D.; Tantillo, D. J. Switching between Concerted and Stepwise Mechanisms for Dyotropic Rearrangements of β-Lactones Leading to Spirocyclic, Bridged γ-Butyrolactones. *J. Org. Chem.* **2011**, *76*, 7167–7174.
(20) Andrés, J.; Queralt, J. J.; Safont, V. S.; Canle L, M.; Santaballa, J. A. Unimolecular Decomposition of the Anionic Form of N -Chloro-α-Glycine. A Theoretical Study. *J. Phys. Chem.* **1996**, *100*, 3561–3568.
(21) Queralt, J. J.; Safont, V. S.; Moliner, V.; Andrés, J. A Theoretical Study of the Unimolecular Decomposition of N-Chloro-α-Amino Acids in Aqueous Solution. *Chem. Phys.* **1998**, *229*, 125–136.
(22) LeBlanc, L. M.; Powers, S. W.; Grossert, J. S.; White, R. L. Competing Fragmentation Processes of β-Substituted Propanoate Ions upon Collision-Induced Dissociation. *Rapid Commun. Mass Spectrom.* **2016**, *30*, 2133–2144.
(23) Batsomboon, P.; Gold, B.; Alabugin, I.; Dudley, G. Tandem Nucleophilic Addition/Fragmentation of Vinylogous Acyl Nonaflates for the Synthesis of Functionalized Alkynes, with New Mechanistic Insight. *Synthesis* **2012**, *44*, 1818–1824.
(24) Castiñeira Reis, M.; López, C. S.; Nieto Faza, O.; Tantillo, D. J. Pushing the Limits of Concertedness. A Waltz of Wandering Carbocations. *Chem. Sci.* **2019**, *10*, 2159–2170.
(25) Mehta, G.; Ravikrishna, C. Base Catalyzed Pentacyclo[4.3.0.02,4.03,8.05,7]Nonan-9-One (Norsnoutanone) → Tricyclo[3.2.1.02,7]Octane Transformation: A Higher Order Fragmentation? *Tetrahedron Lett.* **1996**, *37*, 2655–2658.
(26) Sternbach, D.; Jaisli, F.; Bonetti, M.; Eschenmoser, A.; Shibuya, M. A Fragmentational Approach to Macrolides: (5-E, 8-Z)-6-Methyl-5,8-Undecadien-11-Olide. *Angew. Chem. Int. Ed.* **1979**, *18*, 634–636.
(27) Risch, N.; Langhals, M.; Hohberg, T. Triple (Grob) Fragmentation. Retro-Mannich Reactions of 1-Aza-Adamantane Derivatives. *Tetrahedron Lett.* **1991**, *32*, 4465–4468.
(28) Ess, D. H.; Wheeler, S. E.; Iafe, R. G.; Xu, L.; Çelebi-Ölçüm, N.; Houk, K. N. Bifurcations on Potential Energy Surfaces of Organic Reactions. *Angew. Chem. Int. Ed.* **2008**, *47*, 7592–7601.
(29) Rehbein, J.; Carpenter, B. K. Do We Fully Understand What Controls Chemical Selectivity? *Phys. Chem. Chem. Phys.* **2011**, *13*, 20906.
(30) Hare, S. R.; Tantillo, D. J. Dynamic Behavior of Rearranging Carbocations - Implications for Terpene Biosynthesis. *Beilstein J. Org. Chem.* **2016**, *12*, 377–390.
(31) Hare, S. R.; Tantillo, D. J. Post-Transition State Bifurcations Gain Momentum-Current State of the Field. *Pure Appl. Chem.* **2017**, *89*, 679–698.
(32) Yang, Z.; Houk, K. N. The Dynamics of Chemical Reactions: Atomistic Visualizations of Organic Reactions, and Homage to van 't Hoff. *Chem. Eur. J.* **2018**, *24*, 3916–3924.
(33) Mandal, N.; Datta, A. Dynamical Effects along the Bifurcation Pathway Control Semibullvalene Formation in Deazetization Reactions. *J. Phys. Chem. B* **2018**, *122*, 1239–1244.
(34) Carpenter, B. K. Dynamic Behavior of Organic Reactive Intermediates. *Angew. Chem. Int. Ed.* **1998**, *37*, 3340–3350.
(35) Collins, P.; Carpenter, B. K.; Ezra, G. S.; Wiggins, S. Nonstatistical Dynamics on

Potentials Exhibiting Reaction Path Bifurcations and Valley-Ridge Inflection Points. *J. Chem. Phys.* **2013**, *139*, 154108.
(36) Carpenter, B. K. Energy Disposition in Reactive Intermediates. *Chem. Rev.* **2013**, *113*, 7265–7286.
(37) Tantillo, D. J. *Dynamic Effects on Organic Reactions*; Reedijk, J., Ed.; Elsevier Inc.: Waltham, MA, 2018.
(38) Frisch, M. J.; Trucks, G. W.; Schlegel, H. B.; Scuseria, G. E. .; Robb, G. E.; Cheeseman, J. R.; Scalmani, G.; Barone, V.; Mennucci, B. .; Petersson, G. A.; Nakatsuji, H.; Caricato, M.; Li, X.; Hratchian, H. P. .; Izmaylov, A. F.; Bloino, J.; Zheng, G.; Sonnenberg, J. L.; Hada, M. .; Ehara, M.; Toyota, K.; Fukuda, R.; Hasegawa, J.; Ishida, M.; Nakajima, T. .; Honda, Y.; Kitao, O.; Nakai, H.; Vreven, T.; Montgomery, Jr., J. A. . P.; J. E.; Ogliaro, F.; Bearpark, M.; Heyd, J. J.; Brothers, E. . K.; K. N.; Staroverov, V. N.; Keith, T.; Kobayashi, R.; Normand, J. . R.; K.; Rendell, A.; Burant, J. C.; Iyengar, S. S.; Tomasi, J. . C.; M.; Rega, N.; Millam, J. M.; Klene, M.; Knox, J. E.; Cross, J. B. .; Bakken, V.; Adamo, C.; Jaramillo, J.; Gomperts, R.; Stratmann, R. E.; Yazyev O.; Austin, A. J.; Cammi, R.; Pomelli, C.; Ochterski, J. W.; Martin R. L.; Morokuma, K.; Zakrzewski, V. G.; Voth, G. A.; Salvador, P.; Dannenberg, J. J.; Dapprich, S.; Daniels, A. D.; Farkas O.; Foresman, J. B.; Ortiz, J. V.; Cioslowski, J.; Fox, D. J. *Gaussian 09*, Revision D.01. *Gaussian Inc.* Wallingford, CT 2009.
(39) Fukui, K. The Path of Chemical Reactions -- The IRC Approach. *Acc. Chem. Res.* **1981**, *14*, 363–368.
(40) Gonzalez, C.; Schlegel, H. B. Reaction Path Following In Mass-Weighted Internal Coordinates Cartesians and with Internal Coordinates without Mass-Weighting. *J. Phys. Chem.* **1990**, *94*, 5523–5527.
(41) Maeda, S.; Harabuchi, Y.; Ono, Y.; Taketsugu, T.; Morokuma, K. Intrinsic Reaction Coordinate: Calculation, Bifurcation, and Automated Search. *Int. J. Quantum Chem.* **2015**, *115*, 258–269.
(42) Singleton, D. A.; Hang, C.; Szymanski, M. J.; Greenwald, E. E. A New Form of Kinetic Isotope Effect. Dynamic Effects on Isotopic Selectivity and Regioselectivity. *J. Am. Chem. Soc.* **2003**, *125*, 1176–1177.
(43) Shaik, S.; Ramanan, R.; Danovich, D.; Mandal, D. Structure and Reactivity/Selectivity Control by Oriented-External Electric Fields. *Chem. Soc. Rev.* **2018**, *47*, 5125–5145.
(44) Stuyver, T.; Huang, J.; Mallick, D.; Danovich, D.; Shaik, S. TITAN: A Code for Modeling and Generating Electric Fields—Features and Applications to Enzymatic Reactivity. *J. Comput. Chem.* **2020**, *41*, 74–82.
(45) Kardel, D.; Knoche, W.; Risch, N. Protonation and Gem-Diol Formation of 1-Azaadamantanones. *J. Chem. Soc. Perkin Trans. 2* **1993**, *2*, 1455–1459.
(46) Lampkins, A. J.; Li, Y.; Al Abbas, A.; Abboud, K. A.; Ghiviriga, I.; Castellano, R. K. Assessable Consequences of Through-Bond Donor-Acceptor Interactions in β-Aminoketones. *Chem. Eur. J.* **2008**, *14*, 1452–1463.
(47) Li, H.; Homan, E. A.; Lampkins, A. J.; Ghiviriga, I.; Castellano, R. K. Synthesis and Self-Assembly of Functionalized Donor−σ−Acceptor Molecules. *Org. Lett.* **2005**, *7*, 443–446.
(48) Yuan, L.; Sumpter, B. G.; Abboud, K. A.; Castellano, R. K. Links between Through-Bond Interactions and Assembly Structure in Simple Piperidones. *New J. Chem.* **2008**, *32*, 1924.
(49) Alabugin, I. V. *Stereoelectronic Effects: A Bridge Between Structure and Reactivity*, 1st ed.; John Wiley & Sons, Ltd: Hoboken, NJ, 2016.

(50) Hoffmann, R. Interaction of Orbitals through Space and through Bonds. *Acc. Chem. Res.* **1971**, *4*, 1–9.
(51) Gleiter, R. Effects of Through-Bond Interaction. *Angew. Chem. Int. Ed.* **1974**, *13*, 696–701.
(52) Paddon-Row, M. N. Some Aspects of Orbital Interactions through Bonds: Physical and Chemical Consequences. *Acc. Chem. Res.* **1982**, *15*, 245–251.
(53) Barone, V.; Cossi, M. Quantum Calculation of Molecular Energies and Energy Gradients in Solution by a Conductor Solvent Model. *J. Phys. Chem. A* **1998**, *102*, 1995–2001.
(54) Cossi, M.; Rega, N.; Scalmani, G.; Barone, V. Energies, Structures, and Electronic Properties of Molecules in Solution with the C-PCM Solvation Model. *J. Comput. Chem.* **2003**, *24* (6), 669–681.
(55) Tantillo, D. J. Recent Excursions to the Borderlands between the Realms of Concerted and Stepwise: Carbocation Cascades in Natural Products Biosynthesis. *J. Phys. Org. Chem.* **2008**, *21*, 561–570.
(56) Williams, A. *Concerted Organic and Bioorganic Mechanisms*, 1st ed.; CRC Press LLC, 2000.
(57) Dewar, M. J. S.; Pierini, A. B. Mechanism of the Diels-Alder Reaction. Studies of the Addition of Maleic Anhydride to Furan and Methylfurans. *J. Am. Chem. Soc.* **1984**, *106*, 203–208.
(58) Adcock, W.; Coope, J.; Shiner, Jr., V. J.; Trout, N. A. Evidence for 2-Fold Hyperconjugation in the Solvolysis of 5-(Trimethylsilyl)- and 5-(Trimethylstannyl)-2-Adamantyl Sulfonates. *J. Org. Chem* **1990**, *55*, 1411–1414.
(59) Lambert, J. B.; Salvador, L. A.; So, J. H. The .Gamma. and .Delta. Effects of Tin. *Organometallics* **2005**, *12*, 697–703.
(60) Alabugin, I. V; Manoharan, M. Effect of Double-Hyperconjugation on the Apparent Donor Ability of σ-Bonds: Insights from the Relative Stability of δ-Substituted Cyclohexyl Cations. *J. Org. Chem.* **2004**, *69*, 9011–9024.
(61) Glendening, E. D.; Landis, C. R.; Weinhold, F. NBO 6.0 : Natural Bond Orbital Analysis Program. *J. Comput. Chem.* **2013**, *34*, 1429–1437.
(62) Weinhold, F.; Landis, C. R.; Glendening, E. D. What Is NBO Analysis and How Is It Useful? *Int. Rev. Phys. Chem.* **2016**, *35*, 399–440.
(63) Wiberg, K. B. Application of the Pople-Santry-Segal CNDO Method to the Cyclopropylcarbinyl and Cyclobutyl Cation and to Bicyclobutane. *Tetrahedron* **1968**, *24*, 1083–1096.
(64) Ortega, D. E.; Gutiérrez-Oliva, S.; Tantillo, D. J.; Toro-Labbé, A. A Detailed Analysis of the Mechanism of a Carbocationic Triple Shift Rearrangement. *Phys. Chem. Chem. Phys.* **2015**, *17*, 9771–9779.
(65) Pratihar, S.; Ma, X.; Homayoon, Z.; Barnes, G. L.; Hase, W. L. Direct Chemical Dynamics Simulations. *J. Am. Chem. Soc.* **2017**, *139*, 3570–3590.
(66) Ma, X.; Hase, W. L. Perspective : Chemical Dynamics Simulations of Non-Statistical Reaction Dynamics. *Philos. Trans. R. Soc. A* **2017**, *375*, 20160204.
(67) Paranjothy, M.; Sun, R.; Zhuang, Y.; Hase, W. L. Direct Chemical Dynamics Simulations: Coupling of Classical and Quasiclassical Trajectories with Electronic Structure Theory. *Wiley Interdisciplinary Reviews: Computational Molecular Science*. 2013, pp 296–316.
(68) Hare, S. R.; Tantillo, D. J. Cryptic Post-Transition State Bifurcations That Reduce the Efficiency of Lactone-Forming Rh-Carbenoid C-H Insertions. *Chem. Sci.* **2017**, *8*, 1442–

1449.
(69) Nouri, D. H.; Tantillo, D. J. Hiscotropic Rearrangements: Hybrids of Electrocyclic and Sigmatropic Reactions. *J. Org. Chem.* **2006**, *71*, 3686–3695.
(70) Hong, Y. J.; Tantillo, D. J. Biosynthetic Consequences of Multiple Sequential Post-Transition-State Bifurcations. *Nat. Chem.* **2014**, *6*, 104–111.
(71) Lourderaj, U.; Park, K.; Hase, W. L. Classical Trajectory Simulations of Post-Transition State Dynamics. *Int. Rev. Phys. Chem.* **2008**, *27*, 361–403.
(72) Carpenter, B. K. NONSTATISTICAL DYNAMICS IN THERMAL REACTIONS OF POLYATOMIC MOLECULES. *Annu. Rev. Phys. Chem.* **2005**, *56*, 57–89.
(73) Lourderaj, U.; Hase, W. L. Theoretical and Computational Studies of Non-RRKM Unimolecular Dynamics. *J. Phys. Chem. A* **2009**, *113*, 2236–2253.
(74) Wodrich, M. D.; Corminboeuf, C.; Schleyer, P. V. R. Systematic Errors in Computed Alkane Energies Using B3LYP and Other Popular DFT Functionals. *Org. Lett.* **2006**, *8*, 3631–3634.
(75) Staroverov, V. N.; Davidson, E. R. Transition Regions in the Cope Rearrangement of 1,5-Hexadiene and Its Cyano Derivatives. *J. Am. Chem. Soc.* **2000**, *122*, 7377–7385.
(76) Mandal, N.; Datta, A. Gold(I)-Catalyzed Intramolecular Diels–Alder Reaction: Evolution of Trappable Intermediates via Asynchronous Transition States. *J. Org. Chem.* **2018**, *83*, 11167–11177.
(77) Legault, C. Y. CYLview, 1.0b. *Université de Sherbrooke*. 2009.
(78) Shaik, S.; Mandal, D.; Ramanan, R. Oriented Electric Fields as Future Smart Reagents in Chemistry. *Nat. Chem.* **2016**, *8*, 1091–1098.
(79) Ciampi, S.; Darwish, N.; Aitken, H. M.; Díez-Pérez, I.; Coote, M. L. Harnessing Electrostatic Catalysis in Single Molecule, Electrochemical and Chemical Systems: A Rapidly Growing Experimental Tool Box. *Chem. Soc. Rev.* **2018**, *47*, 5146–5164.
(80) Stuyver, T.; Danovich, D.; Joy, J.; Shaik, S. External Electric Field Effects on Chemical Structure and Reactivity. *WIREs Comput. Mol. Sci.* **2019**, *e1438*.
(81) Meir, R.; Chen, H.; Lai, W.; Shaik, S. Oriented Electric Fields Accelerate Diels-Alder Reactions and Control the Endo /Exo Selectivity. *ChemPhysChem* **2010**, *11*, 301–310.
(82) Akamatsu, M.; Sakai, N.; Matile, S. Electric-Field-Assisted Anion−π Catalysis. *J. Am. Chem. Soc.* **2017**, *139*, 6558–6561.
(83) Bhattacharyya, K.; Karmakar, S.; Datta, A. External Electric Field Control: Driving the Reactivity of Metal-Free Azide–Alkyne Click Reactions. *Phys. Chem. Chem. Phys.* **2017**, *19*, 22482–22486.
(84) Sun, W.-M.; Li, C.-Y.; Kang, J.; Wu, D.; Li, Y.; Ni, B.-L.; Li, X.-H.; Li, Z.-R. Superatom Compounds under Oriented External Electric Fields: Simultaneously Enhanced Bond Energies and Nonlinear Optical Responses. *J. Phys. Chem. C* **2018**, *122*, 7867–7876.
(85) Dudev, T.; Ilieva, S.; Doudeva, L. How an Electric Field Can Modulate the Metal Ion Selectivity of Protein Binding Sites: Insights from DFT/PCM Calculations. *Phys. Chem. Chem. Phys.* **2018**, *20*, 24633–24640.
(86) Yue, L.; Wang, N.; Zhou, S.; Sun, X.; Schlangen, M.; Schwarz, H. The Electric Field as a "Smart" Ligand in Controlling the Thermal Activation of Methane and Molecular Hydrogen. *Angew. Chem. Int. Ed.* **2018**, *57*, 14635–14639.
(87) Arabi, A. A.; Matta, C. F. Effects of Intense Electric Fields on the Double Proton Transfer in the Watson–Crick Guanine–Cytosine Base Pair. *J. Phys. Chem. B* **2018**, *122*, 8631–8641.

(88) Wang, Z.; Danovich, D.; Ramanan, R.; Shaik, S. Oriented-External Electric Fields Create Absolute Enantioselectivity in Diels-Alder Reactions: The Importance of the Molecular Dipole Moment. *J. Am. Chem. Soc.* **2018**, *140*, 13350–13359.
(89) Zang, Y.; Zou, Q.; Fu, T.; Ng, F.; Fowler, B.; Yang, J.; Li, H.; Steigerwald, M. L.; Nuckolls, C.; Venkataraman, L. Directing Isomerization Reactions of Cumulenes with Electric Fields. *Nat. Commun.* **2019**, *10*, 4482.
(90) Geng, C.; Li, J.; Weiske, T.; Schlangen, M.; Shaik, S.; Schwarz, H. Electrostatic and Charge-Induced Methane Activation by a Concerted Double C–H Bond Insertion. *J. Am. Chem. Soc.* **2017**, *139*, 1684–1689.
(91) Aragonès, A. C.; Haworth, N. L.; Darwish, N.; Ciampi, S.; Bloomfield, N. J.; Wallace, G. G.; Diez-Perez, I.; Coote, M. L. Electrostatic Catalysis of a Diels–Alder Reaction. *Nature* **2016**, *531*, 88–91.
(92) Huang, X.; Tang, C.; Li, J.; Chen, L.-C.; Zheng, J.; Zhang, P.; Le, J.; Li, R.; Li, X.; Liu, J.; et al. Electric Field–Induced Selective Catalysis of Single-Molecule Reaction. *Sci. Adv.* **2019**, *5*, eaaw3072.
(93) Kolakowski, R. V.; Manpadi, M.; Zhang, Y.; Emge, T. J.; Williams, L. J. Allene Synthesis via C−C Fragmentation: Method and Mechanistic Insight. *J. Am. Chem. Soc.* **2009**, *131*, 12910–12911.
(94) Eschenmoser, A.; Frey, A. Über Die Spaltung Des Mesylesters von 2-Methyl-2-oxymethyl-cyclopentanon Mit Basen. *Helv. Chim. Acta* **1952**, *35*, 1660–1666.

Chapter 8

The Role of Through-Bond Stereoelectronic Effects in the Reactivity of 3-Azabicyclo[3.3.1]nonanes*

No stereoelectronic explanation, no matter how firm, can be absolutely, positively confirmed.

- Claire M. Filloux (*Angew. Chem. Int. Ed.* **2015**, *54*, 8887)

8.1 Abstract

Hyperconjugation/conjugation through-bond stereoelectronic effects were studied with density functional theory (DFT) in the context of 3-azabicyclo[3.3.1]nonanes to unravel puzzling differences in reactivity between a vinylogous chloride (**4**) and a vinylogous ester (**5**). These compounds—whose structures differ only by one substituent—were found to display strikingly different reactivities in hydrochloric acid by Risch and co-workers (*J. Am. Chem. Soc.* **1991**, *113*, 9411–9412). Computational analyses of substituent effects, noncovalent interactions, natural bond orbitals, isodesmic reactions, and hydration propensities lead to a model for which the role of remote, through-bond stereoelectronic effects is key to explaining **4** and **5**'s diverging reactivity.

* This chapter is a slightly modified version of the following published article: Laconsay, C. J.; Rho, T. C.; Tantillo, D. J., *J. Org. Chem.* **2022**, *87*, 3378-3388 with permission from the American Chemical Society. Copyright American Chemical Society 2022. Tyler C. Rho helped carry out DFT calculations and contributed to the editing and revision of the final manuscript.

8.2 Introduction

Bond, through-bond.[1] Interactions in chemistry can occur through-space and/or through-bond,[2–4] both of which have been the subject of intense research in theoretical chemistry[2,3] and photoelectron spectroscopy.[5–10] These interactions can affect reactivity/selectivity of molecules because their manifestations are net stabilizing or destabilizing and depend on molecular geometry, hence *stereo*electronic.[11–16] For example, many investigations have been sparked by 1-azaadamantane structures (e.g., Scheme 8.1, **1**) because of its unique, conformationally constrained architecture,[17–19] rich in hyperconjugation.[11,20,21] Additionally, 1-azaadamantanes (and derivatives like 1-azaadamantanones) have been synthesized[22,23] and studied in the past for their tendency to undergo Grob fragmentations,[24] for their intramolecular through-bond[16] and charge transfer interactions,[25] and for measuring electron spin distribution through a σ-skeleton by ^{13}C contact shifts in NMR studies.[26] We developed an interest in 1-azaadamantanone structures (e.g., **1**, Scheme 8.1) and their 3-azabicyclo[3.3.1]nonane fragmentation products (e.g., **4** and **5**, Scheme 8.1) for their visually appealing[27] and unusual structures, which hold functional groups of varying nucleophilicity and electrophilicity in particular orientations. 3-Azabicyclo[3.3.1]nonanes[28] are of interest for their pharmaceutical applications[29,30] and use in molecular recognition chemistry.[31,32] The 3-azabicyclo[3.3.1]nonane architecture also arises in *Aristotelia* alkaloid natural products (e.g., hobartine and aristoquinoline).[33,34]

Scheme 8.1 Unusual reorganization of 3-azabicyclo[3.3.1]nonanes through heterolytic fragmentation.

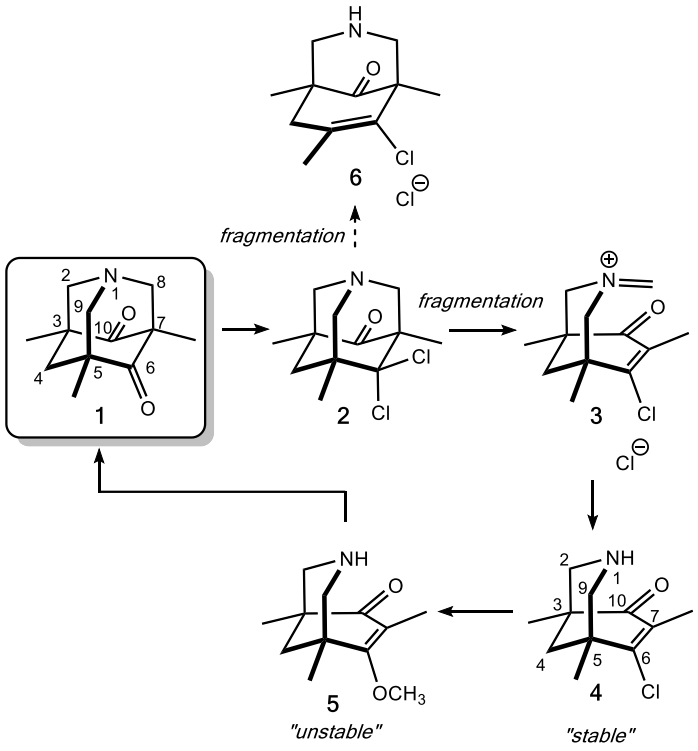

Heterolytic fragmentation reactions (e.g., **2** → **3**) can be useful strategic tools in organic synthesis.[35–41] When applied successfully, fragmentation reactions can effect ring-expansion[42,43]—see, for example, the total synthesis of vinigrol.[44] Examples in which fragmentation reactions have been useful continue to emerge in the literature (e.g., in bioorthogonal self-immolative linkers)[45] and we suspect their utility will only continue to expand. Nevertheless, sparse mechanistic information hinders their broad use. Somewhat cryptic aspects of fragmentations that computational chemistry is uniquely positioned to address include: (1) directing competing divergent mechanisms to control product outcomes,[46] (2) connection between the atom-length of a fragmentation and its concertedness, and (3) tendencies of particular groups to sequentially fragment (in stepwise or concerted but asynchronous pathways).[24] Basic research[47] into simple theoretical model systems that investigate the roles of stereoelectronic interactions in

fragmentations, and intermediates/products born out of them, would therefore be valuable for future investigations of heterolytic fragmentations. To this aim, we consider here through-bond effects in a 3-azabicyclo[3.3.1]nonane product borne out of a fragmentation reaction[48]—orbital effects that could have promoted its formation and that influence its fate.

Compound **1**, reported by Risch's group, piqued our interest because it was reported that **1** fragments to a "stable" intermediate, **4**.[48] Here, stable refers to *kinetic* stability (as opposed to *thermodynamic* stability) with respect to hydrolysis. Specifically, diketone **1** yields **2** when refluxed in thionyl chloride. Molecule **2** then fragments to a 3-azabicyclo[3.3.1]nonane derivative, **4**, upon workup [(1) aqueous ammonia, 25%; (2) methanol/NaOH; (3) concentrated hydrochloric acid].[48] An alternative fragmentation of **2** could generate β,γ-unsaturated ketone **6**, but the authors do not observe **6**. Our calculations are consistent with this result: fragmentation to **6** is kinetically and thermodynamically less favorable than fragmentation to **3** ($\Delta G^{\ddagger}$ = 24.3 kcal mol^{-1}, ΔG = 16.4 kcal mol^{-1} to **6** versus $\Delta G^{\ddagger}$ = 22.2 kcal mol^{-1}, ΔG = 10.2 kcal mol^{-1} to **3**.)* Notably, treatment of **4** with CH_3O^- was reported to give structure **5**, which "immediately reacts with hydrochloric acid at room temperature"[48] to form **1**, presumably via initial hydrolysis to the vinylogous acid.

8.2.1 The Puzzle

Herein, we use density functional theory (DFT) calculations to investigate why **5**, and not **4**, react in acid. While **4** is a vinylogous chloride, **5** is a vinylogous ester. Why **4** and **5** would react so differently in acid is not obviously clear, especially since one would expect an acid chloride to be more susceptible to hydrolysis than an ester. One possible answer is that swapping a chlorine atom

* Data is described in the Supporting Information of *J. Org. Chem.* **2022**, *87*, 3378-3388. See Figure S1.

at C6 in **4** to a methoxy group in **5** results in changes in intramolecular orbital interactions in **4** that are not present, or are of different strengths, in **5**. Here we assess how interactions between the amine and α,β-unsaturated carbonyl substructures influence reactivity, both through-space and through-bond.[49] Our results reveal that the divergent reactivity can be tied to through-bond orbital effects, which are scaffolded by the 1-azaadamantane cage.

8.3 Methods

Density functional theory calculations were carried out using *Gaussian 09*.[50] The Minnesota hybrid functional, M06-2X,[51] was used for geometry optimization and frequency analysis for calculation of Gibbs free energies, as it has been shown to work well for systems involving hyperconjugation and minimizes error associated with extensive electron delocalization.[52,53] A triple-ζ Pople basis set, 6-311+G(d,p), was used with diffuse and polarization functions for all calculations. Intrinsic reaction coordinate (IRC) calculations were carried out to find the minimum energy pathways downhill in energy and each transition state structure's flanking minima.[54–56] To check the robustness of our level of theory, we computed amine proton affinities with B3LYP-D3[57,58] in the gas phase and M06-2X in a polarizable continuum (PCM)[59] solvation model and compared the results to that in Figure 8.2 (*vide infra*). The data gleaned from this case study led to consistent qualitative conclusions across the three levels. Thus, we reasoned that M06-2X/6-311+G(d,p) adequately captures qualitative trends for the systems studied here. All computed structures (including coordinates) can be found on the ioChem-BD repository[60] at the following DOI: https://doi.org/10.19061/iochem-bd-6-120. Energies, file names, and lowest frequencies associated with each structure can also be found in the SI.

Basicities were computed by using the proton transfer equilibrium equation (1) and a formula based on electronic energies (2).[61] Relative basicity values (*B*) obtained from this method establish a reasonable sense of relative basicity for various R-substituted fragmented products (FPs).

$$A + H^+ \rightarrow AH^+ \quad (1)$$

$$B = E(FPH^+ + H_2O) - E(FP + H_3O^+) \quad (2)$$

Noncovalent interaction (NCI) plots[62] were generated using Multiwfn version 3.7 with a medium quality grid.[63] Natural bond orbital (NBO) analysis (version 3.1) was carried out in *Gaussian 09* to obtain second-order perturbation NBO energies.[64,65] Hydration propensities of our substrates were calculated using electronic energies (*E*) in a formula based on thermodynamic data[66]—hydration data may also be determined kinetically[67,68]—with the following equations (3 and 4), where *E* is the non-hydrated species, and E_{hyd} is the hydrated species:

$$\Delta E_{rxn} = E_{hyd} - (E + E_{H_2O}) \quad (3)$$

$$lnK_{hyd} = -(\frac{\Delta E_{rxn}}{RT}) \quad (4)$$

8.4 Results and Discussion

8.4.1 Noncovalent Interactions (NCI) Analysis

Structures **4** and **5** are unique in that the amine and π-system are close enough that a through-space interaction could be relevant between the lone pair of the nitrogen (n_N) and the π-system (i.e., n_N

$\rightarrow \pi^*_{C=C}$ or $n_N \rightarrow \pi^*_{C=O}$) or between the N-H bond and the π-system. If through-space interactions are operative, then a noncovalent interaction (NCI) analysis should reveal any difference in through-space interactions that exist between **4** and **5**. NCI analysis is a useful tool for qualitatively visualizing intra- and intermolecular noncovalent interactions within (or between) molecules.[62] The use of NCI analyses in computational organic chemistry studies has become increasingly important to characterize, visualize, and rationalize the role of weak, noncovalent interactions in mechanistic models.[69–71] Colors in NCI plots indicate the type of interaction: blue indicates strong attraction on one extreme, and red indicates strong repulsion on the other; green lies in the middle of the two extremes and indicates weak interactions (e.g., dispersion interactions). Figure 8.1 shows NCI plots for structures **4** and **5**. The green in each plot indicates that weak interactions exist between the amine and the π-system, but the degree to which it changes from **4** to **5** suggests that through-space effects remain effectively the same in **4** and **5** (analogous results were obtained for the *N*-invertomers of **4** and **5**—**4'** and **5'**—and their *N*-protonated forms; see SI). A through-space interaction argument alone is thus insufficient to explain Risch et al.'s observed diverging kinetic stabilities in acid. Though these plots by themselves do not definitively rule out the existence of strong through-space interactions between the amine and the enone moieties, they weigh against through-space effects having a consequential role in the fate of these structures in acid.

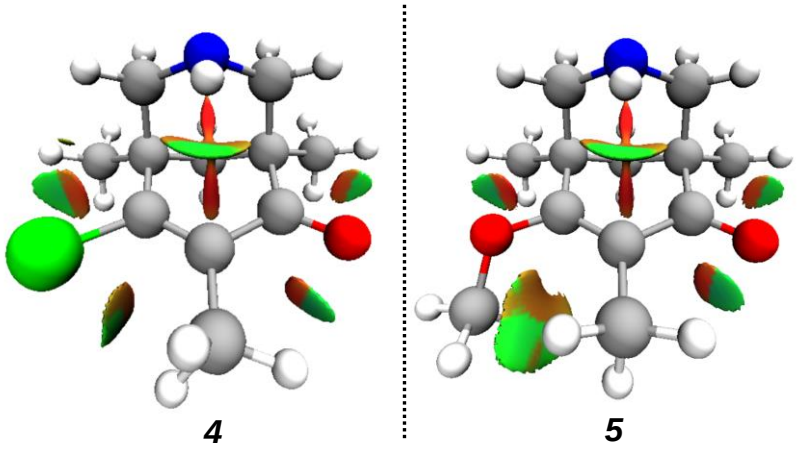

Figure 8.1 NCI index plots (blue, strong attraction; green, weak interaction; red, strong repulsion; isovalue = 0.5) of structures **4** and **5**.

8.4.2 Basicity of Amine and π-system

If, on the other hand, through-bond effects are important for the stabilities in acid of **4** and **5**, we would expect to see a significant difference in computed basicity for the amine, the most basic site of **4** and **5**. The strong basicity of the amine relative to other groups is reflected in our computed basicities: in Figures 8.2a and 8.2b when R = H, the basicities of the amine and ketone are -61.7 and -45.7 kcal mol^{-1}, respectively.

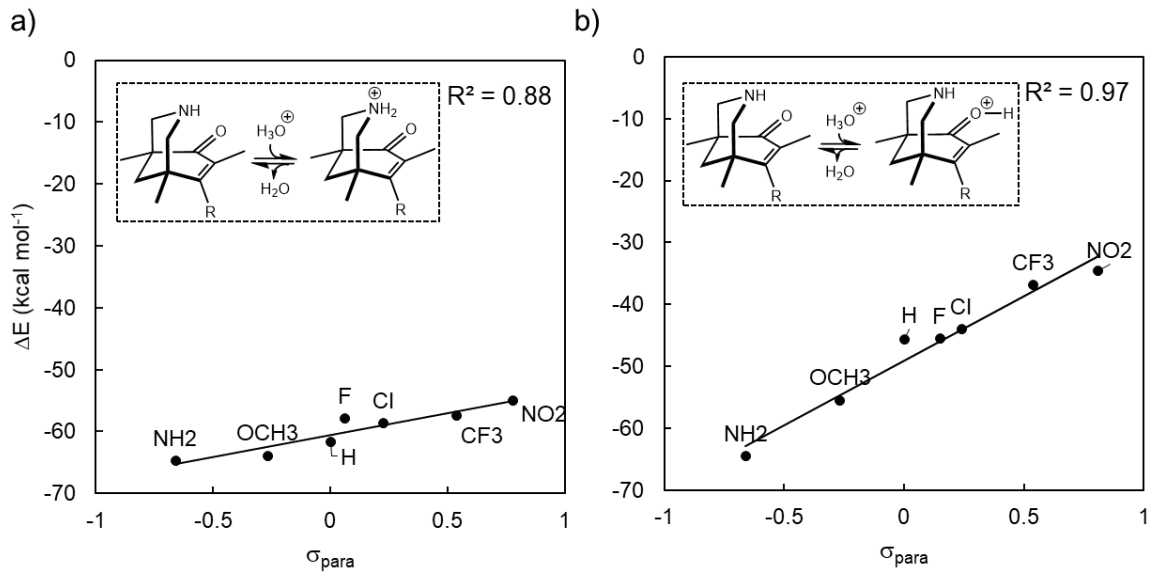

Figure 8.2 Relationship between R substituent σ_{para} constant and (a) basicity of nitrogen (slope = 7.0) and (b) basicity of carbonyl oxygen (slope = 20.8). The energy (ΔE) axis range in both plots is kept consistent for easy comparison.

Both **4** and **5** have local amine functionality and local vinylogous carbonyl derivative functionality. But these local functional groups may communicate with each other by through-bond orbital effects. If this is the case, we would expect to observe changes in amine basicity upon changing the substituent at carbon 6 (C6, Scheme 8.1); it would not be the first time amine basicity is influenced by remote, neighboring functionality.[72,73] Figure 8.2a shows the results of our amine basicity calculations with different C6 substituents plotted against their Hammett σ_{para} constants, which reflect the π electron-donating and -withdrawing ability of R.[74,75] Though the range of basicity (ca. 10 kcal mol^{-1}) for the amine pales in comparison to the range of computed basicity for the ketone (Figure 8.2b, ca. 30 kcal mol^{-1}), the correlation in Figure 8.2a (R^2 = 0.88) with σ_{para} values suggest that the amine lone pair is sensitive to the nature of the R group, an observation consistent with a through-bond interaction. Additionally, the difference in basicity values between

4 and **5**, a $\Delta\Delta E$ = 5.3 kcal mol^{-1}, suggests that a Cl at C6 (**4**) makes the amine notably less basic than when a methoxy group is at C6 (**5**).

The same basicity analysis was applied to the ketone group (Figure 8.2b). Oxygen basicities are highly correlated with the Hammett σ_{para} value (R^2 = 0.97), and more sensitive to R (slope = 20.8 versus slope = 7.0 in Figure 8.2a), as expected. Compound **5** (R = OCH_3) has a greater ketone oxygen basicity than that of **4** (R = Cl): ΔE's = -55.5 kcal mol^{-1} and -44.1 kcal mol^{-1} for **5** and **4**, respectively. The greater basicity of **5** likely contributes to its greater instability in acidic solution by promoting its activation as an electrophile.

One could consider the above discussion of data up until this point being also consistent with a through-space interaction between the R group and the amine group. But, as we argue in subsequent sections, through-space interactions make up only a minor role in comparison. While we acknowledge it is difficult to decouple through-bond and through-space interactions completely, the lack of clear evidence from NCI analysis for through-space interactions, and ample evidence of through-bond interactions, led us to arrive at the considerable role of through-bond interactions in this particular system (*vide infra*).

8.4.3 It Takes Two to Tango—Hyperconjugation/Conjugation Effects

How exactly does changing R influence the basicity of the amine? We surmised based on past literature on 1-azaadamantanones (such as **1**), the precursor to intermediates **4** and **5**, that through-bond interactions may be the major means of modulating amine basicity.[76,77] Despite the nitrogen lone pair being two bonds away from the carbonyl, it still participates in an interaction resembling that of double hyperconjugation or hyperconjugation/conjugation (Scheme 8.2a-f).[78,79] In this particular case, the nitrogen lone pair in 1-azaadamantanones donates electron density into the σ^*

orbital of the adjacent C–C bond, while simultaneously, the σ orbital of the C–C bond donates electron density into the $\pi^*_{C=O}$ (Scheme 8.2e and 8.2f).[80] Both double hyperconjugation (distinct from "two-way" hyperconjugation[81]) and hyperconjugation/conjugation are examples of remote stereoelectronic effects inextricably linked by a mediating single-bond bridge, and ample examples of their effects on organic structure and reactivity are documented.[11,82–86] If intermediates **4** and **5** indeed exhibit through-bond communication between the nitrogen lone pair and the enone substructure, we would expect computed basicities to be sensitive to R's identity, and that is what is observed (Figure 8.2).

Scheme 8.2 Select types of extended hyperconjugation (see ref. 11, Ch. 8 for an in-depth discussion of remote stereoelectronic effects). a) double hyperconjugation, b) hyperconjugation/conjugation, c) negative double hyperconjugation, d-f) negative hyperconjugation/conjugation

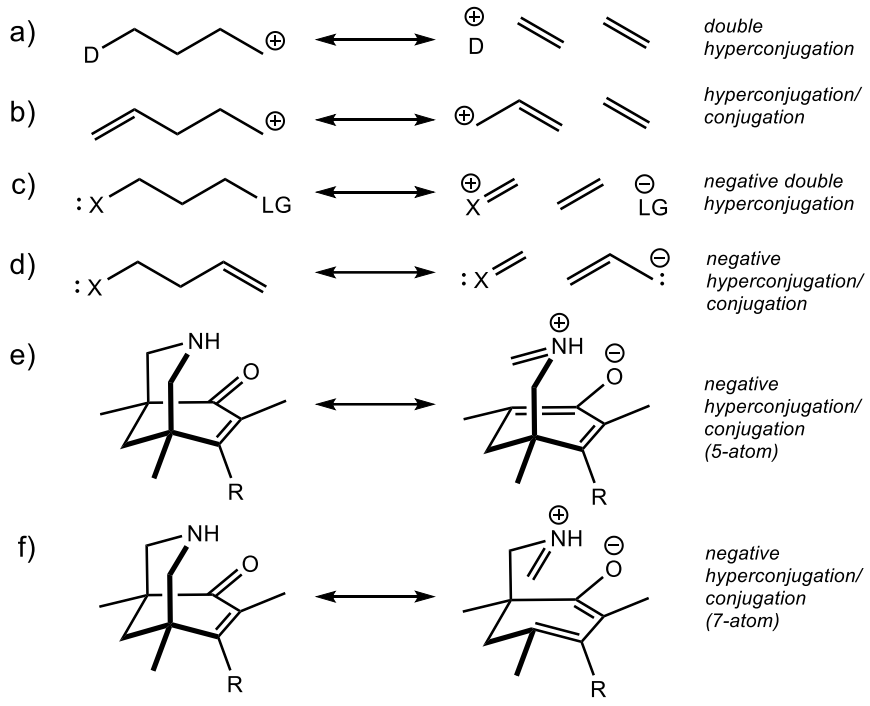

8.4.4 Natural Bond Orbital Analysis

To further explore the possibility of through-bond effects, we computed second-order perturbation NBO energies, an analysis often used to quantify the strength of hyperconjugative donor-acceptor orbital interactions.[20] Second-order perturbation NBO energy (*E*(2), equation 5) analysis measures donor-acceptor electron delocalization that results from filled orbitals interacting with unfilled, antibonding orbitals.[87] In equation (5), n_σ is the population of σ donor orbitals, $F_{i,j}$ is the Fock matrix element between orbitals *i* and *j*, and ε_σ and $\varepsilon_{\sigma*}$ are the energies of σ and σ^* natural bond orbitals (if, for example, one is computing *E*(2) energies between σ and σ^* orbitals).

$$E(2) = -n_\sigma \frac{<\sigma|F|\sigma*>^2}{\varepsilon_{\sigma*} - \varepsilon_\sigma} = -n_\sigma \frac{{F_{i,j}}^2}{\Delta E}. \quad (5)$$

If through-bond effects are relevant to the stability of **4** and **5**, then we would expect to observe qualitative trends in *E*(2) NBO energies. Figure 8.3 plots *E*(2) NBO energies with Hammett σ_{para} values. In the first case (Figure 8.3a), sums of *E*(2) values associated with hyperconjugation from $n_N \rightarrow \sigma^*_{C\text{-}C}$ of both adjacent C–C sigma bonds are plotted against σ_{para} values. A weak correlation ($R^2 = 0.66$) suggests that as the electron-withdrawing ability of the R substituent increases, donation into $\sigma^*_{C\text{-}C}$ antibonding orbitals slightly increases (~1 kcal mol^{-1} increase in *E*(2)). In other words, through-bond communication between the nitrogen lone pair and R is non-negligible. The sum of *E*(2) values corresponding to $n_N \rightarrow \sigma^*_{C\text{-}H}$ hyperconjugation interactions (Figure 8.3b) are slightly better correlated ($R^2 = 0.72$) with respect to σ_{para} values, but smaller in magnitude (at most, 7.1 kcal mol^{-1} when R = NO_2) because $\sigma^*_{C\text{-}H}$ orbitals are worse acceptors, in part, due to their poor orientation for good orbital overlap with respect to the nitrogen lone pair. No correlation between the sum of *E*(2) values corresponding to $\sigma_{C\text{-}C} \rightarrow \pi^*_{C=C}$ and $\sigma_{C\text{-}C}$

$\rightarrow \pi^*_{C=O}$ donor-acceptor interactions and σ_{para} values is observed (Figure 8.3c), To ensure our NBO analyses were reasonable, we checked whether a correlation is observed between the $\pi_{C=C} \rightarrow \pi^*_{C=O}$ donor-acceptor interaction (Figure 8.3d). Indeed, a strong, negative correlation ($R^2 = 0.90$) exists, which is consistent with electron-withdrawing groups weakening a $\pi_{C=C} \rightarrow \pi^*_{C=O}$ interaction.

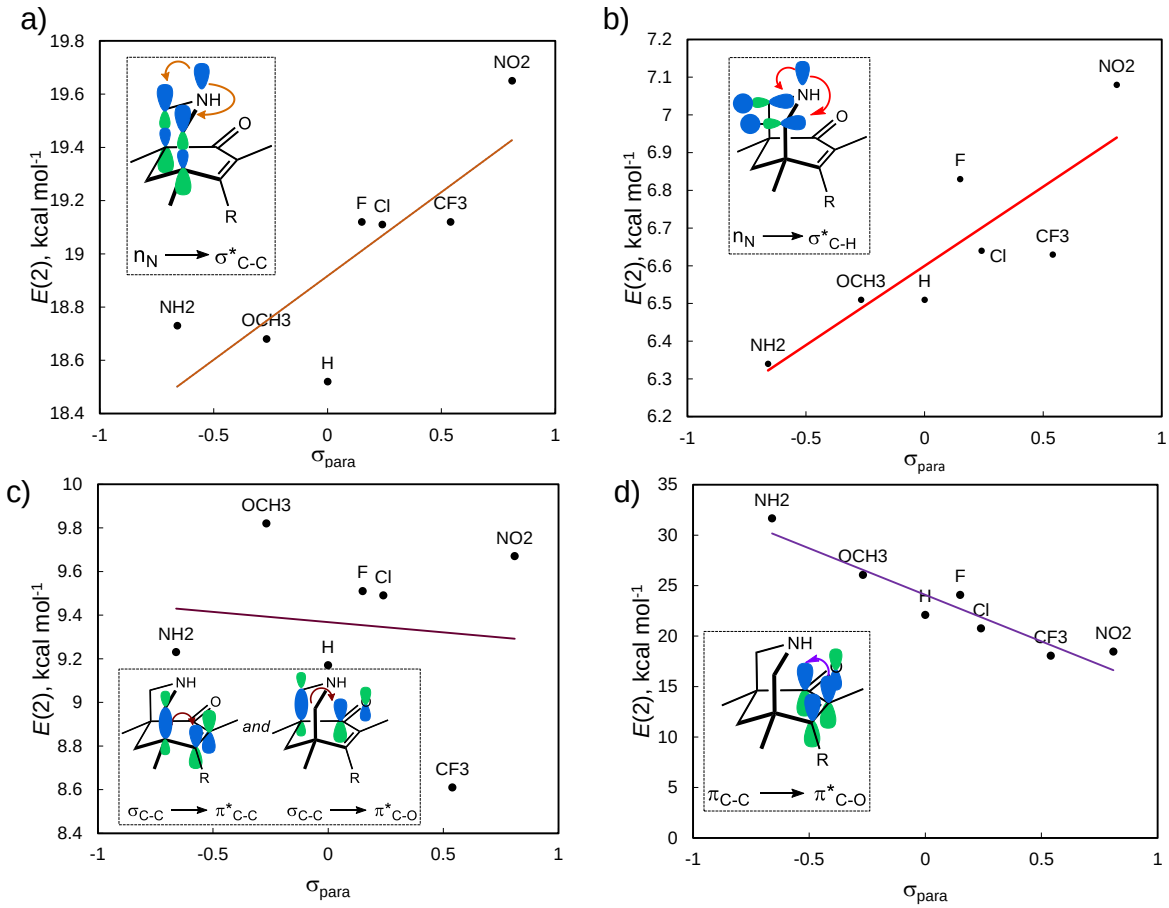

Figure 8.3 Correlations of second-order perturbation NBO energies, *E*(2), and Hammett parameter, σ_{para} (proxy for electron-donating and -withdrawing ability of substituent, R). Shown are correlations of *E*(2) values associated with a) sum of negative hyperconjugation interactions of $n_N \rightarrow \sigma^*_{C-C}$ of adjacent C-C sigma bonds ($R^2 = 0.66$) , b) sum of negative hyperconjugation interactions of $n_N \rightarrow \sigma^*_{C-H}$ of adjacent C-H sigma bonds ($R^2 = 0.72$), c) sum of $\sigma_{C-C} \rightarrow \pi^*_{C=C}$ and $\sigma_{C-C} \rightarrow \pi^*_{C=O}$ interactions ($R^2 = 0.01$), and d) $\pi_{C=C} \rightarrow \pi^*_{C=O}$ interaction ($R^2 = 0.90$).

In Figure 8.3a, we observe a slight correlation with the *sum* of *E*(2) values and π electron-donating and -withdrawing ability, but are the $n_N \rightarrow \sigma^*_{C-C}$ interactions with adjacent C–C σ-bonds

evenly distributed between the two bonds? The range of *E*(2) values in Figure 8.4a for the component associated with the "proximal" donor-acceptor interaction (proximal to the R group) is effectively the same as that in 4b for the "distal" interaction (distal to the R group), ~0.7 kcal/mol, consistent with an evenly delocalized nitrogen lone pair into (seemingly indistinguishable) empty antibonding orbitals. However, we find that there is no correlation ($R^2 = 0.14$) with respect to the proximal $n_N \rightarrow \sigma^*_{C\text{-}C}$ *E*(2) energy (Figure 8.4a) and an excellent correlation ($R^2 = 0.98$) with respect to the distal $n_N \rightarrow \sigma^*_{C\text{-}C}$ *E*(2) energy (Figure 8.4b). The origin of this difference appears to be related to the other partner in the hyperconjugation/conjugation array, i.e., the α,β-unsaturated carbonyl. We observe an unequal distribution of *E*(2) values for donation from C–C bonds into adjacent π^*-antibonding orbitals, with greater *E*(2) values for the distal interaction ($\sigma_{C\text{-}C} \rightarrow \pi^*_{C=O}$, Figure 8.4d) than the proximal interaction ($\sigma_{C\text{-}C} \rightarrow \pi^*_{C=C}$, Figure 8.4c), consistent with $\pi^*_{C=O}$ being a better acceptor than is $\pi^*_{C=C}$. In short, the carbonyl modulates communication between the substituent and the distal C–C bond.

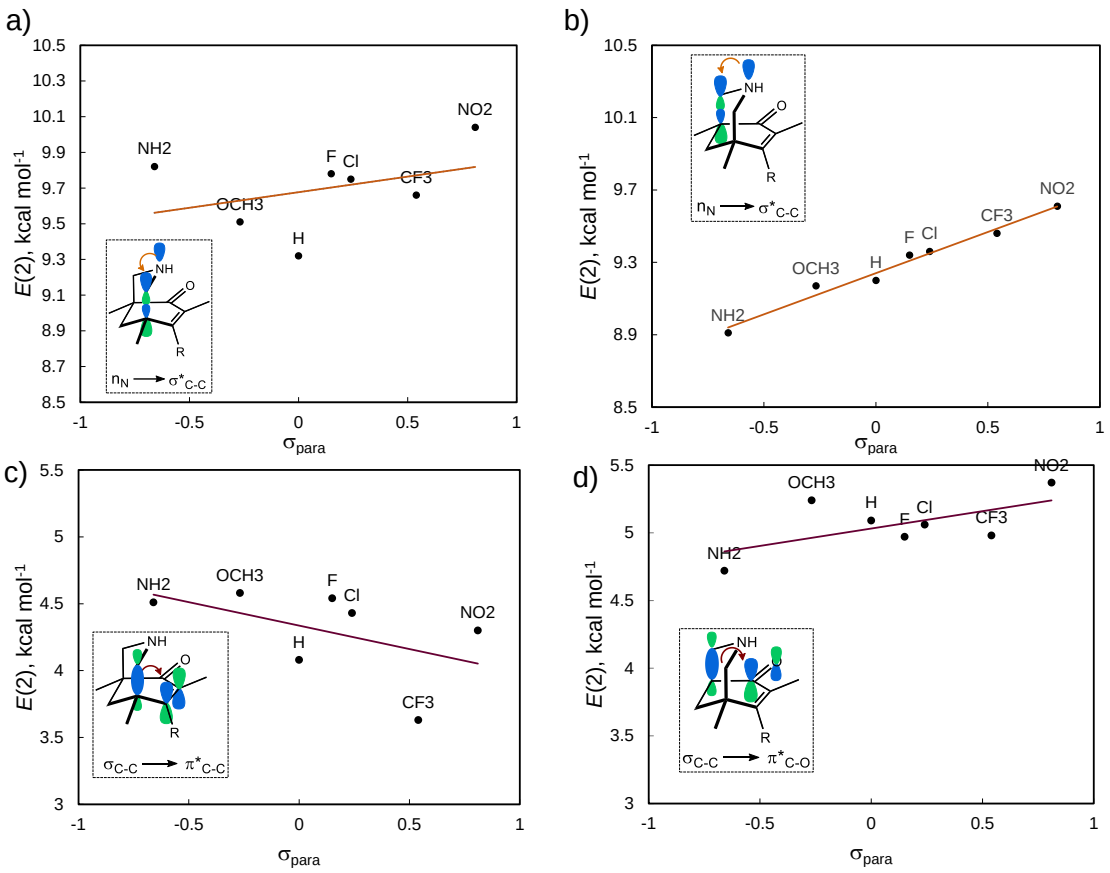

Figure 8.4 Correlations of second-order perturbation NBO energies, *E*(2), and Hammett parameter, σ_{para} (a measure for electron-donating/-withdrawing ability of substituent, R). Shown are correlations of *E*(2) values associated with a) $n_N \rightarrow \sigma^*_{C\text{-}C}$ interaction of proximal C-C sigma bonds ($R^2 = 0.14$), b) $n_N \rightarrow \sigma^*_{C\text{-}C}$ interaction of distal C-C sigma bonds ($R^2 = 0.98$), c) $\sigma_{C\text{-}C} \rightarrow \pi^*_{C=C}$ interaction of proximal C-C sigma bond with $\pi^*_{C=C}$ of enone ($R^2 = 0.25$) and d) $\pi_{C=C} \rightarrow \pi^*_{C=O}$ interaction of distal C-C sigma bond with $\pi^*_{C=O}$ of enone ($R^2 = 0.36$).

8.4.5 Isodesmic Reactions

To isolate key stereoelectronic effects, thermochemical data derived experimentally or computationally are often used in hypothetical reactions (e.g., isogyric, isodesmic, hypohomodesmotic, homodesmotic, hyperhomodesmotic).[88] These reactions can provide useful information for deducing how strong a delocalizing stereoelectronic effect is, but they are challenging to implement in practice because achieving an "ideal" reaction requires careful balancing of changes in bond type, charge, hybridization, and steric effects.[20] Often, changing a

portion of a molecule to probe an effect introduces additional, sometimes undesirable interactions. Figure 8.5, for example, shows simple isodesmic reactions that switch the lone pair position from equatorial to axial (i.e., **4** → **4'** and **5** → **5'**; **4'** and **5'** are examples of concave bases[89]), a transposition that introduces a $\sigma_{N-H} \rightarrow \sigma^*_{C-C}$ interaction at the expense of a $n_N \rightarrow \sigma^*_{C-C}$ interaction—for both **4** and **5**, the reaction is uphill by at least 1 kcal mol^{-1}. Though this hypothetical reaction seems like a reasonable method for acquiring a qualitative measure of the energetic stabilization due to nitrogen lone pair hyperconjugation, by switching the lone pair's position, we also introduce possible through-space effects between the n_N and the π-system (*vide supra*). Like any isodesmic reaction, this one has flaws: the best we can do is asymptotically approach the 'ideal' isodesmic reaction.

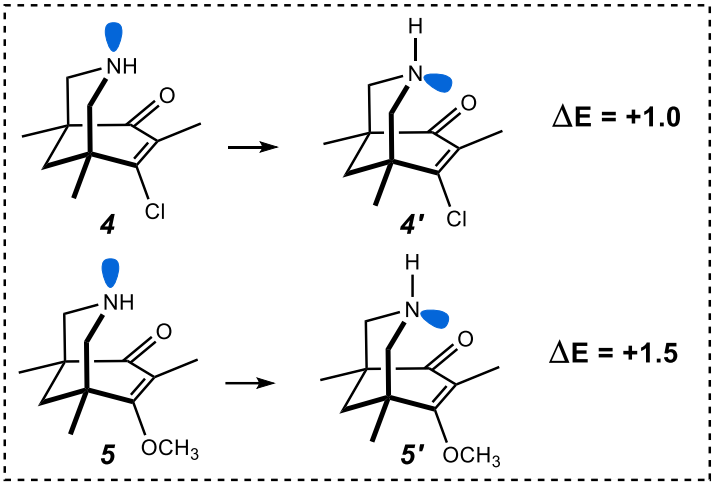

Figure 8.5 Isodesmic reaction. Amine inversion: lone pair from equatorial (**4** and **5**) to axial position (**4'** and **5'**).

The energies from Figure 8.5 reveal that **4'** and **5'** are only 1 to 1.5 kcal mol^{-1} higher in energy than **4** and **5**, respectively, which suggests that we cannot ignore the relevance of this conformation and possible concomitant through-space interactions contributing to the

experimental observation discovered by Risch. However, NCI and NBO analysis on **4'** and **5'** did not provide cogent evidence that through-space effects predominate.[*]

So far, through-*bond* effects appear responsible for **4** and **5**'s kinetic stability in acid, and we have yet to uncover evidence to counter this model. What other isodesmic reactions might we interrogate that would convince us otherwise? Replacing the amine with a methylene (CH_2) group would, in principle, take away any energetic stabilization from the amine lone pair participating in hyperconjugation/conjugation (Figure 8.6a). To keep each side balanced, we added a cyclohexane chair and a piperidine chair on the left and right-hand side, respectively. The ΔE for this reaction is, roughly, a measure of the *difference* between having amine lone pair hyperconjugative stabilization and $\sigma_{C\text{-}H} \rightarrow \sigma^*_{C\text{-}C}$ stabilization from a methylene group, but note that through-space interactions between the π-system and N–H versus C–H bonds are also present (although hopefully not significantly different). Taken together, the reactions shown in Figures 8.5 and 8.6a indicate that the net stabilization energy imparted by $n_N \rightarrow \sigma^*_{C\text{-}C}$ interactions in the context of other intermolecular interactions is likely on the order of 1 kcal mol^{-1} for both **4** and **5**, and slightly more so for the latter.

[*] Ibid, S4 (Figure S3).

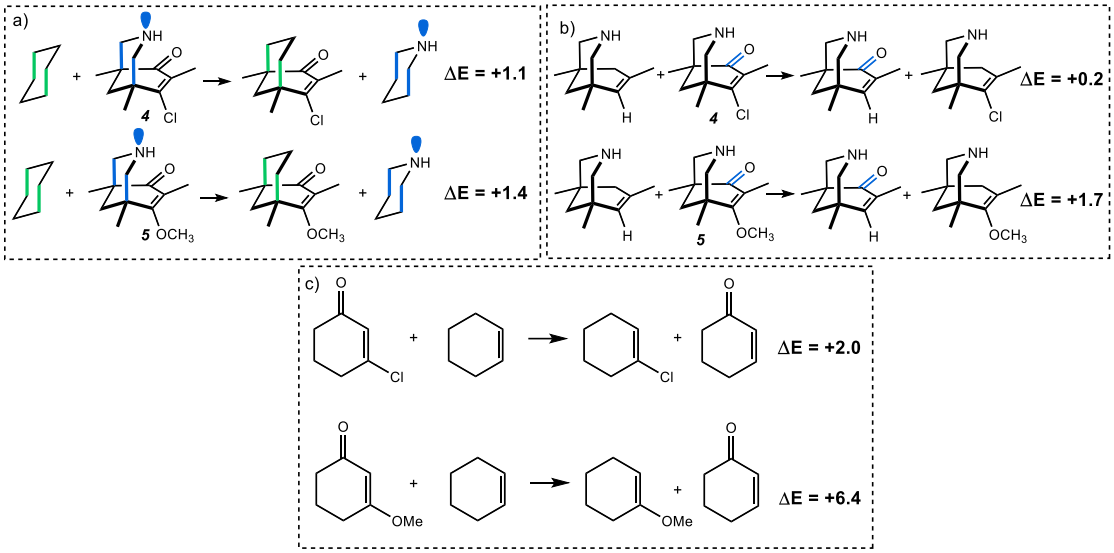

Figure 8.6 Isodesmic reactions. a) Difference in stabilization energy due to amine lone pair versus C-H hyperconjugation into $\sigma^*_{C\text{-}C}$ antibonding orbital for **4** and **5**. b) and c) "Deletion" of ketone functionality.

Is there an isodesmic reaction that measures the stabilization energy associated with the carbonyl group of the enone? Figure 8.6b shows that "deleting" the carbonyl group in **4** costs almost nothing (+0.2 kcal mol^{-1}), while "deleting" the carbonyl group in **5** imposes a 1.7 kcal mol^{-1} energetic penalty, a reasonable reflection of the energetic stabilization due to a donor group at the β position of a carbonyl group. Carbonyl deletion also affects an additional, intertwingled stereoelectronic effect: the so-called 'vinylogous anomeric effect'[11] (VAE, originally named the 'allylic effect'[90]), which results from the in-plane carbonyl oxygen lone pair interacting with the $\sigma^*_{C\text{-}R}$ orbital through the intervening C-C p bond. Contrasting these results to those in Figure 8.6c suggest that the amine in the bicyclic molecule attenuates the cost imposed by ketone "deletion", consistent with the amine reducing the electrophilicity of the carbonyl group via the through-bond interaction described above (here the VAE is still present), i.e., without the amine present, the

communication between the Cl/OCH_3 and the carbonyl group through the intervening π-bond is stronger and the penalty for losing that communication is larger.[*]

8.4.6 A Closer Look—Trends in Basicity and Hydration Propensity

That the ketone oxygen is more basic in **5** than in **4**, and more sensitive to the substituent at the C6 position, is corroborated by the data in Figure 8.2b. This result is not surprising. Changes to amine basicity (Figure 8.2a) were less obvious at the outset, however. Though changes to amine basicity with substituents at the carbonyl β-position are smaller than those to the carbonyl itself, they are substantial (cf. Figure 8.2). As the electron-withdrawing ability of the C6 substituent increases, the amount of through-bond lone pair delocalization increases (approximated with *E*(2) in kcal mol^{-1}), and the amine basicity is curtailed (Figure 8.7).

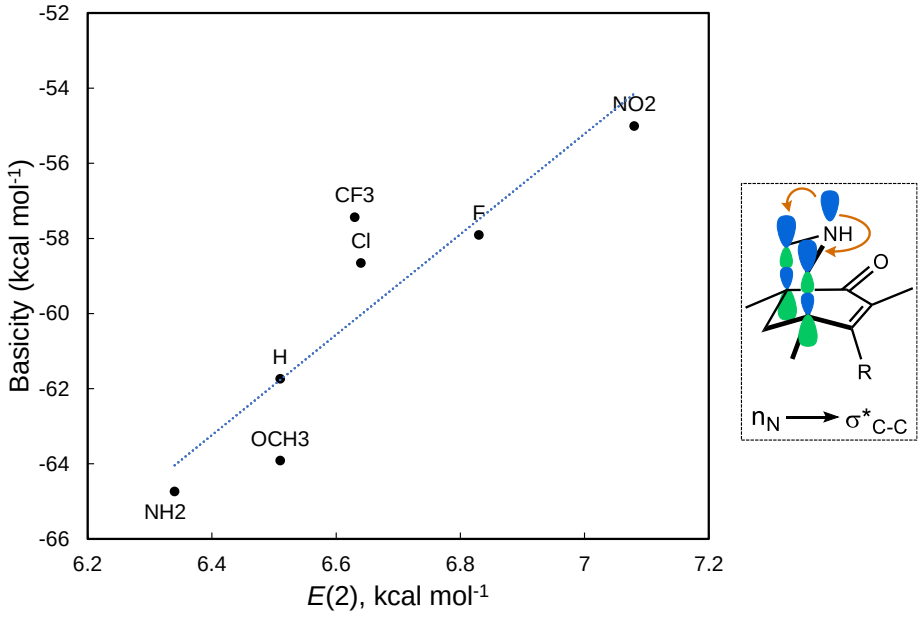

Figure 8.7 Relation of amine basicity to sum of *E*(2) NBO energies from $n_N \rightarrow \sigma^*_{C\text{-}C}$ interaction; $R^2 = 0.80$.

[*] Ibid, S5 (see Figure S4 for additional computed isodesmic reactions).

An increased propensity for carbonyl protonation in **5** versus **4** should lead to increased electrophilicity, more facile attack by water, and more rapid hydrolysis (Scheme 8.3). But might an increased amine basicity have a similar effect? Covalent hydration propensities ($\ln K_{hyd}$) were computed for C6-substituted systems with and without the amine protonated to estimate their reactivity towards water in the hydrolysis from **5** to **6** (Scheme 8.3). The more positive $\ln K_{hyd}$, the greater the equilibrium lies toward the hydrate, suggesting a greater propensity to be attacked by water.

Scheme 8.3 Plausible mechanism from **5** to **1** through hydrolysis and a Mannich reaction.[48]

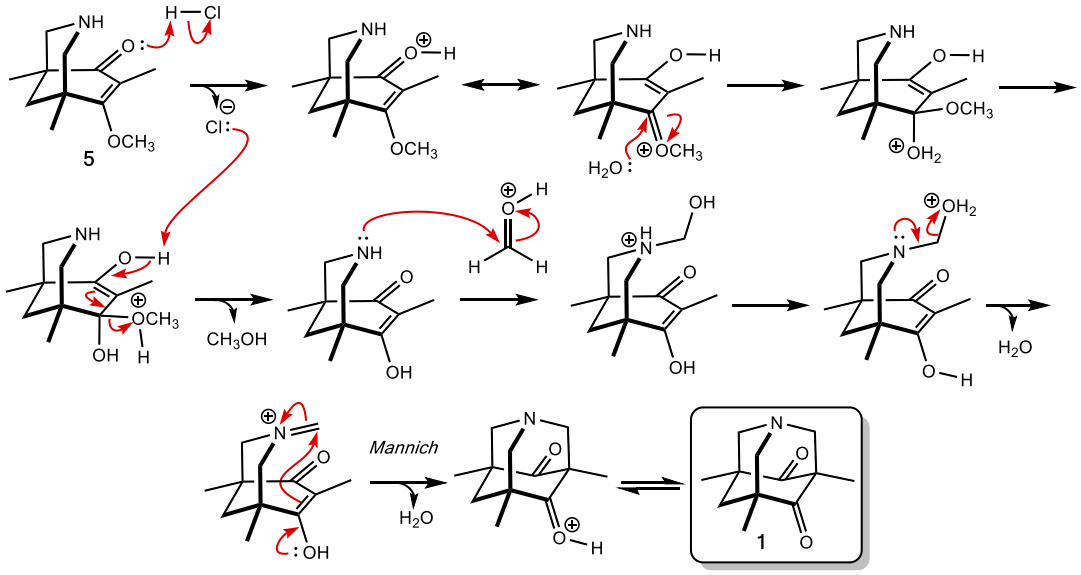

Three hydration sites were considered, for both neutral and *N*-protonated forms of **4** and **5** (a total of six hydration scenarios):* (a) hydration at the carbonyl carbon, (b) hydration at C6 (β-position) resulting from water addition from the "bottom" face (i.e., distal with respect to the amine), and (c) hydration at C6 resulting from water addition from the "top" face (i.e., proximal

* Ibid, S6 (see Figure S5).

with respect to the amine). In all scenarios, *N*-protonated versions showed overall greater hydration propensities than their non-protonated counterparts. Electron-withdrawing groups at C6 also showed greater hydration propensities (e.g., Figure 8.8).*

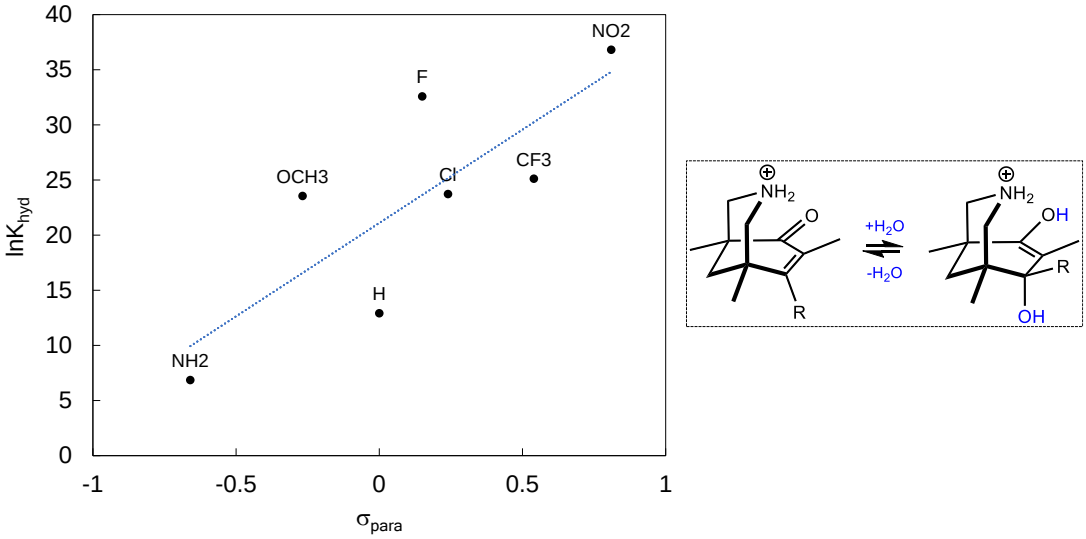

Figure 8.8 Hydration propensities ($\ln K_{hyd}$) increase as electron-withdrawing ability of R increases. The greater $\ln K_{hyd}$ the greater the energetic driving force to be hydrated by H_2O; $R^2 = 0.63$.

For **4** and **5**, whether hydration is favored at the carbonyl carbon or the β-carbon depends on C6 substitution. In the case of **4**, when the amine is protonated, hydration propensities at all possible sites are approximately equal ($\ln K_{hyd} \sim 24$). For **5**, when the amine is protonated, hydration at the β-carbon resulting from "bottom" face attack by water (the face distal with respect to the amine) is most favored ($\ln K_{hyd} = 23.5$). Thus, we proposed a mechanism in Scheme 8.3 wherein water attacks the β-carbon from the "bottom" face ($\ln K_{hyd}$ for "top" face water attack is 17.9). For this hydration scenario, *N*-protonation makes the hydration propensity for **4** ($\ln K_{hyd} = 23.7$) and **5** about equal ($\ln K_{hyd} = 23.5$; Figure 8.8)! An equal susceptibility for water attack such as this is not

* Ibid, S8-S12 (data for other scenarios).

present when the amines of **4** and **5** are not protonated);[*] in fact, in that case, **4** is *more* likely to be hydrated ($\ln K_{hyd}$ = 10.9 for **4** versus 7.2 for **5**). In acid, however, the amines are likely protonated.

These hydration propensity results add yet another explanatory (albeit complex) layer to the mix: that is, despite hydration propensities for **4** and **5** being equal once their amines are protonated, **5**'s amine is *more* basic (Figure 8.7), hence more vulnerable to protonation and subsequent water attack. This result is consistent with the experimental observation that **5** is less kinetically stable under acidic conditions. Though we hesitate to single out any one property responsible for the stability of these molecules, the data is consistent with one overriding message: *through-bond interactions modulate the reactivity of both the amine and enone components of* **4** *and* **5**.

8.5 The Upshot—A Model for Through-Bond Effects in 3-Azabicyclo[3.3.1]nonanes

So, why is **5** unstable in acidic solution and **4** stable? First, it should be emphasized, as was stressed in a recent review article by Alabugin et al.,[52] that "molecular stability always depends on multiple factors. Singling one out of many can be misleading – unless there is a reason." In this study, we singled out particular stereoelectronic interactions to decide if the strengths of these interactions correlated with the π-donating/withdrawing ability of the substituent at C6. While correlation does not equate to causation,[91] and no model based on stereoelectronic interactions can be absolutely confirmed,[92] the data gathered up to this point allow us to suggest a working model rooted in through-bond effects. This model hinges on the reactivity of *both* the more-basic amine nitrogen

[*] Ibid, S10 (see Figure S8).

and the less-basic ketone oxygen, which communicate with each other through intermediary σ-bonds. This study highlights the importance of remote through-bond effects (specifically, negative hyperconjugation/conjugation) in organic reactivity, an area still rich in opportunity for discovery. To not overlook (or underestimate) the importance of such interactions could make the difference between achieving a working model for explaining divergent reactivity of two (or more) molecules and being left in the dark.

8.6 Acknowledgements

Support from the US National Science Foundation (CHE-1856416 and XSEDE) is gratefully acknowledged.

8.7 References

(1) Young, T. *Dr. No*; United Artists: United Kingdom, 1962.
(2) Hoffmann, R. Interaction of Orbitals through Space and through Bonds. *Acc. Chem. Res.* **1971**, *4*, 1–9.
(3) Paddon-Row, M. N. Some Aspects of Orbital Interactions through Bonds: Physical and Chemical Consequences. *Acc. Chem. Res.* **1982**, *15*, 245–251.
(4) Hoffmann, R.; Imamura, A.; Hehre, W. J. Benzynes, Dehydroconjugated Molecules, and the Interaction of Orbitals Separated by a Number of Intervening Bonds. *J. Am. Chem. Soc.* **1968**, *90*, 1499–1509.
(5) Baker, A. D. Photoelectron Spectroscopy. *Acc. Chem. Res.* **1970**, *3*, 17–25.
(6) Dougherty, D.; Brint, P.; McGlynn, S. P. Photoelectron Spectroscopy of Carbonyls. Lone-Pair Interactions in .Alpha.-, .Beta.-, .Gamma.-, and .Delta.-Dicarbonyls. *J. Am. Chem. Soc.* **1978**, *100*, 5597–5603.
(7) Pasman, P.; Rob, F.; Verhoeven, J. W. Intramolecular Charge-Transfer Absorption and Emission Resulting from through-Bond Interaction in Bichromophoric Molecules. *J. Am. Chem. Soc.* **1982**, *104*, 5127–5133.
(8) Martin, H.; Mayer, B. Proximity Effects in Organic Chemistry—The Photoelectron Spectroscopic Investigation of Non-Bonding and Transannular Interactions. *Angew. Chem. Int. Ed.* **1983**, *22*, 283–314.
(9) Rademacher, P. Transannular Interactions in Difunctional Medium Rings - Modelling Bimolecular Reactions. *Chem. Soc. Rev.* **1995**, *24*, 143–150.
(10) Gleiter, R.; Kobayashi, M.; Kuthan, J. The N-Orbital Sequence in 1,3 Diazaadamantane.

Tetrahedron **1976**, *32*, 2775–2781.
(11) Alabugin, I. V. *Stereoelectronic Effects: A Bridge Between Structure and Reactivity*, 1st ed.; John Wiley & Sons, Ltd: Hoboken, NJ, 2016.
(12) Gonikberg, E. M.; Le Noble, W. J. Face Selection in Reactions of 5,7-Diazaadamantan-2-One Derivatives: Mutual Influence of Remote Substituents. *J. Org. Chem.* **1995**, *60*, 7751–7755.
(13) Gonikberg, E. M.; Picart, F.; Le Noble, W. J. Enhanced Stereoselectivity in the Capture of a 5-Substituted 2-Adamantyl Radical by Substitution of C-5 by Negative Boron. *J. Org. Chem.* **1996**, *61*, 9588–9590.
(14) Kaselj, M.; Gonikberg, E. M.; Le Noble, W. J. Effect of Remote Substitution on Face Selection in Addition Reactions of Nor- And Homoadamantan-9-Ones and of Several Analogues. *J. Org. Chem.* **1998**, *63*, 3218–3223.
(15) Adcock, W.; Trout, N. A. Nature of the Electronic Factor Governing Diastereofacial Selectivity in Some Reactions of Rigid Saturated Model Substrates. *Chem. Rev.* **1999**, *99*, 1415–1435.
(16) Lampkins, A. J.; Li, Y.; Al Abbas, A.; Abboud, K. A.; Ghiviriga, I.; Castellano, R. K. Assessable Consequences of Through-Bond Donor-Acceptor Interactions in β-Aminoketones. *Chem. Eur. J.* **2008**, *14*, 1452–1463.
(17) Dekkers, A. W. J. D.; Verhoeven, J. W.; Speckamp, W. N. On the Nature of Sigma-Coupled Transitions. Through-Bond Interactions in 1-Aza-Adamantane Derivatives. *Tetrahedron* **1973**, *29*, 1691–1696.
(18) Sasaki, T.; Eguchi, S.; Kiriyama, T.; Sakito, Y.; Kato, H. Photoelectron Spectroscopic Evidence Concerning Ground-State Through-Sigma-Bond Interaction in the 1,3-Diaza-Adamantan-6-One System. *J. Chem. Soc. Chem. Commun.* **1974**, 725–726.
(19) Bishop, R.; Lee, G.-H. Detection of Non-Conjugative Interactions in Rigid Cyclic Molecules by Using Carbon-13 N.M.R. Shift Values. *Aust. J. Chem.* **1987**, *40*, 249–255.
(20) Alabugin, I. V.; dos Passos Gomes, G.; Abdo, M. A. Hyperconjugation. *WIREs Comput. Mol. Sci.* **2018**, e1389.
(21) Wu, J. I.; Schleyer, P. v. R. Hyperconjugation in Hydrocarbons: Not Just a "Mild Sort of Conjugation." *Pure Appl. Chem.* **2013**, *85*, 921–940.
(22) Risch, N.; Saak, W. Synthesis of Specifically Substituted 1-Azaadamantanes. *Angew. Chem. Int. Ed. English* **1982**, *21*, 923–924.
(23) Risch, N. 1-Aza-Adamantanes from Phloroglucinols. *J. Chem. Soc. Chem. Commun.* **1983**, 532–533.
(24) Risch, N.; Langhals, M.; Hohberg, T. Triple (Grob) Fragmentation. Retro-Mannich Reactions of 1-Aza-Adamantane Derivatives. *Tetrahedron Lett.* **1991**, *32*, 4465–4468.
(25) Worrell, C.; Verhoeven, J. W.; Speckamp, W. N. Through-Bond Interaction in 1-Aza-Adamantane Derivatives. *Tetrahedron* **1974**, *30*, 3525–3531.
(26) Morishima, I.; Okada, K.; Yonezawa, T.; Goto, K. Studies on the Carbon-13 Contact Shifts of a Sigma-Electron System. Conformational Dependence of Carbon-13 Contact Shifts in Six-Membered Rings. *J. Am. Chem. Soc.* **1971**, *93*, 3922–3926.
(27) Hoffmann, R. Molecular Beauty. In *Roald Hoffmann on the Philosophy, Art, and Science of Chemistry*; Oxford University Press, Inc.: New York, 2012; pp 272–292.
(28) Risch, N.; Billerbeck, U.; Meyer-Roscher, B. Azabicyclononane Durch Fragmentierung, II. Regiospezifische (Grob-)Fragmentierung Zur Darstellung von 3-Azabicyclononanen. *Chem. Ber.* **1993**, *126*, 1137–1140.

(29) Ruenitz, P. C.; Mokler, Corwin, M. Analogues of Sparteine. 5. Antiarrhythmic Activity of Selected N,N'-Disubstituted Bispidines. *J. Med. Chem.* **1977**, *20*, 1668–1671.
(30) Thompson, M. D.; Smith, G. S.; Berlin, K. D.; Holt, E. M.; Scherlag, B. J.; Van Der Helm, D.; Muchmore, S. W.; Fidelis, K. A. Synthesis and Antiarrhythmic Properties of Novel 3-Selena-7-Azabicyclo[3.3.1]Nonanes and Derivatives Single-Crystal X-Ray Diffraction Analysis of 7-Benzyl-3-Selena-7-Azabicyclo[3.3.1]Nonan-9-One and 7-Benzyl-3-Selena-7-Azabicyclo[3.3.1]Nonane Hydroperchlo. *J. Med. Chem.* **1987**, *30*, 780–788.
(31) Marshall, L.; Parris, K.; Rebek, J.; Luis, S. V.; Burguete, M. I. A New Class of Chelating Agents. *J. Am. Chem. Soc.* **1988**, *110*, 5192–5193.
(32) Rebek, J. Molecular Recognition with Model Systems. *Angew. Chem. Int. Ed.* **1990**, *29*, 245–255.
(33) Kyburz, R.; Schöpp, E.; Bick, I. R. C.; Hesse, M. 258. Sorellin Und Hobartin, Zwei Neue Indolalkaloide Am Aristoteliu Peduncdaris (LABILL.) HOOK. F. *Helv. Chim. Acta* **1979**, *62*, 2539–2546.
(34) Argade, M. D.; Straub, C. J.; Rusali, L. E.; Santarsiero, B. D.; Riley, A. P. Synthesis of Aristoquinoline Enantiomers and Their Evaluation at the A3β4 Nicotinic Acetylcholine Receptor. *Org. Lett.* **2021**, *23*, 7693–7697.
(35) Eschenmoser, A.; Frey, A. Über Die Spaltung Des Mesylesters von 2-Methyl-2-oxymethyl-cyclopentanon Mit Basen. *Helv. Chim. Acta* **1952**, *35*, 1660–1666.
(36) Grob, C. A.; Schiess, P. W. Heterolytic Fragmentation. A Class of Organic Reactions. *Angew. Chem. Int. Ed.* **1967**, *6*, 1–106.
(37) Weyerstahl, P.; Marschall, H. Fragmentation Reactions. In *Comprehensive Organic Synthesis*; 1991; pp 1041–1070.
(38) Prantz, K.; Mulzer, J. Synthetic Applications of the Carbonyl Generating Grob Fragmentation. *Chem. Rev.* **2010**, *110*, 3741–3766.
(39) Drahl, M. A.; Manpadi, M.; Williams, L. J. C-C Fragmentation: Origins and Recent Applications. *Angew. Chem. Int. Ed.* **2013**, *52*, 11222–11251.
(40) Hoang, T. T.; Dudley, G. B.; Williams, L. J. Fragmentation Reactions. In *Comprehensive Organic Synthesis: Second Edition*; Elsevier Ltd., 2014; Vol. 6, pp 842–860.
(41) Yang, J.; Hoang, T. T.; Dudley, G. B. Alkynogenic Fragmentation. *Org. Chem. Front.* **2019**, *6*, 2560–2569.
(42) Donald, J. R.; Unsworth, W. P. Ring-Expansion Reactions in the Synthesis of Macrocycles and Medium-Sized Rings. *Chem. Eur. J.* **2017**, *23*, 8780–8799.
(43) Clarke, A. K.; Unsworth, W. P. A Happy Medium: The Synthesis of Medicinally Important Medium- Sized Rings via Ring Expansion. *Chem. Sci.* **2020**, *11*, 2876–2881.
(44) Maimone, T. J.; Shi, J.; Ashida, S.; Baran, P. S. Total Synthesis of Vinigrol. *J. Am. Chem. Soc.* **2009**, *131*, 17066–17067.
(45) Ferhati, X.; Salas-Cubero, M.; Garrido, P.; García-Sanmartín, J.; Guerreiro, A.; Avenoza, A.; Busto, J. H.; Peregrina, J. M.; Martínez, A.; Jiménez-Moreno, E.; et al. Bioorthogonal Self-Immolative Linker Based on Grob Fragmentation. *Org. Lett.* **2021**, *23*, 8580–8584.
(46) Laconsay, C. J.; Tsui, K. Y.; Tantillo, D. J. Tipping the Balance: Theoretical Interrogation of Divergent Extended Heterolytic Fragmentations. *Chem. Sci.* **2020**, *11*, 2231–2242.
(47) Schwarz, H. On the Usefulness of Useless Knowledge. *Nat. Rev. Chem.* **2017**, *1*, 1–3.
(48) Risch, N.; Langhals, M.; Mikosch, W.; Boegge, H.; Mueller, A. Unusual Reorganization Reactions of 3-Azabicyclo[3.3.1]Nonanes. *J. Am. Chem. Soc.* **1991**, *113*, 9411–9412.

(49) Gleiter, R.; Stohrer, W.; Hoffmann, R. Orbital Theory of Heterolytic Fragmentation and Remote Effects on Nitrogen Inversion Equilibria. *Helv. Chim. Acta* **1972**, *3*, 893–906.
(50) Frisch, M. J.; Trucks, G. W.; Schlegel, H. B.; Scuseria, G. E. .; Robb, G. E.; Cheeseman, J. R.; Scalmani, G.; Barone, V.; Mennucci, B. .; Petersson, G. A.; Nakatsuji, H.; Caricato, M.; Li, X.; Hratchian, H. P. .; Izmaylov, A. F.; Bloino, J.; Zheng, G.; Sonnenberg, J. L.; Hada, M. .; Ehara, M.; Toyota, K.; Fukuda, R.; Hasegawa, J.; Ishida, M.; Nakajima, T. .; Honda, Y.; Kitao, O.; Nakai, H.; Vreven, T.; Montgomery, Jr., J. A. . P.; J. E.; Ogliaro, F.; Bearpark, M.; Heyd, J. J.; Brothers, E. . K.; K. N.; Staroverov, V. N.; Keith, T.; Kobayashi, R.; Normand, J. . R.; K.; Rendell, A.; Burant, J. C.; Iyengar, S. S.; Tomasi, J. . C.; M.; Rega, N.; Millam, J. M.; Klene, M.; Knox, J. E.; Cross, J. B. .; Bakken, V.; Adamo, C.; Jaramillo, J.; Gomperts, R.; Stratmann, R. E.; Yazyev O.; Austin, A. J.; Cammi, R.; Pomelli, C.; Ochterski, J. W.; Martin R. L.; Morokuma, K.; Zakrzewski, V. G.; Voth, G. A.; Salvador, P.; Dannenberg, J. J.; Dapprich, S.; Daniels, A. D.; Farkas O.; Foresman, J. B.; Ortiz, J. V.; Cioslowski, J.; Fox, D. J. *Gaussian 09*, Revision D.01. Gaussian Inc. Wallingford, CT 2009.
(51) Zhao, Y.; Truhlar, D. G. The M06 Suite of Density Functionals for Main Group Thermochemistry, Thermochemical Kinetics, Noncovalent Interactions, Excited States, and Transition Elements: Two New Functionals and Systematic Testing of Four M06-Class Functionals and 12 Other Function. *Theor. Chem. Acc.* **2008**, *120*, 215–241.
(52) Alabugin, I. V.; Kuhn, L.; Krivoshchapov, N. V.; Mehaffy, P.; Medvedev, M. G. Anomeric Effect, Hyperconjugation and Electrostatics: Lessons from Complexity in a Classic Stereoelectronic Phenomenon. *Chem. Soc. Rev.* **2021**, *50*, 10212–10252.
(53) Nam, S.; Cho, E.; Sim, E.; Burke, K. Explaining and Fixing DFT Failures for Torsional Barriers. *J. Phys. Chem. Lett.* **2021**, *12*, 2796–2804.
(54) Fukui, K. The Path of Chemical Reactions -- The IRC Approach. *Acc. Chem. Res.* **1981**, *14*, 363–368.
(55) Gonzalez, C.; Schlegel, H. B. Reaction Path Following In Mass-Weighted Internal Coordinates Cartesians and with Internal Coordinates without Mass-Weighting. *J. Phys. Chem.* **1990**, *94*, 5523–5527.
(56) Maeda, S.; Harabuchi, Y.; Ono, Y.; Taketsugu, T.; Morokuma, K. Intrinsic Reaction Coordinate: Calculation, Bifurcation, and Automated Search. *Int. J. Quantum Chem.* **2015**, *115*, 258–269.
(57) Becke, A. D. Density-Functional Thermochemistry. III. The Role of Exact Exchange. *J. Chem. Phys.* **1993**, *98*, 5648–5652.
(58) Grimme, S.; Antony, J.; Ehrlich, S.; Krieg, H. A Consistent and Accurate Ab Initio Parametrization of Density Functional Dispersion Correction (DFT-D) for the 94 Elements H-Pu. *J. Chem. Phys.* **2010**, *132*, 154104.
(59) Miertuš, S.; Scrocco, E.; Tomasi, J. Electrostatic Interaction of a Solute with a Continuum. A Direct Utilizaion of Ab Initio Molecular Potentials for the Prevision of Solvent Effects. *Chem. Phys.* **1981**, *55*, 117–129.
(60) Álvarez-Moreno, M.; de Graaf, C.; López, N.; Maseras, F.; Poblet, J. M.; Bo, C. Managing the Computational Chemistry Big Data Problem: The ioChem-BD Platform. *J. Chem. Inf. Model.* **2015**, *55*, 95–103.
(61) Prasad, S.; Tantillo, D. J. Substituent Effects on the Basicity of Patriscabrin A and Lettucenin A: Evolution Favors the Aromatic? *ACS Omega* **2021**, *6*, 29685–29691.
(62) Johnson, E. R.; Keinan, S.; Mori-Sánchez, P.; Contreras-García, J.; Cohen, A. J.; Yang,

W. Revealing Noncovalent Interactions. *J. Am. Chem. Soc.* **2010**, *132*, 6498–6506.
(63) Lu, T.; Chen, F. Multiwfn: A Multifunctional Wavefunction Analyzer. *J. Comput. Chem.* **2012**, *33*, 580–592.
(64) Glendening, E. D.; Reed, A. E.; Carpenter, J. E.; Weinhold, F. NBO Version 3.1 Gaussian Inc. Pittsburgh 2003.
(65) Weinhold, F.; Landis, C. R.; Glendening, E. D. What Is NBO Analysis and How Is It Useful? *Int. Rev. Phys. Chem.* **2016**, *35*, 399–440.
(66) Wedler, H. B.; Palazzo, T. A.; Pemberton, R. P.; Hamann, C. S.; Kurth, M. J.; Tantillo, D. J. Predicting Hydration Propensities of Biologically Relevant α-Ketoamides. *Bioorganic Med. Chem. Lett.* **2015**, *25*, 4153–4157.
(67) Buschmann, H.-J.; Dutkiewicz, E.; Knoche, W. Reversible Hydration of Carbonyl Compounds in Aqueous Solution - 2. the Kinetics of the Keto/Gem-Diol Transition. *Ber. Chem.* **1982**, *86*, 129–134.
(68) Guthrie, J. P. Hydration of Carbonyl Compounds, an Analysis in Terms of Multidimensional Marcus Theory. *J. Am. Chem. Soc.* **2000**, *122*, 5529–5538.
(69) Wagner, J. P.; Schreiner, P. R. London Dispersion in Molecular Chemistry - Reconsidering Steric Effects. *Angew. Chem. Int. Ed.* **2015**, *54*, 12274–12296.
(70) Peng, Q.; Duarte, F.; Paton, R. S. Computing Organic Stereoselectivity-from Concepts to Quantitative Calculations and Predictions. *Chem. Soc. Rev.* **2016**, *45*, 6093–6107.
(71) Maji, R.; Mallojjala, S. C.; Wheeler, S. E. Chiral Phosphoric Acid Catalysis: From Numbers to Insights. *Chem. Soc. Rev.* **2018**, *47*, 1142–1158.
(72) Morgenthaler, M.; Schweizer, E.; Hoffmann-Röder, A.; Benini, F.; Martin, R. E.; Jaeschke, G.; Wagner, B.; Fischer, H.; Bendels, S.; Zimmerli, D.; et al. Predicting and Tuning Physicochemical Properties in Lead Optimization: Amine Basicities. *ChemMedChem* **2007**, *2*, 1100–1115.
(73) Yaremenko, I. A.; Belyakova, Y. Y.; Radulov, P. S.; Novikov, R. A.; Medvedev, M. G.; Krivoshchapov, N. V.; Korlyukov, A. A.; Alabugin, I. V.; Terent'ev, A. O. Marriage of Peroxides and Nitrogen Heterocycles: Selective Three-Component Assembly, Peroxide-Preserving Rearrangement, and Stereoelectronic Source of Unusual Stability of Bridged Azaozonides. *J. Am. Chem. Soc.* **2021**, *143*, 6634–6648.
(74) Hammett, L. P. The Effect of Structure upon the Reactions of Organic Compounds. Benzene Derivatives. *J. Am. Chem. Soc.* **1937**, *59*, 96–103.
(75) Hansch, C.; Leo, A.; Taft, R. W. A Survey of Hammett Substituent Constants and Resonance and Field Parameters. *Chem. Rev.* **1991**, *91*, 165–195.
(76) Kardel, D.; Knoche, W.; Risch, N. Protonation and Gem-Diol Formation of 1-Azaadamantanones. *J. Chem. Soc. Perkin Trans. 2* **1993**, *2*, 1455–1459.
(77) Galasso, V. On the n(N)/n(O) Interaction in Adamantane Cages. *J. Mol. Struct. THEOCHEM* **2000**, *528*, 171–176.
(78) Lambert, J. B.; Ciro, S. M. The Interaction of π Orbitals with a Carbocation over Three σ Bonds. *J. Org. Chem.* **1996**, *61*, 1940–1945.
(79) Alabugin, I. V; Manoharan, M. Effect of Double-Hyperconjugation on the Apparent Donor Ability of σ-Bonds: Insights from the Relative Stability of δ-Substituted Cyclohexyl Cations. *J. Org. Chem.* **2004**, *69*, 9011–9024.
(80) Grob, Cyril A, R. R. Inductive and Hyperconjugative Effects in the Solvolysis of 4-Substituted Bicyclo[2.2.2]Oct-1-Yl p-Nitrobenzenesulfonates. *Tetrahedron Lett.* **1978**, 663–666.

(81) Wu, J. I.; Fernández, I.; Mo, Y.; Schleyer, P. von R. Why Cyclooctatetraene Is Highly Stabilized: The Importance of "Two-Way" (Double) Hyperconjugation. *J. Chem. Theory Comput.* **2012**, *8*, 1280–1287.
(82) Grob, C. A.; Rich, R. Polar Effects in the Solvolysis of 4-Substituted Bicyclo[2.2.2]Octyl P-Nitrobenzenesulfonates. Polar Effects. VII. *Helv. Chim. Acta* **1979**, *62*, 2793–2801.
(83) Adcock, W.; Krstic, A. R.; Duggan, P. J.; Shiner, V. J.; Coope, J.; Ensinger, M. W. Through-Bond Transmission of Substituent Effects in the Bicyclo[2.2.2]Octane Ring System: Solvolysis of 4-Deuterioand 4-Metalloidal ($M(CH_3)_3$, M = Si, Ge, and Sn)-Substituted Bicyclo[2.2.2]Oct-1-Yl p-Nitrobenzenesulfonates and Methanesulfonates. *J. Am. Chem. Soc.* **1990**, *112*, 3140–3145.
(84) Adcock, W.; Trout, N. A. Transmission of Polar Substituent Effects in the Adamantane Ring System As Monitored by ^{19}F NMR: Hyperconjugation as a Stereoinductive Factor. *J. Org. Chem.* **1991**, *56*, 3229–3238.
(85) Lambert, J. B.; Salvador, L. A.; So, J. H. The .Gamma. and .Delta. Effects of Tin. *Organometallics* **2005**, *12*, 697–703.
(86) Vidhani, D. V.; Krafft, M. E.; Alabugin, I. V. Gold(I)-Catalyzed Allenyl Cope Rearrangement: Evolution from Asynchronicity to Trappable Intermediates Assisted by Stereoelectronic Switching. *J. Am. Chem. Soc.* **2016**, *138*, 2769–2779.
(87) Reed, A. E.; Curtiss, L. A.; Weinhold, F. Intermolecular Interactions from a Natural Bond Orbital, Donor—Acceptor Viewpoint. *Chem. Rev.* **1988**, *88*, 899–926.
(88) Wheeler, S. E.; Houk, K. N.; Schleyer, P. V. R.; Allen, W. D. A Hierarchy of Homodesmotic Reactions for Thermochemistry. *J. Am. Chem. Soc.* **2009**, *131*, 2547–2560.
(89) Lüning, U. Concave Reagents: Syntheses of Macrobicyclic Pyridines. *Liebigs Ann.* **1987**, 949–955.
(90) Ferrier, R. J.; Sankey, G. H. Unsaturated Carbohydrates. Part VII. The Preference Shown by Allylic Ester Groupings on Pyranoid Rings for the Quasi-Axial Orientation. *J. Chem. Soc. C Org.* **1966**, 2345.
(91) Johnson, S. R. The Trouble with QSAR (or How I Learned To Stop Worrying and Embrace Fallacy). *J. Chem. Inf. Model.* **2008**, *48*, 25–26.
(92) Filloux, C. M. The Problem of Origins and Origins of the Problem: Influence of Language on Studies Concerning the Anomeric Effect. *Angew. Chem. Int. Ed.* **2015**, *54*, 8880–8894.

Part III

A Collaboration Project on a Diterpene Natural Product

Chapter 9

Deceptive Complexity in Formation of Cleistantha-8,12-diene*

All science can do is turn out the false lights so the true light can get us home.

- Tobias Wolff, *Old School* (2003)

9.1 Abstract

A cleistanthane diterpene natural product, (14*S*)-cleistantha-8,12-diene (**1**), was produced from a diterpene synthase (HvKSL4), isolated from barley (*Hordeum vulgare*). Density functional theory calculations of the computed NMR shifts aided in the structure elucidation of the natural product with ^{1}H, ^{13}C, HSQC, and HMBC spectral data. Subsequent calculations and labeling studies explored two possible mechanisms for the biosynthesis of the diterpene product and provided a plausible mechanistic pathway from pimaradienyl cation. The significant finding from this work suggests that HvKSL4 must steer through a complex energetic landscape, manifesting in a complicated mechanism to **1**.

* This chapter is a modified version of the following published article: Liang, J.; Merrill, A. T.; Laconsay, C. J.; Hou, A.; Pu, Q.; Dickschat, J. S.; Tantillo, D. J.; Wang, Q.; Peters, R. J. Deceptive Complexity in Formation of Cleistantha-8,12-diene, *Org. Lett.* **2022**, *24*, 2646-2649 with permission from the American Chemical Society. Amy T. Merrill (from the Tantillo group) completed the computational NMR portions of this study, and that work is not included here—that can be found in the Supporting Information of the above cited publication. The Peters and Wang groups isolated and characterized the diterpene natural product. The Dickschat group carried out the mechanistic labeling studies. Croix J. Laconsay carried out the DFT mechanistic studies (described herein).

9.2 Introduction

The Poaceae plant family is a particularly rich source of labdane-related diterpenoids.[1,2] The biosynthesis of these diterpenoids begin from the general diterpenoid precursor (*E*,*E*,*E*) geranylgeranyl diphosphate (GGPP) by class II diterpene cyclases to produce the eponymous labdadienyl/copalyl diphosphate (CPP).[3] However, relatively little is known about such biosynthesis in barley (*Hordeum vulgare*), with only the ent-CPP synthase HvCPS1 and ent-kaurene synthase HvKS1 presumably involved in gibberellin phytohormone biosynthesis.[4] Nevertheless, barley contains several genes for KS-like (KSL) terpene synthases. Among these, HvKSL4 is of particular note, as its transcript accumulates in response to either UV-irradiation or infection with the fungus *Piriformospora indica*,[5] similar to KSLs involved in specialized/secondary metabolism of known importance in other Poaceae plant species.[2] Given the importance of barley as a source of drink, food, and fodder, as well as the critical physiological roles for labdane-related diterpenoids in cereal resistance to biotic and abiotic stresses,[6] we selected HvKSL4 for characterization of such specialized metabolism in this key crop plant.

HvKSL4 was cloned from UV-irradiated leaf tissue for biochemical characterization.[*] HvKSL4 was then incorporated into a previously described modular metabolic engineering system that enables expression in *Escherichia coli* engineered to produce potential substrates, specifically the three known stereoisomers of CPP,[7] all of which are produced by Poaceae. HvKSL4 did not react with ent-CPP, but it does with both (normal) CPP (**2**) and syn-CPP. A recent preprint reported that HvKSL4 is found in a biosynthetic gene cluster in the barley genome and also contains HvCPS2 that produces **2**, with derivatives of the resulting **1** found in planta.[8] Herein we study that

[*] Details of the experiment can be found in the Supporting Information of the original *Organic Letters*[68] publication— *Org. Lett.* **2022**, *24*, 2646-2649.

reaction (**1** → **2**).* HvKSL4 reacts with **2** to form an unknown major product (**1**, Figure 9.1a), along with small amounts of a single minor product that was shown to be isopimara-8,15-diene (**3**) by comparison to an authentic standard.†

Scheme 9.1. Example cleistanthane type structures akin to product **1**. All were isolated and reported in four papers by Pinto *et al.* in *Phytochemistry* between 1984 – 1995. Shown above are some example structures reported between 1988-1995.

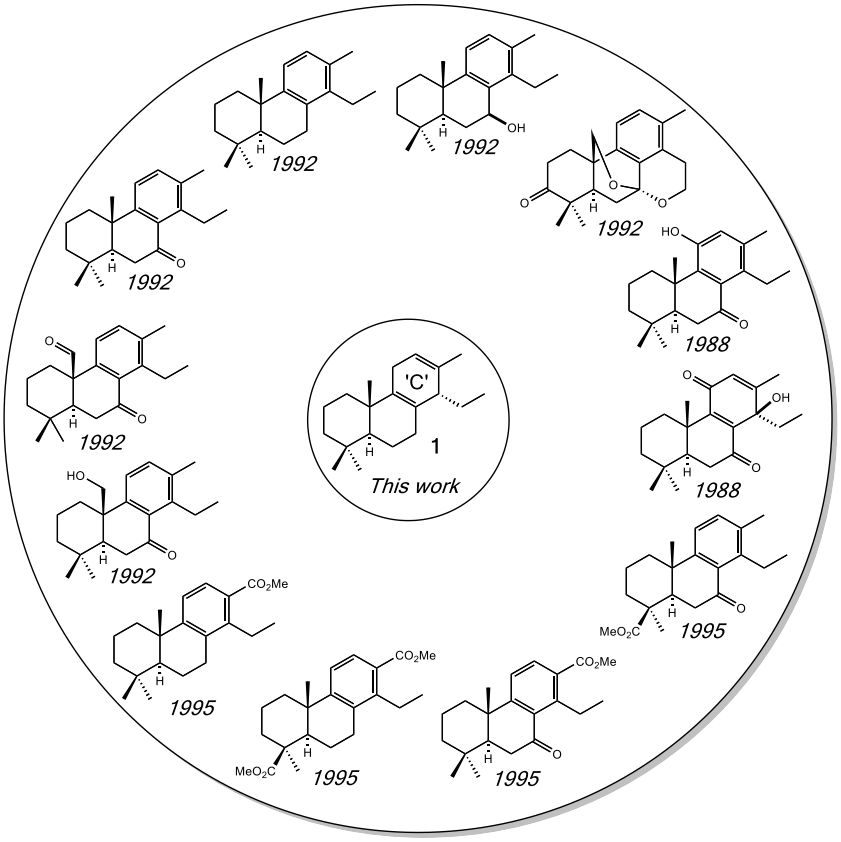

Past literature contains scattered examples of cleistanthane compounds whose backbone resembles that of **1**.[9–12] For instance, from 1984-1995, Pinto *et al.* reported numerous oxygenated and desaturated cleistanthanes (Scheme 9.1), many of which were isolated from plants from the *Vellozia* plant genus.[9–11] Almost all the cleistanthane structures in Scheme 9.1 have aromatic C rings—that is, aromatized versions of **1**—so **1** may be an important precursor in the cleistanthanes

* see Supplemental Figure S1 of *Org. Lett.* **2022**, *24*, 2646-2649 for the results with syn-CPP.
† Ibid, 12, Supplemental Figure S2.

class of natural products. At the outset, literature precedent for the stereochemistry and carbon backbone motif of **1** suggests that this product may be the byproduct of dynamical tendencies (possibly guided by the terpene synthase) in an unexplored post-transition state bifurcation (PTSB) pathway along the complex PES of diterpenes.[13]

9.3 Computational Methods

Gaussian09[14] transition-state structure (TSS) and minima optimizations were carried out with a (99,590) grid (i.e., an ultrafine integration grid).[15] Optimized TSSs were verified with frequency calculations and by identifying one imaginary frequency. Minima were verified as such by the absence of imaginary frequencies. Intrinsic Reaction Coordinate (IRC) calculations were used to further characterize TSSs.[16–18] Becke's hybrid, three-parameter functional with Lee, Yang, and Parr's non-local correlation functional,[19] that is, B3LYP, has been consistently provided sufficient accuracy at a reasonable computational cost for exploring mechanistic possibilities in terpene biosynthesis.[20] Single-point calculations at the B3LYP/6-31+G(d,p) optimized geometries with the mPW1PW91[21] and ωB97X-D[22] functionals—that is, mPW1PW91/6-31+G(d,p)//B3LYP/6-31+G(d,p) and ωB97X-D/6-31+G(d,p)//B3LYP/6-31+G(d,p), respectively—were performed to verify that the B3LYP/6-31+G(d,p) energies were reasonable. Cartesian coordinates of all structures can be found in the ioChem-BD repository[23] at the following DOI: https://doi.org/10.19061/iochem-bd-6-75.*

* Ibid, 54-56, energies and frequencies for all stationary points (see Supplemental Tables S24 – S26).

9.4 Results and Discussion

9.4.1 Metabolic Engineering and Characterization

In order to identify the unknown major product (**1**) resulting from **2**, metabolic engineering was employed to increase metabolic flux toward isoprenoids,[24] and the resulting recombinant *E. coli* grown in larger volumes. This enabled isolation of a sufficient amount of **1** (~2 mg) for structural analysis by NMR.* NMR analysis enabled us to determine that **1** is a perhydrophenanthrene tricycle with a methyl and ethyl substituent on the 'C' ring formed by HvKSL4 (Figure 9.1). However, two potential configurations for the ethyl substituent and double-bond arrangement in this ring could be reasonably proposed.† To help determine the relevant structure, computational predictions of chemical shift data were made for both, with further consideration of the ethyl epimers, and compared to those measured‡ (all structures deposited in ioChem-BD at this DOI: https://doi.org/10.19061/iochem-bd-6-75).[23] The details of the NMR and computational NMR studies are readily available in the original publication and the SI therein. This dissertation chapter from here on solely focuses on an elaborated discussion of the quantum chemical mechanistic studies.

* Ibid, 13 (Supplemental Table S1), and 14-16 (Figures S3−S7).
† Ibid, 16 (Supplemental Figure S8).
‡ Ibid, 17-24, Supplemental Tables S2−S9.

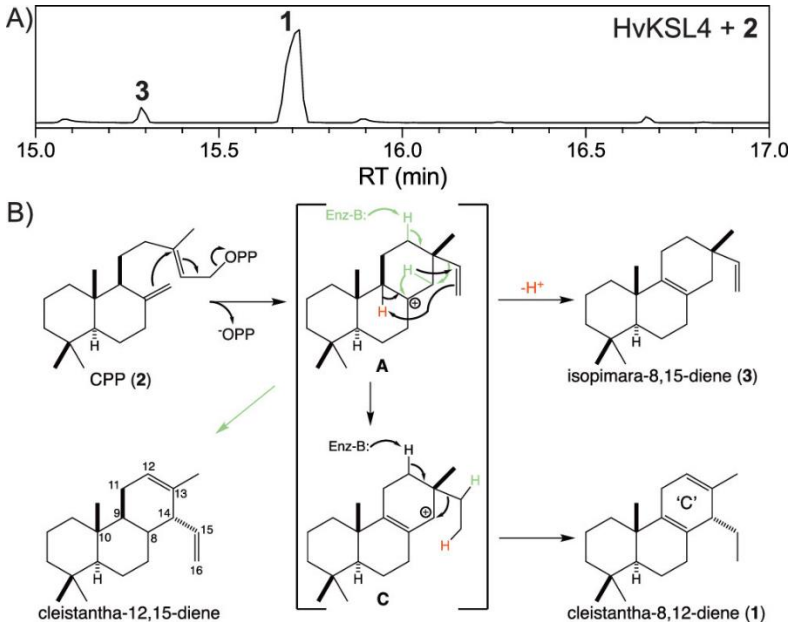

Figure 9.1 HvKSL4 activity with CPP (2). (A) Total ion chromatogram for extract from *E. coli* expressing HvKSL4, engineered to also produce CPP (**2**), with peak numbering as described in the text. (B) Scheme showing **2** and reaction leading to identified products, as well as a "simpler" alternative mechanism leading to a cleistantha-12,15-diene (green arrows), as discussed in the text.

9.4.2 Exploration of Possible Biosynthetic Mechanisms

Possible mechanisms for the formation of **1** from A (Figure 9.2) were investigated using DFT calculations, a tool that has been integral in the exploration of mechanistic proposals for the formation of terpene natural products and the intrinsic reactivity of the carbocation intermediates that precede them.[20,25,26] The mechanism begins with an enzyme-promoted carbocation formation of geranylgeranyl diphosphate as a result of departure of the diphosphate group. Subsequent cyclization steps yield either (-)-CPP or (+)-CPP, which then the terpene synthase uses to cyclize to pimar-15-en-8-yl (or 'pimardienyl cation' [**A**] from here on). The quest to find a reasonable mechanism from (-)-copalyl diphosphate (CPP) to **1**, led us to revisit known mechanistic pathways previously studied by our group.[13,27,28] Building upon these past studies, in which the pimaradienyl cation (**A**) has been shown to lead to a variety of natural and theoretically plausible products, we

found it reasonable to begin our mechanistic exploration from **A**. The biosynthesis of **1** may be closely related to that of key intermediates associated with abietane-type diterpenoids, for example, abietadiene[28–33] and miltiradiene,[27,34,35] which could mean that pimaradienyl cation is a common cationic intermediate between all three structures.

Cation **A** exists on a complex hyperdimensional potential energy surface (PES), which poses a challenge for the synthase, as there may be myriad pathways to different products. Our group previously reported DFT calculations and direct dynamics results that suggest that the PES around **A** (and **A'**) is quite complex: it is flat in some regions, and contains sequential post-transition state bifurcations (PTSBs) along its surface, which means that the inherent reactivity of carbocation intermediates along the reaction pathway are dictated by non-statistical dynamic effects.[36–44] A PTSB is a reaction in which downhill from a single transition-state structure, the path of the reaction bifurcates, which can lead to divergent product outcomes that conventional transition-state theory fails to explain.[45–48] As a result, these reactions can only be studied using molecular dynamics simulations.[49–51] Because of this, terpene synthases face a formidable challenge to control product selectivity, as in the biosynthesis of miltiridiene.[27]

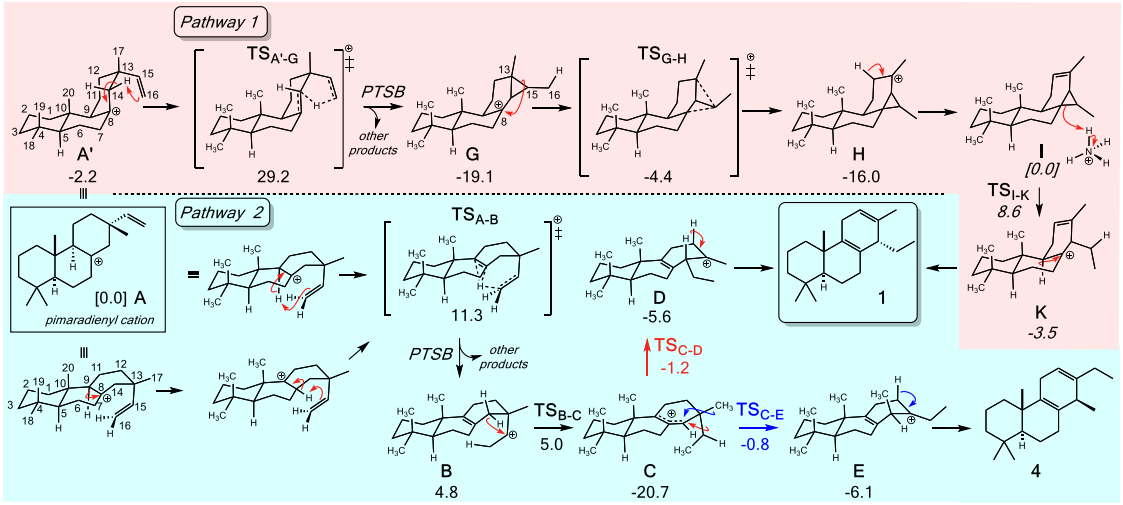

Figure 9.2 Possible mechanistic pathways for the formation of **1**. Pathway 1 (top, shaded in red) and Pathway 2 (bottom, shaded in blue). Also indicated are relative energies (kcal mol^{-1}) of minima and transition state structures calculated using density functional theory (mPW1PW91/6-31+G(d,p)//B3LYP/6-31+G(d,p)). In both pathways the initial proton transfer exhibits a post-transition state bifurcation (PTSB) leading to other products (and sometimes other PTSBs), as previously described.[27,46]

We find that the cationic precursors of **1** can be made *via* two energetically viable pathways from two different conformers of pimaradienyl cation (Figures 9.3 and 9.4).

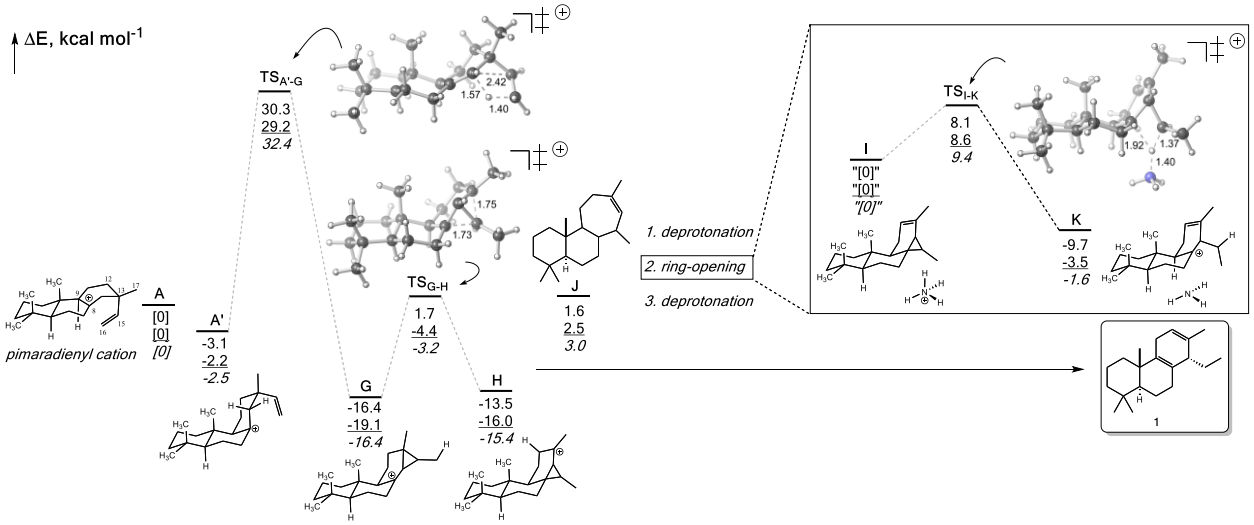

Figure 9.3 Potential energy surface for Pathway 1—**A'** to **1**. Shown are relative electronic energies (in kcal mol^{-1}) at the B3LYP, mPW1PW91 (underlined), and ωB97X-D (italicized) levels of theory with a 6-31+G(d,p) basis set derived from single-point calculations at the B3LYP/6-31+G(d,p) optimized geometries.

Pathway 1 starts from a conformer of pimaradienyl cation, **A'**, which is lower in energy than **A** by about 2 kcal mol^{-1}. From **A'** a cyclopropanated intermediate, **G**, could be formed *via* a TSS that contains a PTSB—this TSS exists on the PES for abietadienyl cation formation, the biosynthetic precursor of abietic acid.[13,28] With an energetic barrier of 30 kcal mol^{-1}, $\mathbf{TS_{A'\text{-}G}}$ is rate-determining and would likely be catalytically controlled by the terpene synthase, as its inherent reactivity[20] would preclude it from traversing such a high barrier under physiological conditions. An unusual 1,3-alkyl shift from **G** to **H** is energetically viable with a barrier of < 20 kcal mol^{-1}.[52] One could envision **H** ring-opening to carbocation **J** (Figure 9.3), but we note that this step would require an energetic barrier of at least 15 kcal mol^{-1}, which is unlikely given that it could be deprotonated (and quenched) at three positions. If **H** is deprotonated at the C12 methylene position (**H** to **I**, Figure 9.3), then the cyclopropyl ring can open if there is an acidic active-site residue (e.g. by a tyrosine/water)[53] to form the cationic precursor, **K**, which by one more deprotonation step would result in **1**. Although lysine residues are not likely found in the active sites of terpene synthases,[54] ammonia molecules and ammonium cations are reasonable model bases and acids, respectively—we have successfully utilized these species in past terpene mechanistic studies.[55–58]

The concerted 1,3-alkyl shift that transforms **G** to **H** may not be so unusual. Literature precedent, both computational and labeling experiments, exists for such "pendular" shifts"[59] in the carbocation cascade mechanisms forming cyclooctat-9-en-7-ol.[60–63] This type of shift is also proposed in the biosynthesis of verrucosan-2β-ol[64] and in the transformation of thujopsene to widdrol.[65] Ultimately, this step can be thought of as a cyclopropylcarbinyl cation – cyclopropylcarbinyl cation rearrangement (a 1,3 alkyl shift from C13 to C8) within the skeleton of the carbocation intermediates.

Pathway 2 begins from conformer **A** and forms **B** *via* a TSS leading to a PTSB.[46] After a hydride shift to an allylic cation, **C**, either an ethyl shift (red arrow) or a methyl shift (blue arrow) result in the cationic precursors of **1** and **4** (**C** and **D**), respectively (Figure 9.4). The TSS for the rate-determining step for this pathway, that is, $\mathbf{TS_{C\text{-}D}}$, is approximately 20 kcal mol^{-1} out of **C**, which is an energetic barrier that is approaching the limit to, but does not preclude, being energetically viable under biological conditions above A.[52] We suspect an enzyme would have a hand in lowering this barrier and/or controlling the prevention of **4** formation, as our computational NMR data provides good evidence that the product isolated is **1**.*

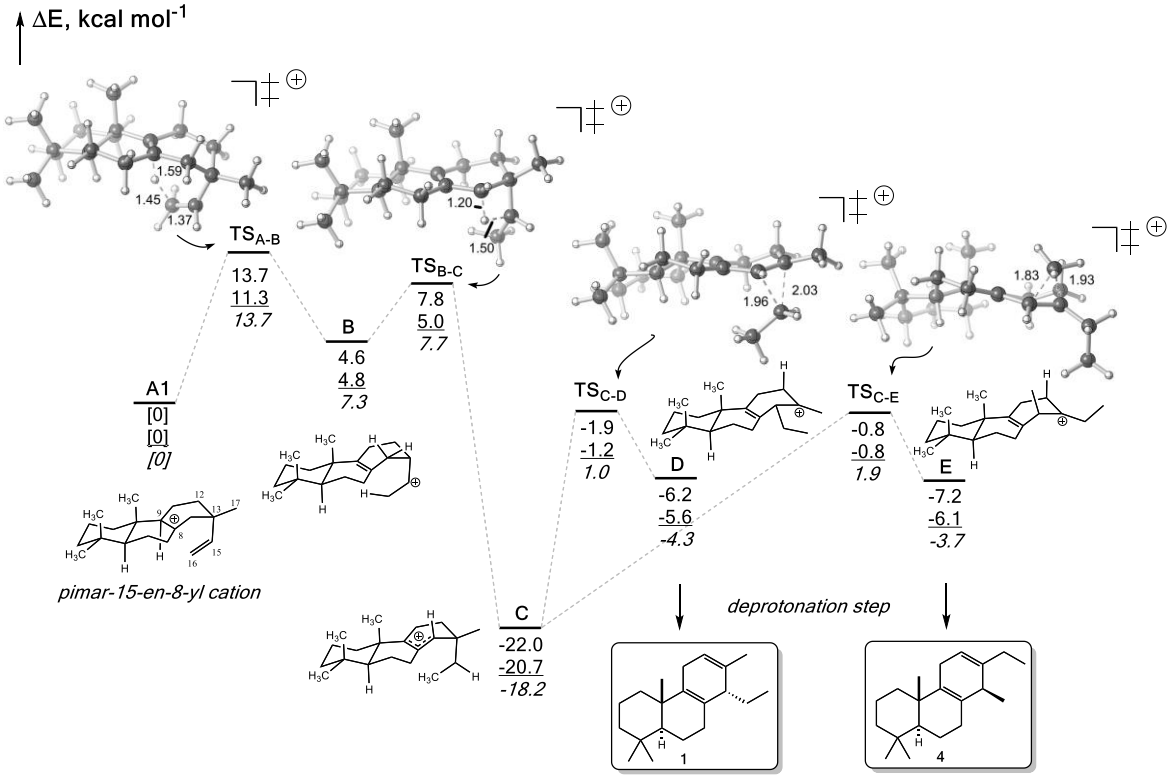

Figure 9.4 Potential energy surface for Pathway 2—**A** to **1** and **4**. Shown are relative electronic energies (in kcal mol^{-1}) at the B3LYP, mPW1PW91 (underlined), and ωB97X-D (italicized) levels of theory with a 6-31+G(d,p) basis set derived from single-point calculations at the B3LYP/6-31+G(d,p) optimized geometries.

* Ibid, 32-33 (Tables S14-S15, for computational NMR results of **4**).

We proposed two energetically viable mechanisms from pimaradienyl cation, **A** or **A'**, to the unexpected, isolated product **1**. After confirming its structure with computational NMR calculations, and subsequent DFT mechanistic studies, two reasonable mechanistic pathways emerge for the biosynthesis **1**. To support or refute our hypothesized pathways, we designed a deuterium-labeling study to distinguish between the two.[66] Our initial design is shown in Figure 9.5. If the methyl group at C14 were deuterated, for example, we hypothesized that we would be able to discern between the pathways: if **1** had deuterium at C14/C16, then that would lend support that Pathway 1 is the relevant pathway, and similarly if C14/C15 were deuterated, then that would lend support in favor of Pathway 2.

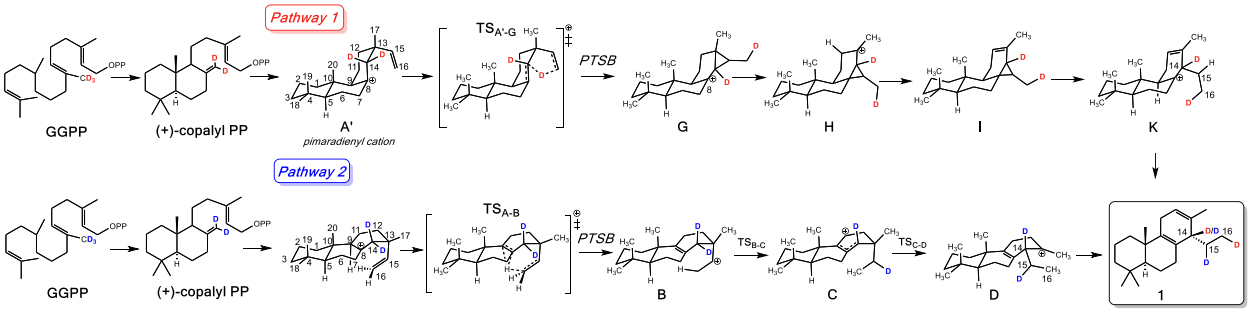

Figure 9.5 Possible isotopic labelling experiment to test theoretical mechanistic hypotheses proposed herein.

9.4.3 Labeling Studies

Collaboration with the Dickschat research group facilitated a realization of these deuterium-labeling studies. In Pathway 1, and in the absence of deuterium in **2**, exogenous deuteration the cyclopropane ring of intermediate **I** (Figure 9.2) would result in a deuterium at C15 (not to be confused with C15 deuterium coming from deuterated **2** from Pathway 2 above). Studies of the reaction in $^{2}H_2O$, including initial cyclization of GGPP to **2** by a class II diterpene cyclase

(which involves incorporation of a deuterium as previously shown[67]) were run to interrogate Pathway 1. Incorporation of an additional deuterium, beyond that found in **2** upon cyclization of **2** to **1** by HvKSL4 was not observed, and weighs against Pathway 1.[68*] Given the frequency of intramolecular proton transfer in terpene synthase catalyzed reactions, the absence of incorporation from an exogenous source does not provide definitive evidence—i.e., as the cyclopropyl might be opened by 1,4-proton transfer from C12 to C15. Accordingly, additional labeling studies were carried out. These relied on generation of labeled GGPP from farnesyl diphosphate and isopentenyl diphosphate, using a GGPP synthase, as previously described,[69–71] along with the synthesis of (15,15,15-$^{2}H_3$)-farnesyl diphosphate reported here.[†] This enabled a series of experiments to more fully investigate the predicted rearrangements (Scheme 9.2).

Scheme 9.2. Labeling Studies of HvKSL4 Production of **1**. Shown for the relevant pathway 2.

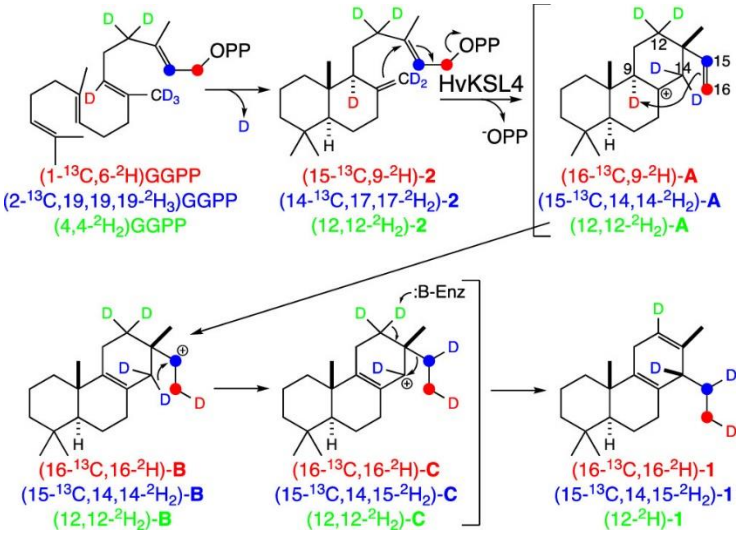

[*] Ibid, 26 (Figure S11).
[†] Ibid, 4 (Supplemental Results S3).

First, a coupled reaction with (1-^{13}C,6-^{2}H)GGPP was carried out, which results in (16-^{13}C,9-^{2}H)-**A**, with observation of a triplet for C16 in the ^{13}C NMR spectra demonstrating derivation to (16-^{13}C,16-^{2}H)-1.* This confirms 1,6-proton transfer within **A** to form isopimara-8-en-15-yl^{+} (**B**). Notably, approximately half of the minor product 3 retains the deuterium, suggesting a mixed origin from deprotonation of either **A** at C9 (loss of ^{2}H) or **B** at C16 (retaining ^{2}H). Second, a coupled reaction with (2-^{13}C,19,19,19-2H3)GGPP was carried out, which results in (15-^{13}C,14,14-$^{2}H_2$)-**A**, with observation of a triplet for C15 in the ^{13}C NMR spectra demonstrating derivation to (15-13C,14,15-$^{2}H_2$)-1.† This confirms the 1,3-proton transfer within **B** to form the allylic carbocation intermediate isopimara-8-en-14-yl^{+} (**C**). The subsequent 1,2-ethyl migration from C13 to C14 formally proceeds from C as isopimara-8-en-14-yl^{+} to yield the rearranged carbocation intermediate cleistantha-8-en-13-yl^{+} (**D**). Finally, a coupled reaction with (4,4-$^{2}H_2$)GGPP was carried out, which results in (12,12-$^{2}H_2$)-**A**, with observation of the loss of a deuterium in the derived (12-^{2}H)-1.‡ This confirms concluding deprotonation of **D** at C12 rather than intramolecular transfer.

Use of pathway 2 by HvKSL4 for production of **1** emphasizes the complexity of the energetic landscape for this reaction, which includes previously reported alternative rearrangements of **B**.[27] There are alternative transition states leading toward ring expansion (barrierless at the mPW1PW91 level of theory utilized here) or the 1,2-methyl migration leading to production of the cyclohexa-1,4-diene abietane miltiradiene (5.2 kcal mol^{-1} relative to **B**), and the inherent barriers for these are similar to that for the production of 1 (0.2 kcal mol^{-1}). Even within the relevant pathway carbocation **C** can undergo an alternative 1,2-methyl shift (leading to

* Ibid, 27 (Supplemental Figure S12).
† Ibid, 28 (Supplemental Figure S13).
‡ Ibid, 29 (Supplemental Figure S14).

a cassane backbone, such as in E and **4**) rather than a 1,2-ethyl shift (c.f. blue vs red arrows in Figure 9.2), and the energetic barrier for each is essentially identical (19.9 versus 19.5 kcal mol^{-1}, respectively, relative to **C**). While the energetic barrier for the 1,2-hydride shift from C14 to C8 within the initially formed **A** to generate the pimar-15-en-14-yl^{+} precursor to vinyl containing cleistantha-12,15-diene (Figure 9.7)* is greater than that for transition to **B** (14.5 versus 11.3 kcal mol^{-1}, respectively), it is still easily surmountable.

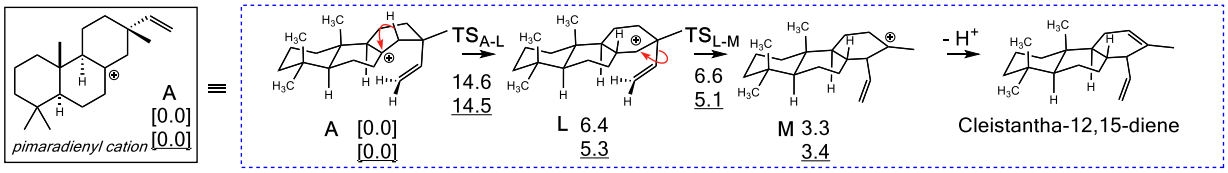

Figure 9.7 Potential energy surface for pathway to the pimar-15-en-14-yl+ precursor to vinyl containing cleistantha-12,15-diene. Relative electronic energies were computed at the B3LYP/6-31+G(d,p) and mPW1PW91/6-31+G(d,p)//B3LYP/6-31+G(d,p) (underlined values) levels of theory; they are reported in kcal mol^{-1}.

Thus, HvKSL4 must steer its reaction through a complex energetic landscape in order to selectively produce 1. This is hypothesized to enable formation of the nearly planar cyclohexa-1,4-diene ring, indicating eventual aromatization in any derived phytoalexins. Indeed, the recent preprint reports that barley produces aromatic derivatives of 1.[8] Accordingly, the work reported here elucidates the ability of terpene synthases to form not only various carbon backbones but also specific olefin isomers that enable further transformations via use of an alternative more extended mechanism, providing an additional contribution to terpenoid natural products biosynthesis.

* Structure **L** is an unusual, non-classical carbocation. Significant hyperconjugation from the shifted hydride and vinyl group gives this carbocation an unusual source of kinetic stability, though not much (only 0.2 kcal/mol is required to shift the vinyl group according to B3LYP). Results from mPW1PW91 indicate that **L** is not a minimum on its surface (5.3 kcal mol^{-1} for **L** versus 5.1 kcal mol^{-1} to shift vinyl group). However, these single-point values were computed from the B3LYP-optimized geometries. On the B3LYP surface, **L** is a minimum (non-underlined values).

9.5 Conclusions

In conclusion, a new diterpene product was isolated and elucidated using computational and spectroscopic NMR analysis. Stereoselectivity and constitutional questions about the structure of (14*S*)-cleistantha-8,12-diene (**1**) were resolved using computational NMR techniques. Computational and experimental labeling studies elucidated a plausible biosynthetic pathway from pimaradienyl cation to **1**.

9.6 References

(1) Zi, J.; Mafu, S.; Peters, R. J. To Gibberellins and Beyond! Surveying the Evolution of (Di)Terpenoid Metabolism. *Annu. Rev. Plant Biol.* **2014**, *65*, 259–286.

(2) Murphy, K. M.; Zerbe, P. Specialized Diterpenoid Metabolism in Monocot Crops: Biosynthesis and Chemical Diversity. *Phytochemistry* **2020**, *172*, 112289.

(3) Peters, R. J. Two Rings in Them All: The Labdane-Related Diterpenoids. *Nat. Prod. Rep.* **2010**, *27*, 1521.

(4) Wu, Y.; Zhou, K.; Toyomasu, T.; Sugawara, C.; Oku, M.; Abe, S.; Usui, M.; Mitsuhashi, W.; Chono, M.; Chandler, P. M.; et al. Functional Characterization of Wheat Copalyl Diphosphate Synthases Sheds Light on the Early Evolution of Labdane-Related Diterpenoid Metabolism in the Cereals. *Phytochemistry* **2012**, *84*, 40–46.

(5) Li, L.; Chen, X.; Ma, C.; Wu, H.; Qi, S. Piriformospora Indica Requires Kaurene Synthase Activity for Successful Plant Colonization. *Plant Physiol. Biochem.* **2016**, *102*, 151–160.

(6) Zhang, J.; Li, R.; Xu, M.; Hoffmann, R. I.; Zhang, Y.; Liu, B.; Zhang, M.; Yang, B.; Li, Z.; Peters, R. J. A (Conditional) Role for Labdane-related Diterpenoid Natural Products in Rice Stomatal Closure. *New Phytol.* **2021**, *230*, 698–709.

(7) Cyr, A.; Wilderman, P. R.; Determan, M.; Peters, R. J. A Modular Approach for Facile Biosynthesis of Labdane-Related Diterpenes. *J. Am. Chem. Soc.* **2007**, *129*, 6684–6685.

(8) Liu, Y.; Balcke, G. U.; Porzel, A.; Mahdi, L.; Scherr-Henning, A.; Zuccaro, A.; Tissier, A. A Barley Gene Cluster for the Biosynthesis of Diterpenoid 1 Phytoalexins. *bioRxiv* **2021**.

(9) Pinto, A. C.; Peixoto, E. M.; Fiorani, N. G. M. Diterpenes with Pimarane and Cleistanthane Skeletons from Vellozia Piresiana. *Phytochemistry* **1984**, *23*, 1293–1296.

(10) Pinto, A. C.; Maçaira, A. M. P. Two Diterpenes with a Cleistanthane Skeleton from Vellozia Nivea. *Phytochemistry* **1988**, *27*, 3973–3974.

(11) Pinto, A. C.; Epifanio, R. D. A.; Pizzolatti, M. G. Diterpenoids from Vellozia Declinans. *Phytochemistry* **1992**, *31*, 4241–4243.

(12) Hussaini, F. A.; Roy, R.; Shoeb, A.; Pragya; Gajhede, M.; Jacobsen, J. P.; Boll, P. M. Structure and Configuration of a New Cleistanthane Diterpenoid from Pogostemon Auricularis. *Nat. Prod. Lett.* **1993**, *3*, 71–77.

(13) Siebert, M. R.; Zhang, J.; Addepalli, S. V; Tantillo, D. J.; Hase, W. L. The Need for Enzymatic Steering in Abietic Acid Biosynthesis: Gas-Phase Chemical Dynamics Simulations of Carbocation Rearrangements on a Bifurcating Potential Energy Surface. *J. Am. Chem. Soc.* **2011**, *133*, 8335–8343.
(14) Frisch, M. J.; Trucks, G. W.; Schlegel, H. B.; Scuseria, G. E. .; Robb, G. E.; Cheeseman, J. R.; Scalmani, G.; Barone, V.; Mennucci, B. .; Petersson, G. A.; Nakatsuji, H.; Caricato, M.; Li, X.; Hratchian, H. P. .; Izmaylov, A. F.; Bloino, J.; Zheng, G.; Sonnenberg, J. L.; Hada, M. .; Ehara, M.; Toyota, K.; Fukuda, R.; Hasegawa, J.; Ishida, M.; Nakajima, T. .; Honda, Y.; Kitao, O.; Nakai, H.; Vreven, T.; Montgomery, Jr., J. A. . P.; J. E.; Ogliaro, F.; Bearpark, M.; Heyd, J. J.; Brothers, E. . K.; K. N.; Staroverov, V. N.; Keith, T.; Kobayashi, R.; Normand, J. . R.; K.; Rendell, A.; Burant, J. C.; Iyengar, S. S.; Tomasi, J. . C.; M.; Rega, N.; Millam, J. M.; Klene, M.; Knox, J. E.; Cross, J. B. .; Bakken, V.; Adamo, C.; Jaramillo, J.; Gomperts, R.; Stratmann, R. E.; Yazyev O.; Austin, A. J.; Cammi, R.; Pomelli, C.; Ochterski, J. W.; Martin R. L.; Morokuma, K.; Zakrzewski, V. G.; Voth, G. A.; Salvador, P.; Dannenberg, J. J.; Dapprich, S.; Daniels, A. D.; Farkas O.; Foresman, J. B.; Ortiz, J. V.; Cioslowski, J.; Fox, D. J. *Gaussian 09*, Revision D.01. Gaussian Inc. Wallingford, CT 2009.
(15) Bootsma, A. N.; Wheeler, S. E. Popular Integration Grids Can Result in Large Errors in DFT-Computed Free Energies. *ChemRxiv* **2019**, 1–20.
(16) Fukui, K. The Path of Chemical Reactions -- The IRC Approach. *Acc. Chem. Res.* **1981**, *14*, 363–368.
(17) Gonzalez, C.; Schlegel, H. B. Reaction Path Following In Mass-Weighted Internal Coordinates Cartesians and with Internal Coordinates without Mass-Weighting. *J. Phys. Chem.* **1990**, *94*, 5523–5527.
(18) Maeda, S.; Harabuchi, Y.; Ono, Y.; Taketsugu, T.; Morokuma, K. Intrinsic Reaction Coordinate: Calculation, Bifurcation, and Automated Search. *Int. J. Quantum Chem.* **2015**, *115*, 258–269.
(19) Becke, A. D. Density-Functional Thermochemistry. III. The Role of Exact Exchange. *J. Chem. Phys.* **1993**, *98*, 5648–5652.
(20) Tantillo, D. J. Biosynthesis via Carbocations: Theoretical Studies on Terpene Formation. *Nat. Prod. Rep.* **2011**, *28*, 1035–1053.
(21) Adamo, C.; Barone, V. Exchange Functionals with Improved Long-Range Behavior and Adiabatic Connection Methods without Adjustable Parameters: The MPW and MPW1PW Models. *J. Chem. Phys.* **1998**, *108*, 664–675.
(22) Chai, J.-D.; Head-Gordon, M. Long-Range Corrected Hybrid Density Functionals with Damped Atom–Atom Dispersion Corrections. *Phys. Chem. Chem. Phys.* **2008**, *10*, 6615.
(23) Álvarez-Moreno, M.; de Graaf, C.; López, N.; Maseras, F.; Poblet, J. M.; Bo, C. Managing the Computational Chemistry Big Data Problem: The ioChem-BD Platform. *J. Chem. Inf. Model.* **2015**, *55*, 95–103.
(24) Morrone, D.; Lowry, L.; Determan, M. K.; Hershey, D. M.; Xu, M.; Peters, R. J. Increasing Diterpene Yield with a Modular Metabolic Engineering System in E. Coli: Comparison of MEV and MEP Isoprenoid Precursor Pathway Engineering. *Appl. Microbiol. Biotechnol.* **2010**, *85*, 1893–1906.
(25) Tantillo, D. J. The Carbocation Continuum in Terpene Biosynthesis - Where Are the Secondary Cations? *Chem. Soc. Rev.* **2010**, *39*, 2847–2854.
(26) Tantillo, D. J. Walking in the Woods with Quantum Chemistry – Applications of

Quantum Chemical Calculations in Natural Products Research. *Nat. Prod. Rep.* **2013**, *30*, 1079.
(27) Hong, Y. J.; Tantillo, D. J. Biosynthetic Consequences of Multiple Sequential Post-Transition-State Bifurcations. *Nat. Chem.* **2014**, *6*, 104–111.
(28) Siebert, M. R.; Manikandan, P.; Sun, R.; Tantillo, D. J.; Hase, W. L. Gas-Phase Chemical Dynamics Simulations on the Bifurcating Pathway of the Pimaradienyl Cation Rearrangement: Role of Enzymatic Steering in Abietic Acid Biosynthesis. *J. Chem. Theory Comput.* **2012**, *8*, 1212–1222.
(29) Phillips, M. A.; Croteau, R. B. Resin-Based Defenses in Conifers. *Trends Plant Sci.* **1999**, *4*, 184–190.
(30) LaFever, R. E.; Vogel, B. S.; Croteau, R. Diterpenoid Resin Acid Biosynthesis in Conifers: Enzymatic Cyclization of Geranylgeranyl Pyrophosphate to Abietadiene, the Precursor of Abietic Acid. *Arch. Biochem. Biophys.* **1994**.
(31) Peters, R. J.; Flory, J. E.; Jetter, R.; Ravn, M. M.; Lee, H.-J.; Coates, R. M.; Croteau, R. B. Abietadiene Synthase from Grand Fir (Abies Grandis): Characterization and Mechanism of Action of the "Pseudomature" Recombinant Enzyme. *Biochemistry* **2000**, *39*, 15592–15602.
(32) Peters, R. J.; Ravn, M. M.; Coates, R. M.; Croteau, R. B. Bifunctional Abietadiene Synthase: Free Diffusive Transfer of the (+)-Copalyl Diphosphate Intermediate between Two Distinct Active Sites. *J. Am. Chem. Soc.* **2001**, *123*, 8974–8978.
(33) Peters, R. J.; Croteau, R. B. Abietadiene Synthase Catalysis: Mutational Analysis of a Prenyl Diphosphate Ionization-Initiated Cyclization and Rearrangement. *Proc. Natl. Acad. Sci.* **2002**, *99*, 580–584.
(34) Gao, W.; Hillwig, M. L.; Huang, L.; Cui, G.; Wang, X.; Kong, J.; Yang, B.; Peters, R. J. A Functional Genomics Approach to Tanshinone Biosynthesis Provides Stereochemical Insights. *Org. Lett.* **2009**, *11*, 5170–5173.
(35) Zhou, Y. J.; Gao, W.; Rong, Q.; Jin, G.; Chu, H.; Liu, W.; Yang, W.; Zhu, Z.; Li, G.; Zhu, G.; et al. Modular Pathway Engineering of Diterpenoid Synthases and the Mevalonic Acid Pathway for Miltiradiene Production. *J. Am. Chem. Soc.* **2012**, *134*, 3234–3241.
(36) Carpenter, B. K. Intramolecular Dynamics for the Organic Chemist. *Acc. Chem. Res.* **1992**, *25*, 520–528.
(37) Carpenter, B. K. Bimodal Distribution of Lifetimes for an Intermediate from a Quasiclassical Dynamics Simulation. *J. Am. Chem. Soc.* **1996**, *118*, 10329–10330.
(38) Carpenter, B. K. Dynamic Behavior of Organic Reactive Intermediates. *Angew. Chem. Int. Ed.* **1998**, *37*, 3340–3350.
(39) Oyola, Y.; Singleton, D. A. Dynamics and the Failure of Transition State Theory in Alkene Hydroboration. *J. Am. Chem. Soc.* **2009**, *131*, 3130–3131.
(40) Ma, X.; Hase, W. L. Perspective : Chemical Dynamics Simulations of Non-Statistical Reaction Dynamics. *Philos. Trans. R. Soc. A* **2017**, *375*, 20160204.
(41) Tantillo, D. J. *Dynamic Effects on Organic Reactions*; Reedijk, J., Ed.; Elsevier Inc.: Waltham, MA, 2018.
(42) Hare, S. R.; Tantillo, D. J. Dynamic Behavior of Rearranging Carbocations - Implications for Terpene Biosynthesis. *Beilstein J. Org. Chem.* **2016**, *12*, 377–390.
(43) Tantillo, D. J. *Beyond Transition State Theory—Non-Statistical Dynamic Effects for Organic Reactions*, 1st ed.; Elsevier Ltd., 2021.
(44) Tantillo, D. J. Dynamic Effects on Organic Reactivity—Pathways to (and from)

Discomfort. *J. Phys. Org. Chem.* **2021**, *34*, 1–9.
(45) Ess, D. H.; Wheeler, S. E.; Iafe, R. G.; Xu, L.; Çelebi-Ölçüm, N.; Houk, K. N. Bifurcations on Potential Energy Surfaces of Organic Reactions. *Angew. Chem. Int. Ed.* **2008**, *47*, 7592–7601.
(46) Hong, Y. J.; Tantillo, D. J. A Potential Energy Surface Bifurcation in Terpene Biosynthesis. *Nat. Chem.* **2009**, *1*, 384–389.
(47) Hare, S. R.; Pemberton, R. P.; Tantillo, D. J. Navigating Past a Fork in the Road: Carbocation−π Interactions Can Manipulate Dynamic Behavior of Reactions Facing Post-Transition-State Bifurcations. *J. Am. Chem. Soc.* **2017**, *139*, 7485–7493.
(48) Hare, S. R.; Tantillo, D. J. Post-Transition State Bifurcations Gain Momentum-Current State of the Field. *Pure Appl. Chem.* **2017**, *89*, 679–698.
(49) Paranjothy, M.; Sun, R.; Zhuang, Y.; Hase, W. L. Direct Chemical Dynamics Simulations: Coupling of Classical and Quasiclassical Trajectories with Electronic Structure Theory. *WIREs Comput. Mol. Sci.* **2013**, *3*, 296–316.
(50) Pratihar, S.; Ma, X.; Homayoon, Z.; Barnes, G. L.; Hase, W. L. Direct Chemical Dynamics Simulations. *J. Am. Chem. Soc.* **2017**, *139*, 3570–3590.
(51) Jayee, B.; Hase, W. L. Nonstatistical Reaction Dynamics. *Annu. Rev. Phys. Chem.* **2020**, *71*, 289–313.
(52) Wang, S. C.; Tantillo, D. J. Theoretical Studies on Synthetic and Biosynthetic Oxidopyrylium−Alkene Cycloadditions: Pericyclic Pathways to Intricarene. *J. Org. Chem.* **2008**, *73*, 1516–1523.
(53) Garms, S.; Köllner, T. G.; Boland, W. A Multiproduct Terpene Synthase from Medicago Truncatula Generates Cadalane Sesquiterpenes via Two Different Mechanisms. *J. Org. Chem.* **2010**, *75*, 5590–5600.
(54) Davis, E. M.; Croteau, R. B. Cyclization Enzymes in the Biosynthesis of Monoterpenes, Sesquiterpenes, and Diterpenes. *Top. Curr. Chem.* **2000**, *209*, 53–95.
(55) Lodewyk, M. W.; Gutta, P.; Tantillo, D. J. Computational Studies on Biosynthetic Carbocation Rearrangements Leading to Sativene, Cyclosativene, α-Ylangene, and β-Ylangene. *J. Org. Chem.* **2008**, *73*, 6570–6579.
(56) Hong, Y. J.; Tantillo, D. J. Consequences of Conformational Preorganization in Sesquiterpene Biosynthesis: Theoretical Studies on the Formation of the Bisabolene, Curcumene, Acoradiene, Zizaene, Cedrene, Duprezianene, and Sesquithuriferol Sesquiterpenes. *J. Am. Chem. Soc.* **2009**, *131*, 7999–8015.
(57) Hong, Y. J.; Tantillo, D. J. Quantum Chemical Dissection of the Classic Terpinyl/Pinyl/Bornyl/Camphyl Cation Conundrum—the Role of Pyrophosphate in Manipulating Pathways to Monoterpenes. *Org. Biomol. Chem.* **2010**, *8*, 4589.
(58) Hong, Y. J.; Tantillo, D. J. Formation of Beyerene, Kaurene, Trachylobane, and Atiserene Diterpenes by Rearrangements That Avoid Secondary Carbocations. *J. Am. Chem. Soc.* **2010**, *132*, 5375–5386.
(59) Bushmelev, V. A.; Genaev, A. M.; Sal'nikov, G. E.; Shubin, V. G. Pendular Rearrangement of Epimeric 3b,4,4a,5-Tetramethyl-3b,4,4a,5-Tetrahydro-4H-Cyclopropa[a]Phenalen-5-Yl Cations. *Russ. J. Org. Chem.* **2007**, *43*, 1656–1660.
(60) Tantillo, D. J. Interrogating Chemical Mechanisms in Natural Products Biosynthesis Using Quantum Chemical Calculations. *WIREs Comput. Mol. Sci.* **2020**, *10*, 2–5.
(61) Meguro, A.; Motoyoshi, Y.; Teramoto, K.; Ueda, S.; Totsuka, Y.; Ando, Y.; Tomita, T.; Kim, S.-Y.; Kimura, T.; Igarashi, M.; et al. An Unusual Terpene Cyclization Mechanism

Involving a Carbon-Carbon Bond Rearrangement. *Angew. Chem. Int. Ed.* **2015**, *54*, 4353–4356.
(62) Hong, Y. J.; Tantillo, D. J. The Energetic Viability of an Unexpected Skeletal Rearrangement in Cyclooctatin Biosynthesis. *Org. Biomol. Chem.* **2015**, *13*, 10273–10278.
(63) Sato, H.; Teramoto, K.; Masumoto, Y.; Tezuka, N.; Sakai, K.; Ueda, S.; Totsuka, Y.; Shinada, T.; Nishiyama, M.; Wang, C.; Kuzuyama, T.; Uchiyama, M. "Cation-Stitching Cascade": Exquisite Control of Terpene Cyclization in Cyclooctatin Biosynthesis. *Sci. Rep.* **2016**, *5*, 18471.
(64) Rieder, C.; Strauß, G.; Fuchs, G.; Arigoni, D.; Bacher, A.; Eisenreich, W. Biosynthesis of the Diterpene Verrucosan-2β-ol in the Phototrophic Eubacterium Chloroflexus Aurantiacus. *J. Biol. Chem.* **1998**, *273*, 18099–18108.
(65) Dauben, W. G.; Friedrich, L. E. The Mechanism of the Transformation of Thujopsene to Widdrol. *Tetrahedron Lett.* **1964**, *5*, 2675–2678.
(66) Dickschat, J. S. Modern Aspects of Isotopic Labellings in Terpene Biosynthesis. *European J. Org. Chem.* **2017**, *2017*, 4872–4882.
(67) Potter, K. C.; Jia, M.; Hong, Y. J.; Tantillo, D.; Peters, R. J. Product Rearrangement from Altering a Single Residue in the Rice Syn -Copalyl Diphosphate Synthase. *Org. Lett.* **2016**, *18*, 1060–1063.
(68) Liang, J.; Merrill, A. T.; Laconsay, C. J.; Hou, A.; Pu, Q.; Dickschat, J. S.; Tantillo, D. J.; Wang, Q.; Peters, R. J. Deceptive Complexity in Formation of Cleistantha-8,12-Diene. *Org. Lett.* **2022**, *24*, 2646–2649.
(69) Rabe, P.; Rinkel, J.; Dolja, E.; Schmitz, T.; Nubbemeyer, B.; Luu, T. H.; Dickschat, J. S. Mechanistic Investigations of Two Bacterial Diterpene Cyclases: Spiroviolene Synthase and Tsukubadiene Synthase. *Angew. Chem. Int. Ed.* **2017**, *56*, 2776–2779.
(70) Mitsuhashi, T.; Rinkel, J.; Okada, M.; Abe, I.; Dickschat, J. S. Mechanistic Characterization of Two Chimeric Sesterterpene Synthases from Penicillium. *Chem. Eur. J.* **2017**, *23*, 10053–10057.
(71) Rinkel, J.; Lauterbach, L.; Dickschat, J. S. A Branched Diterpene Cascade: The Mechanism of Spinodiene Synthase from Saccharopolyspora Spinosa. *Angew. Chem. Int. Ed.* **2019**, *58*, 452–455.

Appendix

Supplementary for Chapter 6

Supplementary Information

Chapter 6: Can Dirhodium Complexes Catalyze Cyclopropanation of Cycloheptatriene Diazo Compounds to Synthesize Substituted-Semibullvalenes?

A-1. Supplementary Figures

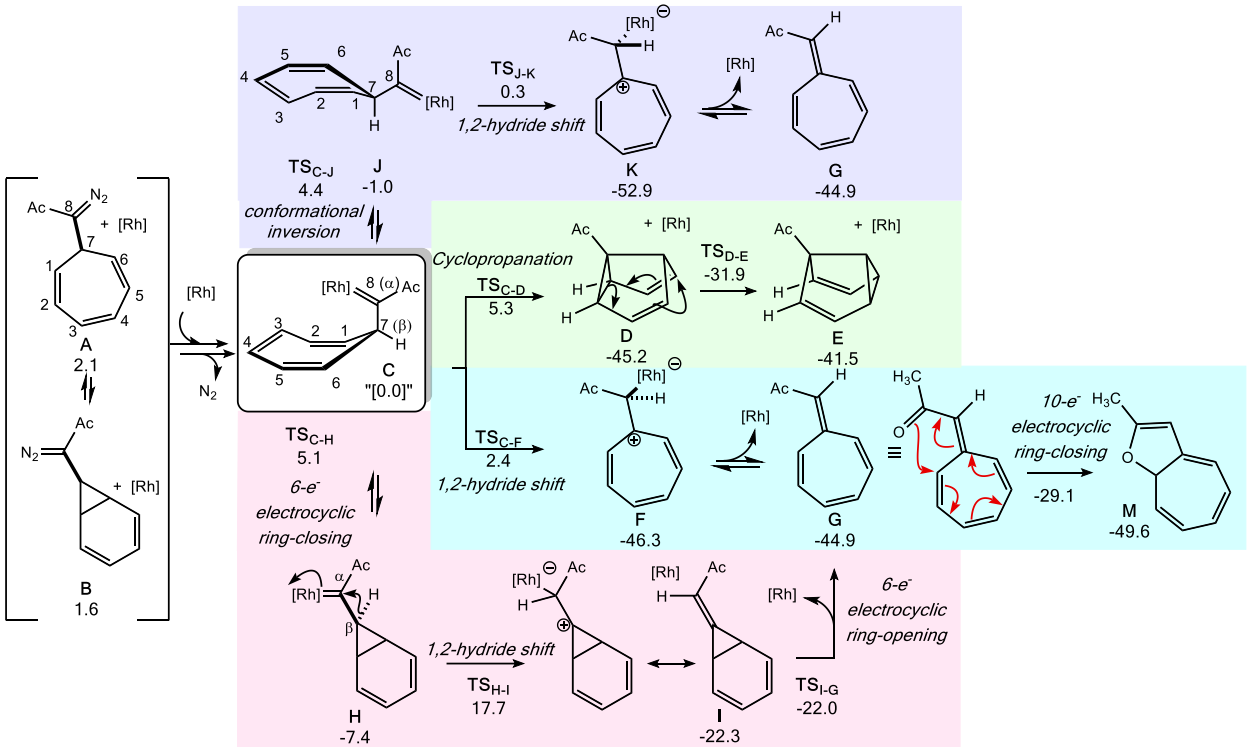

Figure A.1 Relative free energies (kcal mol^{-1}) of donor-acceptor carbene system with the inclusion of **M**. PW6B95/def2-SVP level.

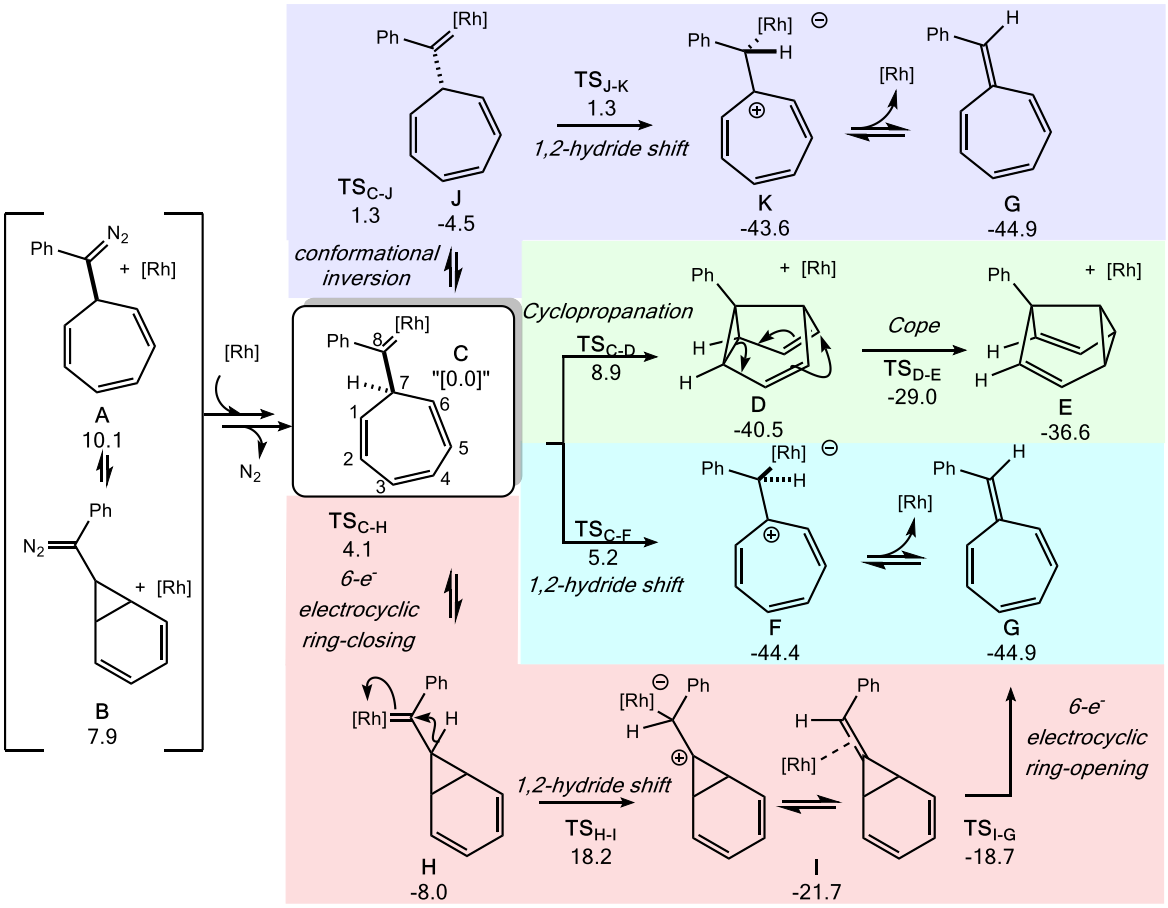

Figure A.2 Relative free energies (kcal mol^{-1}) of donor-donor carbene system. PW6B95/def2-SVP level.

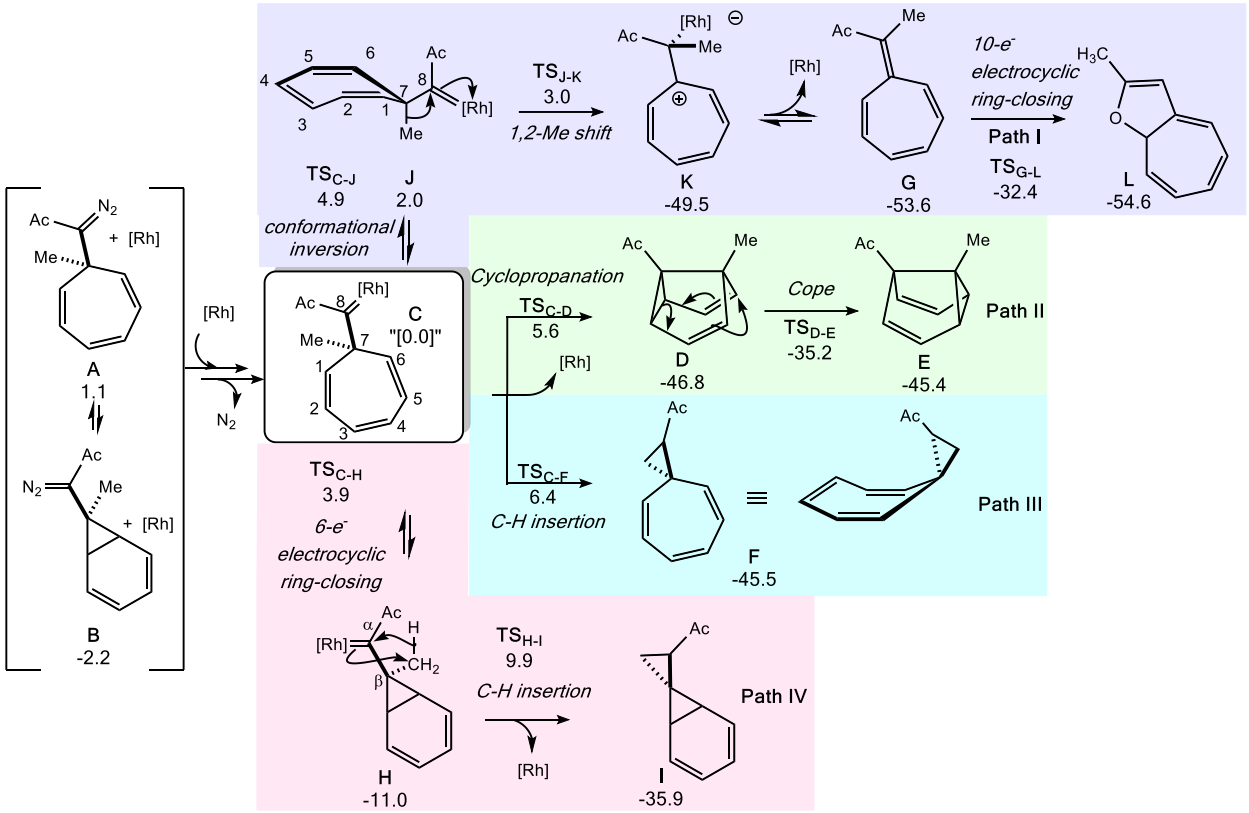

Figure A.3 Relative free energies (kcal mol^{-1}) of donor-acceptor, C7-methyl system. PW6B95/def2-SVP level. Figure 6.2 of Chapter 6 with **TS_{G-L}** and **L** structures.

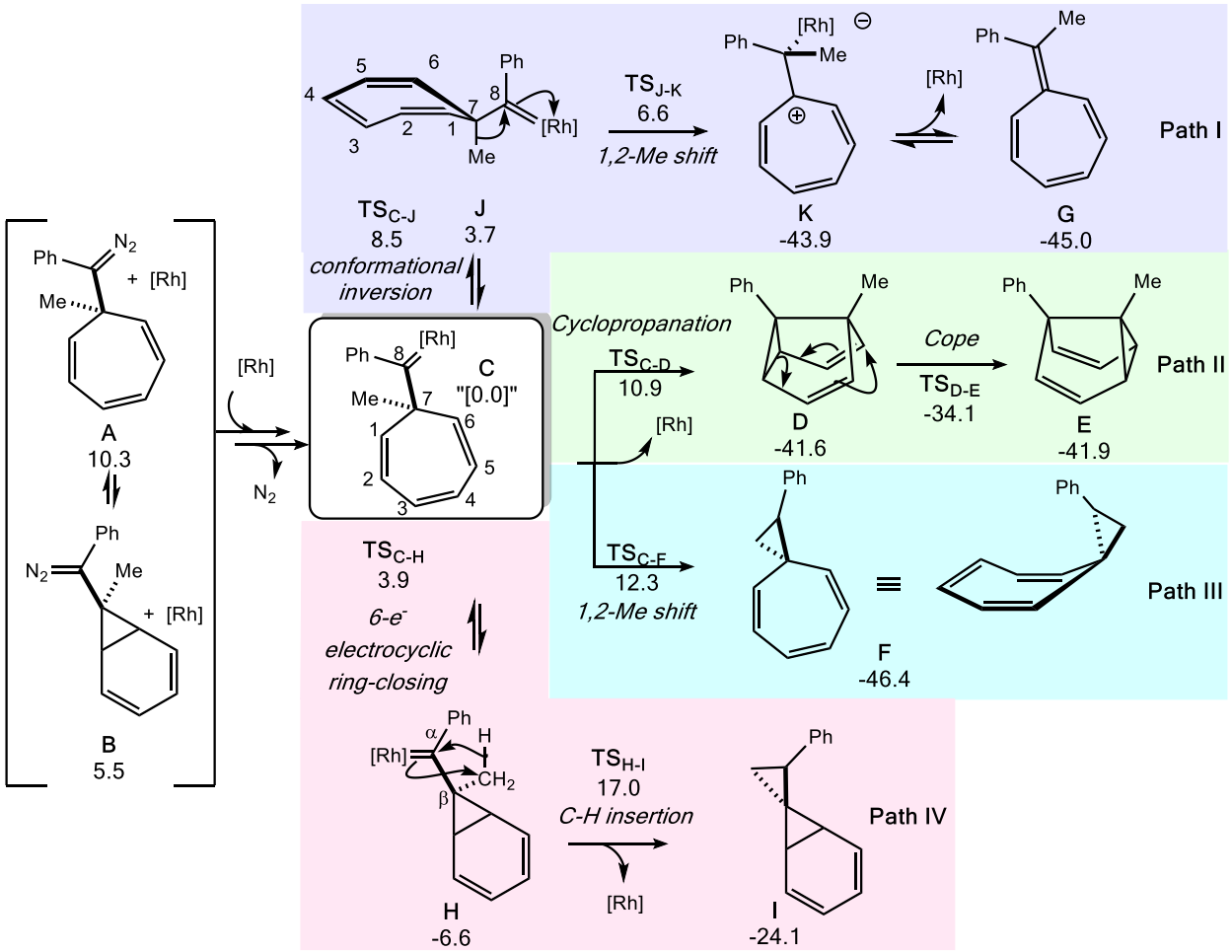

Figure A.4 Relative free energies (kcal mol^{-1}) of donor-donor, C7-methyl system. PW6B95/def2-SVP level.

A-2. Energies and Frequencies

All structures can be found on the ioChem-BD database at the following link: https://iochem-bd.bsc.es/browse/handle/100/216065

Energies and Frequencies for each reported structure can be found in the following Tables.

Table A.1 Energies and lowest frequencies for structures in Figure A.1.

Structure	File Name	G (Hartree)	E (Hartree)	ΔG (kcal mol^{-1})	ΔE (kcal mol^{-1})	Lowest frequency (cm^{-1})
N_2	N2	-109.58265	-109.5699956	-	-	2536.3
A	CHT_diazo_acc	-571.870736	-572.0134621	2.1	3.3	27.9
B	Norc_diazo_acc	-571.87147	-572.0156583	1.6	2.0	51.8
A_inverted	CHT_invert_diazo_acc	-571.871344	-572.0122815	1.7	4.1	18.8
B_inverted	Norc_invert_diazo_acc	-571.871409	-572.0121117	1.6	4.2	3.9
Rh cat	Rh_cat	-1135.530568	-1135.689383	-	-	28.8
C	C_acc	-1597.821946	-1598.138176	[0]	[0]	14.6
TS_{C-D}	TS_C_D_acc	-1597.81356	-1598.131686	5.3	4.1	-181.7
D	D_acc	-1597.893936	-1598.216906	-45.2	-49.4	16.7
TS_{D-E}	TS_D_E_acc	-1597.872801	-1598.193451	-31.9	-34.7	-482.7
E	E_acc	-1597.888109	-1598.211159	-41.5	-45.8	24.8
H	H_acc	-1597.833811	-1598.152008	-7.4	-8.7	22.6
TS_{H-I}	TS_H_I_acc	-1597.793722	-1598.106296	17.7	20.0	-835.3
I	I_acc	-1597.857514	-1598.178614	-22.3	-25.4	21.5
J	J_acc	-1597.823508	-1598.138777	-1.0	-0.4	14.8
TS_{J-K}	TS_J_K_acc	-1597.821391	-1598.135044	0.3	2.0	-668.7
K	K_acc	-1597.906173	-1598.224555	-52.9	-54.2	5.9
TS_{C-F}	TS_C_F_acc	-1597.818188	-1598.133031	2.4	3.2	-108.0
F	F_acc	-1597.895786	-1598.215905	-46.3	-48.8	11.4
G	G_acc	-462.362873	-462.4990248	-44.9	-31.5	13.8
TS_{C-H}	TS_C_H_acc	-1597.813749	-1598.129716	5.1	5.3	-438.6
TS_{C-J}	TS_C_J_acc	-1597.814906	-1598.131023	4.4	4.5	-45.8
TS_{G-L}	TS_G_M_acc	-462.337678	-462.4751012	-29.1	-16.5	-471.2
L	M_acc	-462.370358	-462.5100371	-49.6	-38.4	93.7

Table A.2 Energies and lowest frequencies for structures in Figure A.2.

Structure	File Name	G (Hartree)	E (Hartree)	ΔG (kcal mol^{-1})	ΔE (kcal mol^{-1})	Lowest frequency (cm^{-1})
A	CHT_diazo_don	-650.302791	-650.4884838	10.1	12.3	25.3
B	Norc_diazo_don	-650.306333	-650.4930408	7.9	9.4	32.5
C	C_don	-1676.266856	-1676.627477	[0]	[0]	20.0
TS_{C-D}	TS_C_D_don	-1676.252594	-1676.614596	8.9	8.1	-264.2
D	D_don	-1676.331466	-1676.698097	-40.5	-44.3	24.4
TS_{D-E}	TS_D_E_don	-1676.313013	-1676.676226	-29.0	-30.6	-468.3
E	E_don	-1676.325214	-1676.692448	-36.6	-40.8	30.6
H	H_don	-1676.279569	-1676.635472	-8.0	-5.0	7.2
TS_{H-I}	TS_H_I_don	-1676.237852	-1676.595258	18.2	20.2	13.5
I	I_don	-1676.301422	-1676.664444	-21.7	-23.2	-951.3
TS_{I-G}	TS_I_G_don	-1676.296623	-1676.659328	-18.7	-20.0	-447.0
J	J_don	-1676.274045	-1676.635154	-4.5	-4.8	17.8
TS_{J-K}	TS_J_K_don	-1676.264783	-1676.620822	1.3	4.2	-568.2
K	K_don	-1676.336338	-1676.700694	-43.6	-45.9	16.3
TS_{C-F}	TS_C_F_acc	-1676.258522	-1676.61553	5.2	7.5	-394.8
F	F_acc	-1676.337594	-1676.699875	-44.4	-45.4	13.6
G	G_acc	-540.807892	-540.9871218	-44.9	-31.3	41.1
TS_{C-H}	TS_C_H_don	-1676.260244	-1676.620865	4.1	4.1	-407.3
TS_{C-J}	TS_C_J_don	-1676.264758	-1676.627498	1.3	0.0	-46.6

Table A.3 Energies and lowest frequencies for structures in Figure 6.2 of Chapter 6 and Figure A.3.

Structure	File Name	G (Hartree)	E (Hartree)	ΔG (kcal mol^{-1})	ΔE (kcal mol^{-1})	Lowest frequency (cm^{-1})
A	CHT_diazo_acc_c7_me	-611.178551	-611.3486835	1.1	4.1	56.8
B	Norc_diazo_acc_c7_me	-611.183864	-611.3543773	-2.2	0.6	59.6

C	C_acc_c7_me	-1637.128299	-1637.474647	[0]	[0]	-4.5
TS_{C-D}	TS_C_D_acc_c7_me	-1637.11943	-1637.465999	5.6	5.4	-212.3
D	D_acc_c7_me	-1637.202911	-1637.553619	-46.8	-49.6	22.3
TS_{D-E}	TS_D_E_acc_c7_me	-1637.184429	-1637.532269	-35.2	-36.2	-484.6
E	E_acc_c7_me	-1637.200647	-1637.55029	-45.4	-47.5	22.8
TS_{C-F}	TS_C_F_acc_c7_me	-1637.118155	-1637.463194	6.4	7.2	-412.0
F	F_acc_c7_me	-1637.191972	-1637.540372	-45.5	-46.7	18.8
H	H_acc_c7_me	-1637.136923	-1637.482825	-11.0	-10.6	18.7
TS_{H-I}	TS_H_I_acc_c7_me	-1637.103685	-1637.447131	9.9	11.8	-530.5
I	I_acc_c7_me	-1637.17657	-1637.527327	-35.9	-38.5	25.8
J	J_acc_c7_me	-1637.125119	-1637.468563	2.0	3.8	18.7
TS_{J-K}	TS_J_K_acc_c7_me	-1637.123495	-1637.468623	3.0	3.8	-321.1
K	K_acc_c7_me	-1637.207122	-1637.552411	-49.5	-48.8	9.9
G	G_acc_c7_me	-501.67425	-501.8369771	-53.6	-37.9	40.2
TS_{C-H}	TS_C_H_acc_c7_me	-1637.122124	-1637.465903	3.9	5.5	-416.7
TS_{C-J}	TS_C_J_acc_c7_me	-1637.120438	-1637.464391	4.9	6.4	-53.9
TS_{G-L}	TS_G_L_acc_c7_me	-501.649306	-501.8127448	-32.4	-17.2	-469.8
L	L_acc_c7_me	-501.684686	-501.8502128	-54.6	-40.8	83.8

Table A.4 Energies and lowest frequencies for structures in Figure A.4.

Structure	File Name	G (Hartree)	E (Hartree)	ΔG (kcal mol^{-1})	ΔE (kcal mol^{-1})	Lowest frequency (cm^{-1})
A	A_don_c7_me	-689.609465	-689.8220573	10.3	11.5	27.0
B	B_don_c7_me	-689.617057	-689.8304971	5.5	6.3	39.1
C	C_don_c7_me	-1715.573773	-1715.959848	[0]	[0]	16.2
TS_{C-D}	TS_C_D_don_c7_me	-1715.556462	-1715.944812	10.9	9.4	-258.9
D	D_don_c7_me	-1715.64007	-1716.033051	-41.6	-45.9	22.6
TS_{D-E}	TS_D_E_don_c7_me	-1715.62806	-1716.015864	-34.1	-35.2	-454.5
E	E_don_c7_me	-1715.640508	-1716.031412	-41.9	-44.9	17.0
TS_{C-F}	TS_C_F_don_c7_me	-1715.554171	-1715.940167	12.3	12.3	-464.7
F	F_don_c7_me	-1715.630417	-1716.020631	-46.4	-47.6	16.7
H	H_don_c7_me	-1715.584303	-1715.971183	-6.6	-7.1	11.3
TS_{H-I}	TS_H_I_don_c7_me	-1715.546668	-1715.931295	17.0	17.9	-575.5
I	I_don_c7_me	-1715.612244	-1716.006041	-24.1	-29.0	21.6
J	J_don_c7_me	-1715.567823	-1715.955105	3.7	3.0	15.2
TS_{J-K}	TS_J_K_don_c7_me	-1715.563272	-1715.949484	6.6	6.5	-366.0
K	K_don_c7_me	-1715.643784	-1716.033832	-43.9	-46.4	22.4
G	G_don_c7_me	-580.114887	-580.3199478	-45.0	-31.1	43.4
TS_{C-H}	TS_C_H_don_c7_me	-1715.56758	-1715.954664	3.9	3.3	-393.3
TS_{C-J}	TS_C_J_don_c7_me	-1715.560226	-1715.948586	8.5	7.1	-31.9

Table A.5 Energies and lowest frequencies for structures in Figure 6.3 of Chapter 6.

Structure	File Name	G (Hartree)	E (Hartree)	ΔG (kcal mol^{-1})	ΔE (kcal mol^{-1})	Lowest frequency (cm^{-1})
R	R	-1175.781755	-1176.063456	[0]	[0]	14.88
TS_U-1	TS_U_1	-1175.76417	-1176.045421	11.0	11.3	-285.05
Int_U-1	Int_U_1	-1175.782586	-1176.067892	-0.5	-2.8	10.27
TS_U-2	TS_U_2	-1175.773328	-1176.059304	5.3	2.6	-330.61
Int_U-2	Int_U_2	-1175.777698	-1176.06187	2.5	1.0	5.59
TS_U-3	TS_U_3	-1175.774846	-1176.060434	4.3	1.9	-327.28
P_U	P_U	-1175.780964	-1176.068006	0.5	-2.9	13.58

Table A.6 Energies and lowest frequencies for structures in Figure 6.4 of Chapter 6.

Structure	File Name	G (Hartree)	E (Hartree)	ΔG (kcal mol^{-1})	ΔE (kcal mol^{-1})	Lowest frequency (cm^{-1})
R_O	R_O	-1251.017674	-1251.302855	[0]	[0]	9.48
TS_O-1	TS_O_1	-1251.011988	-1251.299177	3.6	2.3	-175.87
Int_O	Int_O	-1251.07793	-1251.370792	-37.8	-42.6	20.91
TS_O-2	TS_O_2	-1251.060547	-1251.351206	-26.9	-30.3	-423.55
P_O	P_O	-1251.075986	-1251.368401	-36.6	-41.1	24.54